Universitat Autònoma de Barcelona

Electrochemical and optical nanomaterial-based biosensors for diagnostic applications

Alejandro Chamorro García

Thesis dissertation to apply for the PhD in Biotechnology

Department of Genetics and microbiology - Faculty of Biosciences

Autonomous University of Barcelona

PhD director

Prof. Arben Merkoçi
ICREA & Nanobioelectronics and Biosensors Group
Institut Català de Nanociència i Nanotecnologia (ICN2)

2015

The present thesis entitled “Electrochemical and optical nanomaterial based biosensors for diagnostic applications” presented by Alejandro Chamorro Garcia to obtain the degree of Doctor, has been performed at the laboratories of the Nanobioelectronics and Biosensors group at the Intitut Català de Nanociència i Nanotechnologia (ICN2), under the supervision of Prof. Arben Merkoçi.

Bellaterra, 17 September 2015

Director

Prof. Arben Merkoçi
ICREA Professor
Nanobioelectronics & Biosensors Group
Institut Català de Nanociència i Nanotecnologia

Tutor

Prof. Antoni Villaverde Corrales
Autonomous University of Barcelona

Alejandro Chamorro García
Nanobioelectronics & Biosensors Group
Institut Català de Nanociència i Nanotecnologia

Acknowledgement for the financial and logistical support

Nanobioelectronics and Biosensors Group of the *Institut Català de Nanociència i Nanotecnologia* (ICN2) for the financial support to carry out all the research work here presented. Plaxco group at the University of California Santa Barbara (UCSB) as hosting institution in a short research stay.

Acknowledgments are also given for the financial support from several institutions / programs: Spanish MINECO under Project MAT2014-52485-P ; the Severo Ochoa Centers of Excellence Program under Grant SEV-2013-0295; the Generalitat de Catalunya for the project 2014SGR-260; the EU for Marie Curie Actions, Programme "PEOPLE" FP7-PEOPLE-2011-IRSES Proposal No 294901 and FP7 for projects under number 315653 "POC4PETS" and 613844 "SMS"; Hospital San Joan de Dèu (Barcelona, Spain) and Cellex foundation.

by I(tion :

on o cept al new tumor sup
gene and therapeutic targ astoma".

Preface

The presented PhD thesis has been carried out mainly in the Nanobioelectronics and Biosensors Group of the Catalan Institute of Nanoscience and Nanotechnology (ICN2). According to the decision of the PhD Commission of the Autonomous University of Barcelona, this PhD thesis is presented as a compendium of publications.

All the publications and manuscripts accepted by the commission for the compendium are listed below following their appearance in the thesis:

1. Carmen C. Mayorga-Martinez, Alejandro Chamorro-García , Arben Merkoçi. Electrochemical impedance spectroscopy (bio)sensing through hydrogen evolution reaction induced by gold nanoparticles. Biosensors and Bioelectronics, Volume 67, 15 May 2015, Pages 53–58.

2. Carmen C. Mayorga-Martinez, Alejandro Chamorro-García, Lorena Serrano, Lourdes Rivas, Daniel Quesada-Gonzalez, Laura Altet, Olga Francino, Armand Sánchez and Arben Merkoçi. An iridium oxide nanoparticle and polythionine thin film based platform for sensitive Leishmania DNA detection. J. Mater. Chem. B, 2015, **3**, 5166-5171.

In addition other work submitted for publication is included in annexes:

1. Chamorro-Garcia Alejandro, de la Escosura-Muñiz Alfredo, Espinosa-Castañeda Marisol, Rodriguez-Hernandez Carlos, de Torres Carmen, Merkoçi Arben. Detection of Parathyroid Hormone-like Hormone in Cancer Cell Cultures by Gold Nanoparticle-based Lateral Flow Immunoassays. Submitted, in revision.

Thesis overview

This thesis describes the study and development of new biosensing approaches based on novel properties of nanomaterials for the detection of proteins and DNA. The work has been performed in basis of two sensing platforms: first platform, the carbon screen-printed electrodes (SPCEs), were used in a more sensitive detection of gold nanoparticles (AuNPs) through electric impedance measurements. This type of measurement was carried out using gold nanoparticles as labels in a magnetoimmunoassay for the detection of a model protein. Furthemore, the same platform (SPCE) was adapted through polythinione films and iridium oxide nanoparticles (IrOxNPs) for the detection of specific DNA sequences in a label free assay. The second platform, paper-based platforms in format of Flow Immunoassay (LFIA), using gold nanoparticles as labels is adapted for the detection of a specific protein, Parathyroid like Hormone (PTHLH), with the aim to find a new strategy for simpler, non-hazardous, cheaper and faster detection of the protein.

The thesis is presented as a compendium of publications. Significant part of the work carried out during the thesis is still unpublished, and is presented at annexes part. However, background and introductory aspects of the unpublished work are discussed and presented in the introduction chapter of the thesis.

In **Chapter 1** a general overview of the application of nanomaterials for the improvement of biosensors and its application in the field of diagnostics and biomarkers detection is presented. First, a brief overview of diagnostics and biomarkers is given, followed by the advantages and suitability of biosensors in such field, and the interest in developing point of care (POC) sensing techniques. Second, advantages and interesting properties of nanomaterials in the field of biosensing are presented. Third, fundamentals of electrochemical and paper-based optical biosensors as well as application examples are given.

In **Chapter 2** the objectives of the thesis are presented.

Use of SPCE as platform for detection of gold nanoparticles (AuNPs) through electric impedance measurements is presented in **Chapter 3.** Achieving a more sensitive detection than the already reported electrochemical reading modes is the main objective of the work shown in this chapter. The developed technique is successfully applied in the detection of AuNPs of different sizes, and in a magnetoimmnuoassay for the detection of a model protein using AuNPs as electrochemical labels.

In **Chapter 4**, a novel biosensor for the detection of DNA is presented. The system is based in SPCE modified with polymer films and Iridium Oxide nanoparticles, where capturing DNA sequences have been immobilized. Detection of target DNA sequences is performed through electric impedance measurements, based in the blocking effect of the DNA against the diffusion of a redox indicator to

the surface of the electrode. A label free immunoassay for detection of specific sequences of Leishmania parasite's DNA is shown.

In **Chapter 5** general conclusions and future perspectives of the presented work are discussed.

In **Annex A** the work related to the paper-based platform for protein detection is presented. In this annex, detection of a specific protein (parathyroid like hormone, PTHLH) through LFIA strips is described. The developed LFIA strips represent a cheaper, faster and non-hazardous alternative to current available systems for PTHLH detection. Limits of detection (LOD) in the range of ng mL^{-1} for PTHLH in real samples (cell culture media, cell lysates) are reported. Furthermore, although the LOD achieved is higher than the levels found in human serum, the developed system is challenged using human serum spiked with PTHLH, proving the potential of the system to detect PTHLH In human serum. This work was done in collaboration with Hospital San Joan de Déu in Barcelona.

In **Annex B** the work carried out in a research stay at Prof. K. Plaxco's group at the University of California Santa Barbara (UCSB) is presented. In this section fabrication of electrochemical DNA (E-DNA), and electrochemical aptamer (E-Ab) biosensors is described. The aim of the work was focused on adapting the E-DNA and E-Ab technology to SPCE, using AuNPs as connecting platform between the thiol modified DNA and the SPCE.

Annex C represents a research done as a continuation of a previous one done in the group related mostly to the study of compatible materials with interest to be used as cells growth platforms with interest in sensing. As continuation of this work, in Annex C the conditions and materials previously selected to grow cells are applied in a nanochannel platform for the detection of a protein secreted by the cells grown directly on the sensing platform.

Resumen de la tesis

La presente tesis describe el desarrollo de nuevos métodos de sensado basados en nuevas propiedades de nanomateriales aplicados en la detección de proteínas y ADN. El trabajo ha sido basado en dos plataformas de sensado: primero, electrodos serigrafiados de carbono (SPCEs). Estos electrodos fueron aplicados en un ensayo de detección por impedancia eléctrica de nanopartículas de oro (AuNPs) que demostró mayor sensibilidad que métodos anteriores. El tipo de medida desarrollado fue aplicado en un ensayo tipo magnetoimmunosandwich para la detección de una proteína modelo. Del mismo modo, SPCE fueron adaptados mediante films de polythionina y nanopartículas de Iridio (IrOxNPs) para la detección de secuencias de ADN en un ensayo llamado libre de marcas. La segunda plataforma utilizada fue basada en papel y tiene el formato de un inmunoensayo de flujo lateral (LFIA, del inglés *lateral flow immunoassays*). Esta plataforma se adaptó para la detección de una proteína específica *Parathyroid like hormone* (PTHLH) utilizando AuNPs como marcas, con el fin de obtener una nueva estrategia más simple, sin marcaje de isotopos radioactivos, menos costosa y más rápida para la detección de dicha proteína.

La tesis está presentada como compendio de publicaciones. No obstante una parte importante del trabajo desarrollado aún está por publicar, y por lo tanto se presenta en forma de anexos. Igualmente, aspectos introductorios y teóricos referentes al trabajo no publicado se presentan en la introducción general de la tesis.

En el **Capítulo 1** se da una visión general de las aplicaciones llevabas a cabo y mejoras aportadas por parte de nanomateriales en el campo de los biosensores, y las posibles aplicaciones en la detección de biomarcadores en el campo del diagnóstico clínico. Primero, se presenta una breve sección sobre diagnóstico clínico y biomarcadores, seguido por ventajas de los biosensores en dicho campo, y el interés en técnicas de tipo punto de atención (POC, del inglés *point of care*). Segundo, se presentan ventajas y propiedades de nanomaterials en el campo de biosensado. Tercero, se tratan fundamentos de electroquímica y sensores ópticos basados en papel, además de ejemplos publicados.

En el **Capítulo 2** se presentan los objetivos de la tesis.

El uso de SPCE como plataforma para la detección de AuNPs mediante medidas de impedancia se presenta en el **Capítulo 3** consiguiendo una mejor detección en comparación con métodos similares publicados para la detección de AuNPs. La técnica desarrollada es aplicada satisfactoriamente en la detección de AuNPs de diferente tamaño, y en un magnetoinmunoensayo utilizando AuNPs como marca para la detección de una proteína modelo.

En el **Capítulo 4**, se presenta el trabajo relacionado con el desarrollo de nuevos sensores para la detección de DNA. El sistema está basado en la modificación de SPCEs mediante películas de un polímero y nanopartículas de óxido de iridio (IrOxNPs) sobre las cuales se inmovilizan secuencias de captura de DNA. La detección del ADN objetivo se consigue mediante medidas de impedancia eléctrica, basadas en el efecto de bloqueo del ADN hibridado para la difusión de un indicador redox a la superficie del electrodo. El biosensor resultante, que opera en modo libre de marcas (*label-free*), fue utilizado para la detección de secuencias de ADN específicas para el parásito de *Leishmania*.

En el **Capítulo 5** se presentan conclusiones generales y perspectivas futuras.

En el **Annexo A**, se presenta el trabajo relacionado con las plataformas de papel para la detección de una proteína específica, PTHLH. El sistema de detección presentado es del tipo LFIA. La técnica desarrollada supone una alternativa menos costosa, más rápida y sin el uso de marcas radioactivas. El límite de detección (LOD) conseguido está en el rango de ng mL^{-1} en muestras reales (medio de cultivo celular y lisado celulares). Además, pese a que el LOD conseguido no sea suficientemente sensible para detectar PTHLH en suero humano, se comprobó la compatibilidad del método desarrollado con suero humano utilizando suero humano con PTHLH añadido. El trabajo presentado ha sido desarrollado en colaboración con el *Hospital San Joan de Déu de Barcelona*.

En el **Annexo B**, se presenta el trabajo llevado a cabo en una estancia de investigación en el grupo del profesor K. Plaxco en la Universidad de California en Santa Barbara (UCSB). En esta sección se presenta la fabricación de sensores electroquímicos de ADN (E-DNA) y basados en aptameros (E-Ab), y la aplicación de dicha tecnología en sensores serigrafiados de oro y en SPCE modificados con AuNPs.

El **Annexo C** representa la investigación llevada a cabo como continuación de otra hecha anteriormente en nuestro grupo relacionado con el estudio de materiales para uso en plataformas de interés para crecimiento de células para aplicarlo luego en sensores. Como continuación del trabajo, las condiciones y materiales encontrados se aplicaron en la fabricación de una plataforma de nanocanales para la detección de una proteína secretada por células cultivadas directamente sobre la plataforma de sensado.

List of acronyms

Acronym	*Definition*
AAO	Anodic Aluminum Oxide
AC	Alternative current
APTMS	Amino Propyl Trimethoxy Silane
ApoE	Apolipoprotein E
AuNPs	Gold Nanoparticles
CB	Conduction Band
CE	Counter Electrode
CSN	Colloidal semiconductor nanocrystals
CV	Cyclic voltammetry
DC	Direct current
DLS	Dynamic light scattering
DNA	Deoxyribonucleic acid
DPV	Differential Pulse Voltammetry
$_{DS}$DNA	Double Strain DNA
E-AB	Electrochemical Aptamer based sensors
E-DNA	Electrochemical DNA sensor
EIS	Electrochemical Impedance Spectroscopy
Eg	Energy gap
EL	Electroluminiscence
FRET	Föster Resonance Energy Transfer
FTIC	Fluorescein Isothiocyanate
GSPE	Gold screen printed electrodes.
GOx	Glucose Oxidase
HER	Hydrogen Evolution Reaction
hGC	Human Chorionic gonadotropin
hIgG	Human Immunoglobulin
IgG	Immunoglobulin
IrOxNP	Iridium Oxide Nanoparticles
LF	Lateral Flow
LFA	Lateral Flow Assay

LFIA	Lateral Flow Immunoassay
LOD	Limit Of Detection
LSV	Linear Sweep Voltammetry
MB	Molecular Beacons
MtB	Methylene Blue
µPADs	Micropads
QD	Quantum Dots
PAA	Porous Alumina Membranes
PB	Prussian Blue
PBNPs	Prussian Blue nanoparticles
PCR	Polymerase chain reaction
PE	Photoelectorchemistry
POC	Point of Care
PSA	Prostate specific antigen
PVP	Polyvinylpyrrolidone
RE	Reference Electrode
RNA	Ribonucleic acid
SAM	Self-assembled Monolayer
SEM	Scanning electron microscopy
SHE	Standard hydrogen electrode
SPCE	Carbon Screen Printed Electrode
SPE	Screen Printed Electrodes
SPR	Surface Plasmon Resonance
$_{ss}$DNA	Single strain DNA
SV	Staircase voltammetry
SWV	Square wave voltammetry
TCEP	Tris (2-carboxyethyl)phosphine hydrochloride
TEM	Transmission electron microscopy
VB	Valence band
WE	Working electrode
WOR	Water oxidation reaction
Z	Impedance

Index

Chapter 1
Introduction

1.1 Diagnosis and biomarkers

In recent decades medical diagnosis has been greatly improved thanks to the development of new techniques capable of performing detection and quantification of specific molecules and components, the presence or absence of which, give information about the physiological state of a living being. Previously to the discovery of such techniques diagnostics was based on just observable parameters. However having solid data of presence/absence of substances or other parameters to support the diagnosis represent the possibility to perform more accurate forecasts and more robust studies of the situation of the patient. This possibility of gathering precise and solid information of the patient by measuring specific molecular components needs to be complemented by a deep knowledge of the principles related to the physiological state and the mechanism involved in the disorder or diseases. In other words, it is necessary to know which components should be measured and be able to make an interpretation of the results obtained regarding the situation of the patient. Hence, not only is interesting to develop new devices for detecting of certain molecules or components in patients, but also new sensing techniques to allow researchers to carry out studies to improve or generate knowledge around the disease or miss function.

Biomarkers can be defined as parameters which can be objectively measured or evaluated in order to get information of either a physiologic/pathologic situation or as a response to a therapeutic intervention[1]. Although biomarkers can be physically measured (ex. body temperature or thickness of a nerve fibre) most common biomarkers, the so called molecular biomarkers, are measured biochemically, for instance protein concentration in urine, or certain protein in blood[2]. Usually molecular biomarkers are molecules biologically relevant for the intra- or intercellular function, and their expression or presence is altered by a non-regular situation or activity of a living entity. In medicine, the interest of biomarkers lays on the possibility to relate an altered parameter to a certain pathologic condition, for instance: overexpression of maternal superoxide dismutase to screen potential risk of Down syndrome[3], Prostate Specific Antigen (PSA) as biomarker for prostate cancer[4], C reactive protein as inflammation and cardiovascular risk biomarker[5], etc.

Nowadays, thanks to the sophisticated equipment available in laboratories it is possible to make very sensitive detection of a wide range of molecules[1]. Techniques such as 2D gel electrophoresis[6] , mass spectroscopy [7-9] and isotope coded affinity tags[10] allow researchers to make detection of very small amounts of the biomolecules under study. Furthermore, the cited techniques are not only able to perform detection but also capable of giving valuable information about other issues and characteristics of the biomolecules under study, for instance their modification states, conformation,

or interactions with other molecules. Although the great sensitivity, the above mentioned techniques require the analyte in the proper context to perform the detection, therefore there is a need to perform some treatment of the samples prior the detection; these treatments are mainly purification and concentration processes usually done by chromatography. These extra steps represent a huge drawback for the application of the techniques in real situations, and limit enormously the possibilities to process high number of samples and its feasibility in terms of time and costs. Moreover, the experimental procedure has to be carried out by trained personnel with broad expertise in the field. All these characteristics make the cited techniques greatly important and remarkable for basic research studies. However, owing to the drawbacks cited, they do not represent an attractive possibility for routine diagnosis.

1.2 Point of care diagnosis

All the already known and described biomarkers with interests in clinics and diagnosis together with new discoveries in the field of nature sciences have raised the demand of analytical devices for detecting and measuring a wide range of analytes with interest in different fields such as food quality control, bio-security, contaminants/pollutants and specially in diagnosis. The main interest for these types of new devices lays on the reliable monitoring of parameters of interest for the proper control of either the state of goods and environmental conditions (food and drinks, drugs, air and gases, etc), the physiological conditions of living entities (bacteria, cells, organs, plants, animals, …) or drug control tests. Such close control would make more feasible early detection preventing unwanted or hazardous situations. In particular, in the field of clinics, early detection of biomarkers even prior to manifestation of any symptom of the disease is essential for the successful medical treatment and patient survival rates [11,12]. It is worth mentioning the huge interest behind the discovery of reliable biomarkers for early detection of cancer to allow the possibility of quick screening of the population sector in risk [13]. In this context the development of Point of Care (POC) testing devices has been growing in last years[14]. This type of devices is defined as 'testing at or near the site of the patient care'. [15] The main point of this type of sensing is to achieve the *in situ* and immediate patient's parameter testing in order to facilitate the evidence based diagnosis. There is a strong support among physicians towards the possibility to perform primary care either in office or from home (remote self-management) or in emergency medical services[16].

The final goal when developing a POC test is to match the ASSURED criteria: Affordable, sensitive, specific, user friendly, robust, equipment free and deliverable to those in need. Their

characteristics aim to promote bringing tests to general public. This criteria was set by The World Health Organization (WHO), which gives strong priority to the tests that fulfil the mentioned characteristics. Nevertheless, besides the ASSURED criteria, global markets are applying their own driving forces towards more sensitive and specific assays with special interest in those which operate with low volume of clinical samples, minimum user manipulation and eliminating sharps (i.e. needles)[17]. In order to move forward in the field of biosensing new devices and techniques are necessary to ensure the progress and fulfil the new demands which may arise.

Biosensors represent a group of analytical devices which can be adapted to match the characteristics requested for POC testing and ASSURED criteria. Owing to their versatility and applicability in concrete situations of detection, the field of biosensors has experienced a sensational growth[18]. Biosensors are defined as analytical devices in which the recognition system is based on biochemical or biological mechanisms[19]. Thanks to the high specificity of the biological recognition systems, biosensors are provided with a high selectivity tool for detection of the analyte. In general terms, biosensors consist in two integrated components[20]:

i. The receptor, usually a biological element such as enzymes, antibodies, DNA, microorganisms, tissues or even synthetic molecules.

ii. The transducer, part of the sensor which transforms the recognition event into a measurable signal which can be used for the quantification of the analyte.

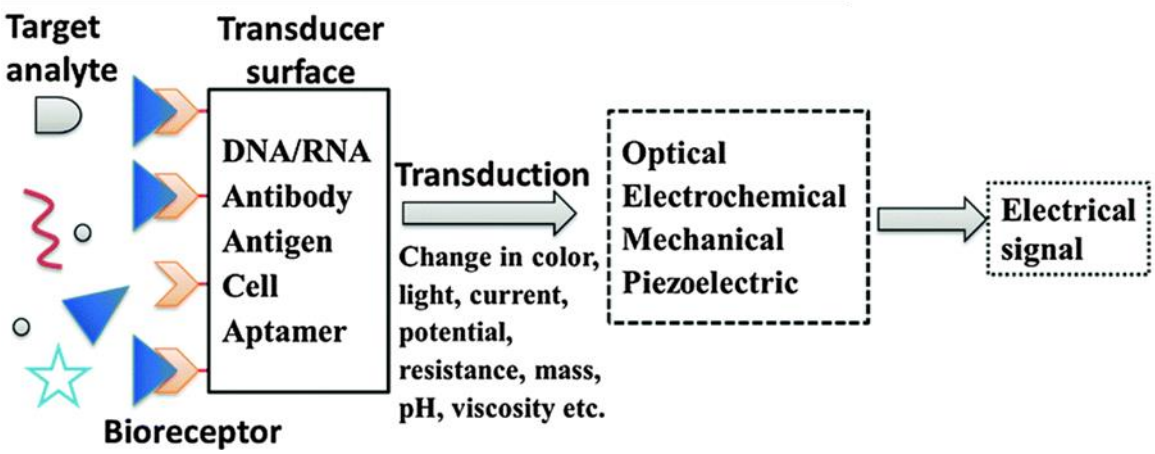

Figure 1.1: General scheme of parts of a biosensor. Obtained from reference: [20].

Biosensors can be classified according to the two components above cited: one based on the biological recognition element[21] such as proteins, enzymes, nucleic acids, whole cells, or tissue. The second main classification mode, and more popular, is based on the transduction mode; which can be optical (surface plasmon resonance, chemiluminescence, fluorescence or optical density),

electromechanical/mass (quartz crystal microbalance, surface acoustic wave, cantilievers), electrochemical (potentiometric, amperometric, conductimetric/impedimetric, ion charge/field effect).

When the recognition event takes places on the biosensor a significant change in the properties of the system is necessary so the transducer can read it and transform the perturbation into an electrical signal. In some cases signal labels are necessary in the system to achieve this readable signal. This type of sensors is referred as label-based biosensors. Usually labels are organic molecules, nanoparticles or proteins (proteins or enzymes) which can generate a fluorescent or electrochemical signal. The other alternative are the so called label-free biosensors, in which the interaction between the target and the recognition element generate a change, physical or chemical, that can be directly read by the transducer and hence used by itself to monitor the interactions in the biosensor.

As general rule label-free biosensors are the preferred possibility due to the disadvantages associated to label-based sensors: the costs of both the labels themselves and labelling the recognition elements, the additional steps in the detection procedure, the alteration of the binding properties of the recognition element due to the attachment of the label and the non-specific signal issues associated with the labelling [22,23] . Unfortunately, the main limitation of label-free assays is the lack of significant changes upon the recognition event of the target. In order to move forward in the field of label free sensing it is necessary to find new strategies in which the binding of the target can arise a significant change such as nanochannels blocking[24], telomerase activity[25], etc. Another possibility is to improve the already existing transducers to be capable of reading even smaller changes related to the target recognition (using sensitive techniques such as SPR[24] or nanomaterials such as nanowires[26] , carbon nanotubes[27] , graphene[28] , etc).

1.3 Nanomaterials

Advances in different disciplines of science and technology have provided the necessary techniques and equipment which make possible to study matter at smaller levels, allowing researcher to work at nanoscale. Thanks to this, the whole field of nanotechnology, as we know today, has been stablished. Although being an emerging discipline, nanotechnology has raised huge interest and expectations among researchers due to the possibilities of application in other fields of science and technology. Most of this enthusiasm comes from the fact that matter behaves in a different way at the nanoscale than at the macroscale, hence new possibilities and properties may emerge from macroscale materials when structured at the nanoscale. Generally, nanomaterials are considered those whose size ranges from 1 to 100nm. The main advantages they offer are related to their large surface-to-volume ratio, their physicochemical properties regarding composition, their shape, and the unusual binding characteristics [29]. In order to classify nanomaterials few groups have been stablished: nanoparticles[30], graphene[31], nanowires[32] and nanotubes[33], nanochannels and nanostructured surfaces[34].

Several reviews in the literature confirm the broad possibilities and applications of nanomaterials improving existing technologies. For instance: generating motility (nanomotors)[35], new biomaterials[36], phototherapy against cancer [37], catalysis[38], energy conversion and storage [39], and especially in the field of sensing: new labels in electrochemical[40] and optical[41] sensors, signal amplification in biosensors [42], detection directly with undiluted real samples [43], enhance pesticide detection and degradation[29], heavy metal detection [44], etc.

In the field of biosensors huge improvements thanks to nanomaterials have been achieved, being the overall aim to obtain smaller, more portable, more sensitive and more robust analytical devices.

Some more details on nanomaterials used in the work presented in this PhD thesis are shown in the following sections.

1.3.1 Nanoparticles

Nanoparticles are considered clusters of atoms or molecules of a size between 1 and 100nm. Beside single materials, alloys[46] or core-shell nanoparticles [47] are also reported. Such compositions may range from metals (gold[48] , copper[49] , silver [50], iron[51], titanium dioxide[52], etc) to carbon (carbon particles, micelles, liposomes) [48,53] or polymers (dendrimers)[54] .

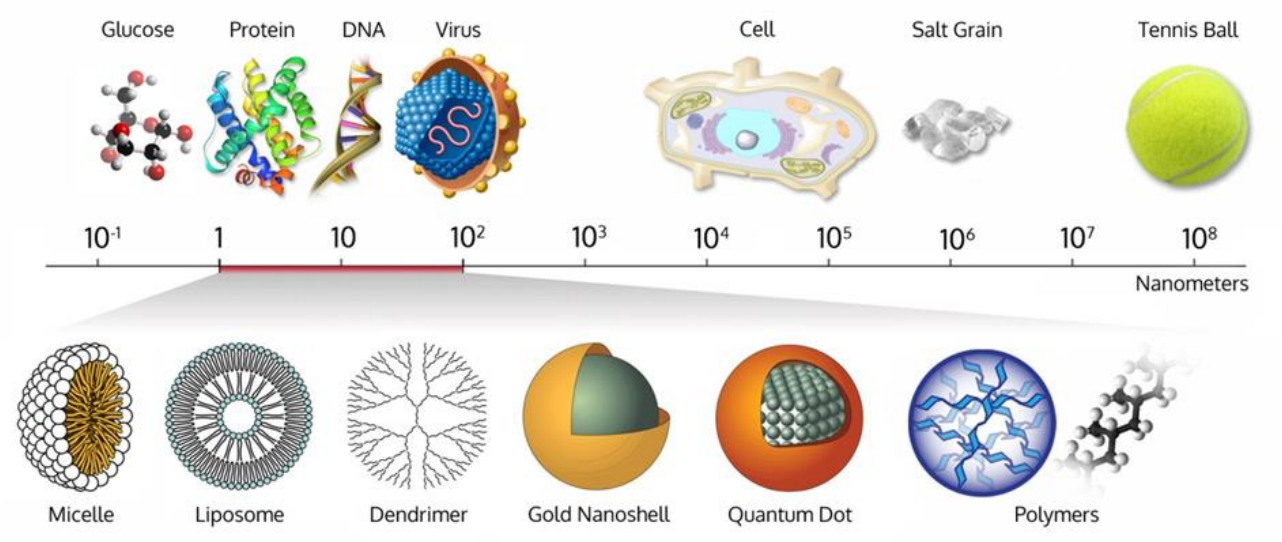

Figure 1.2: Representation of nanoparticle size in the real world. Obtained from reference[45].

Generally nanoparticles can present characteristic properties: optical, electronic, magnetic, chemical, mechanical and catalytic. Furthermore, a very interesting issue is the fact that these properties can be easily tuned by changing parameters of the nanoparticles such as: size, shape and composition[30]. In addition, more functionalities and properties can be introduced into nanoparticles by tailoring different molecules (chemical or biological) on their surface. Together with the high surface to area ratio, nanoparticles can be found in several situations, carrying out different roles: optical/electrochemical labels, catalysers, immobilization platforms, photo therapy, etc.

1.3.1.1 Optical properties of nanoparticles (plasmons)

As already stated previously in the manuscript, nanomaterials present different properties in contrast with the same materials in bulk or at the macroscale. The most obvious issue and easier to notice is the colour of nanoparticles, which thanks to the plasmons, is different from the typical colour that the material shows in bulk. Plasmons can be defined as an oscillation of the free electrons cloud with respect to the fixed position of the atoms in the lattice that conforms the material [55]. When light is incident on nanoparticles, electrons in the conduction band will show collective oscillation due to the interaction with the specific resonant wavelength. These oscillations are also called "localized surface plasmons". Depending on the size, shape, ligands on the surface and composition of the nanoparticle, the scattering would be at certain wavelengths. Thanks to this phenomena nanoparticles can scatter light at a specific wavelength range, which gives the nanoparticles their characteristic colour [56,57] .

1.3.1.2 Gold nanoparticles.

Although these have been historically known and reported, gold nanoparticles (AuNPs), initially known as gold colloids and used to make ruby glass and colouring ceramics, have experience an increase in number of publications and applications[57]. Available from 1 up to 120nm, with special optoelectronic properties, AuNPs represent a versatile tool which can be applied in different fields. Along with the biocompatibility that they show and the possibility to tailor other molecules or biomolecules on the surface, AuNPs play a key role in both nanomedicine based therapies [58] and biosensing methods [48].

1.3.1.2.1 Synthesis of gold nanoparticles

AuNPs are traditionally synthetized by the chemical reduction Au(III) in solution, usually introduced in form of a gold salt ($HAuCl_4$). Besides the gold precursor, two more components are needed for the synthesis of AuNPs, first the reductant, a molecule which will be oxidized in order to provide the electrons needed for the reduction of gold ions into metallic gold Au^0, and second a stabilizing agent which will prevent the reduced gold from aggregating. Several methods have been described in the literature and well collected in several reviews [57-59]. Being the most extended and

popular, the citrate reduction method, an approach reported by Turkevich [60] in 1951, where $HAuCl_4$ is reduced in water by the addition of sodium citrate obtaining gold nanoparticles of 20nm of diameter. In this procedure citrate acts as both reducing and stabilizing agent, therefore the resulting nanoparticles are capped with citrate. Nevertheless, several other methods for AuNPs synthesis with some modifications and improvements have been reported [57]. For instance the Brust-Schiffrin method, is based in the two phase synthesis and stabilization by thiols, where the resulting nanoparticles are thermally and air stable with a narrow size dispersion [48]. Another set of methods for AuNPs are the microemulsion-based ones, reversed micelles, surfactants and membranes based methods; as common feature these techniques share the use of a two-phase system with surfactants which form microemulsions [57]. The advantages of these techniques are the good control of the growing conditions and hence the good size distribution of the resulting AuNPs.

1.3.1.2.2 Conjugation of gold nanoparticles.

Several opportunities and potential that AuNPs offer are based on their possibility to conjugate biomolecules such as proteins and DNA[61]. Modification of the AuNPs with biomolecules allow introduction of new properties and functionalities to the gold, among which, the most interesting is the possibility to make AuNP selective to a specific ligand.

The stabilizing agents used in the synthesis of the AuNPs represent a smart possibility to introduce different functional groups onto the surface of AuNPs, on which other molecules can be anchored through covalent bond formation (for instance the covalent bond formation through the carbodiimide chemistry [62]). In parallel to the modified stabilizers, various AuNPs functionalization routes have been successfully carried out thanks to the interaction of thiols groups (S) with gold (Au) [63], where the S groups show a strong and stable interaction/chemisorption (non-covalent) with Au atoms. Very simple and easy to apply procedures are derived from this principle, in which just mixing the thiolate component with the AuNP will form the conjugate.

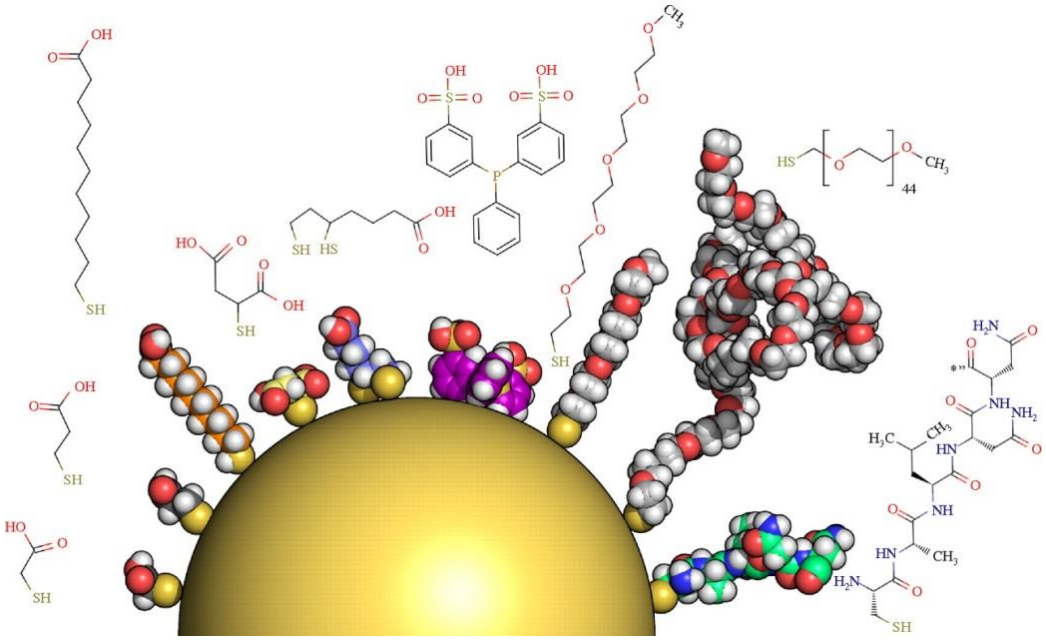

Figure 1.3: Schematic view of gold nanoparticle modified with different ligands through the thiol gold interaction. Obtained from source [64].

Another possibility is the use of electrostatic and weak attraction forces for the immobilization. This is the most popular and used approach due to the acceptable results achieved given the simplicity of the adsorption procedure[59,65]. This interaction can happen thanks to different chemical groups such as amines, carboxyls, hydroxyls, imidazoles, phosphates, etc, present in biomolecules. Since there are different types and degrees of binding interactions with Au surfaces, the resulting conjugate is the product of a complex mixture or electrostatic, hydrogen bonding, and Van der Waals interactions.

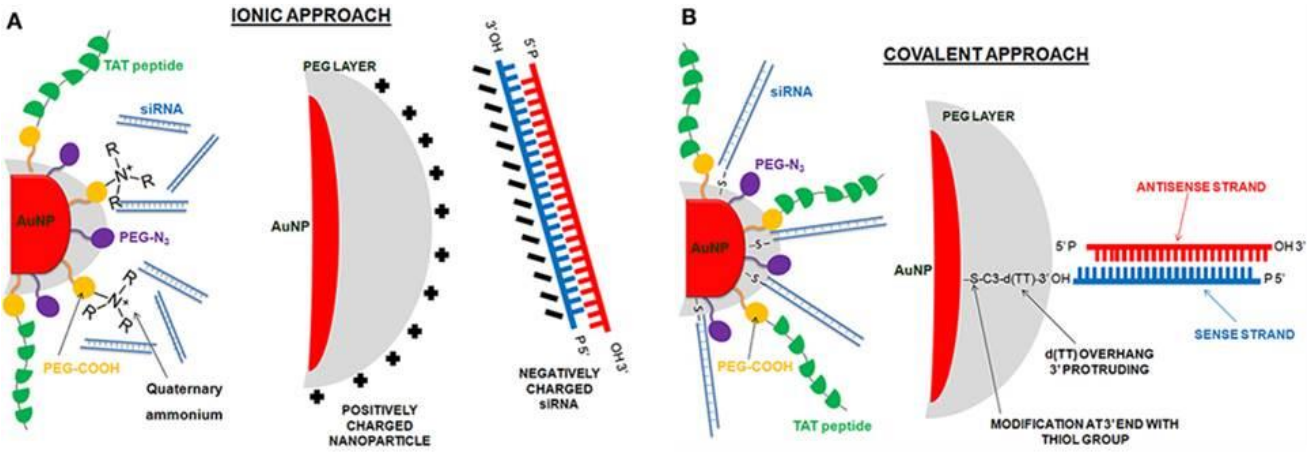

Figure 1.4: Schematic representation of examples of ionic (A) and covalent (B) approaches to immobilize small interference RNA on PEG modified gold nanoparticles. Figure extracted from reference[65].

1.3.1.2.3 Applications of nanoparticles in biosensing

Thanks to their physical and chemical attributes AuNPs represent an excellent nanomaterial to be applied in the fabrication of biological sensors. Thanks to the high surface-to-volume ratio and the good biocompatibility, they represent a proper surface for multifunctionalization with a wide range of chemical and biological ligands to adapt them in detection systems. The conductivity, redox behaviour and plasmon resonance make them good candidates as electrochemical and optical labels. Nevertheless, nanomaterials can be also used to modify transducer surfaces in order to enhance the signals improving the response of the detection system.

1.3.1.2.3.1 Applications in optical sensors

In the field of sensing through optical transducers, nanoparticles may be applied in both, fluorescence based and colorimetric assays. In the first, thanks to the photoluminescence[66] of gold nanoparticles smaller than 8nm, also called gold nanodots, can be used as fluorescent label [67]. Different assays using this kind of labels have been successfully applied to the detection of biomolecules. Hao Kong and co-workers reported the detection of proteins at the nM range using fluorescent AuNPs[68]. On the other hand AuNPs of bigger diameters have been successfully applied as quenchers in fluorescent assays[67]. Finally, both properties of AuNPs (photoluminescence and quencher) used as labels have been brought together in the same assay by Huang et al[69] where they reported the detection of pM amounts of a breast cancer marker protein, PDGFAA, where the authors used a 2nm AuNP as a fluorescent emitter and a 13nm AuNP as quencher.

However, application of gold nanoparticles in optical biosensors is mostly focused on the colorimetric sensing[48] . Thanks to the interparticle coupling of plasmons aggregation of AuNPs a visible colour change from red to blue can be induced. This possibility to induce aggregation and resuspension represents a useful platform to build biosensors easy to be triggered by a proper ligand /analyte. First report in the literature of such detection system is given by Chad Mirkin group [70] , where the authors achieved a system capable of performing detection of fmols of a oligonucleotide. Important contributions since then have been done, developing detection techniques based in similar principles[71]. The same principle has been proved to work for protein detection[72,73] , enzyme activity [74], small molecules and ions[75,76]. Furthermore, this type of detection techniques have proved

to work even in complex samples, for instance Jiang and co-workers reported the detection of glucose in rat brain[77].

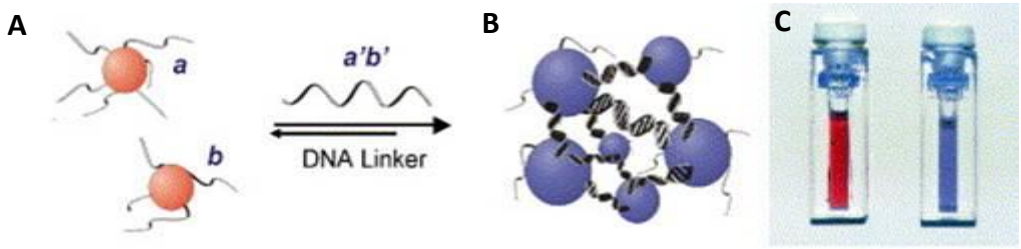

Figure 1.5: Representation of ligand induced aggregation of gold nanoparticles (AuNPs). A) Non aggregated showing the characteristic pink colour. B) Aggregated nanoparticles by the crosslinking action of ligand, and the corresponding colour turning to blue. C) Examples of the suspensions of nanoparticles before and after the aggregation. Figure adapted from ref [71].

1.3.1.2.3.2 Applications in electrochemical sensors

The excellent electro activity of gold nanoparticles together with their catalytic activity for some reactions, make them a strong candidate when evaluating labels for electrochemical detection. In electrochemical sensors AuNPs can be detected by direct or indirect electrochemical detection. In the first, AuNPs are detected by their own redox properties; therefore AuNPs can be detected without any preliminary step, which means that the metal forming the nanoparticles is electrically detected. As strong point, direct detection offers rapid responses with reasonable limit of detection (LOD), a short analysis time and the possibility to perform a compact/integrated assay. Pioneer in direct detection of AuNPs was Costa-Garcia et al.[78] . He and co-workers developed an assay for the detection of antihuman IgG achieving a LOD of 17.8nM. Important contributions in this field have been done since then. Pumera and co-workers reported a new method for the detection of AuNPs adsorbed onto the surface of graphite epoxy composite electrodes, where AuNPs were oxidized in acidic media applying a constant potential. The resulting tetracholoroaurate ions were measured by electrochemical procedure (DPV) with a LOD of $1.8 \cdot 10^{8}$ AuNP cm^{-3} . [79]

On the other hand the indirect electrochemical detection exploits the electro catalytic properties of the AuNPs. As electrocatalyst, nanoparticles take part in the catalysis and contribute to the electron transfer between the electrode and the reagents involved. However, an alternative procedure to perform indirect electrochemical detection is the preliminary oxidative dissolution of the AuNPs in acidic medium followed by the detection of the metal ions released from the particle. Both methods can be easily monitored by electrochemical means [80]. Thanks to the amplification

nature of these procedures, low limits of detection, in order of pM have been achieved. Dequaire *et al.*[81] reported the application of these techniques in the detection of human IgG at levels of 1 pM. Later, Ho Ja-an Annie and co-workers[82] reported a similar approach in which human lung cancer-associated antigen (ENO1) is detected at levels of pg mL^{-1}. A different type of assay, reported by Xiaoli Qin [83], induces the deposition of more gold on the AuNPs once the immunocomplex on the surface of the electrode has been performed (sandwich between capture antibody analyte and labelled detection antibody). Quantification of gold through anodic stripping is afterwards carried out, achieving LODs of 0.3fg/mL for human IgG and 0.1 fg mL^{-1} for human prostate specific antigen (PSA). Similar detection techniques have been previously developed in our group[84], in which silver ions are electrochemically deposited onto the surface of AuNPs in a magneto immunoassay, for the later detection of these silver ions by stripping voltammetry, achieving a LOD of fM.

1.3.1.3 Iridium oxide nanoparticles.

Despite the high cost and low abundance of iridium on earth, iridium oxide has attracted considerable attention for being capable of catalysing water splitting over a broad range of pHs [85]. Although there are other materials capable of catalysing the same water decomposition, iridium oxide presents some other advantages that makes it especially attractive: the good conductivity and capability for decreasing the electrode electrolyte interface[86], the biocompatibility and chemical and thermal stability [87,88].

$$2\,H_2O \rightarrow O_2 + 4\,H^+ + 2\,e^-$$

Figure 1.6: Chemical reaction of water splitting catalysed by iridium oxide.

Fortunately, stable nanoparticles of iridium oxide (IrOxNP) can be synthetized, making possible to take advantage of the increased surface to volume ratio, hence higher catalytic levels than the bulk material have been achieved. Furthermore, capping agents and stabilizers used in the synthesis of Iridium IrOxNP represent an opportunity to introduce functional groups or ligands onto the surface of the nanoparticles. As consequence different applications of IrOxNP can be found in the literature: from the efficient O_2 production[89,90] to its use as electrochemical label [91].

1.3.1.3.1 Synthesis of IrOxNP

Although several methods for the modification of surfaces with iridium such as electrodeposition of Iridium Oxide layers [86,92] and Iridium sputtering [93-95], have been reported relatively scarce number of publications regarding the IrOxNP synthesis can be found. Most of the described synthesis of IrOxNP are based on the chemical reduction of K_2IrCl_6 using different stabilizing agents such as citrate[96], malonate and succinate [97]. Nakagawa and co-workers[89] reported the synthesis without the use of stabilizing ligands by thermal hydrolysis of K_2IrCl_6 salt.

1.3.1.3.2 Applications of IrOxNP in biosensing

The main focus of application for IrOxNP derives from its capability to catalyse the water splitting. The water splitting or water oxidation reaction (WOR) described in Figure 1.6 is an endothermic process (1.23 eV at pH=0.0) that involves four electrons and the formation of an oxygen-oxygen bond. In nature, photosynthetic organisms catalyse water oxidation thanks to Mn complexes located in membrane proteins [98,99], as a result this organisms can perform a light-powered conversion of water into energy and oxygen[100]. No need to say that a huge interest and effort is behind the development of an artificial version of this reaction capable of splitting water into Oxygen and Hydrogen. Nakagawa and co-workers have successfully applied IrOxNP films in the efficient water oxidation for the production of Oxygen [89,90]. Although most of the interest of the related works pursues the application in clean eco-friendly energy production, still the capability to perform redox catalysis in water becomes an attractive application in other fields.

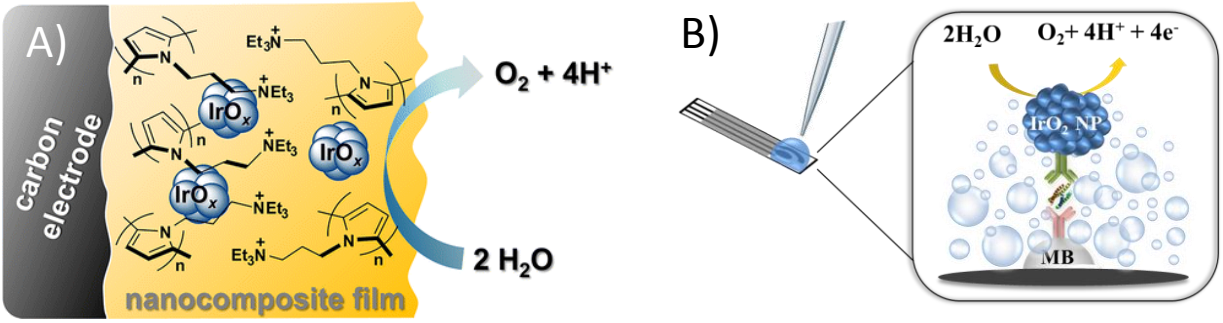

Figure 1.7: Examples of application of Iridium Oxide Nanoparticles (IrOxNP). A) IrOxNP included in composites for the water splitting reaction. B) Use of IrOxNP as labels in a magneto immunoassay for the detection of Apolipoprotein A. Figure composed with images obtained from [101] and [91], respectively.

In the specific case of biosensing, nanoparticle redox tags suffer from the need of a specific solution, usually acidic, in order to allow the catalysis related to the detection. In contrast to conventional redox labels, Iridium Oxide thanks to WOR, can generate an electrochemical signal in the presence of water, hence Iridium Oxide detection can be performed in the detection media itself. Our group has reported the application of IrOxNP as redox labels in the detection of Apolipoprotein E (ApoE) in a magnetoimmunosandwich assay [91]. Beside the catalytic properties towards the WOR, IrOXNP not only can work as immobilization platforms thanks to the carboxylic groups introduced through the stabilizing agent but also as enhancer of the electrochemical signal by decreasing the electrode electrolyte interface. Application of both properties was reported by Rivas *et al.* in the detection of ocratoxin A, through the specific recognition of aptamer immobilized through amida bond on carboxylic groups present on the IrOxNP deposited on carbon electrodes [102].

1.3.1.4 Prussian Blue nanoparticles

Prussian Blue (PB) also known as iron (II, III) hexacyanoferrates (II, III) are a colloidal form of a mixed-valence compound, composed by transition metal hexacyanoferrates. PB follows the general formula of Fe^{+3}_4 $[Fe^{+2}(CN)^-_6]_3 \cdot nH_2O$ [103]. Initially known and used as a dye in ancient times [104], strong attention has been paid to PB lately due to its interesting properties[103]: electrochromic, electrochemical, photophysical, magnetic, etc. Thanks to the electrocatalytic properties PB has been applied as artificial peroxidase in many sensing situations [105,106]. Stable disperse nanoparticles of Prussian Blue (PBNPs) have been successfully synthetized [107]. Furthermore PBNPs have been widely used thanks to their easy surface modification and size control. PB in form of nanoparticles has been used in drug clinic demonstrating its biosafety in human body[104], stability in blood and serum and cellular uptake. Moreover it has been successfully applied in MRI imaging and drug delivery [108], and its potential as new photothermal agent for cancer therapy proved [104]. Nevertheless PBNPs have also found applicability in biosensing thanks to their electrocatalytic properties and suitability in electrochemical sensors as inorganic mediator [109].

1.3.1.4.1 Prussian blue nanoparticles synthesis

It is well known that PBNPs can be chemically synthetized by mixing ferric and hexacyanoferrate ions with different oxidation states of iron. The solutions can be achieved by different combinations of iron solutions either Fe^{2+} and $[Fe(CN)_6]^{3-}$ or from Fe^{3+} and $[Fe(CN)_6]^{4-}$ or

from Fe^{3+} and $[Fe(CN)_6]^{3-}$ [110]. After mixing a dark blue colloid is observed. Miao and co-workers [111] reported a synthesis procedure by mixing $FeCl_3$ with an excess of $K_4Fe(CN)_6$ to obtain well-dispersed and stable PBNPs.

Organic polymers have been used for the preparation of PB nanoparticles. The selection of the polymer determines both the final morphology and size by controlling the growing process and the properties of the surface of the particles [112]. Kitagawa and co-workers developed a simple and smart procedure for the synthesis of PBNPs by mixing $FeCl_2$ with $K_3Fe(CN)_6$ and using Poly(vinylpyrrolidone) (PVP) as protecting polymer. The authors reported the possibility to tune the particle size –between 10 and 30 nm diameter- by changing reagents molarity ratio.

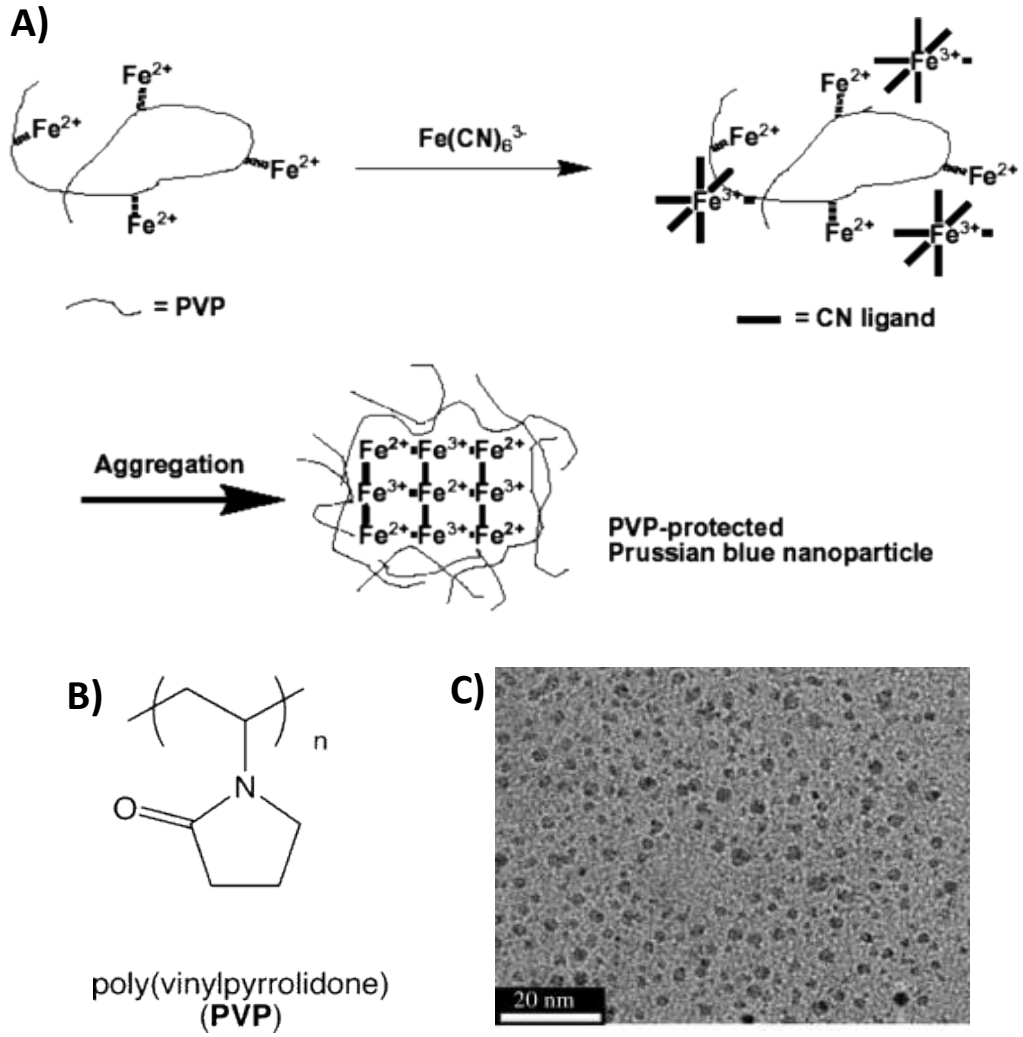

Figure 1.8: Prussian blue nanoparticles (PBNPs) synthetized with Polyvinylpyrrolidone (PVP). A) representation of the process of the PBNPs formation given by Uemura and co-workers[107]. B) Chemical structure of PVP. C) TEM Image of PBNPs reported by Castañeda and co-workers [113].

1.3.1.4.2 Prussian Blue Nanoparticles applied in biosensing.

The main application of PBNPs in biosensings, relies in the development of electrochemical sensors in which PBNPs creates a readable signal[114]. Most of applications of PBNPs are related to the catalysis of hydrogen peroxide. Ricci and collaborators reported several studies of PBNPs on carbon/based electrodes [115,116] applying them successfully in the detection of thiols [117], hydrogen peroxyde[118], acetylcholinesterase[119], or even as pH sensor [120]. Other authors have also adapted the systems for glucose detection, where the activity of glucose oxidase is monitored thanks to PBNPs immobilized with the enzyme on the surface of the electrode [121].

Recently PBNPs were applied as redox indicator in carbon/based electrochemical sensors [113], in which the presence of PBNPs on the electrode is read by Differential Pulse Voltammetry. This presence of PBNPs is modulated by the hindering effect of the analyte, allowing this way the analyte quantification[121].

1.3.1.5 Nanocrystalline semiconductors (Quantum Dots).

Colloidal semiconductor nanocrystals (CSN), which also receive the name of Quantum Dots (QD)[†] , are small crystalline particles with sizes between 1 and 100nm, dispersed in a solvent thanks to the help of a stabilizing ligand on their surface. The most particularity of CSN compared to other nanoparticles is the fact that the size and shape of CSN determine their optical and electrical properties, therefore CSN's properties can be engineered by changing the size of the crystals, without need to change the chemical composition[122]. In semiconductors, the gap energy (Eg) can be understood as the energy need required to excite an electron from the valence band (VB) to the conduction band (CB). As consequence this energy gap determines both the absorption of photons capable to excite electrons from the valence band to the conduction band (excitation wavelength) and the fluorescence emitted by the electrons which relax back to the valence band (emission wavelength). The smaller the particle is, the band structure is shifted to higher energy by the quantum confinement effect[123,124], hence the emission of an excited electron would be at lower wavelengths.

[†] Both names will be used indistinctively during the chapter.

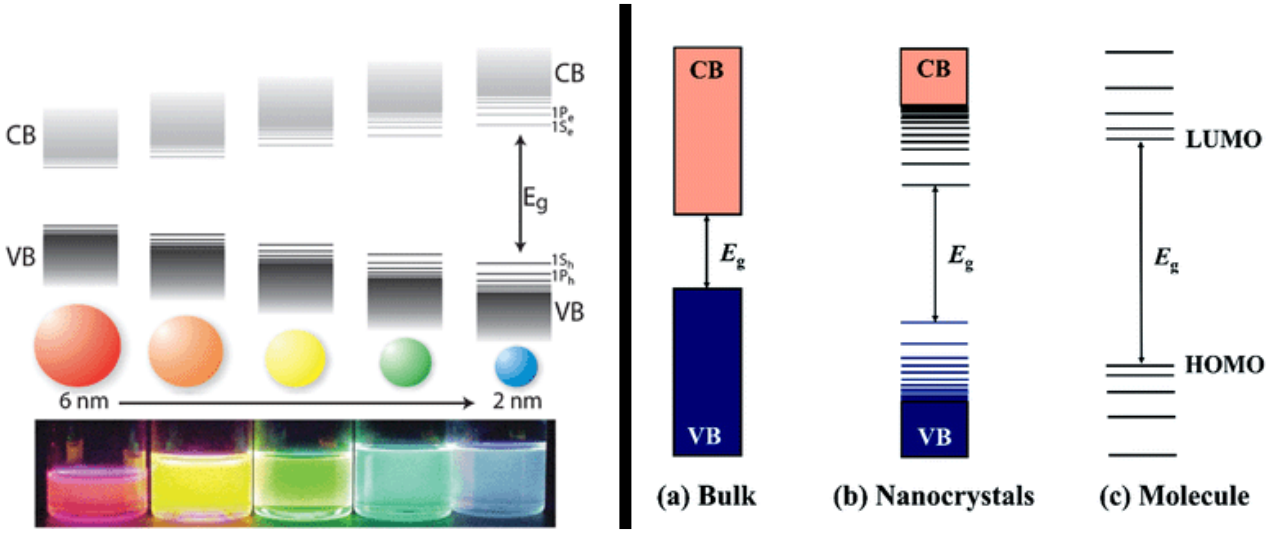

Figure 1.9: Representation of electronic energy states. Conduction bands (CB), Valence Band (VB), Energy gap (Eg) are represented. Left: Energy states of different size colloidal nanocrystals. Right: Comparison of energy states of different scale semi-conductor materials: A) bulk, b) nanocrystals and c) Molecules. Adapted from references [125] and [126] respectively.

1.3.1.5.1 Colloidal semiconductor nanocrystals composition

Despite the possibility to tune CSN properties by the particle size, chemical composition of the nanocrystals still determines the properties of the resulting quantum dots. Generally CSN are composed of an inorganic core, which contains between few hundred to thousands of atoms. Surrounding this core an outer layer of surfactant molecules acts as ligand and helps stabilization. Several materials have been successfully applied in the fabrication of CNS: CdS[66,128-130], CdSe[128] , CdTe[128,131], ZnSe[132,133] , HgTe[134], ZnSeS[135], ZnSeTe[135] , etc.

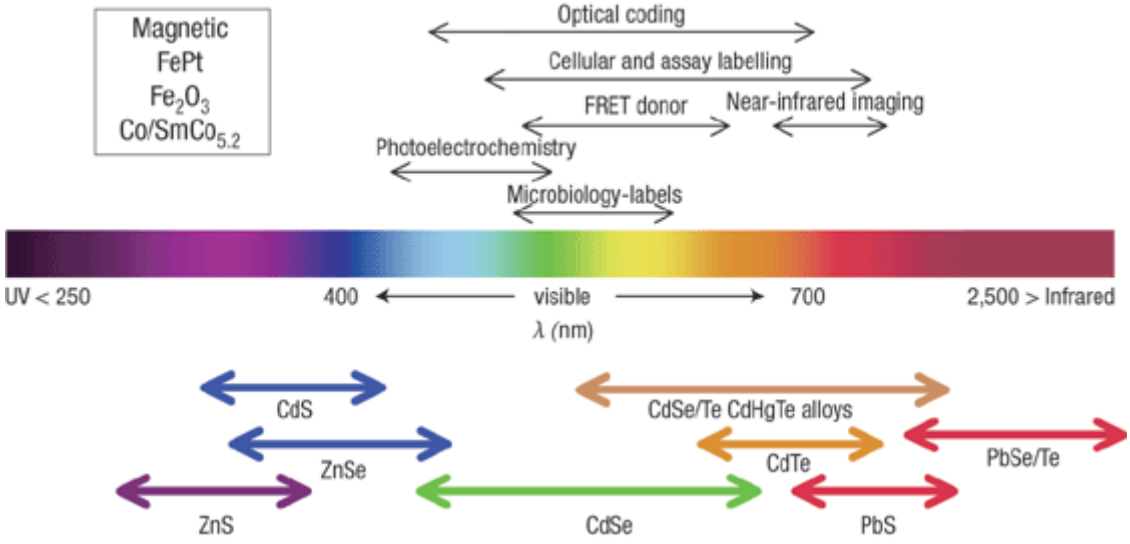

Figure 1.10: Representation of emission spectra of colloidal semiconductors nanocrystals (CSN) of different compositions. Extracted from reference [127].

However, the described type of CSN often presents surface-related trap states which can act as an alternative non fluorescent relaxation process. This represents a fast alternative to fluorescent relaxation reducing significantly the fluorescence quantum yield of the CSN [136]. Passivation of the surface of CSN plays a key role avoiding these non-desired relaxation pathways. Surfactants and organic ligands attached directly onto the surface of the CSN act as passivating agents, partially preventing the alternative channel for relaxation.

With the aim to overcome this limitation and improve the passivation of CSN, a shell of a second semiconductor is overgrown onto the surface of the first, resulting in the conformation of a core/shell systems. This new type of CSN presents an enhanced fluorescence efficiency and better stability against photo-oxidation. Furthermore the composition of core and shell means another degree of freedom in order to tune properties of the CSN [136]. As consequence core/shell structured CSN conforms a new generation of improved QD, being CdSe@ZnS (core/shell) the most applied in the field of biosensing and imaging.

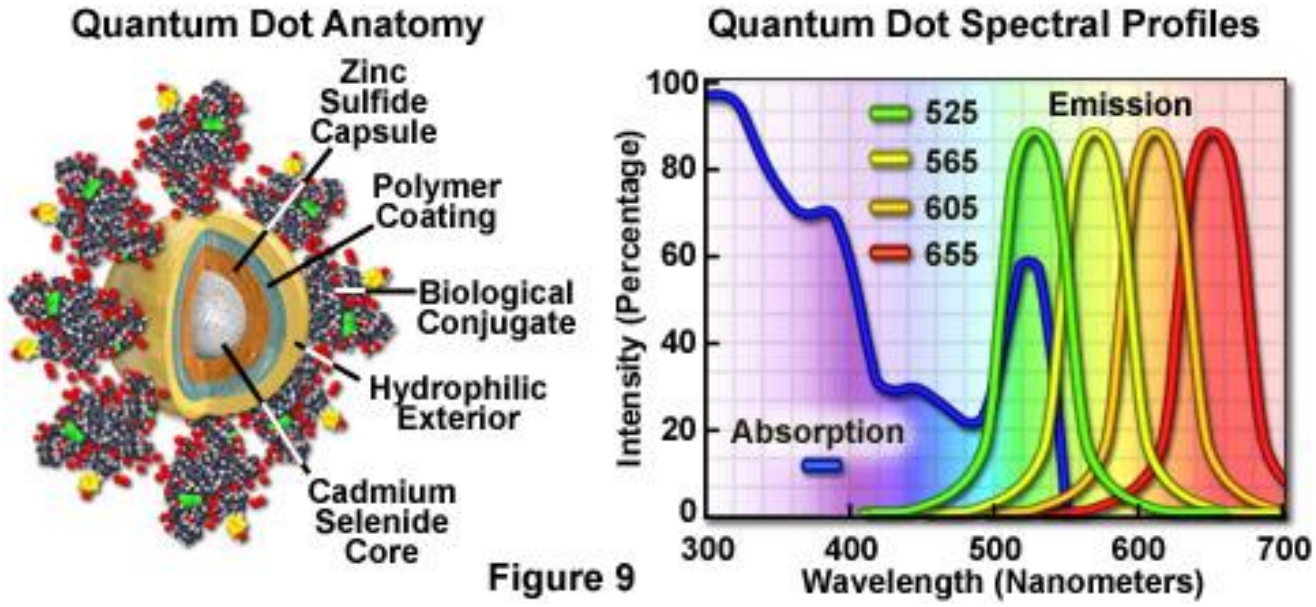

Figure 1.11: Core/shell quantum dots. Left: structure of biofunctionalized core/shell composition CdSe@ZnS quantum dot. Right: Excitation and emission spectra of different size CdSe@ZnS quantum dots. Figure extracted from Olympus web site [137].

1.3.1.5.2 Colloidal semiconductor nanocrystals synthesis

Synthesis of CSN can be achieved by different routes, like vapour-phase methods such as chemical vapour deposition, metal-organic vapour chemical deposition, molecular beam epitaxy, laser ablation, etc. Nevertheless, liquid phase synthesis thanks to the better control of the size and

shape of the resulting CSN in combination with the need of relatively simple lab ware and reagents have become the most popular and spread methods [126]. Synthesis techniques in liquid phase are composed by a first nucleation stage in the homogeneous solution followed by the growing step. Nucleation occurs in the solution thanks to the presence of organic surfactants, which also play a key role in the kinetics of the growing process [138]. The resulting reaction in combination with the appropriate precursors can be further used to coat the formed CSN with another layer of semiconducting material achieving the core/shell quantum dot [128,139,140]. CSN synthetized in organic phase allows a finer control of size, shape and crystallinity than water based synthesis. This better performance is related to the higher working temperatures allowed by high boiling point solvents[126]. However, even the not so good performance of aqueous synthesis, the fact that water is the most widespread environmentally friendly and biocompatible solvent, promotes a strong interest in finding novel and reliable synthetic routes of CSN in aqueous environments, besides the fact that water based synthesis are not restricted to inert atmosphere and can be easily scaled-up[141,142].

1.3.1.5.3 Colloidal semiconductor nanocrystals' applications in biosensing.

One important aspect in molecular biology is the understanding of interactions and localizations of different biological components either in *in vitro* or in *in vivo* situations. In order to study this, optical labels which allow the direct observation become of especial interest for researchers. CSN thanks to their optical properties can be successfully applied as labels for sensing and imaging. In fact CSN present important advantages which make them a good choice compared to traditionally used organic dyes: high quantum yield and molar extinction coefficient, broad absorption with narrow symmetric emission spectra, large effective Stokes shift, high resistance to photobleaching, high resistance to photo and chemical degradation [127].

In order to be applied in biosensing CSN need to be functionalized with the specific molecules necessary to perform the specific recognition. For such purpose, CSNs should present a coating compatible with the molecules to be anchored onto their surface. These coatings are usually polymers –Polyethylene Glycol, polysaccharides, etc- or bifunctional organic molecules, with an anchoring and a functional group at the end of the molecules [143]. Different immobilization strategies can be applied in order to perform the bioconjugation of CSN[144]. Non covalent conjugation has been successfully performed by Mattousi et al., where proteins where attached to the CSN surface by electrostatic interaction. The resulting construct worked for biosensing studies in buffer [145]. Another reported non-covalent binding is based on the modification of the biomolecules with a group which

displaces the capping ligand and binds directly to the CSN surface, being thiol groups the most extended examples [146]. Covalent bond is a strong and stable conjugation, which is possible thanks to functional groups introduced through the coating of the CSN. Thanks to this strategy it has been possible to conjugate CSN with peptides, enzymes, antibodies and DNA. Moreover, the possibility to conjugate streptavidin on CSN meant the consolidation of CSN as an entity for universal immobilization of biomolecules thanks to the widely applied immobilization through the streptavidin – biotin method[147,148]. Unfortunately, since the modification/conjugation of CSN can affect their properties it is necessary to make sure that after the functionalization first, the CSN remain stable and soluble in water, and second, fluorescence properties have not been affected.

CSN have found great applicability in cellular and tissue labelling. Thanks to their stability, resistance to photobleaching and less fading over organic dyes, CSN have been quickly embraced by scientist working in fluorescent microscopy [127]. Quantum dots have been successfully applied in labelling cells [150], tissues [151] and even live animals[152].

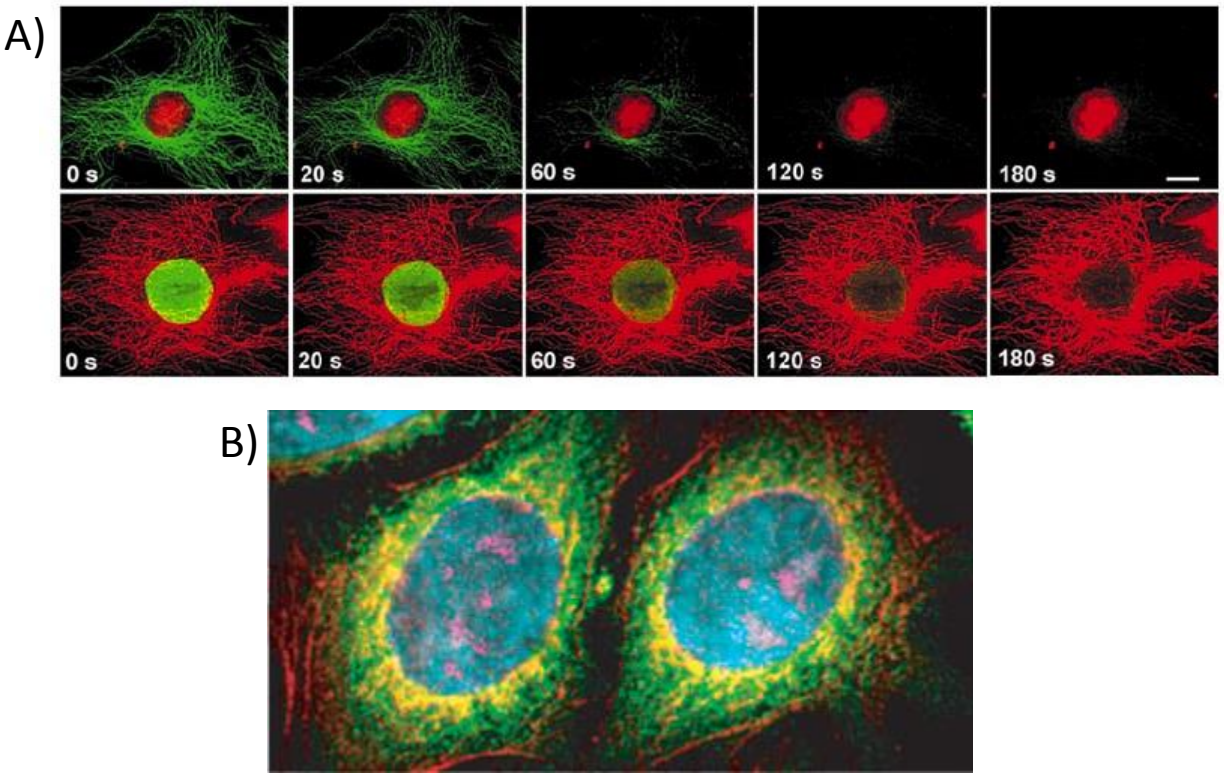

Figure 1.12: Cell culture staining with conjugated quantum dots (QD). A) Comparison of stability of QD 630 (red) *vs* Alexa 488 (green). Top row: nucleus labelled with the quantum dots 630 and microtubules labelled with Alexa 488. Bottom row: nucleus labelled with Alexa 488 and microtubules with Quantum Dots 630. B) Fixed human epithelial cells. Cyan corresponds to 655-nm QD labelling the nucleus, magenta 605-Qdots labelling Ki-67 protein, orange 525-Qdots labelling mitochondria, green 565-Qdots labelling microtubules and red 705-Qdots labelling actin filaments. Obtained from [149] and [127] respectively.

CSN have been applied to *in vitro* sensing as fluorescent and electrochemical label in multiple type of assays. Detection of ions such as Cu^{2+} [153], Hg^{2+} [154], Cd^{2+} [155], Ag^{+} [156], etc, with the use of CSN have been reported. The principle of detection is related to the quenching related to the binding of the ion onto the surface of the CSN. This binding onto the surface can either be through a specific recognition element previously attached onto the CSN or direct affinity of the ions towards the surface of the CSN [157].

Typically CSNs have been applied as substitutes of the fluorescent labels in traditional assays in regular sandwich assays: direct/indirect, competitive, etc. First example of protein detection using CSNs was reported by Chan and Nie [148], where IgG were conjugated to the CSN. Detection was based in the agglutination of modified CSN through the agglutination caused by the crosslinking between two or more quantum dots due to the analyte. CSNs have been applied in other regular types of assays such as detection on nitrocellulose membranes [159], western blott[160] , Lateral Flow [161], ELISA[162] and even flow cytometry[163] . Furthermore, CSNs have also been successfully applied as labels in fluorescence micro arrays[164], for instance Alivisatos an co-workers [165] were pioneers reporting the detection of Hepathytis B and C virus and Small Nucleotide Polymorfisms (SNP) in a microarray assay. Later several improvements have been applied in order to achieve better LOD and higher throughput [166]. In our group a quantum dot based microarray for the detection of ApoE has been developed [158].

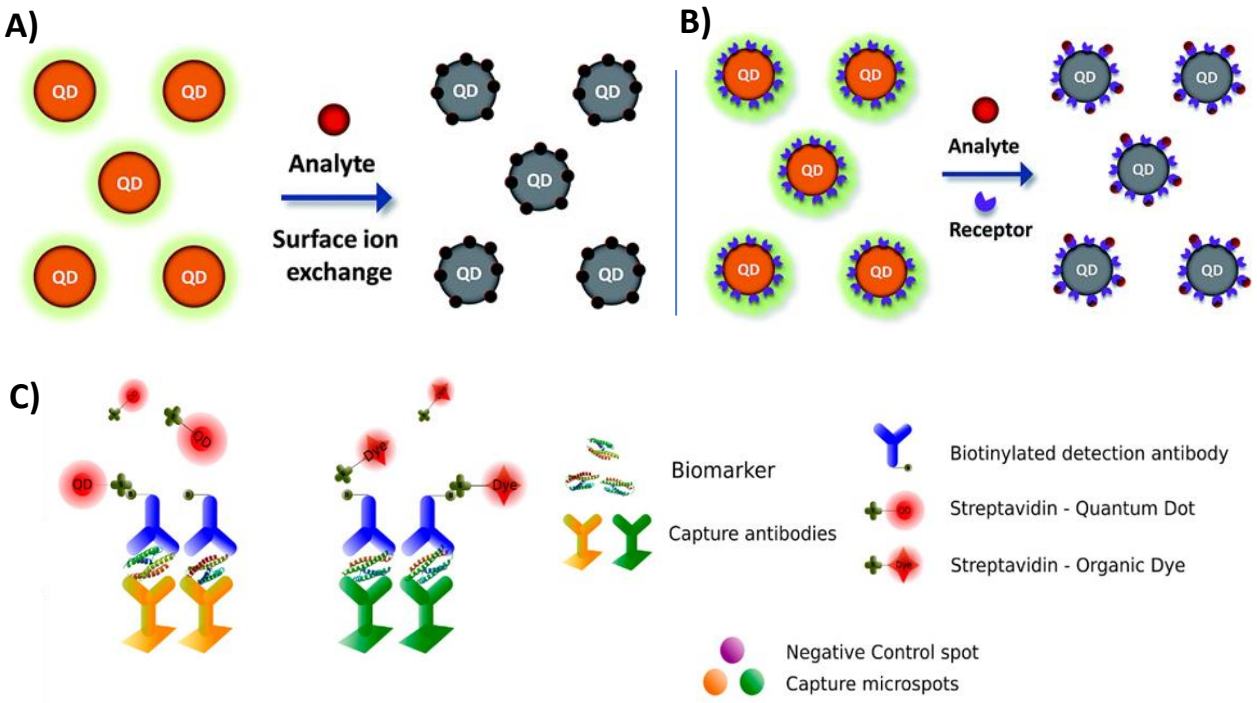

Figure 1.13: Quantum Dots (QD) in sensing assays. A) Detection of analyte by ion surface exchange, when binding events happen fluorescence of the QD is affected. B) Similar principle of detection as A), using a ligand instead of the native ion exchange on surface of the QD. Obtained from reference [158]. C) Use of QD labels compared to organic dyes in an immunosandwich assay detection. Obtained from reference [158] .

CSN can interact with certain molecules in such a way that the resulting fluorescence emission is affected; this modulation can be used with sensing and biosensing purposes. Several detection schemes can be built out of this principle (see Figure 1.13).

A highly exploded phenomena is the Föster Resonance Energy Transfer (FRET). Briefly, it is a phenomenon that takes place between two components. The acceptor is the one that reaches an excited state due to light irradiation. This goes either through its own relaxation or in case it is close to another component it can present non-radiative relaxation transferring part of the energy to the other component. The emitter reaches an excited state with the energy received from the acceptor and relaxes emitting fluorescence. As a result, when there is no interaction between the two components the acceptor would relax according to its own process. In case it can interact with the emitter, the fluorescence of the emitter would be achieved. FRET depends in the molecular disposition and is sensitive to changes of distance between the acceptor and the emitter, since the effectivity of energy transfer varies with $1/R^6$, where R is the distance between acceptor and the emitter. The systems are sensitive to changes between 1 and 10nm. At this point it becomes quite obvious that FRET has been widely applied in the study of molecular interactions, especially in the field of interactions and folding of biomolecules[167-172] . Despite the capping and passivating layers of QDs which introduce some spacer between the quencher and the QD, effective FRET can be achieved [173-175] . CSN can act as donors for other fluorescent molecules. Mattoussi et al. proved the principles using a QD as fluorescent donor and Cy3 immobilized on maltose binding protein as acceptor. Tza-Huei Wang applied the principle in a smart method for DNA detection[176], using biotinylated DNA oligonucleotides and Cy5 modified target.

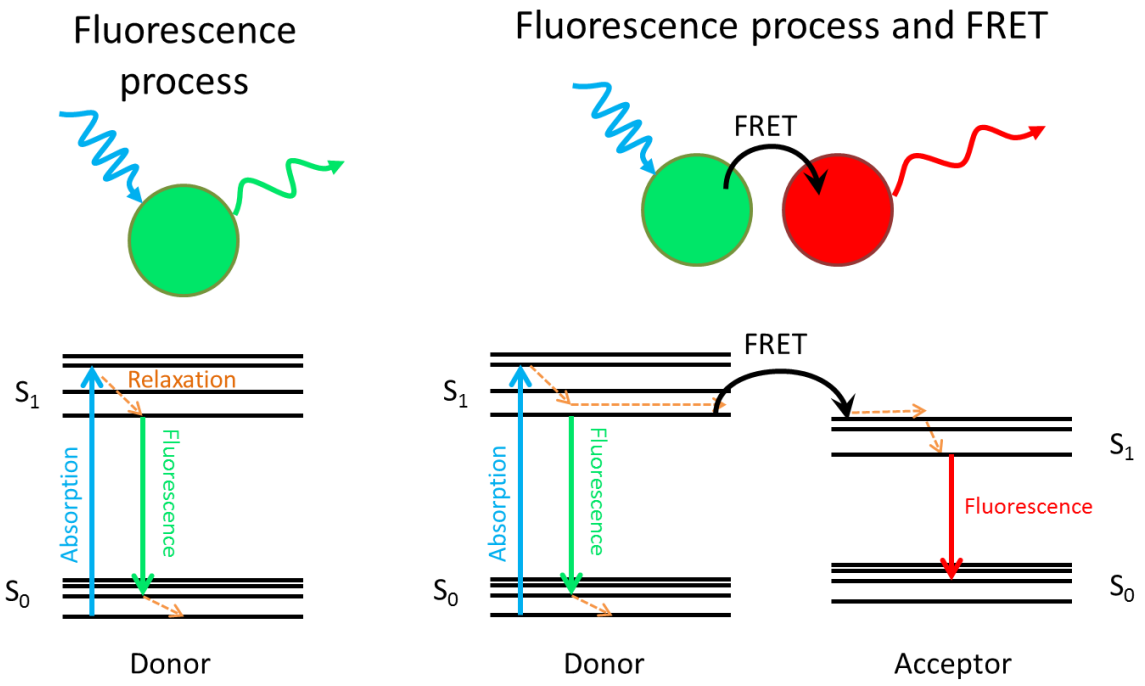

Figure 1.14: Representation of fluorescence and Föster resonance energy transfer (FRET) processes through Jablonsky diagrams. **Left:** situation of excitation and fluorescence relaxation process of a fluorophore. **Right:** Emission phenomena through FRET process, the excited donor, thanks to the proximity with the acceptor can relax through FRET and excite the acceptor which will relax through a fluorescence process emitting light at different wavelength than the emission wavelength of the donor in a regular fluorescent process.

A different scheme would be this in which the acceptor presents a non-radiative relaxation, therefore the fluorescence signal would be quenched and no fluorescence will be emitted by the acceptor. As an example Niko *et al* [177] reported an approach in which the detection antibody is labelled with a molecule that quenches the emission of the quantum dot. When the immunosandwich with the analyte is formed both QD and quencher are brought close enough to see a decrease in the emission of the QD. A different type of detection by QD quenching has been reported by our group[178], where the analyte is captured by an antibody conjugated to a quantum dot and graphene oxide is used as quencher. The presence of the analyte keeps the graphene oxide far from the QD, thus the more analyte the less quenching is observed.

Molecular beacons (MB) are short single stranded DNA sequences which contain a fluorophore on one end and a quencher on the other[179,180]. When the DNA strand interacts with its complementary sequence or the corresponding ligand the conformation change induced brings the fluorophore and the quencher to different positions altering their interaction and consequently the fluorescence signal (see Figure 1.15). After years proving its capabilities and good performance using organic fluorescent dyes[181], MB were conjugated to QD as fluorescent emitters[182].

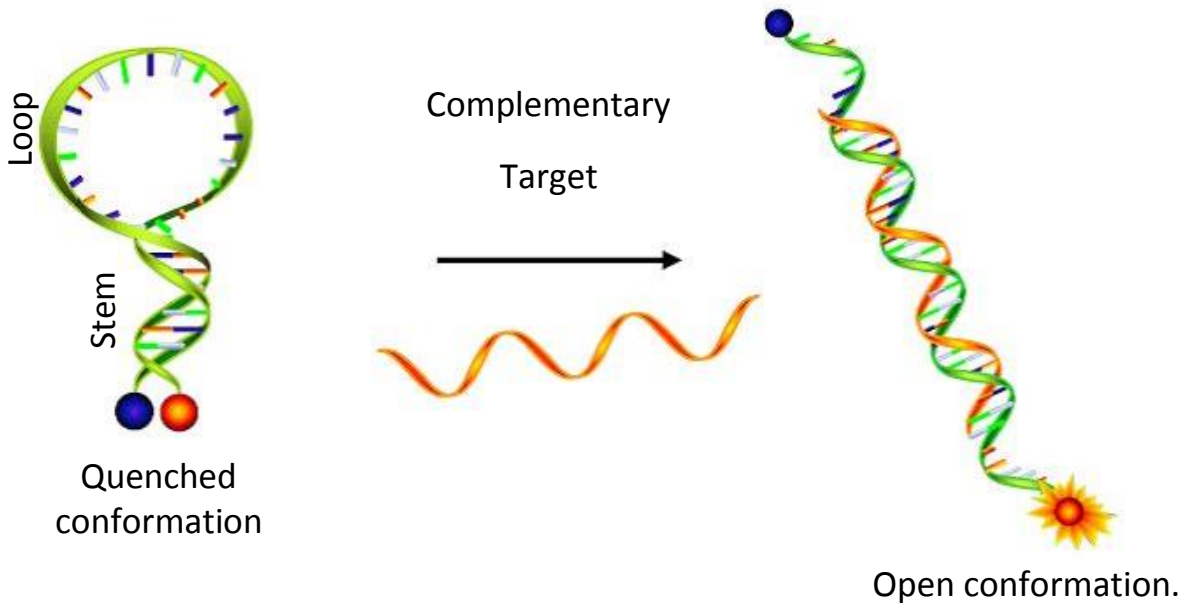

Figure 1.15: Example of working principle of molecular beacons (MB). A DNA based molecular beacon is displayed. **Left:** The stem holds the closed conformation, in which the quencher is placed close to the fluorophore and prevents the fluorescent signal emission. **Right:** interaction of the target with its complementary region (the loop sequence in the molecular beacon) open stem region opening the molecular beacon, pulling the quencher away from the fluorophore. Resulting in the opening configuration, which allows the emission of the fluorophore. Figure extracted from reference[183].

Due to the nature itself of the molecular interactions most of the MB-based approaches are performed in solution, however it is possible to find application of the described principles in different solid state platforms like plastic biochips [184], multi well plates[185] or microfluidic and lab on a chip devices[186]. Besides the application in conventional platforms such as glass, silicon or plastic, FRET based assays have been successfully applied in paper substrates [187]. Krull et al. have reported several approaches of biosensing through QD – FRET on paper substrates, performing a simple assay [188] or multiplexed detection with different QD [189]. They even proved the compatibility of the developed assay with a portable device as signal reader [190].

Although electrochemical detection of CSN has not reached such a high impact and popularity as fluorescence based assays, still represents an interesting and useful approach regarding the possibilities to be miniaturized and integrated within portable devices [192]. CSNs can be electrochemically detected by different means. Due to the charge transfer reaction they can catalyse[193] simple electrochemical procedures (cyclic voltammetry, differential pulse voltammetry, etc) [194,195] can be applied. Other possibilities are based in dissolving of the CSN and stripping voltammetry of the released metal ions[196] . Both possibilities make CSN suitable candidates for use as electrochemical labels. In our group, detection of ApoE by dissolving of quantum dots followed by in chip integrated electrochemical stripping was reported by Medina, M. *et al* [191].

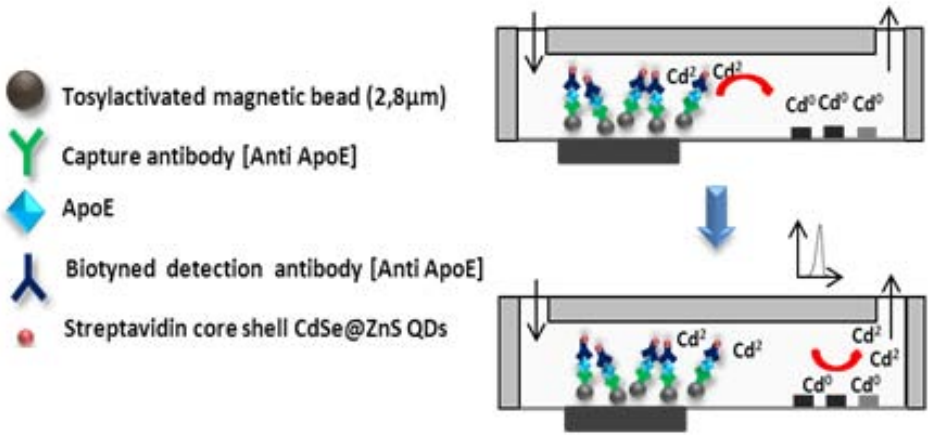

Figure 1.16: On chip electrochemical detection of ApoE using CdSe@ZnS quantum dots (QDs). Adapted from reference [191].

CSNs have also proved their feasibility to be used in electroluminescence (EL) and photoelectrochemistry (PE)[197]. EL is the process of light emission triggered by electrochemical excitation of the CSN , while PE is the electrical signal generation thanks to the light interaction with the CSN [198]. Combination of optics and electrochemistry brings unique advantages such as rapidity, high sensitivity. Moreover, as analytical technique they do not require an external light source, therefore limitations regarding scattered light and luminescent impurities are avoided, achieving a low optical background and noise[199]. After Bard and co-workers reported the EL phenomena with Silicon CSN [200], several applications in sensing have been reported: for instance Ju and co-workers developed a hydrogen peroxide sensor based in a paraffin impregnated graphite electrode modified with CdSe QD [201]. Jinghong and co-workers[201] reported label free DNA detection based on the photoluminescence signal change due to the hybridization of the target with the capture probe immobilized onto the surface of titanium dioxide electrodes. Similar approach was developed by Cosnier and co-workers for the detection of anticholera-toxin antibody [202].

1.3.2 Nanochannels

Nanochannels and nanopores have emerged as systems inspired by ion channels and pores already found in cell membranes [203]. Different authors have coincided setting the definition and differences between nanopores and nanochannels[24,204]; According to these authors, when the pore depth is much larger than the diameter the resulting structure will be considered nanochannel. Pores with diameters within 1 and 100nm are considered nanopores, as long as the pore diameter is larger than the depth.

These pore and channel elements found in nature act as "smart gates" in charge of transport of specific molecules across biological membranes. This transport mechanism across barriers allows the cell to control a steady state situation and the presence of certain molecules inside and outside of the cell. This principle of transport control caught easily the attention of researchers and its applicability to sensing was rapidly accepted [205]. The fundamental sensing using nanochannels is based on the concept of Coulter counter [206,207]: a device consisting in two chambers filled with electrolytes and connected with one or more microchannels. When a microscopic particle enters through a μchannel, a change in the electrical conductance would be recorded as electric current pulse. This electric pulse can be correlated with the nature and properties of the particle. This approach for detection of particles at the microscale was the pioneer of later works adapted to perform detection at the nanoscale using pores and channels with nanometric sizes. Initially most of the works were driven by the development of sensors for ions and DNA detection. There is a especial interest of developing nanochannel based sensors for DNA detection, this is related to the possibility to perform direct DNA sequencing while the DNA strain is travelling in a linear conformation through the pore/channel through [208].

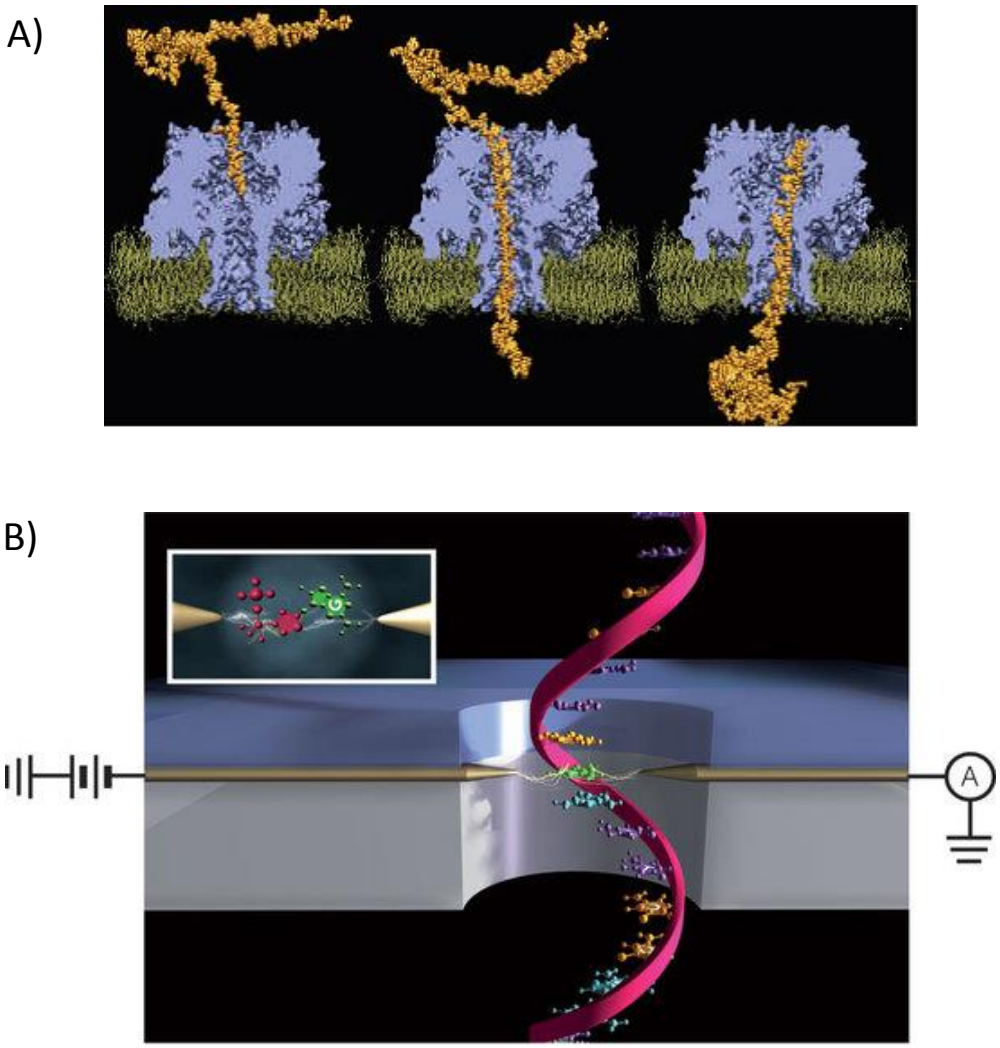

Figure 1.17: Example nanochannels. A) Snapshots of DNA being transported through a nanopore protein transporter. B) Example of single strain DNA flowing through a solid state nanopore in a sequencing approach. Obtained from reference [205] and [208] respectively.

Biological nanopores and nanochannels found in nature are not only made by organic materials but also embedded in lipid bilayers, becoming especially susceptible to deterioration when subjected to certain harsh conditions such as pH, temperature, mechanical stress, etc[209]. Much effort has been applied with the aim to create stable and robust solid-state nanopores/nanochannels, for the application in sensing [210]. With this aim several nanopore based sensors have been developed, for example Wanunu and co-workers[211] reported the detection of microRNA using a nanopore based device, where the pore has been performed in a free-standing SiN membrane in a silicon chip as frame. Meller and his team achieved the detection of DNA through a similar suspended SiN structure with a nanopore[212]. Another similar approach was reported by Branton *et al.* [213] where pores were done by ion beam and the size of the pores tuned afterwards by

alumina atomic layer deposition. Several more examples of this type of detection can be found in the literature. However fabrication of single pore device for analysis is limited by the real applicability. Fabrication procedures of a single device require long and tedious clean room procedures, with several time consuming and expensive steps. Furthermore the signals that can be achieved with such small devices require very specific and sophisticated instrumentation. In order to overcome these drawbacks nanochannels arrays emerged as a solution. First, the array global result can be understood as the parallel and simultaneous behaviour of all the single channels [214], hence the small signal coming from a single channel is magnified as the sum of all channels in the array generating a larger signal easier and more feasible to read. Second, the device fabrication of a bigger area with an array of channels represents an easier and more feasible alternative that can be performed through conventional chemistry procedures in contrast with the equipment and facilities necessary for single pore/channel fabrication[214].

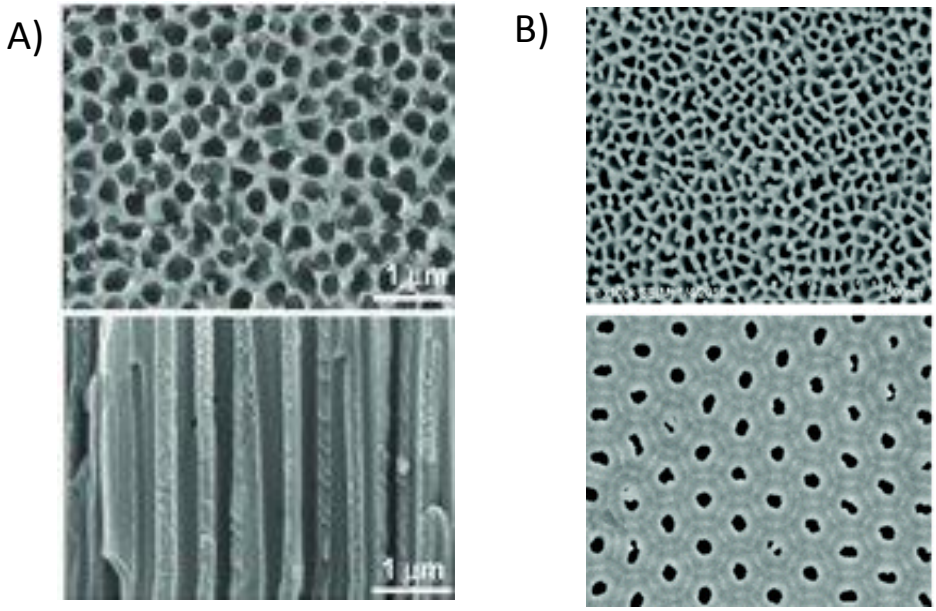

Figure 1.18: SEM images with examples of nanochannel arrays in porous alumina membranes (PAA). A) Top view and cross view of 200 nm commercial, whatmann PAA. Extracted from reference [215]. B) Above: top view of 20 nm whatman PAA. Below: homemade 40 nm pore PAA. Obtained from reference [216].

In our group several works related to the use of nanochannel arrays in biosensing have been carried out [24,203]. These works are based on the use of commercially available membranes: Porous alumina membranes (PAA). In Figure 1.18 SEM images of this type of commercial and homemade

membranes are shown, the whole membranes are disks of 1.2 cm diameter which contains the array of nanochannels that cross them vertically.

1.3.2.1 Solid state nanochannels array fabrication and functionalization

Different methods for the preparation of solid-state nanochannels have been reported: anodization[217], ion sputtering[218], quantum lithography[219], microchannel compression[220], electron-beam lithography[221], µcontact printing[222] and micromolding[223] , water assisted self-assembly[224] , nanoimprintlithography[225] , and ordered mesoporous thin films formation[226].

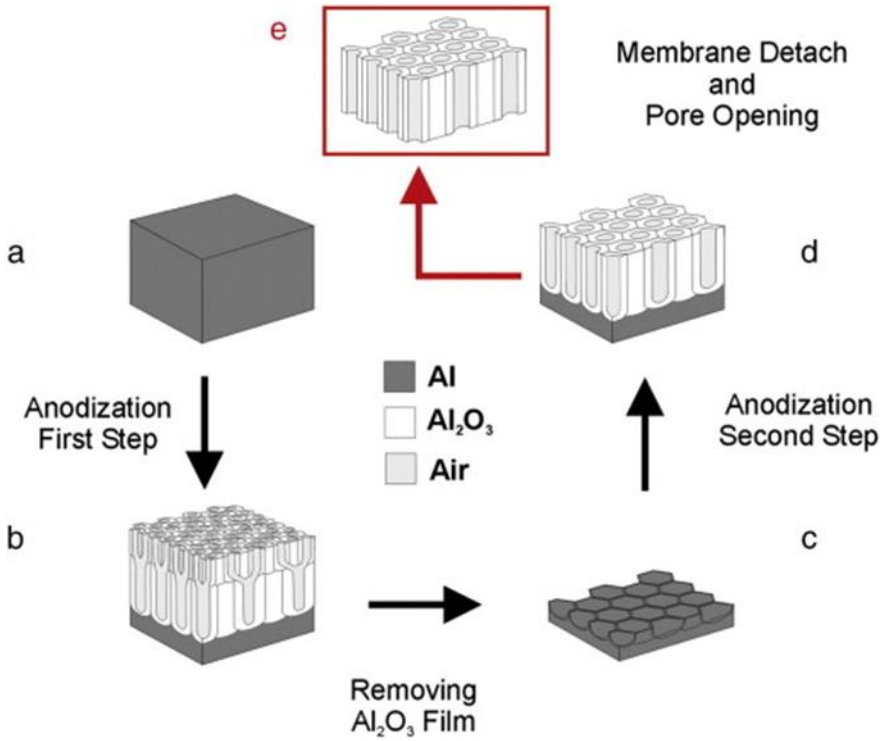

Figure 1.19: Scheme of nanochannel membrane array fabrication through aluminum anodization. A) Annealed and electropolished aluminium substrate. B) Nanoporous anodic aluminium with a protective layer under the ordered pores. c) Patterned Aluminum substrate after removing the oxide film. D) Nanoporous anodic aluminium membrane with straight and closed pores. E) Nanoporous anodic aluminium membrane with straight and open pores after performing the membrane detach and the pore opening at the same time. Obtained from reference [227].

As previously stated, nanochannels used in the works presented in this thesis are the commercially available PAA. These membranes are composed of anodic aluminium oxide (AAO), a rigid membrane of a dense porous material, which is chemically and thermally stable. The most interesting issue of AAO are the perfectly ordered and size controlled nanopores they present[228]. The fabrication process is based in the easy and inexpensive electrochemical anodization. It becomes

an interesting process thanks to its wide accessibility, capability of top-bottom fabrication with nanoscale precision and possibility to perform high aspect ratio structures[227].

The structure of AAO can be described as a close-packed hexagonal parallel cell array, where each cell contains the cylindrical nanochannel perpendicular to the surface. The resulting membrane is an AAO rich in hydroxyl groups which makes it suitable to be modified with organic molecules. This possibility gives the chance to incorporate binding ligands to the AAO membranes. These ligands play a crucial role in the recognition of other molecules necessary for sensing purposes.

One of the most common surface modifications is the wet chemical approach, in which organolakoxysilane molecules capable to covalently attach to the oxide groups of the AAO are used to introduce the amino or carboxylic groups necessary for the subsequent biomolecule immobilization. Since the most interesting aspect of membrane modification is the incorporation of ligands or recognition elements inside the nanochannels, the chemical modification mainly refers to the chemical reactions on the inner wall of the nanochannels with molecules in the solution. Figure 1.20 shows a schematic representation the reaction mechanism of the PAA bioconjugation and confocal images indicate the efficient immobilization of FTIC labelled antibodies inside AAO channels.

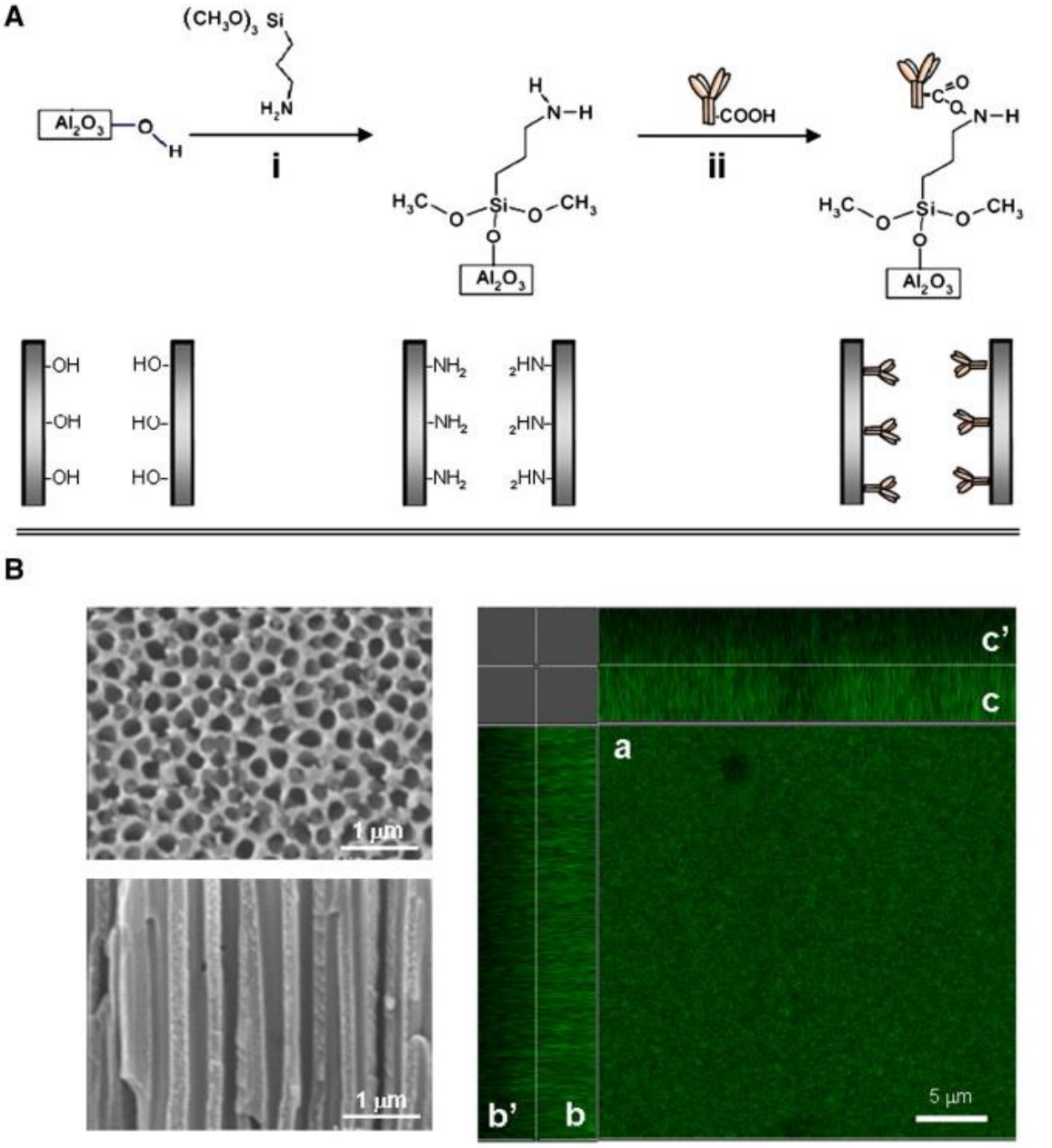

Figure 1.20: Porous aluminium membrane (PAA) biofunctionalization. A) Scheme of chemical bonds formation through wet chemistry inside the nanochannels. "i)" modification of OH- groups with Amino propyl trimethoxy silane (APTMS) to introduce amino groups on the surface. "ii)" use of $-NH_3^+$ and $-COO^-$ coupling for the amide bond formation achieving the immobilization of the biomolecules containing –COOH on the PAA surface. B) Left: SEM images of PAA, top and cross view. Right: Optical confocal microscope of an antibody labelled with a fluorescent dye (FTIC), immobilized on PAAs with nanochannels of 200 nm of diameter. Where "a" is the plain view, "b" and "c" the view in depth from the top surface and "b' " and "c' " the view in depth from the bottom surface. Figure extracted from reference [229].

1.3.2.2 Principles of solid state nanochannel arrays for biosensing

The simplest and most straightforward application of solid-state nanochannels arrays in sensing is their integration / coupling with conventional electrotransducer surfaces such as screen printed carbon electrodes (SPCEs). The parameter measured is the electrochemical response generated by electroactive species (redox indicators) that are able to diffuse through the channel and reach the transducer (SPCE) surface. When analyte is captured by the ligands immobilized on the walls of the nanochannels, the assembly formed prevents the electroactive species from reaching the transducer surface, thus decreasing the electrochemical signal read by the sensor. An important issue to take into account is the fact that the achievable signal change is related to the blocking capabilities of the analyte once captured by the ligand immobilized on the nanochannel array. The more bulky the analyte is, or more electrostatic repulsion with the electroactive indicator has, the more sensitive the system will be.

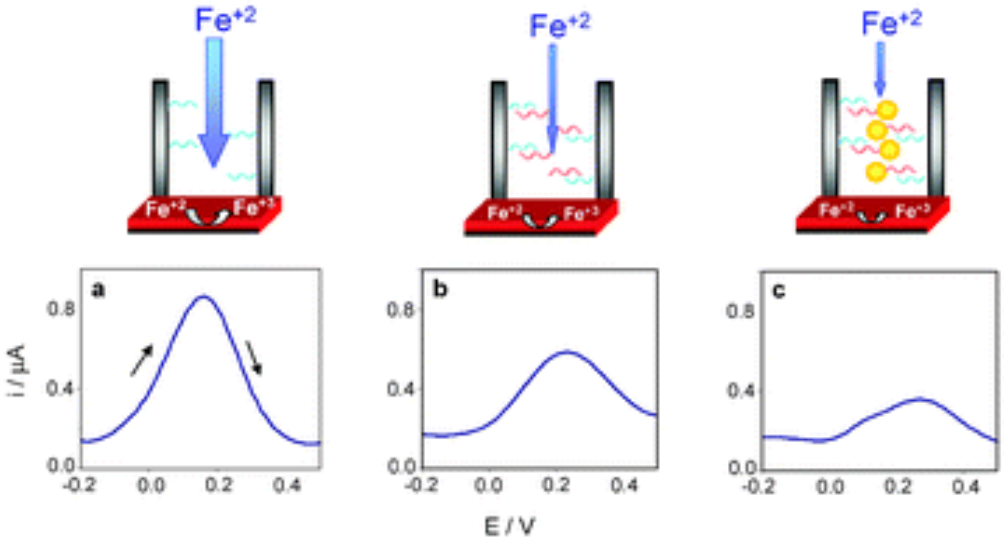

Figure 1.21: Principle of electrochemical detection using anodic aluminium oxide (AAO) nanochannel array membranes. $[Fe(CN)_6]^{4-}$, the redox indicator, is oxidized to $[Fe(CN)_6]^{3-}$ by Differential Pulse Voltammetry (DPV). (Top) Scheme of the sensing principle for a non-specific assay (left) and for a specific assay with unlabeled (middle) and 20 nm AuNPs labeled (right) target ssDNA. (Bottom) The corresponding differential pulse voltammograms (DPVs) for non-specific target ssDNA (a) and for unlabeled (b) and 20 nm AuNPs labeled specific target ssDNA (c). Obtained from [203].

An example of universal electrochemical indicator widely used in electrochemistry is $[Fe(CN)_6]^{4-}$, which can be oxidized to $[Fe(CN)_6]^{3-}$ and this signal read by differential pulse voltammetry (DPV). The oxidation or reduction peak at the corresponding potential is selected as analytical signal [203,229]. In the described nanochannel sensing approach maximum signal is achieved

in absence of ligands and analyte. When the detection is performed in the nanochannels, the blockage of the pores occurs causing smaller DPV signals [203]. Figure 1.21 illustrates the detection phenomena.

Nevertheless, the indicator properties are tightly related with the signal achieved with the detection system. For instance for the specific case of a small and mobile molecule used as indicator, such as $[Fe(CN)_6]^{4-}$, the final performance of the sensor is partially limited owing to the fact that the indicator would easily diffuse around the detection assembly –ligand and analyte- and along the channel to reach the electrode surface. The use of bigger and not so diffusive indicators can enhance the performance of the detection system. In our group, Espinosa-Castañeda *et al.*[113] used Prussian blue nanoparticles as indicators (as substitutes of $[Fe(CN)_6]^{4-}$) enhancing the detection possibilities of a protein analyte.

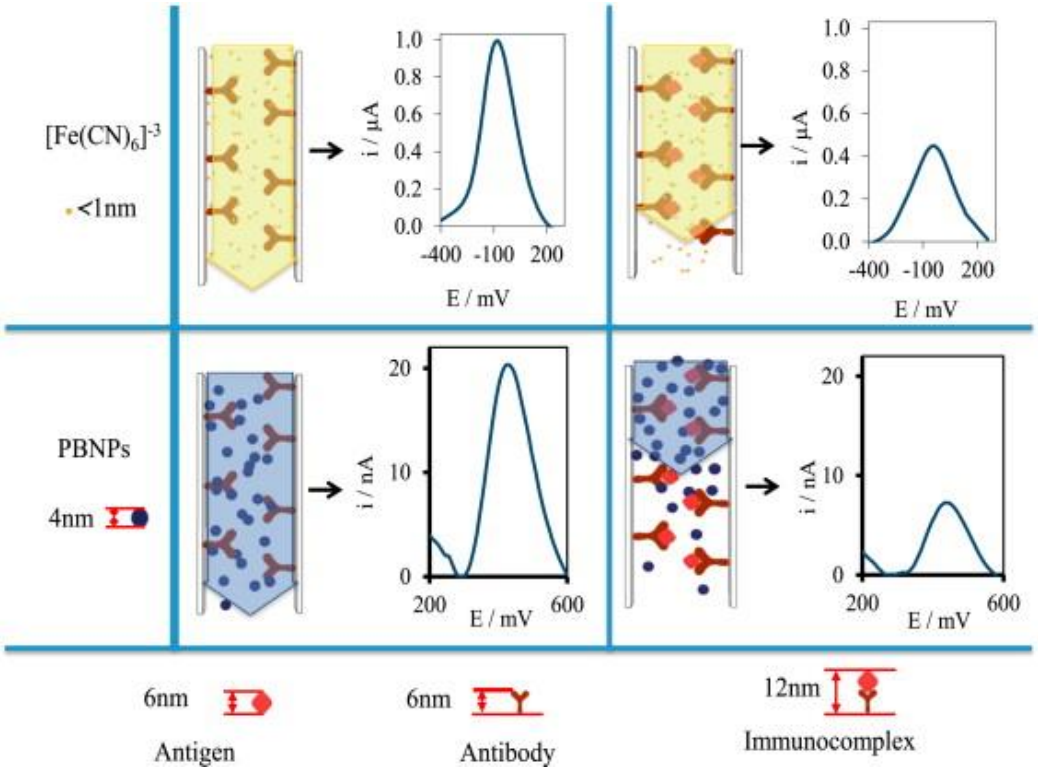

Figure 1.22: Electrochemical indicator Ferrocyanide vs Prussian Blue Nanoparticles (PBNPs). Schematic representation of the effect of the immunocomplex formation towards the voltammetric signal using $[Fe(CN)_6]^{-3}$ (top) and PBNPs (bottom) as redox indicator. DPV signals correspond to blank samples (left) and samples containing the antigen: hIgG (right) [113].

In some cases, direct contact of certain molecule or components in the sample may interfere or foul the sensing surface disrupting the measurement; solid-state nanochannels arrays offer the possibility to be used as barrier protecting the electrode being reported as filtering platform avoiding interference caused by red blood cells [215].

1.3.2.3 Examples of nanochannel arrays based biosensors

Several approaches of successful detection of biomolecules using the described solid-state nanochannel arrays through electrochemical reading have been reported. For instance detection of human IgG in the μg mL^{-1} range, using 200 nm and 20 nm pore PAA, and $[Fe(CN)_6]^{4-}$ oxidation as analytical signal [229]. Another successful application found in the literature is the detection of CA15-3, a breast cancer biomarker spiked in whole blood[215]. The system proved its capability to detect 52 UmL^{-1}.

Since the detection principle is based in the nanochannel blocking, sensitivity can be improved thanks to tags and modifications which enhance the blocking; de la Escosura-Muñiz *et al.* reported the use of AuNPs modified oligonucleotides to enhance the signal of short DNA sequences detection [203]. Same authors reported a sandwich format assay for the detection of thrombin using a DNA aptamer as capture and a AuNP modified antibody as labelled recognition, proving the possibility to use labelled antibodies as amplification[230]. Espinosa-Castañeda and co-workers reported the detection of ng mL^{-1} of parathyroid like hormone (PTHLH) using 20 nm pore PAA and PBNPs as indicator[113].

1.4 Nanomaterial-based Electrochemical Biosensors

Nanomaterials in electrochemical biosensors can be incorporated as modifiers of the transducer's surface offering advantages for signal enhancement. Modification can be usually classified in few different ways: a) Binding with functional groups on the surface of the electrode (either the very surface or groups introduced through SAM). b) By direct deposition onto the electrode surface. c) Addition of the nanomaterials in a composite form. d) Growing the materials directly onto the electrode.

Regarding the use of nanoparticles to modify the transducer surface several works have been reported; Gouzhen Liu *et al* reported the covalent anchoring of AuNPs onto the electrode surface for the detection of Cd^{2+} ions, with a limit of detection of 0.1nM [231]. Ding et al. [232] reported the electrodeposition of AuNPs to an ionic liquid carbon paste electrode for detection of α-fetoprotein at clinical relevant levels 0.25 ng mL^{-1} . Use of a nontoxic conductive composite containing AuNPs on a glassy carbon electrode was reported by Chen *et al* [233]. The developed technique was applied to the detection of human chorionic gonadotrophin (hGC) with a LOD 40 times lower than the minimum necessary for reliable pregnancy diagnostic. Finally, several examples of direct growing of the nanomaterial onto the electrode surface can be found in the literature. Cunningham and co-workers electroplated gold on a carbon electrode, creating AuNPs on the surface, this AuNPs worked as immobilization platform to anchor aptamers specific for thrombin, achieving a LOD of 30 nM.

Among the various electrodes used in electrochemical biosensors, screen-printed ones are gaining priority given their simplicity and cost efficiency. These are the one used in this PhD thesis and some further details on their fabrication are given in the next section.

1.4.1.1.1 Screen printed electrodes

The screen printing microfabrication technology is commonly used for large-scale production of inexpensive and yet highly reproducible electrochemical sensors[234]. Thanks to the low costs this type of electrodes, screen printed electrodes (SPE) made possible the development of "on shot" [235-237] sensors such as glucose sensors. Usually in line with the low cost fabrication the most interesting material to fabricate SPE is carbon, therefore most popular carbon screen printed electrodes (SPCE) are the most reported.

Basic principle in the SPE fabrication is the deposition of the printable material onto a planar substrate through a patterned stencil or mask. The inks are forced to flow across the open regions in the mask (the patterns) by applying pressure with squeegees or blades (see Figure 1.23). The result of the process is the substrate modified with the patterns transferred by the mask. After the printing process, the resulting electrodes have to be cured at temperatures usually around 90 – 100 Celsius degrees. Once the baking process is finished, subsequent layers can be printed on top of the previous one. This allows to make fabrication of all the components of the electrode in the same device, resulting a sensor with the three electrodes: working (WE), counter (CE) and reference (RE) integrated in a small area, as shown in the inset in Figure 1.23, capable of performing measurements in small volumes (few µL liquid sample), without the need of an electrochemical cell where all the electrodes have to be immersed.

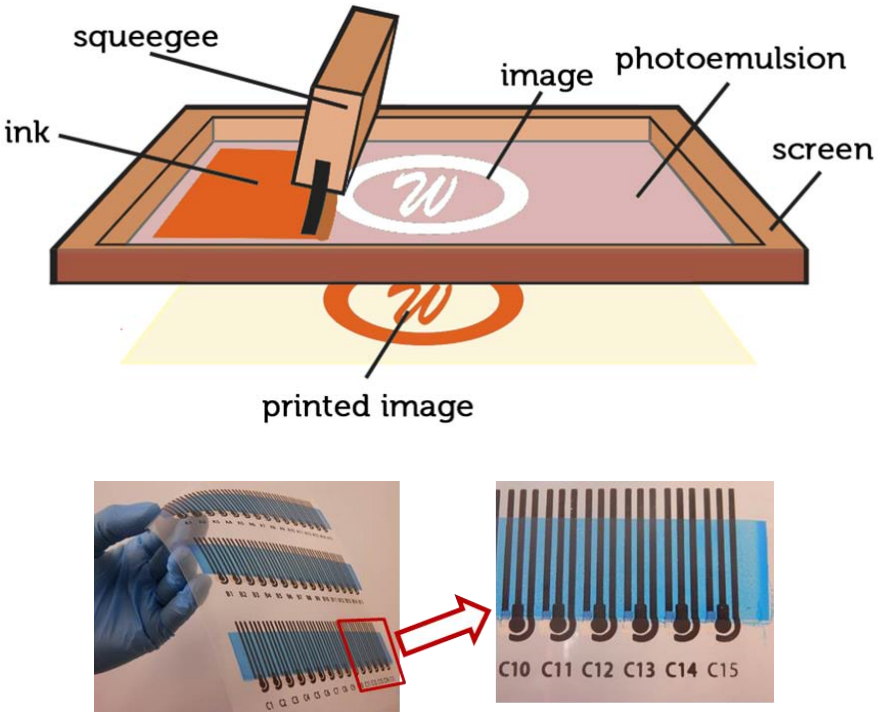

Figure 1.23: Screen-printing technology and examples of screen printed electrodes. Top: Schematic view of the fabrication of screen printed electrodes (SPE). Image obtained from reference[238]. Bottom: examples of carbon screen printed electrodes (SPCE) fabricated in the group. Electrodes are composed by three layers, carbon layer (black), pseudoreference electrode Ag/AgCl (silver colour) and isolating layer (blue).

1.4.2 Electrochemical detection techniques

Main classification distinguishing types of electrochemical techniques is based on the application of electrical charge in the system, which can be direct current (techniques such as amperometry or voltammetry) or alternative (impedance). Some useful tips and detailed consideration of interesting techniques used in this thesis are given in the continuation.

1.4.2.1 Hydrogen evolution reaction

De la Escosura and co-workers from our group have developed several amperometric assays using gold nanoparticles as electroactive/electrocatalitic labels and applied them in immunosandwich based assays, where a AuNP labelled antibody binds the analyte captured onto a surface. The amount of gold is quantified by reading the current of the sample in acidic media at -1.35Volts. This signal is achieved thanks to the role of gold catalysing the proton reduction to hydrogen (hydrogen evolution reaction, HER). The current signal is caused by the hydrogen formation and can be correlated to the amount of gold, which is in direct relation to the amount of analyte. Examples of this are the detection of Escherichia Coli O:157:H7 through an immunoassay on magnetic beads in samples minced beef and drinking water[239], detection of ApoE performing the immunoassay on magnetic porous microspheres[240], detection of cancer cells through antibody labelled with AuNPs against specific proteins of the tumour cell lines[241,242].

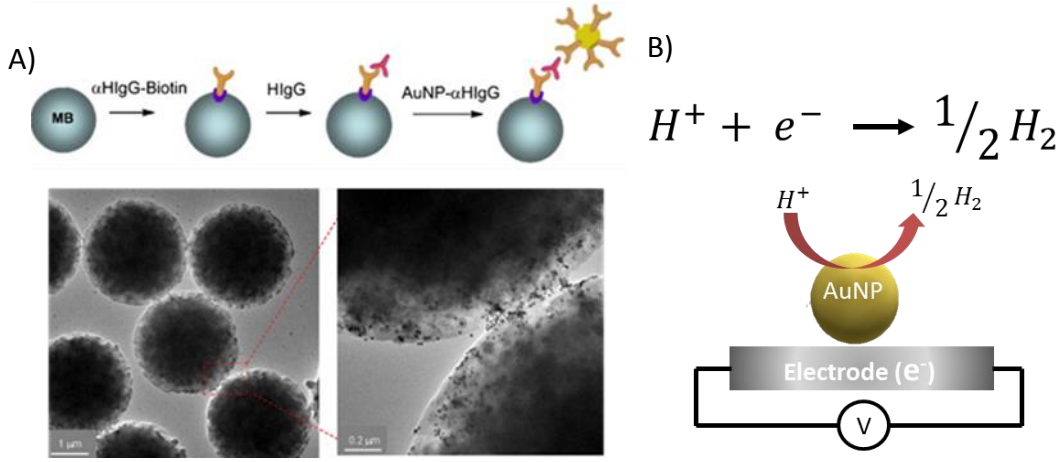

Figure 1.24: Example of biosensors based in hydrogen evolution reaction (HER)[243] catalysed by gold nanoparticles (AuNPs) . A) Above: Scheme of steps in a magnetoimmunoassay where "MB": Streptavidin modified Magnetic Beads. "αHIgG-Biotin": Biotin labelled anti-human IgG. "HIgG": human IgG. "AuNP-αHIgG" AuNPs labelled anti human IgG. Below: TEM images of magneto-immunosandwiches as described in the scheme above. Magnification inset shows the AuNPs attached on the surface of the magnetic beads through the immunoassembly. B) Example of Hydrogen evolution reaction (HER) catalysed by AuNPs, and scheme of AuNPs catalysing HER on an electrode. Images adapted from references[244,245].

1.4.2.2 Square wave voltammetry

In square wave voltammetry (SWV), the changes of potential are applied in a staircase waveform [246,247]. Potential pulses and intervals between pulses have the same duration, which is established by setting the frequency of the waveform. In SWV a progressive change of potential (see Figure 1.25 B) is performed by introducing a forward and backward potential change around the previous potential. Current is measured before each pulse, the resulting difference of the two current signals is the value represented over the average of the applied potentials. The principle behind this procedure is that at the end of each pulse the capacitive/charging current is negligible compared to the current related to the signal[248]. This slightly sophisticated procedure is done to prevent effects of charging currents in the sensor and remove background signal in the measurement. Moreover, another advantage of SWV is the possibility to work at high frequencies, as a result the analysis time is remarkably reduced, making possible to obtain results in few seconds[248].

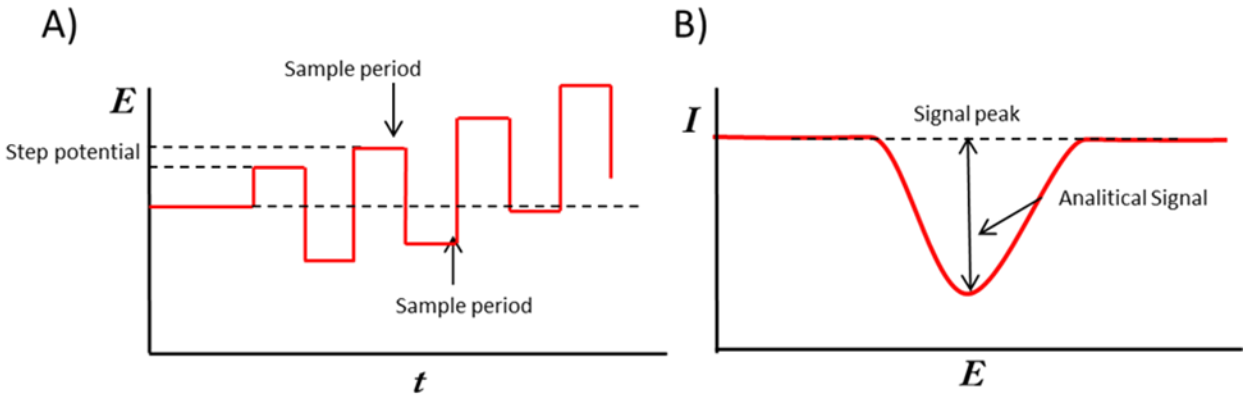

Figure 1.25: Examples of square wave voltammetry (SWV). A) Scheme of potential pulse performed overtime. B) Scheme of signal obtained from a SWV, and representation of intensity peak used as analytical value. [249].

SWV have been successfully applied in several biosensing approaches. For example Plaxco and co-workers reported a reagentless, selective and reusable biosensor[250] based in a surface attached DNA sequence modified with a redox tag. The sensor was interrogated by SWV, obtaining a signal (peak) due to the redox tag. The interaction of the surface attached DNA with its complementary strand introduced a conformational change placing the redox tag in another position and altering the electron transfer to the surface and consequently altering the SWV signal. This pioneer work served to set the electrochemical DNA sensor (E-DNA) technology [251], which later was successfully

applied in multiple situations, for either DNA detection or protein/antibodies/ transcription factors detection [252-257], heavy metals [258], or even other small molecules. This diversification in target detection was possible thanks to the use of aptamers with affinity for different ligands, or nucleic acids modified with ligands capable of interacting with analytes in a sample.

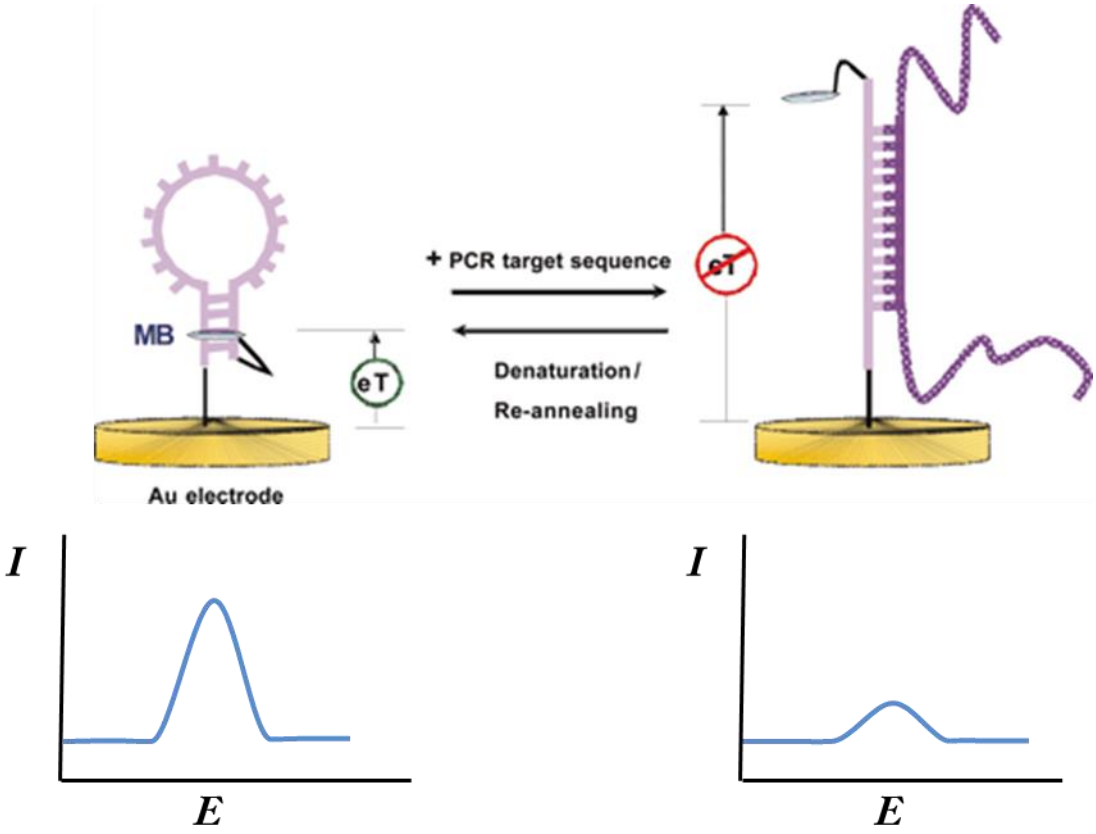

Figure 1.26: Scheme of working principle of the reagentless electrochemical DNA sensor reported by Plaxco and coworkers applied in the detection of PCR products[259], using Methylene Blue (MtB), acting as redox label. Top: scheme of the labelled DNA attached to the electrode surface, in closed conformation (left) and open conformation (right) due to interaction with the PCR product. Below: the SWV signal resulting from the represented conformation above. The change of conformation brings the MtB away from the electrode, disrupting the electron transfer and reducing the peak signal in the SWV. Figure adapted from reference [259].

Other authors have also applied successfully SWV in biosensing. Goyal and coworkers used carbon nanutubes to modify pyrolytic graphite electrodes to perform detection of adenine and andenosine-5'-monophosphate (5'-AMP) at the range of 5 to 100 nM. Carcinoembryonic antigen was detected through a immunosandwich using antibodies labelled with AuNPs conjugated with Methylene blue (MtB) as redox labels[260]. Xiao and collaborators[261] reported a carbon nanotube modified glassy carbon electrode capable of detecting E. coli between $2{\cdot}10^{2}$ and $2{\cdot}10^{8}$ cells mL^{-1}. Interferon-γ on a gold electrode through a MtB labelled aptamer detection with a LOD of 60 pM was reported by Liu and co-workers[262].

1.4.2.3 Electrochemical Impedance Spectroscopy (EIS)

Electrochemical Impedance Spectroscopy (EIS) is a powerful electrochemical method that has recently become popular in the field of biosensing, mostly thanks to advances in equipment and software that made it accessible for researchers working in detection[20].

In order to extract the useful information from experimental data obtained in an impedance measurement an equivalent circuit model is used. Circuit elements are used to represent different components or phenomena taking place in the sensor during the measurement. For instance, the electron transfer happening on the electrode surface is described as a resistance, the double layer is understood as a capacitor and the conductivity of the bulk of the solution as a resistance. This are the components involved in the most popular and most used equivalent circuit, the Randless circuit (Figure 1.27 B). In some cases another component is included, the Warburg impedance (Z_w), this component is used to describe the diffusion processes between the bulk and the surface of the electrode.

It is important to keep in mind that there is not a unique model or perfect correspondence between circuit elements and the physical process underneath. Equivalent circuits are just models built and used to extract information from the experimental data, trying to make the proper interpretation.

Alternatively to impedance in which a sweep of frequency is performed it is possible to measure at a single frequency. Hence, setting a constant frequency allows making measurements of impedance over time. Constant impedance has to be set carefully to the one at which the phenomena under study is maximized in the resulting signal. For instance, when studying the charge transfer resistance on an electrode, frequency set should be around the frequencies at which the Rtc dominates the signal, example of marked point with R_{tc} in Figure 1.27 B).

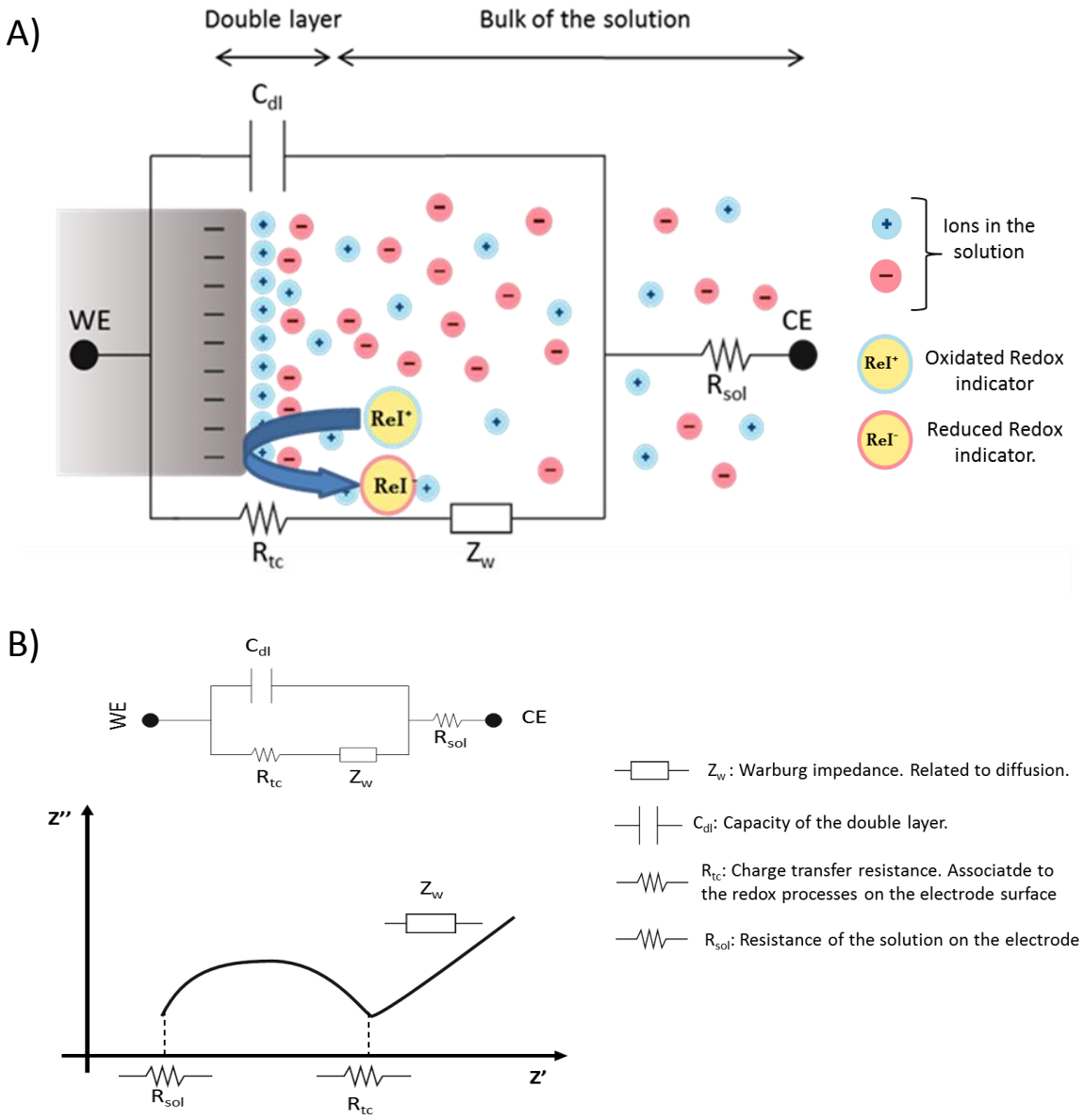

Figure 1.27: A) Representation of the electric components in an electrified interface of a sensor with the solution and the redox mediators. B) Example of impedance data plot (Argand diagram). Each electric component is defined by certain values in the measurement.

1.4.2.3.1 EIS in biosensing

As already stated EIS can be used to monitor electrochemical changes induced by a recognition/interaction or modification event on the surface of the electrode. This fact makes possible to apply the technique in biosensing. In the field of biosensors EIS becomes especially well-suited for the detection of binding events which take place on the electrodes surface. This capability to discriminate small changes on surfaces makes EIS capable of detecting interactions of biomolecules close to the surface of the electrodes; since the signal is obtained due to the

recognition event there is no need of labels, allowing the possibility of performing label free detection[263]. Nevertheless, the high sensitivity and label free detection of EIS has to be carefully managed, since these characteristics bring some drawbacks; in the same way that EIS can register subtle changes, nonspecific changes can be registered and be included in the signal of the interaction event when they are caused by a different principle, leading to false positive signals [264].

Several approaches of detection through EIS are based in the use of a redox indicator (see Figure 1.28), in these systems the signal readout is the charge transfer associated to the redox process of the indicator on the electrode surface, this is represented as a resistance (R_{tc}) in the equivalent circuit. The presence of immobilized capture agent, for instance a DNA sequence, on the surface prevents the redox indicator from reaching the electrode altering the resulting resistance associated to the process. When the target sequence hybridizes with the immobilized capture DNA it conforms a stronger barrier for the redox indicator, decreasing its possibility to access the electrode surface and increasing the R_{tc} value change[265]. Thanks to the strong negative charge of the DNA chains, redox indicator with net negative charge would be especially suitable for DNA detection by this principle.

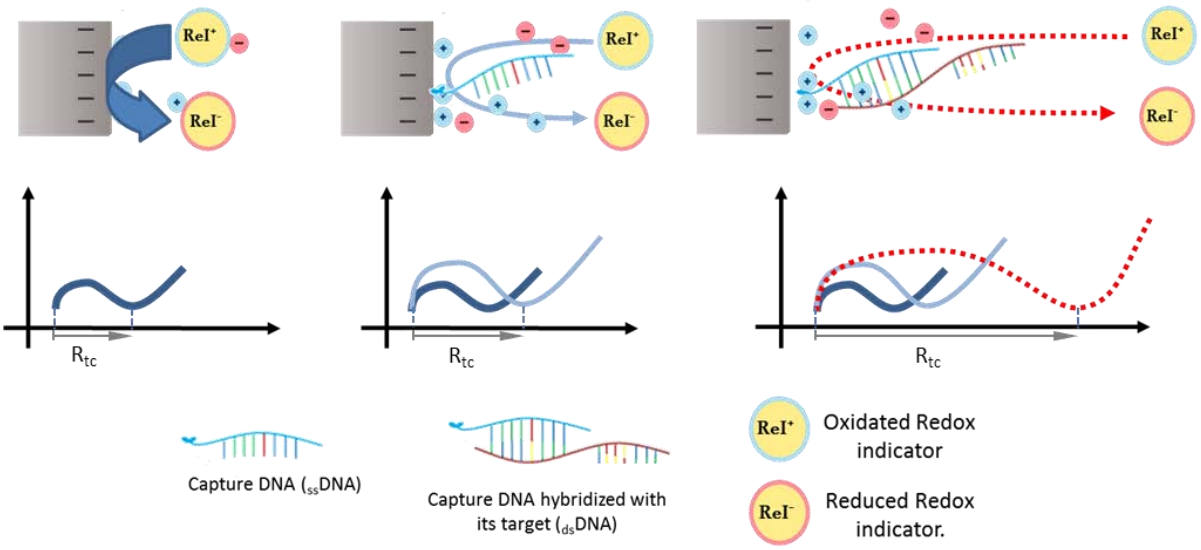

Figure 1.28: Example of principle detection of DNA using impedance measurements. Pictures above represent the situation of the sensor, below plot of the data corresponding to the situation. On the left image a situation of bare electrode is shown, where the redox mediator founds no obstacle reaching the surface and consequently the electron transfer rate is high, therefore a small Rtc is found. In the centre, electrode modified with capture DNA increases slightly the Rtc due to covering effect of the capture DNA. On the right, the target DNA once hybridized with the capture presents a greater obstacle to the redox mediator, preventing it more from reaching the electrodes surface, consequently Rtc is substantially increased.

1.4.2.3.2 Impedimetric biosensors based in DNA as recognition element

Label free EIS sensors have been successfully applied in detection of biomolecules, especially DNA EIS sensors are particularly popular and used. Main reasons to this are the fact that DNA oligonucleotides are available in purified form, they are stable in wide range of different conditions (temperature, ionic force, solvent polarity, etc), immobilization chemistry is well known and mature, and hybridization selectivity is relatively robust. Single strain DNA ($_{ss}$DNA) can be easily immobilized on the surface of the electrode. When the immobilized strain hybridizes with its complementary sequence can introduce changes on the surface electrode that can be monitored by impedance.

DNA detection based in the R_{tc} monitoring using a redox indicator has been widely reported. Initially gold electrodes were used, mainly promoted by the good performance of the electrodes and easiness of chemistry to immobilize DNA through gold interaction with thiol groups added on the DNA probes. Immobilized DNA was used to perform detection of complementary DNA sequences or proteins with affinity for the sequences[266], for instance cytochrome C[267] .

Rivas and co-workers[102] developed a biosensor for Ocratoxin (OTA) detection using SPCE electrodes. The recognition is performed by an aptamer immobilized on a polythionin layer deposited on the carbon area of the WE. The aptamer due to the conformation change after the binding with the analyte, prevents the $Fe(CN)_6^{3-/4-}$ indicator from reaching the electrode surface, hence the R_{tc} associated is altered, achieving limits of detection of 14 pM.

1.4.2.3.3 Impedimetric biosensors based in proteins as recognition element.

Protein detection appears to be the more likely real applications of biosensors worldwide. EIS biosensors are especially well suited for protein detection due to the possibility of performing label-free detection. In contrast to DNA, proteins are less stable and more labile to changes in the environment. Stability of the recognition element on the sensor is often compromised and in cases of EIS biosensors, these changes related to degradation and denaturation represents a significant drawback. Although different non-proteic capturing molecules to detect proteins such as aptamers[268,269] are available for sensor modifications, still the main molecules used for sensing proteins are mainly antibodies, or other proteins with affinity for the target protein.

Several examples of EIS based biosensors using proteins as capturing agents have been successfully developed and reported. Detection of Listeria cells using cell wall binding domain of protein from a bacteriophage immobilized on a gold screen-printed electrodes, achieving LOD of $1 \cdot 10^4$ CFU mL^{-1} in milk, was reported by Zourob and collaborators[270]. In the study $Fe(CN)_6^{3-/4-}$ was used as redox indicator. The blocking effect of the analyte captured on the surface was monitored through the changes of the R_{tc}. Su-Moon P. and collaborators reported detection of p53 protein at levels of 0,1 – 30 µg mL^{-1}, through the modulation of the R_{tc} of $Fe(CN)_6^{3-/4-}$ by the binding of the p53 to a capturing antibody immobilized on a SAM modified gold disk electrode. Lin K. and collaborators successfully developed a biosensor for the detection of a cardiovascular biomarker (C reactive Protein) by monitoring changes in capacitance[271], capable of detecting down to 1 pg mL^{-1} showing a linear range of response until 1µg mL^{-1}. Davis J and Collaborators reported the detection of insulin in undiluted blood serum, through specific antibodies immobilized on polymer coated gold electrodes, achieving detection of insulin in the pM range, by measuring changes of capacitance on the surface of the electrode [272].

1.5 Optical paper based biosensors

Optical biosensors compromise the use of optical transducers for the specific detection of analytes through a biological or biochemical based recognition principle. In fact, optical biosensors represent a special subset developed in basis of traditional optical sensors used in chemistry, adapted by introducing biological components as recognition elements [273]. Among optical biosensors two main categories can be established. First, these in which fundamental properties of the light (phase and amplitude) are monitored. The analyte interaction with the recognition element changes the properties of the reflected light, this interference is used to find out the presence and quantify the analyte. Examples of these biosensors are circular dichroism, surface plasmon resonance (SPR), etc. Second, those based in the use of optical labels, or molecules optically active which can absorb light or perform fluorescence emission.

Often, costs, availability of equipment, need of trained personnel, cost of operation and time of answer are probably the hardest obstacles for the diffusion and application of biosensors in several situations [274]. Nanomaterials can provide important advantages in the design of novel biosensing systems or improvements of the existing devices. Despite the high level of integrated technologies and knowledge that nanotechnology represents, nanotechnology derived achievements grant the tools to develop simple and smart sensing and biosensings systems. An interesting application resulting from these possibilities is the developing of more easy–to–use, less equipment demanding, and more efficient biosensors. In particular paper-based biosensors represent a promising answer to this simplicity-related demand of biosensors. Since paper is inexpensive and abundant, affordable biosensors can be produced. Furthermore, sensitive and specific assays on paper can be developed based on immunoreactions or nucleic acids hybridizations. User friendly capability is very important and examples of this are the pregnancy tests on strips that represent the most used POC biosensor. The same tests are example of rapidness and robustness that paper-based biosensors can achieve. In less than few minutes the response of these devices can be developed. Sometimes they can be equipment free, read by naked eye without need of specific equipment. Nevertheless, if quantitative detection is required, equipment is portable and inexpensive. Finally, versatility and possibility to quickly prototype/develop new and alternative approaches gives them a huge potential for real world applications. Paper-based biosensors use to involve also inkjet [275], wax printing [276], or screen printing [277] in the case of further microfluidics improvements and electrochemical/electrical detection integration.

Paper-based biosensors can be divided into three main categories: dipstick assay, lateral flow Assays (LFA) and micropads (µPADs).

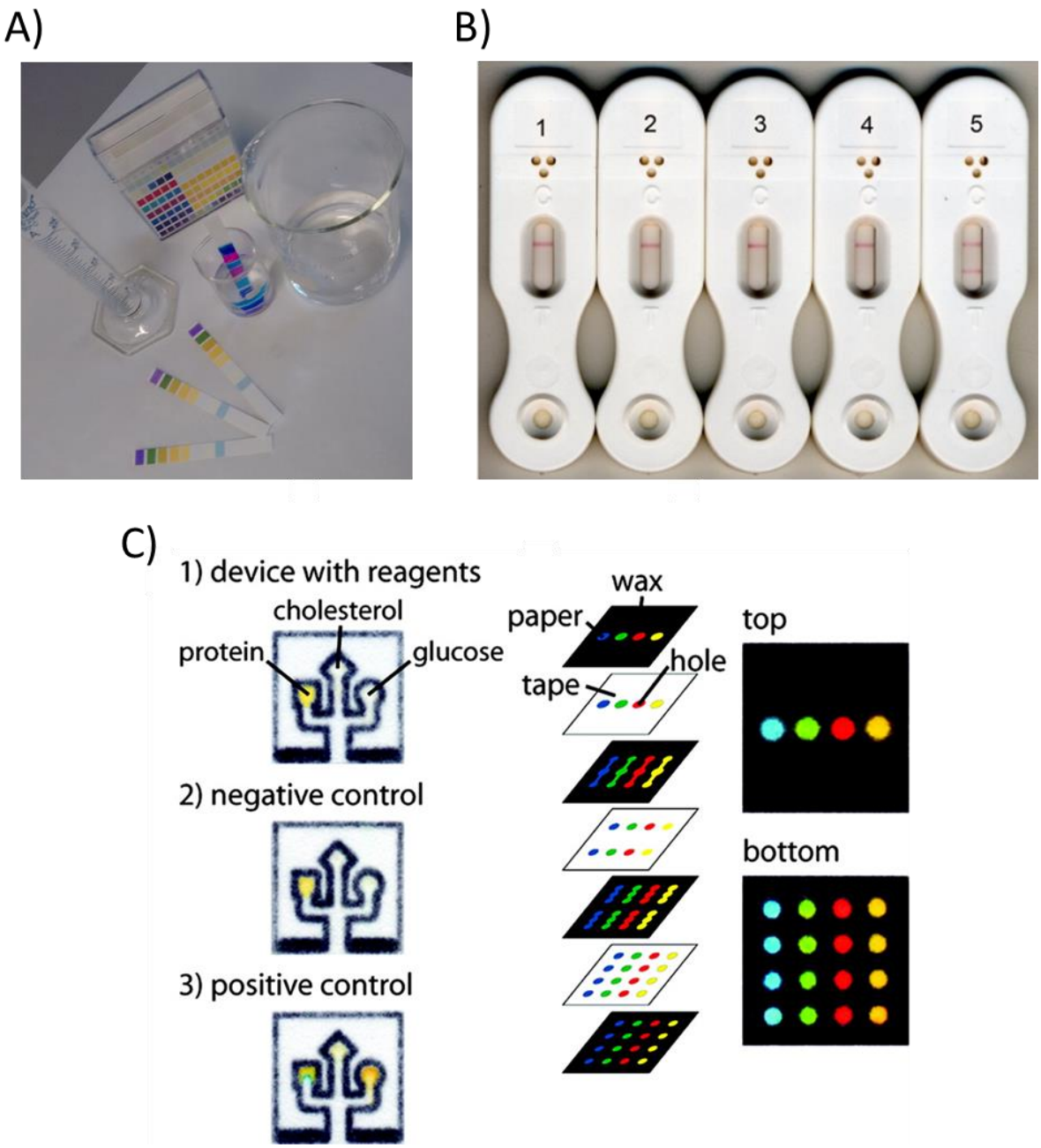

Figure 1.29: (A) Example of dipstick assays: pH strips. (B) Lateral flow: assay for detection of Aspergillius, from left to right: (1) Blank, negative control with (2) Candida albicans, (2) Pseudallescheria boydii, (3) Rizhopus oryzae, (5) Fusarium solani and positive (5) sample for Apergillius fumigatus. MicroPADs (C) paper devices with application in biosensing. B) and C) Figures extracted from [276,278] respectively.

Among the three cited assays dipstick represent the simplest assay: they are based on the blotting of the sample onto a paper pre-stored with reagents; the best known examples is the pH strip (Figure 1.29 A). Lateral flow assays, as in the dipstick, all the reagents are pre-stored in the

strip. However in the lateral flow, the flow plays a key role, since it is used to make the reagents flow through different zones allowing to perform a whole assay integrated in one step. µPADS are devices which combine advantages of paper and microfluidics: by creating hydrophilic and hydrophobic regions of the paper to guide the liquids along the storage or detection regions on the device. Lateral flow, the type of paper based optical biosensor used in the experimental section of this thesis is presented and discussed in more detail in next section.

1.5.1 Lateral flow technology

The concept of rapid body fluid has been reported and documented in history since thousands of years ago. In ancient Egypt a urine test for determining pregnancy of women was reported 1350-1200 BC, based in the capability of pregnant women's urine to make wheat grains grow [279,280]. In middle ages and renaissances, pregnancy and other diseases could be diagnosed by properties of urine. In nineteenth century physicians still practiced the examination of urine in a more rational way including scientific approaches but it was not until 1900 that the term "hormones" was introduced by Ernest Starling[281]. After this study, scientist began to explore in detail a particular hormone, human chorionic gonadotropin (hCG)[282], that can be found only in pregnant woman. In this context, interest in molecular diagnosis through human fluid samples pushed forward several achievements in the field of methods for rapid diagnostics, being the lateral flow devices among the most important.

Basic operational principles date back to the '50s with the work by Plotz and Singer using latex beads agglutination test[283]. Later, in 1980 Leuvering *et al.*[284] reported the sol particle immunoassay in which silver and gold colloids were used as labels for sandwich immunoassays obtaining remarkable limits of detection compared to already existing techniques.

The main application of the agglutination test and sandwich assays were in the human pregnancy test develop in mid '70s: a home-diagnostic methods called "early pregnancy test" (e.p.t^{TM}) developed by Warner-Chilcott, a complex system that involved the use of different tubes and reagents and results were obtained after 2h end point ambiguous to determine. The launching and success of this method allowed the progress of these type of biosensors. Later in 1988, Unipad Ltd, launched the first LFA strip test that allowed non trained users to get a reliable response in few minutes by just adding a small volume of the sample to one of the pads of the pregnancy test. The test was qualitative: two blue lines meant that the patient was pregnant, while just one line meant that the patient is not. The test was based in detection of hCG, which levels are raised in women 9-

10 weeks after conception. Later tests evolved allowing more accurate responses like stage of pregnancy, also test have been integrated with electronics to achieve semi-quantitative results. Due to the success as biosensor in detection of hCG, LFA technology has been adapted in several situations and different contexts for the detection of a wide range of analytes[285].

1.5.1.1 Operation principles of lateral flow assays

The LFAs are based on chromatographic principle in which sample flows through a solid substrate via capillary action. Each strip is composed by dry pre-stored reagents and different porous membranes that have specific functions. As pre-requisite for the proper functioning of LFA, all the components of the strips must be previously treated in order to make them hydrophilic to be solubilized again. The membranes with the pre-loaded regents are assembled overlapping each other on an adhesive backing card in such a way that guarantees the continuous flow of the sample towards the detection lines (see Figure 1.30).

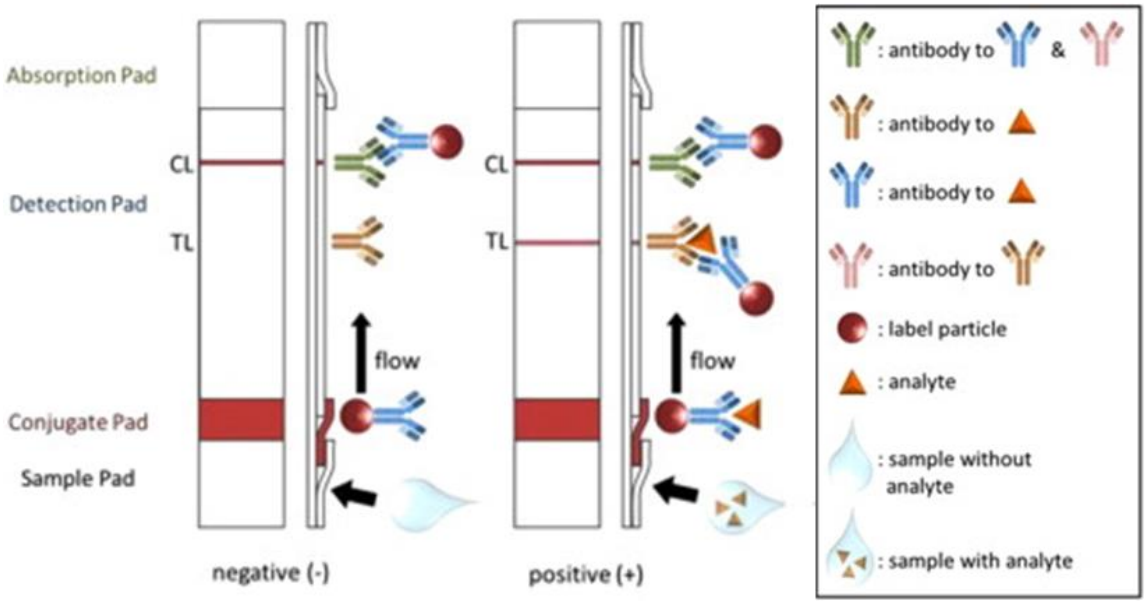

Figure 1.30: Example of working principle of typical Lateral Flow Immunoassay strip (for both negative and positive responses). A direct assay using antibodies as recognition elements in both, the test/control lines and the conjugates. Different components of the strips are represented: Sample pads, Conjugate pad, detection pad with the Test line (TL) and control line (CL), and absorption pad. Extracted from reference [286].

The fluid sample is applied at one end of the strip (sample pad) and migrates towards the next membrane, conjugate pad, where labelled recognition elements are preabsorbed. In this step the analyte interacts with the labelled recognition elements forming a complex. The sample and components solubilized in the conjugate pad flow by capillarity towards the detection pad, composed by a porous membrane in which the biological complementary part of the assay has been

previously immobilized in form of lines. When the complexes (labelled recognition element plus the analyte) reach these lines they are captured by sandwich formation of the two recognition elements connected by the analyte. This accumulation of conjugates in the detection line results in the formation of a readable signal correlated with the detection of the analyte. Unbound conjugates keep migrating to the control line, where recognition elements to capture conjugates have been deposited. This line is necessary to check the proper state of conjugates. The excess of reagents is absorbed by an absorbent pad located after the detection pad. Depending on the label used in the conjugates, naked eye detection can be performed, or specific readers are required in order to read the signal. Direct assay is the simplest and most used type of LFA assay (displayed in Figure 1.30). However, for the detection of small molecules or molecules with one binding site, the sandwich formation of a direct assay becomes rather difficult to perform or achieve, therefore indirect assays were developed. In these assays the analytes act as capturing agent in the detection line, competing with the analyte present in the sample. The fading or loss of intensity in the detection line is related to the presence of analyte in the sample. Since the conjugates will be blocked with the analyte in solution will not be retained in the detection line, hence they will flow away. Control line in an indirect assay works in the same way as in a direct assay.

Most common type of LFA is based in the use of antibodies as recognition elements either in the detection pad or the conjugates (example shown in Figure 1.30), conforming the so called Lateral Flow Immunoassay (LFIA).

1.5.1.2 Components in a Lateral Flow immunoassay Strips

Samples pads. Its purpose is to receive and distribute the sample in a controlled and uniform way, releasing the analyte with the optimal rate [287]. Additionally it controls the flow that enters in the conjugation pad preventing flooding of the device. Typically, sample pads are made of cellulose fibre. These pads are usually pre-treated by impregnation with proteins, buffers and detergents. This pretreatment avoid nonspecific absorption of sample components in the sample pad, thus the reagents present in the sample pad can modulate sample viscosity (parameter involved in the migration time of the components of the assay, which is closely related with the optimal conditions for maximum signal achievement).

Conjugate pads are required to keep dried conjugates particles retained and stable until the test is run. A critical issue is that conjugates should be retained and stable but not irreversibly attached. When the sample flows through the pad, the conjugates have to be solubilized, recognize the

analyte and the formed complexes move to the detection pad. Additionally conjugates should have low nonspecific interaction with other components, except from the analyte, in order to ensure the suitable formation of the sandwich complex in the detection line with low background signal. Conjugate deposition and treatment for drying play a key role in the proper performance of the conjugate pad. In order to achieve an optimal release of the sample, the pad must be pre-treated with pH adjusted buffer containing proteins, surfactants, or even sugars, followed by a suitable drying. Deposition of conjugates can be performed manually or by using a dispensing machine, that delivers them in a continuous mode on the pads. Typical materials used for conjugate pads are glass fibers, cellulose filters, polyester or polypropylene filters and rayon.

Detection pad is the one where detection is performed. It main purpose is to bind irreversibly the capturing agents at the tests and control lines, in order to make possible the formation of lines and visualization of coloured bands indicating the presence or absence of analyte in the sample. Although detection pads can be made out of several materials such as polyethersulfone, nylon, etc. Most common material used is nitrocellulose. Nitrocellulose has proved its suitability to absorb biomolecules and a proper behaviour in biological assays over decades. Proof of this is the successful application of nitrocellulose membranes in blotting techniques for detection of proteins (western blott)[288], DNA (southern blott)[289] and RNa (Northern blott)[290] . Nitrocellulose is hydrophobic by nature, however they may become hydrophilic allowing aqueous liquids to flow through thanks to the presence of surfactants added during membrane production[287]. Deposition of capturing agents on detection pads at both test and control lines can be carried out either with contact or non-contact systems. In principle noncontact deposition such as ink jet or spotting system is preferred to avoid possible physical damage of the membrane. However, low contact dispenser systems can be found and successfully applied for printing/depositing capturing agents; in this system thin nozzles dispense the capturing agents with minimal mechanical stress on the membrane.

Immobilization mechanism of the biomolecules in charge of the recognition in both test and control line is still not clear. There are two main mechanisms proposed. First, absorption of biomolecules by non-covalent interactions. Second, electrostatic interactions between the dipoles of NO_3 groups of the nitrocellulose and COOH in the biomolecules. Either way, independently of the different forces involved in the absorption process(hydrogen bonding, hydrophobic and electrostatic interactions), immobilization of capturing agents on nitrocellulose results in a stable, non-reversible and reliable attachment of capturing agents in the required areas (test and control line).

Binding of the analyte to the conjugates and detection line (sandwich formation) occurs within the detection pads, making it a key component of the assay. Porosity of the detection pad

membranes has direct influence in the final performance of the assay in terms of sensitivity. The pore size determines the flow rate and time in which conjugate and analyte meet and are exposed to the detection line, as consequence, the more time the reagents spent on the membrane, the sandwich complex formation in the detection line is more efficient. Therefore, sensitivity increases when pore size in the detection pad decreases. Another relevant parameter is the thickness of the detection pad, since has direct influence on the bead volume of the assay and signal visibility. When liquid sample is casted onto the membrane the liquid penetrates and moves laterally. In a thin membrane, the spreading of reagents will take place since the insufficient depth causes the diffusion of the liquid through the whole membrane causing difficulties visualizing signals. Furthermore, too deep membranes would mask part of the colorimetric signal in the test and control line, due to the depth.

Absorbent pad: Located at the end of the strip, its main function is to drain the fluid excess from the detection pad. Using absorbent pad, the volume of the sample used can be increased, being the background signal reduced and the sensitivity of the assay improved. Usually absorbent pad are made out of cellulose fibre and no treatment is need.

1.5.1.3 Labels used in Lateral Flow immunoassays

Immunoassay conjugates consists of a recognition element labelled with an appropriate label which function is to generate a signal that correlates with the complex formation and, hence, with the analyte, allowing the detection by reading the signal using techniques such as colorimetry, fluorescence and luminescence[291].

Most of commercial LFIA tests use coloured labels because they allow visual detection[291]. However, LFIA intended to be quantitative require from the use of readers systems, the system varies on the type of label used. Among traditional labels latex beads represent a widely used label. They are based in beads with high capacity of protein binding and are also capable to incorporate colour and fluorescent dyes [291]. Other labels are liposomes[292] which contain the dye encapsulated within, carbon nanoparticles which represent the most inexpensive label show good colour contrast with nitrocellulose[293], fluorescent labels: both organic dyes and quantum dots have been successfully applied [161,294,295].

1.5.1.3.1 Gold nanoparticles based Lateral Flow immunoassays

Due to the work done in the present thesis, special interest is given to gold nanoparticle-based LFIA.

AuNPs have been used for years in biomedical applications and their unique properties already discussed in section 1.3.1.2 make them attractive for areas such as diagnostics, therapy and immunology[30,48,58,71,77,80,296]. Nowadays, AuNPs are the most used labels for LFA due to their signalling properties combined with their biocompatibility and low toxicity overall for in-vitro applications. As stated in sections 1.3.1.2.1 and 1.3.1.2.2 AuNPs can be synthetized following different protocols, allowing to obtain well dispersed and size controlled AuNP colloidal solutions.

In the specific situation of LFIA, thanks to the possibility to easily immobilize antibodies on the AuNPs surface, conjugates for LFIA can be performed and applied in a conjugate pad . The optimum size of AuNPs for LFIA is around 15-40 nm: below 10 nm AuNPs have not bright and intense colour, while above 40 nm AuNPs tend to flocculate. Lou *et al*.[297] Studied the influence of nanoparticle size (14 nm, 16 nm, 35 nm and 38 nm) in LFIA assays. They found differences in conjugation optimal parameters (antibody concentration and pH), however, they proved that 16 nm AuNPs remained stable at the lowest concentration of antibody but the resulting assay in real samples was less sensitive than using 38 nm. In a similar study reported by Safenkova and co-workers[298] , optimal parameters of a AuNPs based LFIA for the detection of potato virus X were found, achieving LOD of 2 ng mL^{-1} using 33.4 nm diameter AuNPs (conjugated with 15 µg mL^{-1} of antibody in pH 9.0) proving the importance to find the optimal conditions in each individual assay.

1.5.1.4 Lateral flow assays applied in biosensing

Lateral flow technology has diverse in different sectors being successfully applied in numerous tests and assays. Proof of this is the significant market of commercial LFA by a great number of companies. In addition, high number of approaches for detection of different analytes have been reported in recent years[299]. Several formats and types of LFA, using different types of recognition elements and labels for the conjugates, applied in the detection of proteins, DNA, toxins, heavy metals and pesticides have been reported.

LFA for detection of protein analytes have been widely described. Xu *et al.*[300] described a more sensitive LFA for thrombin detection using aptamers, as capturing agents in the test line, than the

traditional LFIA using antibodies. Furthermore, LFA has been successfully applied in approaches for cancer biomarkers: Zeng and co-workers[301] developed a LFA for detection of carcinoembryonic antigen in human serum, achieving LOD of 5 ng mL^{-1} in a 10 min assay. In this report, the main interest of the proposed technique is not related to the LOD, since it is similar to the already obtained by the commercially available ELISA kit, but the time of assay which was considerably shorter. Fernandez-Sánchez *et al.* developed[302,303] and optimized a LFA for detection of total and free prostate specific antigen (PSA) achieving a LOD of 1 ng mL^{-1}.

DNA detection represents an important molecular diagnosis, due to the interest in human and veterinary research. Usually, DNA detection is performed using traditional molecular biology techniques such as polymerase chain reaction (PCR) combined with the fluorescent label of oligonucleotides. Integrated POC assays for detection of specific DNA sequences of interest, in a fast and robust assay become of especially interesting alternative to traditional molecular biology techniques. Unfortunately, DNA presence in samples often is too low as to be detected directly, therefore LFA for DNA detection require an amplification system (usually by PCR) coupled to the detection assay in order to guarantee the amount of detectable DNA. Roskos *et al.* [304] developed a device for the detection of mycobacterium tuberculosis DNA, based in a LFA enclosed in a cartridge with the DNA amplification system included in a fully integrated device where only the samples has to be added to perform the assay. Xiao and co-workers[305] reported a LFA for detection of single DNA mutations, by using AuNPs as label and circular displacement reaction for amplification of the target sequence and T4 DNA ligase, an enzyme, for the high specific recognition of DNA single base mismatches. With this strategy LOD of 0.01 fM is achieved. Nevertheless, LFA has been applied in detection of small molecules such as heavy metals using competitive assays [306,307], toxins [102,308,309] and pesticides [310].

1.5.1.5 Lateral flow assays advantages and limitations

LFA is a well-established technology with many advantages and successfully applied in many real world situations. The main interesting points are: a) rapid qualitative or semi-quantitative tests. b) easy to use (results can be interpreted by untrained personnel). c) No need of sophisticated equipment for performing the test. d) Prolonged shelf-life and sometimes even without refrigeration. e) Small volumes of sample require. f) Relatively low cost production. h) Versatility and possibility of integration with other systems.

Despite the cited advantages, LFA present some limitations, mainly related to reproducibility and sensitivity of the technique: a) higher volumes could deteriorate the strip. b) Pre-treatment is required for non-liquid samples. c) Less sensitivity than other molecular biology techniques (radioimmunoassays, ELISA, etc). d) Multiple detection limited by the setup for lateral flow strips fabrication.

1.6 Conclusions and future perspectives

In past decades the field of biosensing technology has experienced a strong demand for detection techniques and approaches to be applied in diagnostics. Most appreciated and requested improvements are focused in assays with low cost, fast response, simple to use without needing specific training. In this context, nanotechnology represents a remarkable source of alternatives and possibilities to achieve such improvements with interest not only in clinical diagnostics but in environmental and food analysis as well.

Undoubtedly through the application of nanomaterials and nanostructured materials, several advantages can be achieved. Electrochemical methods and paper-based optical techniques, both using nanoparticles and also explored in this thesis, are shown to be the most important techniques with interest in biosensors.

Applicability of developed biosensing strategies becomes an issue tackled by researchers nowadays. Works done with low cost devices such carbon electrodes printed on plastics and paper-based devices result with interest due to the low costs of production and hence being close to real devices efficient to be exploited in the market. In particular, Lateral Flow immunoassays (LFIAs), represent a suitable platform to develop new sensing strategies given the well-established market that it has. Proof of this is the number of commercially available LFAs for detection of a wide range of analytes.

1.7 Bibliography

(1) Kumar, S.; Mohan, A.; Guleria, R. *Biomarkers* **2006**, *11*, 385-405.

(2) Golubnitschaja, O.; Flammer, J. *Survey of Ophthalmology* **2007**, *52*, S155-S161.

(3) Ognibene, A.; Ciuti, R.; Tozzi, P.; Messeri, G. *Prenatal Diagnosis* **1999**, *19*, 1058-1060.

(4) Thompson, I. M.; Pauler, D. K.; Goodman, P. J.; Tangen, C. M.; Lucia, M. S.; Parnes, H. L.; Minasian, L. M.; Ford, L. G.; Lippman, S. M.; Crawford, E. D.; Crowley, J. J.; Coltman, C. A. *New England Journal of Medicine* **2004**, *350*, 2239-2246.

(5) Pepys, M. B.; Hirschfield, G. M. *The Journal of Clinical Investigation* **2003**, *111*, 1805-1812.

(6) Hanash, S. M. *ELECTROPHORESIS* **2000**, *21*, 1202-1209.

(7) Jiang, L.; Chughtai, K.; Purvine, S. O.; Bhujwalla, Z. M.; Raman, V.; Paša-Tolić, L.; Heeren, R. M. A.; Glunde, K. *Analytical Chemistry* **2015**.

(8) Cheng, F.; Wang, Z.; Huang, Y.; Duan, Y.; Wang, X. *Clinica Chimica Acta* **2015**, *447*, 23-31.

(9) Nwosu, C.; Yau, H. K.; Becht, S. *Analytical Chemistry* **2015**.

(10) Gygi, S. P.; Rist, B.; Gerber, S. A.; Turecek, F.; Gelb, M. H.; Aebersold, R. *Nat Biotech* **1999**, *17*, 994-999.

(11) de la Escosura-Muñiz, A.; Merkoçi, A. *Expert Opinion on Medical Diagnostics* **2010**, *4*, 21-37.

(12) Ali, M. M.; Aguirre, S. D.; Xu, Y.; Filipe, C. D. M.; Pelton, R.; Li, Y. *Chemical Communications* **2009**, 6640-6642.

(13) Pepe, M. S.; Etzioni, R.; Feng, Z.; Potter, J. D.; Thompson, M. L.; Thornquist, M.; Winget, M.; Yasui, Y. *Journal of the National Cancer Institute* **2001**, *93*, 1054-1061.

(14) Luppa, P. B.; Müller, C.; Schlichtiger, A.; Schlebusch, H. *TrAC Trends in Analytical Chemistry* **2011**, *30*, 887-898.

(15) Kost, G. J.; Tran, N. K.; Louie, R. F. In *Encyclopedia of Analytical Chemistry*; John Wiley & Sons, Ltd: 2006.

(16) Imaging, E. o. b. o. t. N. I. o. B.; Bioengineering/National Heart, L.; Faculty, B. I. N. S. F. W.; Price, C. P.; Kricka, L. J. *Clinical Chemistry* **2007**, *53*, 1665-1675.

(17) Yetisen, A. K.; Akram, M. S.; Lowe, C. R. *Lab on a Chip* **2013**, *13*, 2210-2251.

(18) Turner, A. P. F. *Chemical Society Reviews* **2013**, *42*, 3184-3196.

(19) Thévenot, D. R.; Toth, K.; Durst, R. A.; Wilson, G. S. *Biosensors and Bioelectronics* **2001**, *16*, 121-131.

(20) Rackus, D. G.; Shamsi, M. H.; Wheeler, A. R. *Chemical Society Reviews* **2015**.

(21) Ronkainen, N. J.; Halsall, H. B.; Heineman, W. R. *Chemical Society Reviews* **2010**, *39*, 1747-1763.

(22) Luo, X.; Davis, J. J. *Chemical Society Reviews* **2013**, *42*, 5944-5962.

(23) Daniels, J. S.; Pourmand, N. *Electroanalysis* **2007**, *19*, 1239-1257.

(24) de la Escosura-Muñiz, A.; Merkoçi, A. *ACS Nano* **2012**, *6*, 7556-7583.

(25) Yang, W.; Zhu, X.; Liu, Q.; Lin, Z.; Qiu, B.; Chen, G. *Chemical Communications* **2011**, *47*, 3129-3131.

(26) Ishikawa, F. N.; Chang, H.-K.; Curreli, M.; Liao, H.-I.; Olson, C. A.; Chen, P.-C.; Zhang, R.; Roberts, R. W.; Sun, R.; Cote, R. J.; Thompson, M. E.; Zhou, C. *ACS Nano* **2009**, *3*, 1219-1224.

(27) Kauffman, D. R.; Star, A. *Chemical Society Reviews* **2008**, *37*, 1197-1206.

(28) Ohno, Y.; Maehashi, K.; Yamashiro, Y.; Matsumoto, K. *Nano Letters* **2009**, *9*, 3318-3322.

(29) Aragay, G.; Pino, F.; Merkoçi, A. *Chemical Reviews* **2012**, *112*, 5317-5338.

(30) Zamborini, F. P.; Bao, L.; Dasari, R. *Analytical Chemistry* **2012**, *84*, 541-576.

(31) Geim, A. K.; Novoselov, K. S. *Nat Mater* **2007**, *6*, 183-191.

(32) Schmidt, V.; Wittemann, J. V.; Senz, S.; Gösele, U. *Advanced Materials* **2009**, *21*, 2681-2702.

(33) Guldi, D. M. *Angewandte Chemie International Edition* **2006**, *45*, 695-695.

(34) Variola, F.; Brunski, J. B.; Orsini, G.; Tambasco de Oliveira, P.; Wazen, R.; Nanci, A. *Nanoscale* **2011**, *3*, 335-353.

(35) Guix, M.; Mayorga-Martinez, C. C.; Merkoçi, A. *Chemical Reviews* **2014**, *114*, 6285-6322.

(36) Saito, N.; Haniu, H.; Usui, Y.; Aoki, K.; Hara, K.; Takanashi, S.; Shimizu, M.; Narita, N.; Okamoto, M.; Kobayashi, S.; Nomura, H.; Kato, H.; Nishimura, N.; Taruta, S.; Endo, M. *Chemical Reviews* **2014**, *114*, 6040-6079.

(37) Cheng, L.; Wang, C.; Feng, L.; Yang, K.; Liu, Z. *Chemical Reviews* **2014**, *114*, 10869-10939.

(38) Alves, A.; Berutti, F.; Sánchez, F. In *Nanostructured Materials for Engineering Applications*; Bergmann, C., de Andrade, M., Eds.; Springer Berlin Heidelberg: 2011, p 93-117.

(39) Zhang, Q.; Uchaker, E.; Candelaria, S. L.; Cao, G. *Chemical Society Reviews* **2013**, *42*, 3127-3171.

(40) Liu, G.; Lin, Y. *Talanta* **2007**, *74*, 308-317.

(41) Yao, J.; Yang, M.; Duan, Y. *Chemical Reviews* **2014**, *114*, 6130-6178.

(42) Lei, J.; Ju, H. *Chemical Society Reviews* **2012**, *41*, 2122-2134.

(43) Khor, S. M.; Liu, G.; Peterson, J. R.; Iyengar, S. G.; Gooding, J. J. *Electroanalysis* **2011**, *23*, 1797-1804.

(44) Aragay, G.; Pons, J.; Merkoçi, A. *Chemical Reviews* **2011**, *111*, 3433-3458.

(45) http://wichlab.com/research/, W. L.

(46) Guczi, L. *Catalysis Today* **2005**, *101*, 53-64.

(47) Ghosh Chaudhuri, R.; Paria, S. *Chemical Reviews* **2012**, *112*, 2373-2433.

(48) Saha, K.; Agasti, S. S.; Kim, C.; Li, X.; Rotello, V. M. *Chemical Reviews* **2012**, *112*, 2739-2779.

(49) Zhang, Q.; Zhang, K.; Xu, D.; Yang, G.; Huang, H.; Nie, F.; Liu, C.; Yang, S. *Progress in Materials Science* **2014**, *60*, 208-337.

(50) Ravindran, A.; Chandran, P.; Khan, S. S. *Colloids and Surfaces B: Biointerfaces* **2013**, *105*, 342-352.

(51) Laurent, S.; Forge, D.; Port, M.; Roch, A.; Robic, C.; Vander Elst, L.; Muller, R. N. *Chemical Reviews* **2008**, *108*, 2064-2110.

(52) Chen, X.; Mao, S. S. *Chemical Reviews* **2007**, *107*, 2891-2959.

(53) Li, H.; Zhang, Y.; Wang, L.; Tian, J.; Sun, X. *Chemical Communications* **2011**, *47*, 961-963.

(54) Pecher, J.; Mecking, S. *Chemical Reviews* **2010**, *110*, 6260-6279.

(55) Rycenga, M.; Cobley, C. M.; Zeng, J.; Li, W.; Moran, C. H.; Zhang, Q.; Qin, D.; Xia, Y. *Chemical Reviews* **2011**, *111*, 3669-3712.

(56) Tokel, O.; Inci, F.; Demirci, U. *Chemical Reviews* **2014**, *114*, 5728-5752.

(57) Daniel, M.-C.; Astruc, D. *Chemical Reviews* **2004**, *104*, 293-346.

(58) Boisselier, E.; Astruc, D. *Chemical Society Reviews* **2009**, *38*, 1759-1782.

(59) Sapsford, K. E.; Algar, W. R.; Berti, L.; Gemmill, K. B.; Casey, B. J.; Oh, E.; Stewart, M. H.; Medintz, I. L. *Chemical Reviews* **2013**, *113*, 1904-2074.

(60) Turkevich, J.; Stevenson, P. C.; Hillier, J. *Discussions of the Faraday Society* **1951**, *11*, 55-75.

(61) Mout, R.; Moyano, D. F.; Rana, S.; Rotello, V. M. *Chemical Society Reviews* **2012**, *41*, 2539-2544.

(62) Parolo, C.; de la Escosura-Muñiz, A.; Polo, E.; Grazú, V.; de la Fuente, J. M.; Merkoçi, A. *ACS Applied Materials & Interfaces* **2013**, *5*, 10753-10759.

(63) Mirkin, C. A.; Letsinger, R. L.; Mucic, R. C.; Storhoff, J. J. *Nature* **1996**, *382*, 607-609.

(64) Sperling, R. A.; Parak, W. J. *Philosophical Transactions of the Royal Society of London A: Mathematical, Physical and Engineering Sciences* **2010**, *368*, 1333-1383.

(65) Conde, J.; Dias, J. T.; Grazú, V.; Moros, M.; Baptista, P. V.; De La Fuente, J. M. *Frontiers in Chemistry* **2014**, *2*.

(66) Zheng, J.; Zhang, C.; Dickson, R. M. *Physical Review Letters* **2004**, *93*, 077402.

(67) Chen, L.-Y.; Wang, C.-W.; Yuan, Z.; Chang, H.-T. *Analytical Chemistry* **2015**, *87*, 216-229.

(68) Kong, H.; Lu, Y.; Wang, H.; Wen, F.; Zhang, S.; Zhang, X. *Analytical Chemistry* **2012**, *84*, 4258-4261.

(69) Huang, C.-C.; Chiang, C.-K.; Lin, Z.-H.; Lee, K.-H.; Chang, H.-T. *Analytical Chemistry* **2008**, *80*, 1497-1504.

(70) Elghanian, R.; Storhoff, J. J.; Mucic, R. C.; Letsinger, R. L.; Mirkin, C. A. *Science* **1997**, *277*, 1078-1081.

(71) Thaxton, C. S.; Georganopoulou, D. G.; Mirkin, C. A. *Clinica Chimica Acta* **2006**, *363*, 120-126.

(72) Chen, Y.-M.; Yu, C.-J.; Cheng, T.-L.; Tseng, W.-L. *Langmuir* **2008**, *24*, 3654-3660.

(73) Pavlov, V.; Xiao, Y.; Shlyahovsky, B.; Willner, I. *Journal of the American Chemical Society* **2004**, *126*, 11768-11769.

(74) Liu, R.; Liew, R.; Zhou, J.; Xing, B. *Angewandte Chemie International Edition* **2007**, *46*, 8799-8803.

(75) Watanabe, S.; Seguchi, H.; Yoshida, K.; Kifune, K.; Tadaki, T.; Shiozaki, H. *Tetrahedron Letters* **2005**, *46*, 8827-8829.

(76) Watanabe, S.; Sonobe, M.; Arai, M.; Tazume, Y.; Matsuo, T.; Nakamura, T.; Yoshida, K. *Chemical Communications* **2002**, 2866-2867.

(77) Jiang, Y.; Zhao, H.; Lin, Y.; Zhu, N.; Ma, Y.; Mao, L. *Angewandte Chemie International Edition* **2010**, *49*, 4800-4804.

(78) González García, M. B.; Costa García, A. *Bioelectrochemistry and Bioenergetics* **1995**, *38*, 389-395.

(79) Pumera, M.; Aldavert, M.; Mills, C.; Merkoçi, A.; Alegret, S. *Electrochimica Acta* **2005**, *50*, 3702-3707.

(80) de la Escosura-Muñiz, A.; Parolo, C.; Merkoçi, A. *Materials Today* **2010**, *13*, 24-34.

(81) Dequaire, M.; Degrand, C.; Limoges, B. *Analytical Chemistry* **2000**, *72*, 5521-5528.

(82) Ho, J.-a. A.; Chang, H.-C.; Shih, N.-Y.; Wu, L.-C.; Chang, Y.-F.; Chen, C.-C.; Chou, C. *Analytical Chemistry* **2010**, *82*, 5944-5950.

(83) Qin, X.; Xu, A.; Liu, L.; Deng, W.; Chen, C.; Tan, Y.; Fu, Y.; Xie, Q.; Yao, S. *Chemical Communications* **2015**, *51*, 8540-8543.

(84) de la Escosura-Muñiz, A.; Maltez-da Costa, M.; Merkoçi, A. *Biosensors and Bioelectronics* **2009**, *24*, 2475-2482.

(85) Zhao, Y.; Hernandez-Pagan, E. A.; Vargas-Barbosa, N. M.; Dysart, J. L.; Mallouk, T. E. *The Journal of Physical Chemistry Letters* **2011**, *2*, 402-406.

(86) Mayorga Martinez, C. C.; Madrid, R. E.; Felice, C. J. *Sensors and Actuators B: Chemical* **2008**, *133*, 682-686.

(87) O'Hare, D.; Parker, K. H.; Winlove, C. P. *Medical Engineering and Physics*, *28*, 982-988.

(88) Huang, W.-D.; Cao, H.; Deb, S.; Chiao, M.; Chiao, J. C. *Sensors and Actuators A: Physical* **2011**, *169*, 1-11.

(89) Nakagawa, T.; Beasley, C. A.; Murray, R. W. *The Journal of Physical Chemistry C* **2009**, *113*, 12958-12961.

(90) Nakagawa, T.; Bjorge, N. S.; Murray, R. W. *Journal of the American Chemical Society* **2009**, *131*, 15578-15579.

(91) Rivas, L.; de la Escosura-Muñiz, A.; Pons, J.; Merkoçi, A. *Electroanalysis* **2014**, *26*, 1287-1294.

(92) Petit, M. A.; Plichon, V. *Journal of Electroanalytical Chemistry* **1998**, *444*, 247-252.

(93) Cogan, S. F.; Ehrlich, J.; Plante, T. D.; Smirnov, A.; Shire, D. B.; Gingerich, M.; Rizzo, J. F. *Conference proceedings : ... Annual International Conference of the IEEE Engineering in Medicine and Biology Society. IEEE Engineering in Medicine and Biology Society. Conference* **2004**, *6*, 4153-4156.

(94) Wang, K.; Liu, C.-C.; Durand, D. M. *IEEE transactions on bio-medical engineering* **2009**, *56*, 6-14.

(95) Klein, J. D.; Clauson, S. L.; Cogan, S. F. *Journal of Materials Research* **1989**, *4*, 1505-1510.

(96) Kuwabara, T.; Tomita, E.; Sakita, S.; Hasegawa, D.; Sone, K.; Yagi, M. *The Journal of Physical Chemistry C* **2008**, *112*, 3774-3779.

(97) Hoertz, P. G.; Kim, Y.-I.; Youngblood, W. J.; Mallouk, T. E. *The Journal of Physical Chemistry B* **2007**, *111*, 6845-6856.

(98) Dau, H.; Zaharieva, I. *Accounts of Chemical Research* **2009**, *42*, 1861-1870.

(99) Vinyard, D. J.; Ananyev, G. M.; Charles Dismukes, G. *Annual Review of Biochemistry* **2013**, *82*, 577-606.

(100) Meyer, T. J. *Nature* **2008**, *451*, 778-779.

(101) Lattach, Y.; Rivera, J. F.; Bamine, T.; Deronzier, A.; Moutet, J.-C. *ACS Applied Materials & Interfaces* **2014**, *6*, 12852-12859.

(102) Rivas, L.; Mayorga-Martinez, C. C.; Quesada-González, D.; Zamora-Gálvez, A.; de la Escosura-Muñiz, A.; Merkoçi, A. *Analytical Chemistry* **2015**, *87*, 5167-5172.

(103) Farah, A. M.; Billing, C.; Dikio, C. W.; Dibofori-Orji, A. N.; Oyedeji, O. O.; Wankasi, D.; Mtunzi, F. M.; Dikio, E. D. *Int. J. Electrochem. Sci.* **2013**, *8*, 12132-12146.

(104) Fu, G.; Liu, W.; Feng, S.; Yue, X. *Chemical Communications* **2012**, *48*, 11567-11569.

(105) Moscone, D.; D'Ottavi, D.; Compagnone, D.; Palleschi, G.; Amine, A. *Analytical Chemistry* **2001**, *73*, 2529-2535.

(106) Nossol, E.; Zarbin, A. J. G. *Advanced Functional Materials* **2009**, *19*, 3980-3986.

(107) Uemura, T.; Kitagawa, S. *Journal of the American Chemical Society* **2003**, *125*, 7814-7815.

(108) Shokouhimehr, M.; Soehnlen, E. S.; Hao, J.; Griswold, M.; Flask, C.; Fan, X.; Basilion, J. P.; Basu, S.; Huang, S. D. *Journal of Materials Chemistry* **2010**, *20*, 5251-5259.

(109) Ricci, F.; Palleschi, G. *Biosensors and Bioelectronics* **2005**, *21*, 389-407.

(110) Hornok, V.; Dékány, I. *Journal of Colloid and Interface Science* **2007**, *309*, 176-182.

(111) Miao, Y.; Chen, J.; Wu, X. *Colloid J* **2007**, *69*, 334-337.

(112) Uemura, T.; Ohba, M.; Kitagawa, S. *Inorganic Chemistry* **2004**, *43*, 7339-7345.

(113) Espinoza-Castañeda, M.; Escosura-Muñiz, A. d. l.; Chamorro, A.; Torres, C. d.; Merkoçi, A. *Biosensors and Bioelectronics* **2015**, *67*, 107-114.

(114) Karyakin, A. A. *Electroanalysis* **2001**, *13*, 813-819.

(115) Ricci, F.; Goncalves, C.; Amine, A.; Gorton, L.; Palleschi, G.; Moscone, D. *Electroanalysis* **2003**, *15*, 1204-1211.

(116) Ricci, F.; Palleschi, G. *Biosensors & Bioelectronics* **2005**, *21*, 389-407.

(117) Ricci, F.; Arduini, F.; Amine, A.; Moscone, D.; Palleschi, G. *Journal of Electroanalytical Chemistry* **2004**, *563*, 229-237.

(118) Ricci, F.; Palleschi, G.; Yigzaw, Y.; Gorton, L.; Ruzgas, T.; Karyakin, A. *Electroanalysis* **2003**, *15*, 175-182.

(119) Suprun, E.; Evtugyn, G.; Budnikov, H.; Ricci, F.; Moscone, D.; Palleschi, G. *Anal Bioanal Chem* **2005**, *383*, 597-604.

(120) Ricci, F.; Amine, A.; Palleschi, G.; Moscone, D. *Biosensors & Bioelectronics* **2003**, *18*, 165-174.

(121) Li, J.; Wei, X.; Yuan, Y. *Sensors and Actuators B: Chemical* **2009**, *139*, 400-406.

(122) Trindade, T.; O'Brien, P.; Pickett, N. L. *Chemistry of Materials* **2001**, *13*, 3843-3858.

(123) Steigerwald, M. L.; Brus, L. E. *Accounts of Chemical Research* **1990**, *23*, 183-188.

(124) Bawendi, M. G.; Steigerwald, M. L.; Brus, L. E. *Annual Review of Physical Chemistry* **1990**, *41*, 477-496.

(125) Donega, C. d. M. *Chemical Society Reviews* **2011**, *40*, 1512-1546.

(126) Chang, J.; Waclawik, E. R. *RSC Advances* **2014**, *4*, 23505-23527.

(127) Medintz, I. L.; Uyeda, H. T.; Goldman, E. R.; Mattoussi, H. *Nat Mater* **2005**, *4*, 435-446.

(128) Murray, C. B.; Norris, D. J.; Bawendi, M. G. *Journal of the American Chemical Society* **1993**, *115*, 8706-8715.

(129) Spanhel, L.; Haase, M.; Weller, H.; Henglein, A. *Journal of the American Chemical Society* **1987**, *109*, 5649-5655.

(130) Rogach, A. L.; Kornowski, A.; Gao, M.; Eychmüller, A.; Weller, H. *The Journal of Physical Chemistry B* **1999**, *103*, 3065-3069.

(131) Rogach, A. L.; Katsikas, L.; Kornowski, A.; Su, D.; Eychmüller, A.; Weller, H. *Berichte der Bunsengesellschaft für physikalische Chemie* **1996**, *100*, 1772-1778.

(132) Zheng, Y.; Yang, Z.; Ying, J. Y. *Advanced Materials* **2007**, *19*, 1475-1479.

(133) Li, C. L.; Nishikawa, K.; Ando, M.; Enomoto, H.; Murase, N. *Colloids and Surfaces A: Physicochemical and Engineering Aspects* **2007**, *294*, 33-39.

(134) Rogach, A.; Kershaw, S. V.; Burt, M.; Harrison, M. T.; Kornowski, A.; Eychmüller, A.; Weller, H. *Advanced Materials* **1999**, *11*, 552-555.

(135) Shavel, A.; Gaponik, N.; Eychmüller, A. *The Journal of Physical Chemistry B* **2004**, *108*, 5905-5908.

(136) Reiss, P.; Protière, M.; Li, L. *Small* **2009**, *5*, 154-168.

(137) http://www.olympusconfocal.com/theory/fluorophoresintro.html, O. w. s.

(138) Talapin, D. V.; Lee, J.-S.; Kovalenko, M. V.; Shevchenko, E. V. *Chemical Reviews* **2010**, *110*, 389-458.

(139) Dabbousi, B. O.; Rodriguez-Viejo, J.; Mikulec, F. V.; Heine, J. R.; Mattoussi, H.; Ober, R.; Jensen, K. F.; Bawendi, M. G. *The Journal of Physical Chemistry B* **1997**, *101*, 9463-9475.

(140) Peng, X.; Schlamp, M. C.; Kadavanich, A. V.; Alivisatos, A. P. *Journal of the American Chemical Society* **1997**, *119*, 7019-7029.

(141) Lesnyak, V.; Gaponik, N.; Eychmuller, A. *Chemical Society Reviews* **2013**, *42*, 2905-2929.

(142) Zhuang, Z.; Peng, Q.; Li, Y. *Chemical Society Reviews* **2011**, *40*, 5492-5513.

(143) Blanco-Canosa, J. B.; Wu, M.; Susumu, K.; Petryayeva, E.; Jennings, T. L.; Dawson, P. E.; Algar, W. R.; Medintz, I. L. *Coordination Chemistry Reviews* **2014**, *263–264*, 101-137.

(144) Mansur, H. S. *Wiley Interdisciplinary Reviews: Nanomedicine and Nanobiotechnology* **2010**, *2*, 113-129.

(145) Mattoussi, H.; Mauro, J. M.; Goldman, E. R.; Anderson, G. P.; Sundar, V. C.; Mikulec, F. V.; Bawendi, M. G. *Journal of the American Chemical Society* **2000**, *122 (49)*, 12142-12150.

(146) Sutherland, A. J. *Current Opinion in Solid State and Materials Science* **2002**, *6*, 365-370.

(147) Xing, Y.; Chaudry, Q.; Shen, C.; Kong, K. Y.; Zhau, H. E.; Chung, L. W.; Petros, J. A.; O'Regan, R. M.; Yezhelyev, M. V.; Simons, J. W.; Wang, M. D.; Nie, S. *Nat. Protocols* **2007**, *2*, 1152-1165.

(148) Chan, W. C. W.; Nie, S. *Science* **1998**, *281*, 2016-2018.

(149) Wu, X.; Liu, H.; Liu, J.; Haley, K. N.; Treadway, J. A.; Larson, J. P.; Ge, N.; Peale, F.; Bruchez, M. P. *Nat Biotech* **2003**, *21*, 41-46.

(150) Gao, X.; Nie, S. *Trends in Biotechnology* **2003**, *21*, 371-373.

(151) Åkerman, M. E.; Chan, W. C. W.; Laakkonen, P.; Bhatia, S. N.; Ruoslahti, E. *Proceedings of the National Academy of Sciences* **2002**, *99*, 12617-12621.

(152) Kim, S.; Lim, Y. T.; Soltesz, E. G.; De Grand, A. M.; Lee, J.; Nakayama, A.; Parker, J. A.; Mihaljevic, T.; Laurence, R. G.; Dor, D. M.; Cohn, L. H.; Bawendi, M. G.; Frangioni, J. V. *Nat Biotech* **2004**, *22*, 93-97.

(153) Wu, D.; Chen, Z.; Huang, G.; Liu, X. *Sensors and Actuators A: Physical* **2014**, *205*, 72-78.

(154) Ke, J.; Li, X.; Zhao, Q.; Hou, Y.; Chen, J. *Sci. Rep.* **2014**, *4*.

(155) Banerjee, S.; Kar, S.; Santra, S. *Chemical Communications* **2008**, 3037-3039.

(156) Han, J.; Zhang, X.; Zhou, Y.; Ning, Y.; Wu, J.; Liang, S.; Sun, H.; Zhang, H.; Yang, B. *Journal of Materials Chemistry* **2012**, *22*, 2679-2686.

(157) Cui, L.; He, X.-P.; Chen, G.-R. *RSC Advances* **2015**, *5*, 26644-26653.

(158) Morales-Narváez, E.; Montón, H.; Fomicheva, A.; Merkoçi, A. *Analytical Chemistry* **2012**, *84*, 6821-6827.

(159) Berlina, A. N.; Taranova, N. A.; Zherdev, A. V.; Sankov, M. N.; Andreev, I. V.; Martynov, A. I.; Dzantiev, B. B. *PLoS ONE* **2013**, *8*, e77485.

(160) Ornberg, R. L.; Harper, T. F.; Liu, H. *Nat Meth* **2005**, *2*, 79-81.

(161) Berlina, A.; Taranova, N.; Zherdev, A.; Vengerov, Y.; Dzantiev, B. *Anal Bioanal Chem* **2013**, *405*, 4997-5000.

(162) Luo, Y.; Zhang, B.; Chen, M.; Jiang, T.; Zhou, D.; Huang, J.; Fu, W. *Journal of Translational Medicine* **2012**, *10*, 24-24.

(163) Akinfieva, O.; Nabiev, I.; Sukhanova, A. *Critical Reviews in Oncology/Hematology* **2013**, *86*, 1-14.

(164) Rousserie, G.; Sukhanova, A.; Even-Desrumeaux, K.; Fleury, F.; Chames, P.; Baty, D.; Oleinikov, V.; Pluot, M.; Cohen, J. H. M.; Nabiev, I. *Critical Reviews in Oncology/Hematology* **2010**, *74*, 1-15.

(165) Gerion, D.; Chen, F.; Kannan, B.; Fu, A.; Parak, W. J.; Chen, D. J.; Majumdar, A.; Alivisatos, A. P. *Analytical Chemistry* **2003**, *75*, 4766-4772.

(166) Huang, A.; Qiu, Z.; Jin, M.; Shen, Z.; Chen, Z.; Wang, X.; Li, J.-W. *International Journal of Food Microbiology* **2014**, *185*, 27-32.

(167) Joo, C.; Balci, H.; Ishitsuka, Y.; Buranachai, C.; Ha, T. *Annual Review of Biochemistry* **2008**, *77*, 51-76.

(168) Selvin, P. R. *Nat Struct Mol Biol* **2000**, *7*, 730-734.

(169) Claussen, J. C.; Hildebrandt, N.; Medintz, I. In *FRET – Förster Resonance Energy Transfer*; Wiley-VCH Verlag GmbH & Co. KGaA: 2013, p 397-429.

(170) Pons, T. In *FRET – Förster Resonance Energy Transfer*; Wiley-VCH Verlag GmbH & Co. KGaA: 2013, p 323-356.

(171) Robinson, P. J.; Woolhead, C. A. In *FRET – Förster Resonance Energy Transfer*; Wiley-VCH Verlag GmbH & Co. KGaA: 2013, p 357-396.

(172) Spindel, S.; Granek, J.; Sapsford, K. E. In *FRET – Förster Resonance Energy Transfer*; Wiley-VCH Verlag GmbH & Co. KGaA: 2013, p 269-322.

(173) Gill, R.; Zayats, M.; Willner, I. *Angewandte Chemie International Edition* **2008**, *47*, 7602-7625.

(174) Algar, W. R.; Massey, M.; Krull, U. J. In *FRET – Förster Resonance Energy Transfer*; Wiley-VCH Verlag GmbH & Co. KGaA: 2013, p 475-605.

(175) Algar, W. R.; Krull, U. *Anal Bioanal Chem* **2008**, *391*, 1609-1618.

(176) Zhang, C.-Y.; Yeh, H.-C.; Kuroki, M. T.; Wang, T.-H. *Nat Mater* **2005**, *4*, 826-831.

(177) Wegner, K. D.; Jin, Z.; Lindén, S.; Jennings, T. L.; Hildebrandt, N. *ACS Nano* **2013**, *7*, 7411-7419.

(178) Morales-Narváez, E.; Hassan, A.-R.; Merkoçi, A. *Angewandte Chemie International Edition* **2013**, *52*, 13779-13783.

(179) Tan, W.; Fang, X.; Li, J.; Liu, X. *Chemistry – A European Journal* **2000**, *6*, 1107-1111.

(180) Chen, T.; Tan, W. *Molecular Beacons*; Springer Berlin Heidelberg, 2013.

(181) Tyagi, S.; Kramer, F. R. *Nat. Biotechnol.* **1996**, *14*, 303-308.

(182) Cady, N. C.; Strickland, A. D.; Batt, C. A. *Molecular and Cellular Probes* **2007**, *21*, 116-124.

(183) Kim, Y.; Sohn, D.; Tan, W. H. *Int. J. Clin. Exp. Pathol.* **2008**, *1*, 105-116.

(184) Sabella, S.; Vecchio, G.; Cingolani, R.; Rinaldi, R.; Pompa, P. P. *Langmuir* **2008**, *24*, 13266-13269.

(185) Petryayeva, E.; Algar, W. R.; Krull, U. J. *Langmuir* **2013**, *29*, 977-987.

(186) Varghese, S. S.; Zhu, Y.; Davis, T. J.; Trowell, S. C. *Lab on a Chip* **2010**, *10*, 1355-1364.

(187) Petryayeva, E.; Algar, W. R. *Analytical Chemistry* **2013**, *85*, 8817-8825.

(188) Noor, M. O.; Shahmuradyan, A.; Krull, U. J. *Analytical Chemistry* **2013**, *85*, 1860-1867.

(189) Noor, M. O.; Krull, U. J. *Analytical Chemistry* **2013**, *85*, 7502-7511.

(190) Noor, M. O.; Krull, U. J. *Analytical Chemistry* **2014**, *86*, 10331-10339.

(191) Medina-Sánchez, M.; Miserere, S.; Morales-Narváez, E.; Merkoçi, A. *Biosensors and Bioelectronics* **2014**, *54*, 279-284.

(192) Huang, H.; Zhu, J.-J. *Analyst* **2013**, *138*, 5855-5865.

(193) Kissling, G. P.; Miles, D. O.; Fermin, D. J. *Physical Chemistry Chemical Physics* **2011**, *13*, 21175-21185.

(194) Arben, M.; Luiz Humberto, M.-J.; Sergio, M.; Orlando, F.-F.; Salvador, A. *Nanotechnology* **2007**, *18*, 035502.

(195) Amelia, M.; Lincheneau, C.; Silvi, S.; Credi, A. *Chemical Society Reviews* **2012**, *41*, 5728-5743.

(196) Wang, J.; Liu, G.; Merkoçi, A. *Journal of the American Chemical Society* **2003**, *125*, 3214-3215.

(197) Zhao, W.-W.; Wang, J.; Zhu, Y.-C.; Xu, J.-J.; Chen, H.-Y. *Analytical Chemistry* **2015**.

(198) Finklea, H. O. *Journal of Chemical Education* **1983**, *60*, 325.

(199) Wu, P.; Hou, X.; Xu, J.-J.; Chen, H.-Y. *Chemical Reviews* **2014**, *114*, 11027-11059.

(200) Ding, Z.; Quinn, B. M.; Haram, S. K.; Pell, L. E.; Korgel, B. A.; Bard, A. J. *Science* **2002**, *296*, 1293-1297.

(201) Lu, W.; Wang, G.; Jin, Y.; Yao, X.; Hu, J.; Li, J. *Applied Physics Letters* **2006**, *89*, 263902.

(202) Haddour, N.; Chauvin, J.; Gondran, C.; Cosnier, S. *Journal of the American Chemical Society* **2006**, *128*, 9693-9698.

(203) de la Escosura-Muniz, A.; Mekoci, A. *Chemical Communications* **2010**, *46*, 9007-9009.

(204) Hou, X.; Jiang, L. *ACS Nano* **2009**, *3*, 3339-3342.

(205) Dekker, C. *Nat Nano* **2007**, *2*, 209-215.

(206) Coulter, W. H.; Coulter, Wallace H.: United States, 1953.

(207) Graham, M. D. *Journal of the Association for Laboratory Automation* **2003**, *8*, 72-81.

(208) Venkatesan, B. M.; Bashir, R. *Nat Nano* **2011**, *6*, 615-624.

(209) Wen, L.; Tian, Y.; Ma, J.; Zhai, J.; Jiang, L. *Physical Chemistry Chemical Physics* **2012**, *14*, 4027-4042.

(210) Xia, D.; Yan, J.; Hou, S. *Small* **2012**, *8*, 2787-2801.

(211) Wanunu, M.; Dadosh, T.; Ray, V.; Jin, J.; McReynolds, L.; Drndic, M. *Nat Nano* **2010**, *5*, 807-814.

(212) Singer, A.; Wanunu, M.; Morrison, W.; Kuhn, H.; Frank-Kamenetskii, M.; Meller, A. *Nano Letters* **2010**, *10*, 738-742.

(213) Chen, P.; Mitsui, T.; Farmer, D. B.; Golovchenko, J.; Gordon, R. G.; Branton, D. *Nano Letters* **2004**, *4*, 1333-1337.

(214) Sawafta, F.; Clancy, B.; Carlsen, A. T.; Huber, M.; Hall, A. R. *Nanoscale* **2014**, *6*, 6991-6996.

(215) de la Escosura-Muñiz, A.; Merkoçi, A. *Small* **2011**, *7*, 675-682.

(216) Li, S.-J.; Li, J.; Wang, K.; Wang, C.; Xu, J.-J.; Chen, H.-Y.; Xia, X.-H.; Huo, Q. *ACS Nano* **2010**, *4*, 6417-6424.

(217) Wang, K.; Liu, G.; Hoivik, N.; Johannessen, E.; Jakobsen, H. *Chemical Society Reviews* **2014**, *43*, 1476-1500.

(218) Tian, Y.; Hou, X.; Jiang, L. *Journal of Electroanalytical Chemistry* **2011**, *656*, 231-236.

(219) Stephen, Y. C.; Wen-Di, L.; Xiaogan, L. *Nanotechnology* **2009**, *20*, 155303.

(220) Li, J.-M.; Liu, C.; Ke, X.; Duan, Y.-j.; Fan, Y.; Li, M.; Zhang, K.-p.; Xu, Z.; Wang, L.-d. *Microsyst Technol* **2013**, *19*, 1845-1850.

(221) Devlin, N. R.; Brown, D. K.; Kohl, P. A. *Journal of Vacuum Science & Technology B* **2009**, *27*, 2508-2511.

(222) Quist, A.; Pavlovic, E.; Oscarsson, S. *Anal Bioanal Chem* **2005**, *381*, 591-600.

(223) Po-Chun, W.; Seung-Joon, P.; Shuodan, C.; Rajaraman, S.; Seong-Hyok, K.; Allen, M. G. *Microelectromechanical Systems, Journal of* **2013**, *22*, 1041-1053.

(224) Zhang, W.; Meng, Z.; Zhai, J.; Heng, L. *Chemical Communications* **2014**, *50*, 3552-3555.

(225) Li, X.; You, H.; Jiang, H.; Lin, R.; Kong, D.; Jiang, R.; Zhu, L.; Gao, J.; Tang, M.; Wang, X.; Fu, S. Fabrication of size controllable SU-8 nanochannels using nanoimprint lithography and low-pressure thermal bonding methods. *Micro & Nano Letters* [Online Early Access]. Published Online: 2014. http://digital-library.theiet.org/content/journals/10.1049/mnl.2013.0674.

(226) Yamaguchi, A.; Teramae, N. *Analytical Sciences* **2008**, *24*, 25-30.

(227) Santos, A.; Formentín, P.; Ferré-Borrull, J.; Pallarès, J.; Marsal, L. F. *Materials Letters* **2012**, *67*, 296-299.

(228) Kasi, A. K.; Kasi, J. K.; Afzulpurkar, N.; Hasan, M. M.; Mahaisavariya, B. *Journal of Vacuum Science & Technology B* **2012**, *30*, 031805.

(229) de la Escosura-Muñiz, A.; Merkoçi, A. *Electrochemistry Communications* **2010**, *12*, 859-863.

(230) de la Escosura-Muñiz, A.; Chunglok, W.; Surareungchai, W.; Merkoçi, A. *Biosensors and Bioelectronics* **2013**, *40*, 24-31.

(231) Liu, G.; Zhang, Y.; Qi, M.; Chen, F. *Analytical Methods* **2015**, *7*, 5619-5626.

(232) Ding, C. Z., F; Ren, R ; Lin, JM *TALANTA* **2009**, *78*, 1148-1154.

(233) Chen, J.; Tang, J.; Yan, F.; Ju, H. *Biomaterials* **2006**, *27*, 2313-2321.

(234) Wang, J.; Tian, B.; Nascimento, V. B.; Angnes, L. *Electrochimica Acta* **1998**, *43*, 3459-3465.

(235) Galán-Vidal, C. A.; Muñoz, J.; Domínguez, C.; Alegret, S. *TrAC Trends in Analytical Chemistry* **1995**, *14*, 225-231.

(236) Renedo, O. D.; Alonso-Lomillo, M. A.; Martínez, M. J. A. *Talanta* **2007**, *73*, 202-219.

(237) Hart, J. P.; Wring, S. A. *Electroanalysis* **1994**, *6*, 617-624.

(238) http://www.saxoprint.co.uk/blog/screen-printing-process/.

(239) Hassan, A.-R. H. A.-A.; de la Escosura-Muñiz, A.; Merkoçi, A. *Biosensors and Bioelectronics* **2015**, *67*, 511-515.

(240) de la Escosura-Muñiz, A.; Plichta, Z.; Horák, D.; Merkoçi, A. *Biosensors and Bioelectronics* **2015**, *67*, 162-169.

(241) Maltez-da Costa, M.; de la Escosura-Muñiz, A.; Nogués, C.; Barrios, L.; Ibáñez, E.; Merkoçi, A. *Nano Letters* **2012**, *12*, 4164-4171.

(242) Maltez-da Costa, M.; de la Escosura-Muñiz, A.; Nogués, C.; Barrios, L.; Ibáñez, E.; Merkoçi, A. *Small* **2012**, *8*, 3605-3612.

(243) de la Escosura-Muñiz, A.; Maltez-da Costa, M.; Sánchez-Espinel, C.; Díaz-Freitas, B.; Fernández-Suarez, J.; González-Fernández, Á.; Merkoçi, A. *Biosensors and Bioelectronics* **2010**, *26*, 1710-1714.

(244) http://www.medpagetoday.com/MeetingCoverage/AADE/47136.

(245) Costa, M. M.-d.; la Escosura-Muñiz, A. d.; Merkoçi, A. *Electrochemistry Communications* **2010**, *12*, 1501-1504.

(246) Chen, A.; Shah, B. *Analytical Methods* **2013**, *5*, 2158-2173.

(247) Ramaley, L.; Krause, M. S. *Analytical Chemistry* **1969**, *41*, 1362-1365.

(248) Gupta, V. K.; Jain, R.; Radhapyari, K.; Jadon, N.; Agarwal, S. *Analytical Biochemistry* **2011**, *408*, 179-196.

(249) Nieto, D.; Gonzalez-Vadillo, A. M.; Bruna, S.; Pastor, C. J.; Rios-Luci, C.; Leon, L. G.; Padron, J. M.; Navarro-Ranninger, C.; Cuadrado, I. *Dalton Transactions* **2012**, *41*, 432-441.

(250) Fan, C.; Plaxco, K. W.; Heeger, A. J. *Proceedings of the National Academy of Sciences* **2003**, *100*, 9134-9137.

(251) Xiao, Y.; Lai, R. Y.; Plaxco, K. W. *Nat. Protocols* **2007**, *2*, 2875-2880.

(252) Bonham, A. J.; Hsieh, K.; Ferguson, B. S.; Vallee-Belisle, A.; Ricci, F.; Soh, H. T.; Plaxco, K. W. *Journal of the American Chemical Society* **2012**, *134*, 3346-3348.

(253) Bonham, A. J.; Paden, N. G.; Ricci, F.; Plaxco, K. W. *Analyst* **2013**, *138*, 5580-5583.

(254) Rowe, A. A.; White, R. J.; Bonham, A. J.; Plaxco, K. W. *Journal of visualized experiments : JoVE* **2011**.

(255) Vallee-Belisle, A.; Ricci, F.; Uzawa, T.; Xia, F.; Plaxco, K. W. *Journal of the American Chemical Society* **2012**, *134*, 15197-15200.

(256) White, R. J.; Kallewaard, H. M.; Hsieh, W.; Patterson, A. S.; Kasehagen, J. B.; Cash, K. J.; Uzawa, T.; Soh, H. T.; Plaxco, K. W. *Analytical Chemistry* **2012**, *84*, 1098-1103.

(257) Xiao, Y.; Dane, K. Y.; Uzawa, T.; Csordas, A.; Qian, J.; Soh, H. T.; Daugherty, P. S.; Lagally, E. T.; Heeger, A. J.; Plaxco, K. W. *Journal of the American Chemical Society* **2010**, *132*, 15299-15307.

(258) Porchetta, A.; Vallee-Belisle, A.; Plaxco, K. W.; Ricci, F. *Journal of the American Chemical Society* **2013**, *135*, 13238-13241.

(259) Lai, R. Y.; Lagally, E. T.; Lee, S.-H.; Soh, H. T.; Plaxco, K. W.; Heeger, A. J. *Proceedings of the National Academy of Sciences of the United States of America* **2006**, *103*, 4017-4021.

(260) Kong, F.-Y.; Xu, Z.; Xu, M.-T.; Xu, J.-J.; Chen, H.-Y. *Electrochimica Acta* **2011**, *56*, 9386-9390.

(261) Xiao, X.; Zhu, G.; Liao, L.; Liu, B.; Yuan, Y.; Wang, Y.; He, J.; He, B.; Wu, Y. *Electrochimica Acta* **2012**, *74*, 105-110.

(262) Liu, Y.; Tuleouva, N.; Ramanculov, E.; Revzin, A. *Analytical Chemistry* **2010**, *82*, 8131-8136.

(263) Lisdat, F.; Schäfer, D. *Anal Bioanal Chem* **2008**, *391*, 1555-1567.

(264) Bogomolova, A.; Komarova, E.; Reber, K.; Gerasimov, T.; Yavuz, O.; Bhatt, S.; Aldissi, M. *Analytical Chemistry* **2009**, *81*, 3944-3949.

(265) Gebala, M.; Schuhmann, W. *Physical Chemistry Chemical Physics* **2012**, *14*, 14933-14942.

(266) Keighley, S. D.; Li, P.; Estrela, P.; Migliorato, P. *Biosensors and Bioelectronics* **2008**, *23*, 1291-1297.

(267) Lisdat, F.; Ge, B.; Krause, B.; Ehrlich, A.; Bienert, H.; Scheller, F. W. *Electroanalysis* **2001**, *13*, 1225-1230.

(268) Nimjee, S. M.; Rusconi, C. P.; Sullenger, B. A. In *The Aptamer Handbook*; Wiley-VCH Verlag GmbH & Co. KGaA: 2006, p 131-166.

(269) Potyrailo, R. A.; Conrad, R. C.; Ellington, A. D.; Hieftje, G. M. *Analytical Chemistry* **1998**, *70*, 3419-3425.

(270) Tolba, M.; Ahmed, M. U.; Tlili, C.; Eichenseher, F.; Loessner, M. J.; Zourob, M. *Analyst* **2012**, *137*, 5749-5756.

(271) Lin, K.-C.; Kunduru, V.; Bothara, M.; Rege, K.; Prasad, S.; Ramakrishna, B. L. *Biosensors and Bioelectronics* **2010**, *25*, 2336-2342.

(272) Luo, X.; Xu, M.; Freeman, C.; James, T.; Davis, J. J. *Analytical Chemistry* **2013**, *85*, 4129-4134.

(273) Ramsden, J. J. *Journal of Molecular Recognition* **1997**, *10*, 109-120.

(274) Yager, P.; Edwards, T.; Fu, E.; Helton, K.; Nelson, K.; Tam, M. R.; Weigl, B. H. *Nature* **2006**, *442*, 412-418.

(275) Su, S.; Ali, M. M.; Filipe, C. D. M.; Li, Y.; Pelton, R. *Biomacromolecules* **2008**, *9*, 935-941.

(276) Carrilho, E.; Martinez, A. W.; Whitesides, G. M. *Analytical Chemistry* **2009**, *81*, 7091-7095.

(277) Savolainen, A.; Zhang, Y.; Rochefort, D.; Holopainen, U.; Erho, T.; Virtanen, J.; Smolander, M. *Biomacromolecules* **2011**, *12*, 2008-2015.

(278) Thornton, C. R. *Clinical and Vaccine Immunology : CVI* **2008**, *15*, 1095-1105.

(279)

(280) Ghalioungui, P.; Khalil, S. H.; Ammar, A. R. *Medical History* **1963**, *7*, 241-246.

(281) *The Lancet* **1905**, *166*, 339-341.

(282) Butt, W. R.; Crooke, A. C.; Cunningham, F. J. *Proceedings of the Royal Society of Medicine* **1961**, *54*, 647-648.

(283) Payne, R. B. *Journal of Clinical Pathology* **1961**, *14*, 309-312.

(284) Leuvering, J. H. W.; Thal, P. J. H. M.; Waart, M. v. d.; Schuurs, A. H. W. M. *Z. Anal. Chem.* **1980**, *301*, 132-132.

(285) Ngom, B.; Guo, Y.; Wang, X.; Bi, D. *Anal Bioanal Chem* **2010**, *397*, 1113-1135.

(286) Quesada-González, D.; Merkoçi, A. *Biosensors and Bioelectronics* **2015**, *73*, 47-63.

(287) *Millipore corporation. Rapid Lateral Flow Test Strips. Considerations for product development.* **2002**.

(288) Mahmood, T.; Yang, P.-C. *North American Journal of Medical Sciences* **2012**, *4*, 429-434.

(289) Brown, T. In *Current Protocols in Immunology*; John Wiley & Sons, Inc.: 2001.

(290) Brown, T. In *Current Protocols in Immunology*; John Wiley & Sons, Inc.: 2001.

(291) Wild, D.; Wild, D., Ed.; Elsevier: Oxford, 2013, p 1036.

(292) Edwards, K.; Baeumner, A. *Anal Bioanal Chem* **2006**, *386*, 1335-1343.

(293) Posthuma-Trumpie, G. A.; Wichers, J. H.; Koets, M.; Berendsen, L. B. J. M.; van Amerongen, A. *Anal Bioanal Chem* **2012**, *402*, 593-600.

(294) Wang, Y.; Nugen, S. *Biomed Microdevices* **2013**, *15*, 751-758.

(295) Xu, Y.; Liu, Y.; Wu, Y.; Xia, X.; Liao, Y.; Li, Q. *Analytical Chemistry* **2014**, *86*, 5611-5614.

(296) Perfezou, M.; Turner, A.; Merkoci, A. *Chemical Society Reviews* **2012**, *41*, 2606-2622.

(297) Lou, S.; Ye, J.-y.; Li, K.-q.; Wu, A. *Analyst* **2012**, *137*, 1174-1181.

(298) Safenkova, I.; Zherdev, A.; Dzantiev, B. *Anal Bioanal Chem* **2012**, *403*, 1595-1605.

(299) Rosen, S. In *Lateral Flow Immunoassay*; Wong, R., Tse, H., Eds.; Humana Press: 2009, p 1-15.

(300) Xu, H.; Mao, X.; Zeng, Q.; Wang, S.; Kawde, A.-N.; Liu, G. *Analytical Chemistry* **2009**, *81*, 669-675.

(301) Qingxiang, Z.; Xun, M.; Hui, X.; Shengfu, W.; Guodong, L. *Am. J. Biomed. Sci.* **2009**, *1*, 70-79.

(302) Fernández-Sánchez, C.; McNeil, C. J.; Rawson, K.; Nilsson, O. *Analytical Chemistry* **2004**, *76*, 5649-5656.

(303) Fernández-Sánchez, C.; McNeil, C. J.; Rawson, K.; Nilsson, O.; Leung, H. Y.; Gnanapragasam, V. *Journal of Immunological Methods* **2005**, *307*, 1-12.

(304) Roskos, K.; Hickerson, A. I.; Lu, H.-W.; Ferguson, T. M.; Shinde, D. N.; Klaue, Y.; Niemz, A. *PLoS ONE* **2013**, *8*, e69355.

(305) Xiao, Z.; Lie, P.; Fang, Z.; Yu, L.; Chen, J.; Liu, J.; Ge, C.; Zhou, X.; Zeng, L. *Chemical Communications* **2012**, *48*, 8547-8549.

(306) Lopez Marzo, A. M.; Pons, J.; Blake, D. A.; Merkoci, A. *Analytical Chemistry* **2013**, *85*, 3532-3538.

(307) Lopez-Marzo, A. M.; Pons, J.; Blake, D. A.; Merkoci, A. *Biosensors & Bioelectronics* **2013**, *47*, 190-198.

(308) Sharma, S. K.; Eblen, B. S.; Bull, R. L.; Burr, D. H.; Whiting, R. C. *Applied and Environmental Microbiology* **2005**, *71*, 3935-3941.

(309) Ching, K. H.; He, X.; Stanker, L. H.; Lin, A. V.; McGarvey, J. A.; Hnasko, R. *Toxins* **2015**, *7*, 1163-1173.

(310) Wang, S.; Zhang, C.; Zhang, Y. In *Biosensors and Biodetection*; Rasooly, A., Herold, K., Eds.; Humana Press: 2009; Vol. 504, p 237-252.

Chapter 2

Objectives

2.1 Objectives

The general objective of this thesis is the study and development of new sensing techniques exploiting novel properties of nanomaterials for the improvement of the analytical performance of biosensors with interest for diagnostic applications.

More in detail specific objectives of the present work can be summarized as follows:

- Development of a novel method for characterization/detection of gold nanoparticles (AuNPs) and application in biosensing. The biosensing mode will be based on AuNPs characterisation/detection by electrochemical impedance spectroscopy (EIS) through hydrogen evolution reaction (HER) catalysis. Application of the developed EIS/HER-based detection system to the characterization of different diameter AuNPs, and use of AUNPs as electrochemical labels in a magenotoimmunosandwich assay.

- Development of a label free impedimetric biosensor for DNA detection, based on carbon screen printed electrodes (SPCE) modified with polythionin and Iridium oxide nanoparticles (IrOx NPs). Application of the developed detection technology for sensing of specific DNA sequences of Leishmania parasite.

- Design of a Lateral flow immunoassay (LFIA) for the detection of a specific protein Parathyroid like hormone (PTHLH) in cell cultures and proof of concept of its potential applicability for detection in human serum samples.

- Application of electrochemical detection based in the use of methylene blue labelled DNA probes on screen printed electrodes.

- Development of a nanochannel-based detection system in which cells secreting the target protein are cultured directly on top of the sensing platform.

Chapter 3

Electrochemical Impedance Spectroscopy (bio)sensing through hydrogen evolution reaction induced by gold nanoparticles

Related publication

Biosensors & Bioelectronics, 67 ,(2015), 53-58

Electrochemical Impedance Spectroscopy (bio)sensing through hydrogen evolution reaction induced by gold nanoparticles

Carmen C. Mayorga-Martinez[a,1], Alejandro Chamorro-Garcia[a,b,1], Arben Merkoçi [a,c]

[a] Nanobioelectronics&Biosensors Group, Institut Català de Nanociencia I Nanotecnologia (ICN2), Edifici ICN2, Campus UAB, Bellaterra (Barcelona), 08290, Spain.

[b] Autonomous University of Barcelona, UAB Campus, 08193 Bellaterra, Spain.

[c] Intitució Catalana per la Recerca I Estudis Avançats (ICREA), Passeig Lluis Companys 23, 08010, Barcelona, Spain.

[1] These Authors contributed equally.

Summary

In this chapter, a new gold nanoparticles (AuNPs) based detection strategy using Electrochemical Impedance Spectroscopy (EIS) through Hydrogen Evolution Reaction (HER) is proposed. This EIS-HER method is used as an alternative to the conventional EIS based on $[Fe(CN)6]^{3-/4-}$ or $[Ru(NH3)6]^{3+/2+}$ indicators. The proposed method is based on the HER induced by AuNPs. EIS measurements for different amounts of AuNP are registered and the charge transfer resistance (Rct) was found to correlate and be useful for their quantification. Moreover the effect of AuNP size on electrical properties of AuNPs for HER using this sensitive technique has been investigated. Different EIS-HER signals generated in presence of AuNPs of different sizes (2, 5, 10, 15, 20, 50 nm) are observed, being the corresponding phenomena extendible to other nanoparticles and related catalytic reactions. This EIS-HER sensing technology is applied to a magneto immunosandwich assay for proteins model (IgG) detection achieving improvements of the analytical performance in terms of a wide linear range (2 – 500 ng mL-1) with a good limit of detection (LOD) of 0.31 ng mL−1 and high sensitivity. Moreover, with this methodology a reduction of one order of magnitude in the LOD for IgG detection was archived, compared with chronoamperometric technique normally used.

3.1 Introduction

Gold nanoparticles (AuNPs) possess unique electrochemical and optical properties including and high surface-to-volume ratio and excellent biocompatibility making these interesting material in developing a variety of biosensors [1].

Hydrogen evolution reaction (HER) induced by AuNPs have been used in a variety of analytical applications for novel and improved sensing and biosensing devices with high specificity and high sensibility [2-8]. In addition AuNPs are also used in Electrochemical Impedance Spectroscopy (EIS) to either enhance the impedimetric signal or modify electrodes in order to increase the amount of analites adsorbed onto their surface, or to exploit a dendritic signal amplification in various applications [1,9-12].

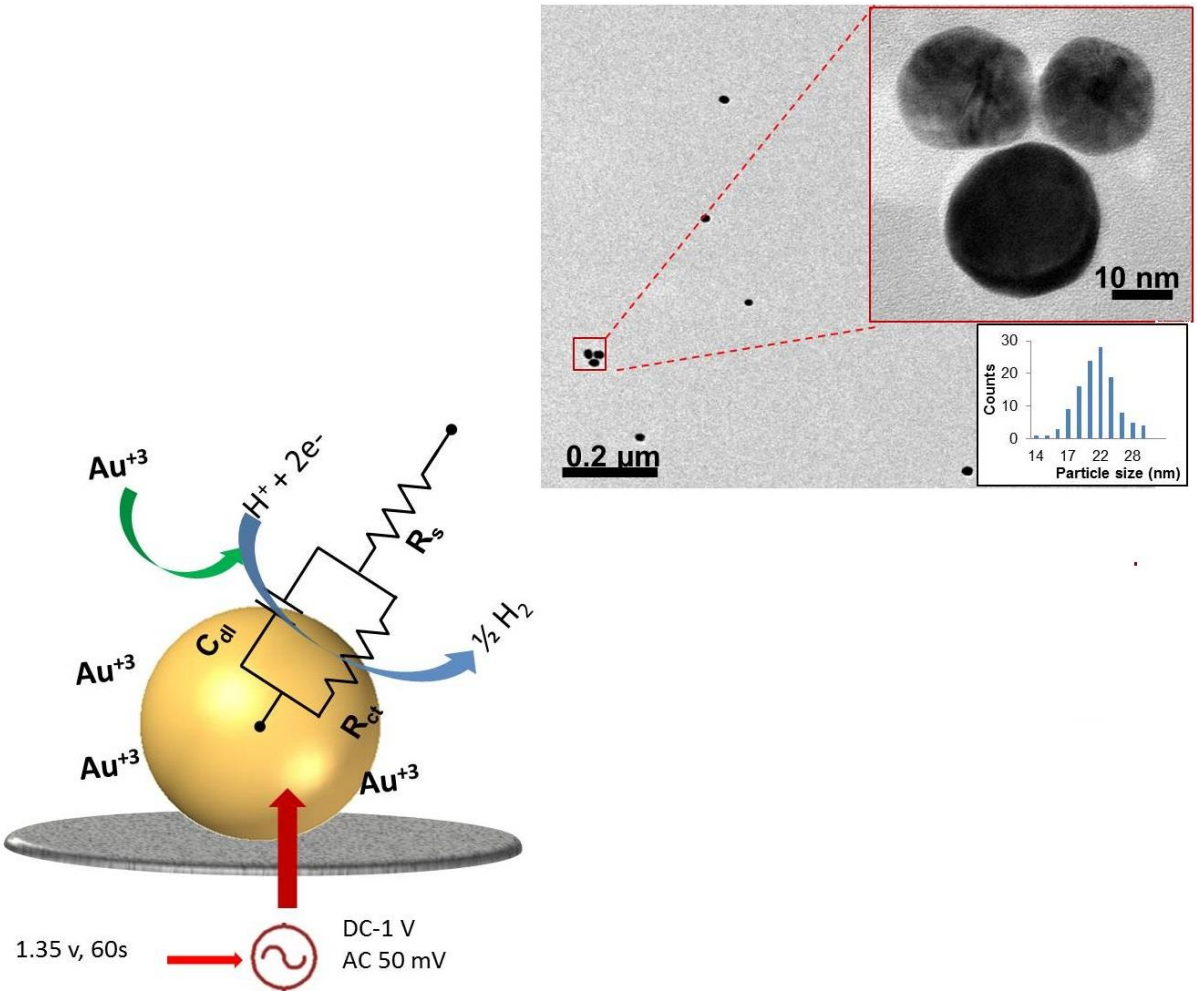

Figure 3.1: Schematic view of EIS sensing principle through hydrogen evolution reaction induced by gold nanoparticles (AuNPs). Randless circuit used to extract parameter values is overlapped on the AuNP. Top right corner Inset: Transmission Electron Microscopy (TEM) images of AuNPs including a magnified imaged.

EIS is a powerful, non-destructive and highly informative technique, which is usually used for interface characterization and kinetic parameter determination for different reactions carried out on interfaces [13-17]. EIS beside other techniques is used to study HER at different pure metals (Pd, Pt, Ni, Re, Au, Ir) and alloys (Pt- Rh, Ni – rare earth) establishing a qualitative relation between metal loading and potential variation [18-21].

In the current study a new and efficient AuNPs-based detection strategy using EIS and HER in acid solution monitored through carbon screen printed electrodes (SPCE) is described. Chronoamperometry and differential pulse voltammetry (DPV) are commonly used techniques to detect AuNPs [2-7]. This EIS-HER method is used as an alternative to the conventional EIS based on the $[Fe(CN)_6]^{3-/4-}$ or $[Ru(NH_3)_6]^{3+/2+}$ indicators [22-24]. This new detection approach is successfully applied in a magneto immuno sandwich assay for HIgG detection achieving a low limit of detection (0.31 ng mL^{-1}). Furthermore, the effect of size on the EIS signals of AuNPs has been investigated demonstrating the applicability of these techniques to evaluate the particles size. This EIS-HER method is very sensitive toward AuNPs quantification and consequently may be offered for several biosensing applications.

3.2 Materials and methods

3.2.1 Chemicals

Magnetic beads (Dynabeads M-280 Tosylactivated) were purchased to Invitrogen™ (Paisley, UK).Gold colloid, gold nanoparticles of different diameters (2, 5, 10, 15, 20, 50 nm) were obtained from British Biocell (BBi, Cardiff, UK). Tetrachloroauric acid, sodium citrate, boric acid, , PBS 10mM pH 7.4, Albumin from Bovine Serum (BSA) in powder, HCl 37% (v/v) , human IgG from serum and antihuman IgG produced in goat were purchased from Sigma Aldrich (SA, St Quentin Fallavier, France). The anti-human IgG produced in rabbit was purchased from Sigma Aldrich (Schnelldorf, Germany). Polyester substrates were purchased from MacDermid Autotype. All the inks, Carbon ink, Ag/AgCl ink and the insulating ink were purchased from Acheson™, Henkel group.

3.2.2 Apparatus

For electrochemical measurement Autolab302 potentiostat/galvanostat/ frequency-response analyzer PGST30, controlled by GPES/FRA Version 4.9 was used. Transmission electron microscope (TEM) images were taken with a JEM-2011 (Jeol, Ltd., Japan).

3.2.3 Gold nanoparticles synthesis

Gold nanoparticles were made following the procedure reported before (Turkevich et al. 1951). A solution of 0.01% (w/v) of tetrachloroauric acid is brought to boiling point under vigorous stirring, then 1.25 mL of sodium citrate at 1% (w/v) are added quickly maintaining the same conditions of stirring and the temperature for 15 more minutes until the colour of the solution turned to deep red. It was left to cool down keeping the stirring. The concentration of gold nanoparticles in the resulting product is 3nM. For the study, different concentrations of gold nanoparticles were used; 3 nM, 300 pM, 30 pM, 3 pM and 0 pM. For the characterization of gold nanoparticles at different sizes, the commercial gold nanoparticles of different diameters (2, 5, 10, 15, 20, 50 nm) were used at a concentration of 3 nM. The initial concentration of the gold nanoparticles in the commercial samples was given by the ier.

3.2.4 Screen printed electrodes fabrication

Screen printed electrodes (SPCE) consists of counter electrode, reference electrode of Ag/AgCl and working Electrode. They are fabricated on sheets of polyester substrate by the sequential deposition of different ink layers, first the graphite ink layer on the polyester substrate for working and counter electrodes, next the Ag/AgCl ink for the reference electrode and finally the isolating ink. Each layer is printed using a screen printing machine with a stencil specific for each layer, which contains the patterns of the electrodes. After its deposition each layer was cured by keeping the printed sheet at 120 ºC for 30 minutes.

3.2.5 Magneto-immunosandwich formation

The magneto immunosandwich were prepared according to previously reported procedures [2,5,25]. To prepare the immunosandwich assembly magnetic beads (Dynabeads M-280) were used as support (3 mg mL^{-1} per sample). The magnetic beads are washed in borate buffer pH 9.2, and

incubated overnight (37 ºC and agitation of 400 rpm) with Anti- human IgG, at a final concentration of 40 µg mL^{-1}l in the mixture. After the incubation the samples were washed with PBS Tween 20 at 0,5 % (v/v). In order to perform a blocking step, the conjugated magnetic beads were resuspended in a solution of PBS and 5 % (w/v) BSA for 1 hour. After the blocking step the samples were washed with PBS. Then the blocked conjugate is incubated with the antigen (in this specific case human IgG) for 1 hour at 25ºC and 400 rpm.

For the gold nanoparticle conjugation to the anti-human IgG, first the pH of the gold nanoparticle is adjusted to 9.2 using borate buffer. Then the gold nanoparticles are incubated with the antibody at a final concentration of 5 µg mL^{-1} for 1 hour at 25 ºC and 400 rpm. After the incubation a solution of BSA in milliQ water was added to reach a final concentration of 0,15 mg mL^{-1} and incubated for 1 hour at 650 rpm and 25 ºC. Next, the sample was centrifuged at 14000 rpm for 20 min at 4 ºC. The pellet was reconstituted to the initial volume in PBS.

The last incubation consisted in mixing the magnetic bead assembly with the conjugated gold nanoparticles at a ratio of 1:1 (v/v). The incubation was done for 30 minutes long under 600rpm agitation and 25 ºC. After the incubation different washing steps with PBS tween 20 at 5% (v/v), PBS and milliQ water were carried out. The assembly was finally resuspended in milliQ water.

3.2.6 Electrochemical measurements

In the EIS-HER measurements a first oxidation step for 60 s at +1.35 V was applied followed by a signal composed of DC of -1 V plus AC of 0.05 V_{RMS}. The range of frequencies went from 0.1 to 10000 Hz. The resulting data was fitted in a regular Randless circuit to extract the value of charge transfer resistance (Rtc).

The magneto immunosandwich assay for HIgG detection using EIS-HER was done. A small magnet is placed under the working electrode of the SPCE to direct the magnetic beads towards it. A mixture of 25µl of the magnetoimmunosandwich and 25µl of a 2M HCl solution is placed onto the surface of the electrode.

3.3 Results and discussion

AuNPs, prepared by the Turkevich method [26] were characterized by Transmission Electron Microscopy (TEM). Figure 3.1 (inset) shows a typical TEM image of AuNPs. Highly regular and uniform nanoparticles in the size range of 21 ± 3 nm can be observed. In order to explore the HER of AuNPs by EIS reading, a fixed concentration of AuNPs solution (1500 pM) were measured by holding the working electrodes (where AuNPs were deposited) at a constant potential of +1.35 V for 1min (electro-oxidizing Au to Au^{+3}) followed by applying a composed signal of high negative DC potential (polarization potential) plus 0.05 V of AC potential in a range frequency from 0.1 Hz to10 KHz . Different DC potentials were evaluated; Figure 3.2 shows the Nyquist representation.

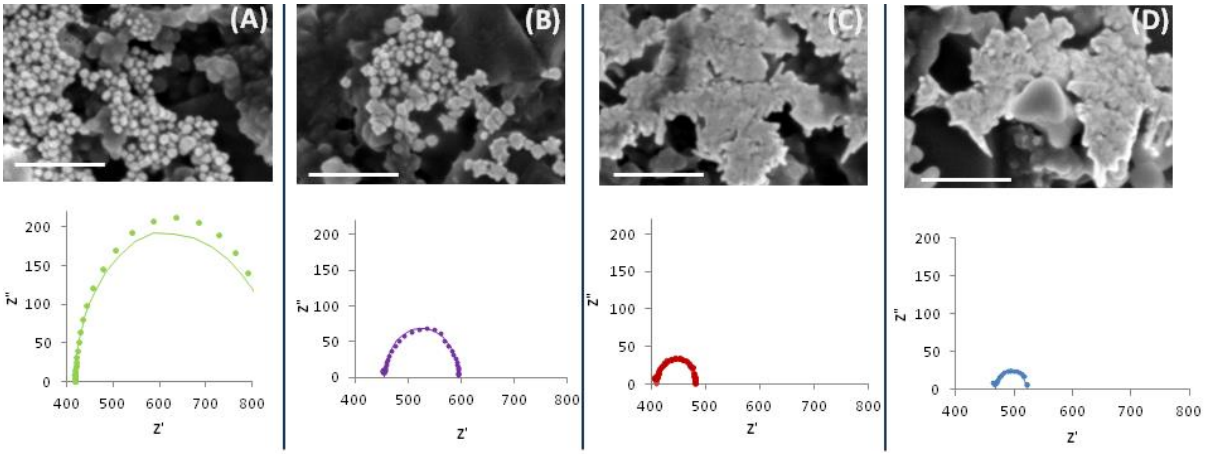

Figure 3.2: Scanning electron microscopy (SEM) images and Nyquist plot for AuNPs after potentiostatic cathodic polarization: (A) -0.6 V, (B) -0.8 V, (C) -1 V and (D) -1.2 V. The scale bare of all the SEM images is 250 nm and continuous line correspond to fit data.

For interface modelling, equivalent circuit (corresponds to Randles model) which includes the solution resistance (Rs), double layer capacitance (Cdl) and the charge transfer resistance (Rtc) is used (see scheme in Figure 3.1). The performed fitting using Randles model is fairly good and the calculated parameters obtained at different potentials (see Table 3.1) show that the Rct values decrease when the polarization potential increases. These measurements show the impedance response dependency from the applied DC potential.

Polarization potential (V)	Rs (Ω)	Rct (Ω)	C (μF)
-0.6	418	422	16.45
-0.8	456	138	21.97
-1.0	409	72	15.50
-1.2	467	54	15.78

Table 3.1: Dependence of fitting parameters on polarization potential using the Randles model shown in Figure 3.1. Rct(Ω) corresponds to the charge transfer resistance associated to the electron transfer for hydrogen evolution reaction (HER) catalysed by gold.

This fact is due to a large dependence of the HER kinetics on AuNPs' surfaces in HCl solution and at negative over potentials. The total two-electron process of hydrogen evolution proceeds at least in two steps: first, the proton donors discharge with formation of adsorbed H atoms, and, second, desorption of these atoms. In this case the hydrogen adsorption by the AuNPs is not observed, for these reason the experimental data was fitted in a common Randless circuit and used to evaluate HER. This phenomenon has been reported for metal electrodes such as gold that poorly adsorbs hydrogen [20].

From the SEM images shown in Figure 3.2 it is possible to notice the physical deformation of the circular shape of the AuNPs, which after hydrogen evolution becomes irregular, furthermore the level of irregularities in the shape increases with the increase of the negative potential applied on the AuNPs (Figure 3.2 B,C,D). This indicates that high negative potential applied changes the nanostructure of AuNPs. For later measurements -1 V was fixed as a polarization potential due to the stable impedance response and less observed deformation of the circular shape of the AuNPs compared to the case where higher potentials are used.

Different AC potentials (10, 20, 50 y 100 mV) were tested, Figure 3.3 shows the Nyquist plot obtained, not much difference was observed in terms of Rct. Nevertheless, at low potentials (10, 20 mV) the impedance response is not stable for low frequency points. On the other hand 100 mV AC was so large potential, for this reason we fixed 50 mV as AC.

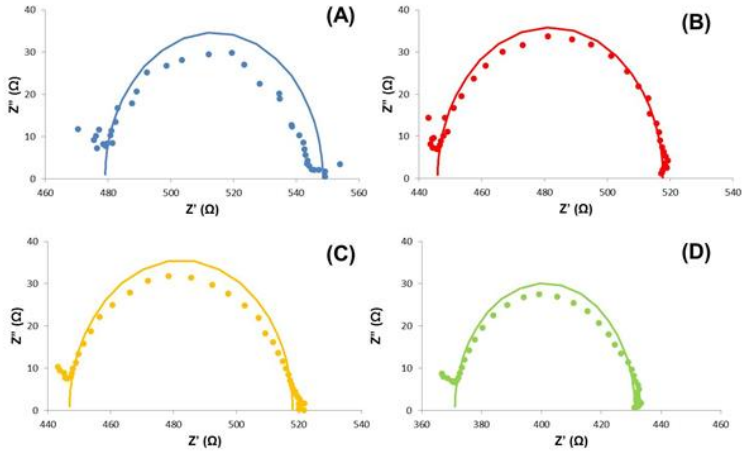

Figure 3.3: Nyquist plot of hydrogen evolution reaction induced by gold nanoparticles (AuNPs) obtained using a DC of -1V and applying different AC potentials: 10 (A), 20 (B), 50(C) y 100 (D) mV.

Finally, the +1.35 V was applied for released Au^{+3} in the solutions from the surface of the gold nanoparticles to enhance the catalytic effects on the HER. This pre-treatment condition was previous optimized and reported in different publications[2,5,25].

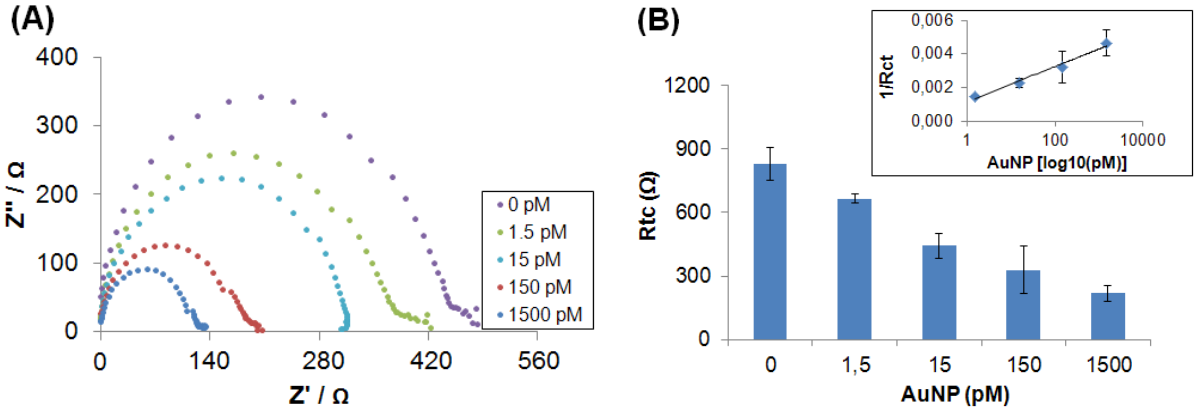

Figure 3.4: (A) Argand Diagram of increasing concentrations of AuNPs in 1 M HCl ranging from 1.5 to 1500 pM (top to bottom). (B) Histogram representing R_{tc} as a function of different AuNPs concentrations. Inset: calibration curb obtained by plotting the R_{tc} inverse value *vs* logarithm of AuNPs concentration.

After optimizing the experimental procedure, a series of EIS measurements for different amounts of AuNP are registered under the optimal conditions. Figure 3.4 A shows the impedance measurements in a Nyquist plot. The smallest semicircle corresponds to the 1500 pM AuNPs, while the biggest semicircle corresponds to the blank (HCl without AuNP). The resulting charge transfer resistances are directly represented in a histogram (Figure 3.4 B) and the inverse of these resistances are plotted vs. the logarithm of the concentration to adjust the calibration curve (inset Figure 3.4 B).

The LOD of 0.67 pM is calculated by the value obtained by interpolation of the blank plus three times its standard deviation. The method shows high reproducibility being its RSD of around 13 %, obtained for 3 repetitive assays.

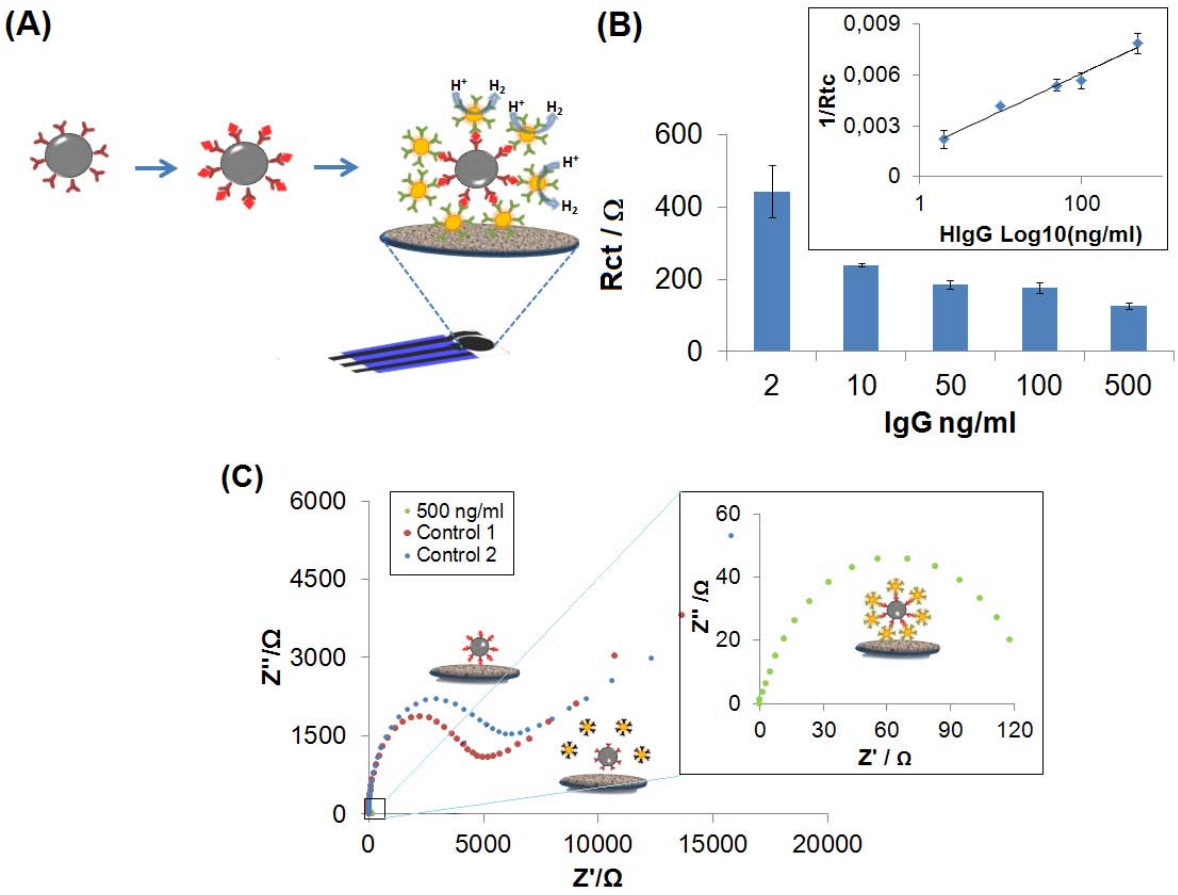

Figure 3.5: (A) Schematic of the magneto sandwich immunoassay for HIgG detection using AuNPs as label. (B) Rct values vs different concentrations of HIgG. Inset: Calibration curve obtained by plotting 1/Rct vs. the logarithm of different concentrations of HIgG.(C)Selectivity of the immunosandwich assay: Nyquist plots obtained for the control 1 (BSA), no antibody as a control two and 500 ng mL^{-1} as a positive.

Once the impedimetric detection of AuNP catalysis was performed and its effectiveness as a transduction method demonstrated, it is afterwards applied in a standard immunoassay for protein detection. In Figure 3.5(A) a schematic of the performed magneto inmunosandwich for human IgG (HIgG) detection is displayed. The capturing antibody, immobilized onto the magnetic bead, is an antihuman IgG, polyclonal, developed in goat. The detection antibody, conjugated with gold nanoparticles, is another antihuman IgG developed in rabbit. Figure 3.5(B) shows the obtained Rct values with the corresponding error bars achieved using different amounts of HIgG. The signal of AuNP is directly related to the amount of the formed immunoconjugates. A linear biosensing response within the range from 2 – 500 ng mL^{-1} IgG with 0.31 ng mL^{-1} as limit of detection (LOD) was obtained from the inverse of the obtained Rct.

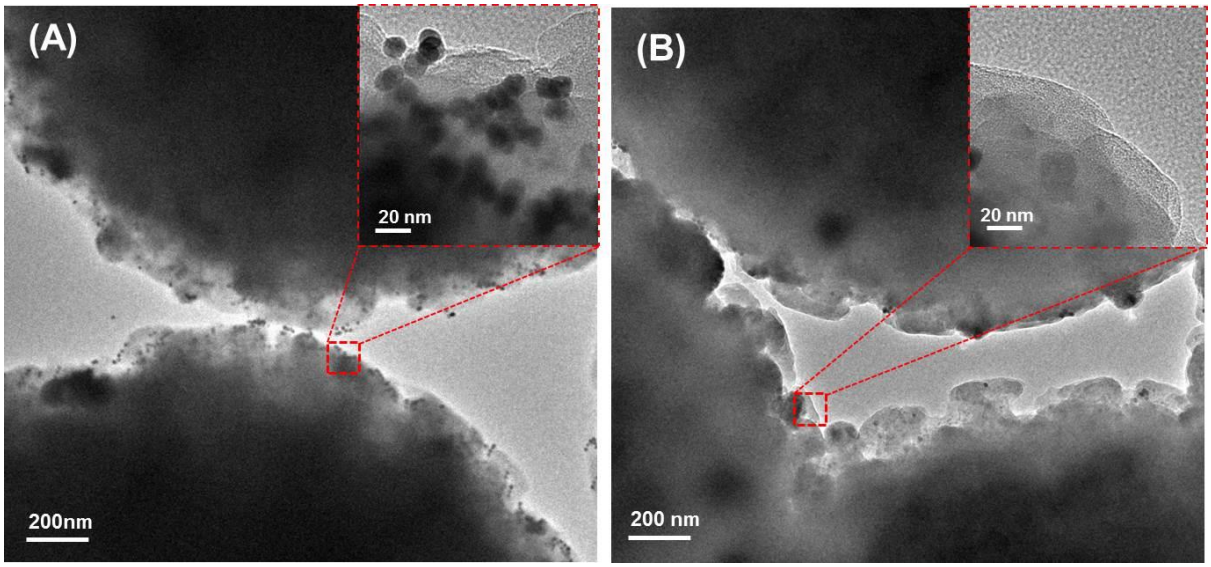

Figure 3.6: Transmission electron microscope (TEM) of magnetic beads modified with (A) and without (B) AuNP anchored through the immunosandwich (magnetic bead-anti-human IgG / human IgG / anti human IgG – AuNPs).

Figure 3.6 shows TEM image of magnetic beads with (Figure 3.6 A) and without (Figure 3.6 B) gold nanoparticles anchored through the inmunosandwich (Magnetic bead -Anti- human IgG / humanIgG/ Anti- human IgG-Au NPs). The small black points corresponding to AuNPs covering the surface of the MBs (big spheres) can be observed in Figure 3.6 A) demonstrating the magneto inmunosandwich formation.

LOD was calculated by the interpolation of the blank plus three times the standard deviation of the blank. With this new AuNP based strategy using EIS the LOD is improved in comparison to the previously one obtained when the chronoamperometry was used for AuNPs detection[5]. Moreover, high reproducibility with a RSD of around 13% was observed for HIgG detection. The selectivity of the assay is demonstrated performing two control assays using a non-specific protein (BSA instead of HIgG) as 'control 1' and another one without AuNPs as 'control 2' (see Figure 3.5 C).

On the other hand, the Au NP size effect in the electrochemical signal amplification was evaluated before[13]. For this reason, this new method represents a quite fast and cost efficient method to determine the size of AuNPs. **Figure 3.7** shows the results of EIS-HER characterization of AuNPs (from BritishBiocell) of different sizes (2, 5, 10, 15, 20, 50 nm). In Figure 3.7 A the EIS-HER data is presented in a Nyquist plot, showing the semicircles resulting from the measurement of the

nanoparticles of different diameters. The biggest semicircles correspond to the smallest gold nanoparticles (2 nm diameter) with a clear tendency of EIS decrease when AuNPs size is increased. Although EIS is applied before for AuNP size evaluation [13] this EIS-HER method clearly shows an improvement of the sensitivity and a better discrimination of AuNPs in the size range of 2-50 nm. The histograms for different AuNPs sizes as a function of Rct were represented in **Figure 3.7** B and the corresponding TEM images as insets are also shown. High reproducibility of the EIS-HER measurements with a RSD of 12 % is observed.

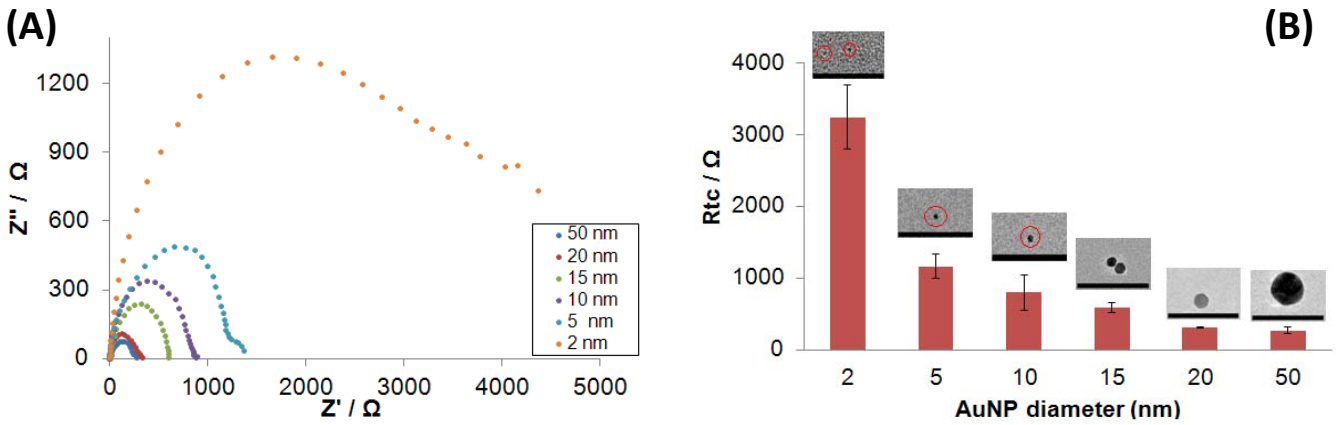

Figure 3.7: Impedimetric measurement of AuNPs of various diameters and in the same concentration. Nyquist plot (A) and histograms of Rct value vs. AuNPs diameter (B). The scale bare of all the TEM images is 100 nm.

3.4 Conclusions

In summary we have demonstrated that the Electrochemical Impedance Spectroscopy (EIS) combined with hydrogen evolution reaction (HER) constitutes a high reproducible and efficient method for the detection of different amounts of AuNPs in acidic medium. This EIS-HER method combines the advantages of EIS with HER induced by AuNPs. Furthermore, the proposed method displays dramatic improvements of the analytical performance in terms of a wide linear range (2 – 500 ng mL^{-1}) of response along with a good LOD (0.31 ng mL^{-1}) and sensitivity for a model protein (Human IgG) detection in a magnetoimmunoassay and the gold nanoparticle size characterization. In addition, it is also important to emphasize that with this new strategy for the magneto immunosandwich a reduction of one order of magnitude in the LOD is obtained, compared with chroamperometric technique normally used for this detection reported before. On the other hand, the use of this EIS-HER as a sensitive technique capable of differentiating the signal generated by the presence of AuNPs of different sizes can be extended to other nanoparticles and related catalytic

reactions. We envisage the use of such sensing technology to be with interest for various sensing and biosensing applications where nanoparticles or other nanomaterials may be involved.

3.5 Bibliorgaphy

(1) Bonanni, A.; Esplandiu, M. J.; del Valle, M. *Electrochim. Acta* **2008**, *53*, 4022-4029.

(2) de la Escosura-Muñiz, A.; Maltez-da Costa, M.; Sánchez-Espinel, C.; Díaz-Freitas, B.; Fernández-Suarez, J.; González-Fernández, Á.; Merkoçi, A. *Biosensors and Bioelectronics* **2010**, *26*, 1710-1714.

(3) de la Escosura-Muniz, A.; Parolo, C.; Maran, F.; Merkoci, A. *Nanoscale* **2011**, *3*, 3350-3356.

(4) Espinoza-Castañeda, M.; de la Escosura-Muñiz, A.; González-Ortiz, G.; Martín-Orúe, S. M.; Pérez, J. F.; Merkoçi, A. *Biosensors and Bioelectronics* **2013**, *40*, 271-276.

(5) Maltez-da Costa, M.; de la Escosura-Muniz, A.; Merkoci, A. *Electrochem. Commun.* **2010**, *12*, 1501-1504.

(6) Maltez-da Costa, M.; de la Escosura-Muniz, A.; Nogues, C.; Barrios, L.; Ibanez, E.; Merkoci, A. *Small* **2012**, *8*, 3605-3612.

(7) Maltez-da Costa, M.; de la Escosura-Muniz, A.; Nogues, C.; Barrios, L.; Ibanez, E.; Merkoci, A. *Nano Lett.* **2012**, *12*, 4164-4171.

(8) Saha, K.; Agasti, S. S.; Kim, C.; Li, X. N.; Rotello, V. M. *Chem. Rev.* **2012**, *112*, 2739-2779.

(9) Ren, Y.; Deng, H.; Shen, W.; Gao, Z. *Anal. Chem.* **2013**, *85*, 4784-4789.

(10) Gao, Z.; Deng, H.; Shen, W.; Ren, Y. *Anal. Chem.* **2013**, *85*, 1624-1630.

(11) Derkus, B.; Emregul, E.; Yucesan, C.; Cebesoy Emregul, K. *Biosensors and Bioelectronics* **2013**, *46*, 53-60.

(12) Shen, W.; Deng, H.; Ren, Y.; Gao, Z. *Biosensors and Bioelectronics* **2013**, *44*, 171-176.

(13) Bonanni, A.; Pumera, M.; Miyahara, Y. *Phys. Chem. Chem. Phys.* **2011**, *13*, 4980-4986.

(14) Katz, E.; Willner, I. *Electroanalysis* **2003**, *15*, 913-947.

(15) Park, S. M.; Yoo, J. S. *Anal. Chem.* **2003**, *75*, 455A-461A.

(16) Xianzong, X.; Rieth, L.; Caldwell, R.; Diwekar, M.; Tathireddy, P.; Sharma, R.; Solzbacher, F. *Biomedical Engineering, IEEE Transactions on* **2013**, *60*, 2943-2951.

(17) Xie, X.; Rieth, L.; Merugu, S.; Tathireddy, P.; Solzbacher, F. *Applied Physics Letters* **2012**, *101*, -.

(18) Castro, B. E.; Milocco, R. H. *J. Electroanal. Chem.* **2005**, *579*, 113-123.

(19) Chen, F. Y.; Liu, J. G.; Chen, H.; Yan, C. W. *Int. J. Electrochem. Sci.* **2012**, *7*, 3750-3764.

(20) Khanova, L. A.; Krishtalik, L. I. *J. Electroanal. Chem.* **2011**, *660*, 224-229.

(21) Ortega-Chavez, L.; Herrera-Peraza, E.; Verde, Y. *J. New Mat.Electrochem. Syst.* **2008**, *11*, 125-130.

(22) Chang, B. Y.; Park, S. M. In *Annual Review of Analytical Chemistry, Vol 3*; Yeung, E. S., Zare, R. N., Eds.; Annual Reviews: Palo Alto, 2010; Vol. 3, p 207-229.

(23) Rodriguez, M. C.; Kawde, A. N.; Wang, J. *Chem. Commun.* **2005**, 4267-4269.

(24) Wei, Y.; Kong, L. T.; Yang, R.; Wang, L.; Liu, J. H.; Huang, X. J. *Chem. Commun.* **2011**, *47*, 5340-5342.

(25) Ambrosi, A.; Castañeda, M. T.; Killard, A. J.; Smyth, M. R.; Alegret, S.; Merkoçi, A. *Anal. Chem.* **2007**, *79*, 5232-5240.

(26) Turkevich, J.; Stevenson, P. C.; Hillier, J. *Discussions of the Faraday Society* **1951**, 55-&.

Chapter 4

An Iridium oxide nanoparticle and polythionine thin film based platform for sensitive Leishmania DNA detection

Related publication

Journal of Materials Chemistry B, 2015, 3, 5166-5171.

An iridium oxide nanoparticle and Polythionine thin film based platform for sensitive Leishmania DNA detection.

Carmen C. Mayorga-Martinez[‡a], Alejandro Chamorro-Garcia[‡a,b], Lorena Serrano [c], Lourdes Rivas [a,b], Daniel Quesada-Gonzalez[a,b], Laura Altet[c], Olga Francino[b,c], Armand Sánchez[c,e] and Arben Merkoçi [a,d]

[a] Nanobioelectronics&Biosensors Group, Institut Catala de Nanociencia I Nanotecnologia (ICN2) Edifici ICN2, Campus UAB, BEllaterra (Barcelona) 08193, Spain.

[b] Autonomous University of Barcelona, UAB campus, 08193 Bellaterra, Spain

[c] Ventgenomics, Edifici Eureka, Parc de recerca de la UAB, 08193 Bellaterra (Barcelona), Spain

[d] Institució Catalana per la Recerca i Estudis avançats (ICREA) Passeig Lluis Companys 23, 08010, Barcelona, Spain

[e] Centre for Research in Agricultural Genomics-CSI-IRTA-UAB-UB, Campus UAB, 08193 Cerdanyola del Valles, Catalonia, Spain

[‡] These authors contributed equally to this work.

Summary

An impedimetric label-free genosensor for high sensitive DNA detection is developed. This system is based on a screen-printed carbon electrode modified with thionine layer and iridium oxide nanoparticles (IrOxNPs). Aminated oligonucleotide probe is immobilized onto the IrOxNPs NP/polythionine modified electrode and ethanolamine was used as a blocking agent. Different diluted PCR amplified DNA samples have been detected. The selectivity and reproducibility of this system is studied and the system was high reproducible with RSD ≈ 15 % and sensitive enough while using 2% of ethanolamine during the blocking step employed for the genosensor preparation.

4.1 Introduction

In the field of biosensors electrochemical impedance spectroscopy (EIS) becomes especially well-suited for the detection of binding events which take place on the electrode's surface [1-3]. This capability to discriminate small changes on surfaces makes EIS capable of detecting interactions of biomolecules close to the surface of the electrodes, and hence enabling a label free detection of a biomolecules thanks just to the changes caused by them due to the biological recognition event [3]. Specially, impedimetric label free DNA genosensors based on nucleic acid hybridization have received considerable attention due to screening of samples in research of specific DNA sequences related to a specific disease, or state of risk and represent a powerful tool in the field of diagnosis [4-6]. They offer great advantages due to simplicity, speed, miniaturization, sensitivity, selectivity and low cost for detection of desired DNA sequence or mutant genes [5,7].

The EIS response depends on the modifications of the electrode surface and the interaction of the analyte with the specific recognition elements. Such alterations affect the capability of the redox indicator to reach the electrode surface and consequently its redox conversion. In this way the charge transfer may either increase or decrease. In this type of measurements becomes of special importance the nature of the electrode surface, which determines in great deal the electron transference between the electrode and the redox indicator. It is common to find in the bibliography examples of electrode surface modifications by electropolymerized layers or self-assembled monolayers, in order to enhance the electron transfer between the electrode surface and a redox indicator[8]. With this aim, polythinoine layers have been reported to be used for proper modifications of sensors [9,10].

The immobilization of the single strand DNA (ss-DNA; to be used as receptor) has been studied over a variety of substrates/electrodes using various methods such as adsorption, covalent coupling and entrapment [11-14]. However, various issues like poor compatibility of immobilizing materials onto the transducer, poor binding of DNA, creation of inactive or poor conducting layers and less surface area including poor stability were raised.[15,16] Nanomaterials including metal nanoparticles, nanowires, nanorods, carbon nanotubes, and graphene have been successfully used in impedimetric biosensors to amplify detection signal and achieve lower detection limit due to their high surface area, favourable electronic properties and electrocatalytic activity as well as good biocompatibility induced by the nanometer size and specific physicochemical characteristics [17]. Nanoparticles, due to their small size, display interesting properties at the nanoscale level. First, due to their shape and size they can increase the surface area. Second, thanks to the electrostatic interactions they can be

adsorbed or attached onto different surfaces. Third, thanks to the functional groups on their surface, they can be used as anchor points for other molecules [18].

Here we exploit the iridium oxide nanoparticles (IrOxNPs) deposited over a polythionine layer which has been electro polymerized onto the carbon transducer with the aim to enhance the properties of the sensor for the detection of amplified DNA (see Figure 4.1). IrOxNPs has proved to be good candidates for being applied in biosensing platforms, especially thanks to the citrate groups they present on their surface. The citrate groups allow tailoring of different biomolecules thanks to the non-covalent bond formation between with amino groups on the biomolecule.[19,20] The platform developed shows good performance for electrochemical sensing of PCR amplified DNA of dog affected by leishmania, this target is used as a proof a concept. Different dilutions of PCR amplified DNA samples are detected showing high sensitivity while detecting up to 1000 times diluted samples. The system offers the possibility to be applied for diagnostics based on DNA detection, as the pathogen detection (or infectious disease) both in veterinary and human file.

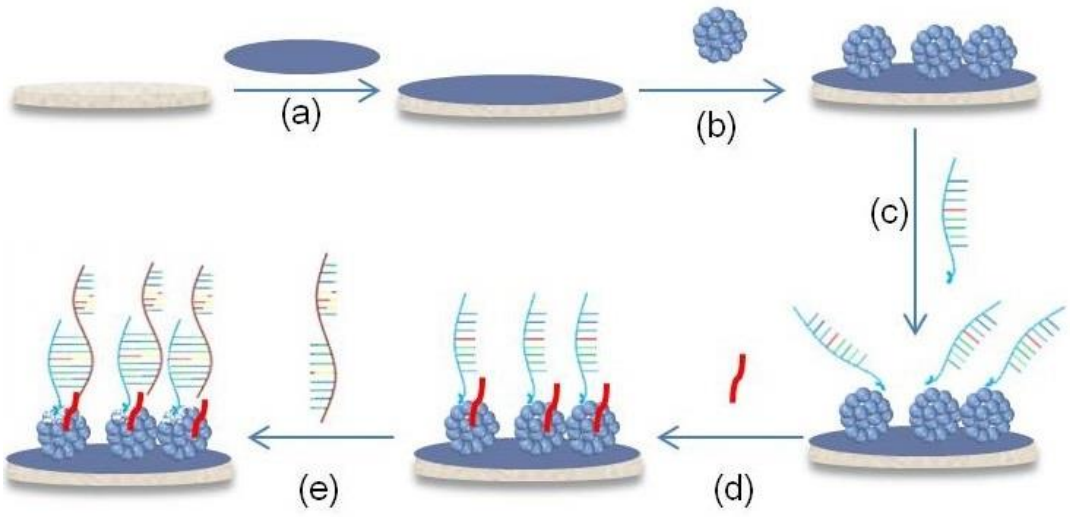

Figure 4.1: Schematic representation of the procedure for the impedimetric label-free genosenor fabrication. Thionine electropolymerization (a), deposition of Iridium oxide nanopartciles (IrOxNPs) (b), immobilization of ss-DNA (c), blocking step with etanolamine (d) and hybridization with complementary target (e).

4.2 Experimental section

4.2.1 Reagents and solutions

The reagents used for SPCEs fabrication were: Autostat HT5 polyester sheet (McDermid Autotype, UK), Electrodag 423SS carbon ink, Electrodag 6037SS silver/silver chloride ink, and Minico 7000 Blue insulating ink (Acheson Industries, The Netherlands). Trizma hydrochloride, sodium chloride, sodium citrate, ethylenediamine-tetraacetic acid disodium salt dihydrate (EDTA), ethanolamine, potassium hexachloroiridate-(IV), sodium hydrogencitrate and thionine acetate were purchased from Sigma-Aldrich (St. Louis, MO). Potassium hexacyanoferrate(II) three hydrate, potassium hexacyanoferrate (II) and sulphuric acid were purchased from Panreac Quimica S.A (Barcelona, Spain). Milli-Q water was obtained from purification system and all solutions were prepared with ultra-pure water from a Millipore-MilliQ system. Washing solutions in the label-free assay consisted of TE (0.01M tris and 0.001M EDTA) buffer, pH 8, 2xSSC (300 mM Sodium Chloride and 30 mM sodium citrate) buffer, pH 7.2, containing 1% ethanolamine and Tris (0.1 M) buffer, pH 7.2 containing 1% ethanolamine.

4.2.2 Apparatus

Electrochemical experiments were performed using an electrochemical analyzer Autolab 20 (Eco-Chemie, The Netherlands) which was connected to a personal computer using a software package GPS 4.9 (General Purpose Electrochemical System). Impedance measurements were performed by using an Autolab302 potentiostat/galvanostat/frequency-response analyzer PGST30, controlled by GPES/FRA Version 4.9. A semi-automatic screen-printing machine DEK248 (DEK International, Switzerland) was used for the fabrication of the screen-printed carbon electrodes (SPCEs).

4.2.3 Synthesis of iridium Oxide Nanoparticles

Potassium hexachloroiridate-(IV) 2.6x10-5 M solution was mixed with sodium hydrogencitrate 1.6x10-2 M solution. The pH of the red brown solution was adjusted to pH 7.5 with a 0.25 M NaOH solution and then refluxed in an oil bath with constant stirring for 30 min. As the mixture cooled to room temperature, the pH was again adjusted to 7.5 with a reflux for 30 min. This procedure was repeated until pH reached a constant value of 7.5. Finally the solution was refluxed 2 h more with

oxygen bubbling. At the end of this step, a deep blue solution of IrO_2 nanoparticles was obtained. The solution was stocked in a glass-stoppered flask and at 4ºC when not in use.

4.2.4 PCR amplified products

The samples used in the study are PCR amplified products of extracted DNA as described in Francino et al 2006.[21] Briefly, for the DNA extraction, peripheral whole blood was washed in TE buffer pH 8.0 to disrupt the erythrocyte membranes until the leukocyte pellet was white. Leukocytes were then lysed by incubation of the pellet in 0.1ml of PK buffer (50mM KCl, 10mM Tris pH 8.0, 0.5% Tween-20 and 23µg of proteinase K) at 56ºC for 5h. Before running the PCR the proteinase K was inactivated by incubation of the samples at 90ºC for 10min. DNA was then diluted 1/5 in water.

The PCR amplification Leishmania, is the target used as a proof of concept for the developed system. TaqMan-MGB probe (FAM-50-AAAAATGGGTGCAGAAAT-30-non-fluorescent quencher-MGB) and PCR primers (Forward: AACTTTTCTGGTCCTCCGGGTAG and Reverse: ACCCCCAGTTTCCCGCC) were used to target conserved DNA regions of the kinetoplast minicircle DNA from L. infantum. Leishmania primers and probe were added at 900 and 200 nM, respectively. PCR was carried out in 25 ml final volume reaction mixture containing TaqMan Universal PCR Master Mix with UNG Amperase (Life technologies). The thermal cycling profile was 50 ºC for 2 min, 95 ºC for 10 min, 40 cycles at 95 ºC for 15 s and 60 ºC for 1 min. Each amplification run contained positive and negative controls.

4.2.5 Genosensor preparation

Screen printing electrodes were fabricated by sequential deposition of a graphite ink, Ag/AgCl ink and insulating ink on a polyester substrate. The polyester substrate was dried at 120 °C for 45 min (graphite) and 30 min (Ag/AgCl and insulating) after the deposition of each layer.

Before modification with thionine layer and IrOxNPs, SPCEs were activated by applying a 3 µA current during 120 sec in 0.1 M H_2SO_4 and then the electrodes were washed with Milli-Q water. 100µL Of thionine solution 0.5 mM was dropped onto the working surface of SPCE, and 20 CVs scans from 0.1 to -0.55 V at 50 mV/s were applied. The electrodes were washed with TE buffer. Afterwards 8µL solution of IrOxNPs suspension were dropped onto the working surface of SPCE and dried at room temperature (1 hour), and the electrodes were washed with TE buffer.

After modification of SPCE with thionine and IrOxNPs, adsorption of a 0.5 ng μL^{-1} of 3'aminated oligonucleotide probe (5'-NH_2-TEG-

atatatatatatataTTTTCTGGTCCTCCGGGTAGGGGCGTTCTG-3') onto the electrode modified surface was performed, leaving an aliquot of 10 µL overnight at 4 °C. Then the electrode was washed with TE buffer pH, to remove the excess of oligonucheotide. Free surface sites were blocked placing a drop of 40 µL of ethanolamine solution contained desired concentration for 90 min, followed by a washing step with SSC, pH 7.2, buffer containing 1% ethanolamine.

Hybridization step was performed using synthetic oligonucleotide (for system optimization) and PCR amplified product. The hybridization with synthetic oligonucleotide target was performed at room temperature by placing 30 µL of synthetic complementary target solutions (5'-TTTCTGCACCCATTTTTCCATTTTCGCAGAACGCCCCTACCCGGAGGACCAGAAAA-3') in 2xSSC buffer, pH 7.2, containing 1% ethanolamine, onto the surface of the genosensor for 45 min and then rinsing with Tris buffer pH 7.2 containing 1% ethanolamine.

The PCR amplified DNA of dog with Leishmania (140 bp) was used to perform the hybridization instead of commercial oligonucleotide target using the same experimental condition as those used for commercial oligonucleotide. Before the hybridization, the PCR amplified DNA was denatured by heating at 95ºC for 5min followed by immersing in ice until the use. The experimental control was performed using PCR amplified DNA of dog without Leishmania (blank).

4.2.6 Electrochemical measurements

The electrochemical measurement was performed by electrochemical impedance spectroscopy (EIS) in 1mM $[Fe(CN)_6]^{3-/4-}$ with 0.1 M KCl as redox probe. A sinusoidal potential modulation of ± 10 mV amplitude in the 0.1 Hz to 100 kHz frequency range, with logarithmic scale of 10 points per decade, was superimposed onto the formal potential of the redox couple, $[Fe(CN)_6]^{3-/4-}$ (0.24 V vs Ag/AgCl). Nyquist diagrams were also recorded. Electrochemical experiments were carried out at room temperature.

4.3 Results and discussion

Electrochemical impedance spectroscopy (Figure 4.2) and cyclic voltammetry (Figure 4.3) were used for the characterization of each fabrication step of the genosensor. Impedance data is usually

studied using an equivalent circuit which helps understanding the behavior of the electrode-electrolyte interface onto the biosensor surface.[2]

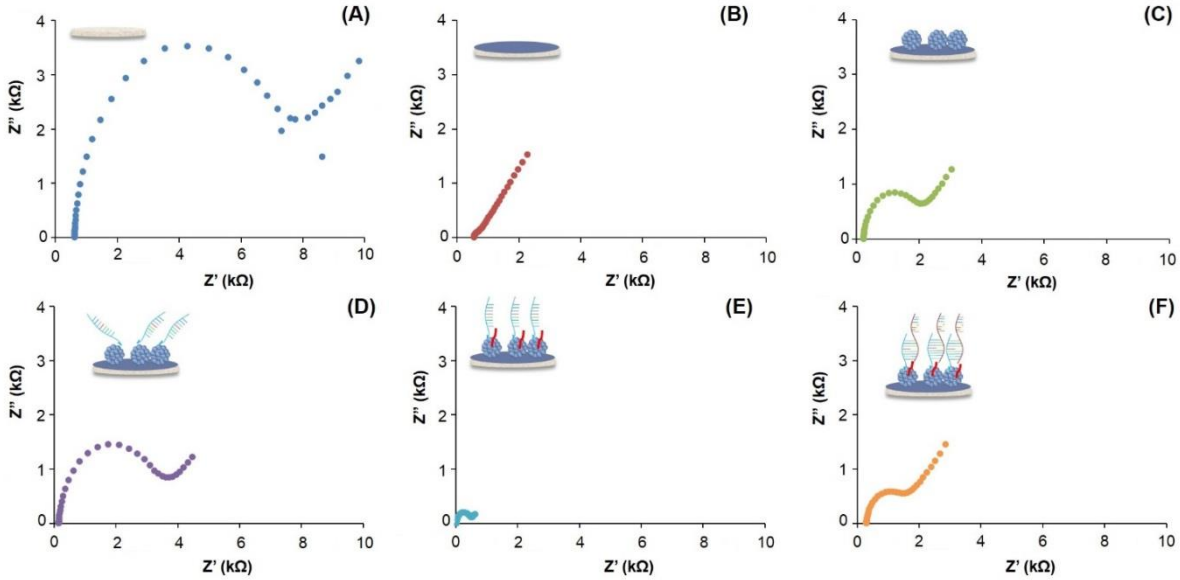

Figure 4.2: EIS characterization of the bare electrode (A) and after of: electrodeposition of polythionine (B), Iridium oxide (IrOxNPs) adsorption (C), oligonucleotide probe immobilization (D), blocking step with ethanolamine (E) and hybridization with complementary target (F).

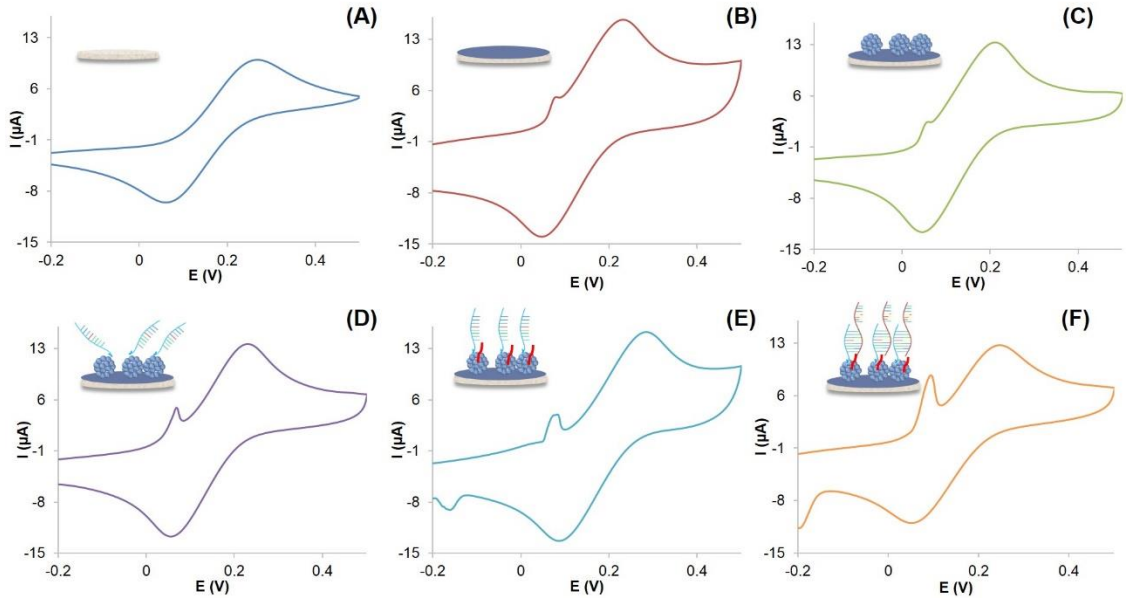

Figure 4.3: Ciclic voltamperograms of bare electrode (A) and after of: electrodeposition of polythionine (B), Iridium oxide (IrOxNPs) adsorption (C), oligonucleotide probe immobilization (D), blocking step with ethanolamine (E) and hybridization with complementary target (F).

The observed high electron transfer rate (Figure 4.2 A and Figure 4.3 A) indicates that the redox mediator doesn't face any obstacle while reaching the surface of the bare electrode. Nevertheless, when the electrode is modified by electrodeposited polythionine layer, the Rct value decreases and a capacitive behavior is observed (Figure 4.2 B and Figure 4.3 B). This demonstrates that the polythionine layer is well deposited and it enhances the electron transfer. However, once IrOxNPs are adsorbed onto the modified electrode, a well-defined semicircle (Figure 4.2 C) and a decreasing of the ΔE of around 20 mV (Figure 4.3 C) were observed. The improvement of the change transfer was probably due to an electrode effective area increases (see SEM images of Figure 4.4) and the redox activity of the IrOxNPs.[19,22-24] After the oligonucleotide capture probe was attached to the IrOxNPs a charge transfer increase is observed (Figure 4.2 D). The negative charges surrounding the IrOxNPs allow the attachment of the positively charged amino groups through non-covalent bonding. The charge transfer increase is due to negative charge from oligonucleotide capture probe that acts as an electrostatic barrier between SPCE/PTH and the redox indicator. The blocking effect of ethanolamine was evidenced by a decrease of charge transfer (Figure 4.2 E and Figure 4.3 E). The hybridization of DNA target with the capture probe represents a greater obstacle to the redox mediator due to the negative charge of phosphate backbone of DNA (Figure 4.2 F and Figure 4.3 F).

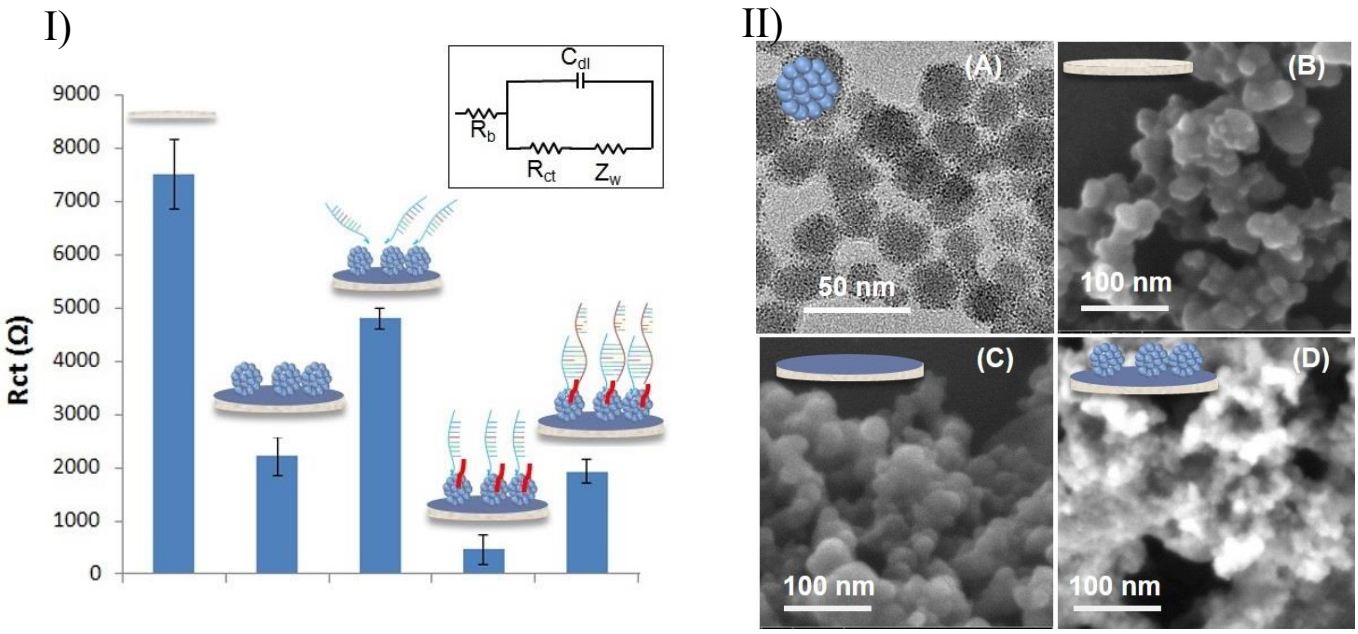

Figure 4.4: Characterization of Iridium Oxide Nanoparticles (IrOxNPs) and the modification of the screen printed Carbon electrodes by TEM and SEM and electrochemically by Electrochemical Impedance spectroscopy (EIS). **Left I)**: Rct values each fabrication step of the genosensor. Inset: equivalent electrical circuit: Randless model modified with Warburg impedance (Zw) composed by resistance of the solution (Rb) on the electrode, capacity of the double layer (Cdl) and charge transfer resistance (Rct) associated to the redox processes on the electrode surface used to calculate Rct value. Error bars correspond to the standard deviations obtained from triplicate experiments. **Right II):** (A) TEM images of IrO2 NPs. SEM images of SPCE (B), SPCE with polythionine electrodeposited onto the working electrode surface (C) and SPCE/polythionine with IrO2 NPs adsorbed onto its surface (D). SEM images were taken using backscattered electrons mode.

The morphological modification of SPE is also studied using scanning electron microscopy (SEM) image. Figure 4.4 II)(B) shows a SPE after activation step using H_2SO_4, while Figure 4.4 II)(C) displays the polythionine layer as a thin film smoothing the SPE surface. Finally in Figure 4.4 II)(D), the distribution of the IrOxNPs (brighter dots) onto the SPE/polythionine are observed. Backscatter electrons mode was used for the enhancement of the contrast between IrOxNPs and SPE/polythionine surface.

The Rct values obtained from Nyquist plots after each surface modification step of the proposed system are shown in Figure 4.3 and Figure 4.4 I). On the basis of the charge transfer kinetics of the $[Fe(CN)_6]^{3/4}$ (redox probe), the faradaic impedance spectra were modelled using the equivalent circuit approach of Randles model modified with Warburg impedance (see Figure 4.4 I) inset).

The morphological characterization of IrOxNPs was studied. Figure 4.4 (A) displays a transmission electron microscopy (TEM) micrograph, where a clusters morphology of around 20 nm composed by smaller IrOxNPs was observed.

X-ray photoelectron spectroscopy and UV-visible spectrophotometry studies also were performed (see Figure 4.5 and Figure 4.6). Figure 4.6 shows the survey XPS analysis (Figure 4.6 A) and high-resolution XPS spectra of the Ir 4f and O 1s regions (Figure 4.6 B). The XPS spectra of the Ir 4F region revealed two main features with signals at 62.5 and 65.3 eV, which correspond to Ir 4f 7/2 and Ir 4f 5/2 orbitals, respectively. Furthermore, the O 1s region shows two features. The position of the main feature is around 532.5 eV that is similar of O 1s observed in standard IrOxNPs single crystal,[25] the additional feature present the binding energy of 530.2 eV. The UV-Vis spectra reveals a characteristic peak of Ir(IV) oxides with a maximum around 580 nm (Figure 4.5). These results are in good agreement with high oxidation state 4^+ of iridium reported before. [19,24,25]

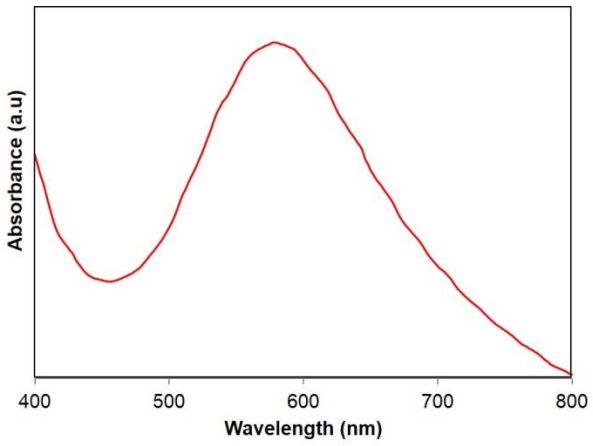

Figure 4.5: UV-Vis spectra of Iridium Oxide Nanoparticles (IrOxNPs).

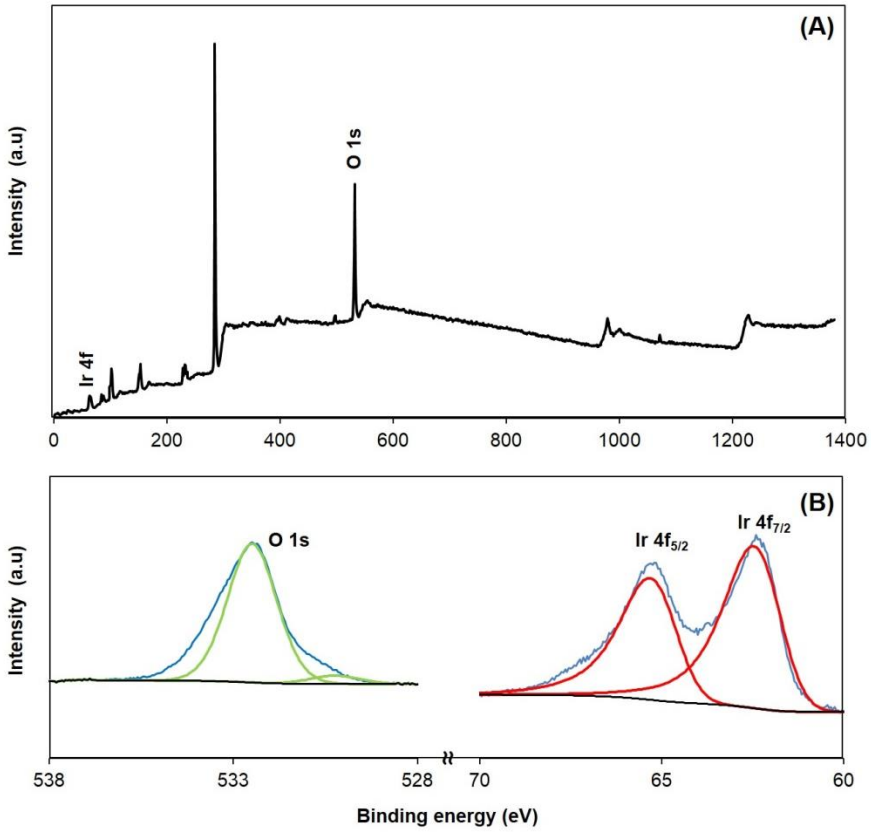

Figure 4.6: Survey XPS analysis (A) and high resolution XPS spectra of O 1s and Ir 4f of IrO_2 NPs (B).

Different dilutions of PCR amplified DNA (1:10, 1:100 and 1:1000) were detected using the system described above. The Rtc values were recorded as a function of PCR amplified DNA (Figure 4.7 A) showing lower impedance values for more diluted samples. These results demonstrate that the system is suitable to detect DNA but with a relatively poor reproducibility (RSD of 26%).

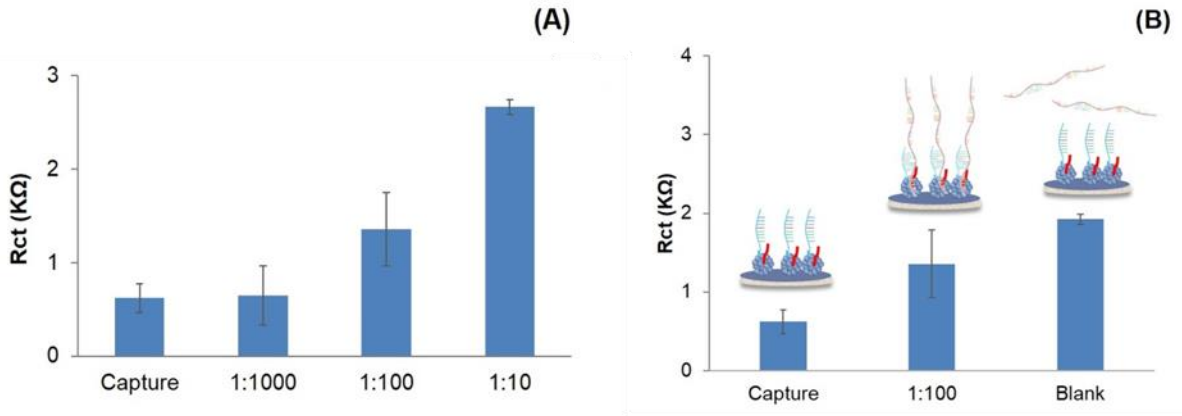

Figure 4.7 : (A) Rct as a function of different dilutions of PCR amplified DNA samples. (B) Comparison of Rct values of the genosensor modified with the capture probe and hybridized with PCR amplified DNA samples of dog affected (Positive) or not (Blank) with Leishmania. Dilutions of 1:10 and 1:100 for the blank and positive samples respectively and 0.1% ethanolamine during the blocking step was used.

Selectivity is a very important parameter to be considered for DNA genosensors. To evaluate the selectivity of this system, PCR product of dog with (positive) and without (blank) Leishmania were compared. Blank diluted 1:10 had a signal comparable to the positive sample diluted 1:100. (see Figure 4.7). To improve the selectivity and the reproducibility of this system, the blocking step during genosensor fabrication was modified using 2% of ethanolamine instead of 0.1%. The resulting data are shown in Figure 4.8. The Rct values are quite different for the different dilutions of the PCR product (RSD of 15%) therefore we could say that this system is more sensitive. A good selectivity of the genosensor toward DNA detection also was evidenced by the neglected responses toward blank (see Figure 4.8) while the difference between capture probe and blank was of 0.09 kΩ.

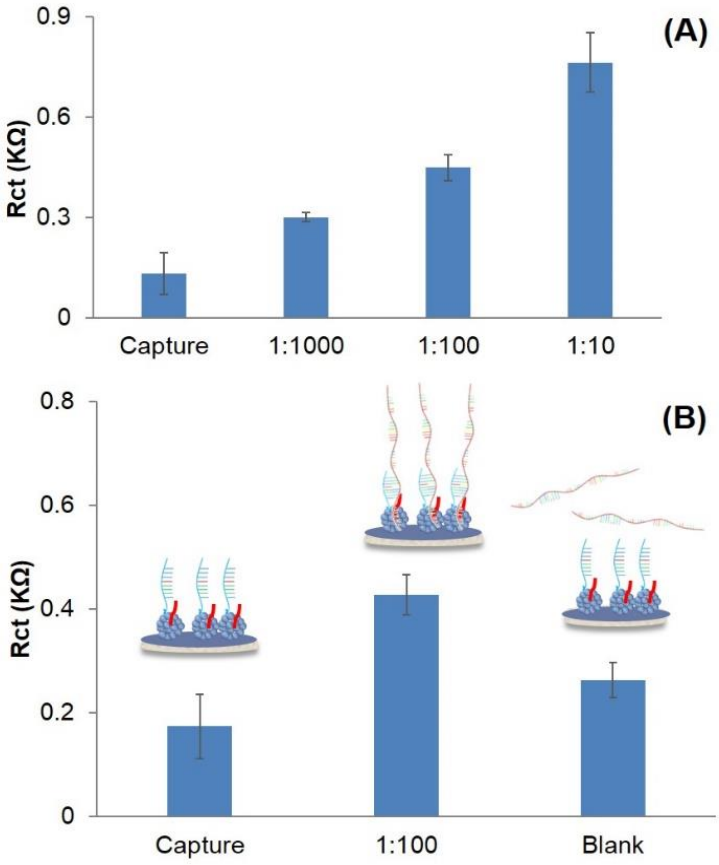

Figure 4.8: (A) Rct as a function of different dilutions of PCR amplified DNA samples. (B) Comparison of Rct values of the genosensor modified with the capture probe and hybridized with PCR amplified DNA samples of dog affected (Positive) or not (Blank) with Leishmania. Dilutions of 1:10 and 1:100 for the blank and positive samples respectively, and 2% ethanolamine during the blocking step was used.

4.4 Conclusions

A simple and sensitive platform for the impedimetric label free genosensor taking advantage of conventional screen printed carbon electrode (SPCE) modified by polythionine and IrO_2 nanoparticles is developed. Although the SPCE electrodes have several advantages such as low cost, miniaturization, mass production, etc. they are not directly suitable as such for impedimetric label free detections, mainly because they present a high resistivity and rough surface. In order to overcome these limitations a polythionine layer was electrodeposited on the surface of the working electrode. This modification at the same time decreases the roughness and increases the conductivity of the working electrode. Furthermore, the IrO_2 NPs show suitable redox properties in addition to the capability to attach the bioreceptor thanks to the surrounding citrate groups used as capping agent. Moreover, regarding the adsorption of capture DNA probe, the blocking procedure and hybridization steps have been optimized. To improve selectivity, reproducibility and sensitivity the concentration of ethanolamine used as blocking agent was optimized and found to be 2%(v/v) the optimal concentration level. This new genosensor is able to detect up to 1000 times diluted samples of PCR amplified DNA.

4.5 Bibliography

(1) Bonanni, A.; del Valle, M. *Analytica Chimica Acta* **2010**, *678*, 7-17.

(2) Chang, B.-Y.; Park, S.-M. *Annual Review of Analytical Chemistry* **2010**, *3*, 207-229.

(3) Lisdat, F.; Schaefer, D. *Analytical and Bioanalytical Chemistry* **2008**, *391*, 1555-1567.

(4) Xu, Q.; Davis, J. J. *Electroanalysis* **2014**, *26*, 1249-1258.

(5) Spain, E.; Kojima, R.; Kaner, R. B.; Wallace, G. G.; O'Grady, J.; Lacey, K.; Barry, T.; Keyes, T. E.; Forster, R. J. *Biosensors and Bioelectronics* **2011**, *26*, 2613-2618.

(6) Tosar, J. P.; Brañas, G.; Laíz, J. *Biosensors and Bioelectronics* **2010**, *26*, 1205-1217.

(7) Ito, T.; Hosokawa, K.; Maeda, M. *Biosensors and Bioelectronics* **2007**, *22*, 1816-1819.

(8) Emr, S. A.; Yacynych, A. M. *Electroanalysis* **1995**, *7*, 913-923.

(9) Gao, Q.; Cui, X. Q.; Yang, F.; Ma, Y.; Yang, X. R. *Biosensors & Bioelectronics* **2003**, *19*, 277-282.

(10) Yang, R.; Ruan, C. M.; Dai, W. L.; Deng, J. Q.; Kong, J. L. *Electrochimica Acta* **1999**, *44*, 1585-1596.

(11) Peng, H.; Soeller, C.; Vigar, N.; Kilmartin, P. A.; Cannell, M. B.; Bowmaker, G. A.; Cooney, R. P.; Travas-Sejdic, J. *Biosensors and Bioelectronics* **2005**, *20*, 1821-1828.

(12) Liu, S.; Liu, J.; Wang, L.; Zhao, F. *Bioelectrochemistry* **2010**, *79*, 37-42.

(13) Bonanni, A.; Esplandiu, M. J.; del Valle, M. *Biosensors and Bioelectronics* **2009**, *24*, 2885-2891.

(14) Honorato Castro, A. C.; França, E. G.; De Paula, L. F.; Soares, M. M. C. N.; Goulart, L. R.; Madurro, J. M.; Brito-Madurro, A. G. *Applied Surface Science* **2014**, *314*, 273-279.

(15) Gebala, M.; Schuhmann, W. *Phys. Chem. Chem. Phys.* **2012**, *14*, 14933-14942.

(16) Doneux, T.; De Rache, A.; Triffaux, E.; Meunier, A.; Steichen, M.; Buess-Herman, C. *ChemElectroChem* **2014**, *1*, 147-157.

(17) Wang, Y.; Ye, Z.; Ying, Y. *Sensors* **2012**, *12*, 3449-3471.

(18) Murray, R. W. *Chemical Reviews* **2008**, *108*, 2688-2720.

(19) Rivas, L.; de la Escosura-Muñiz, A.; Pons, J.; Merkoçi, A. *Electroanalysis* **2014**, *26*, 1287-1294.

(20) Kurbanoglu, S.; Mayorga-Martinez, C. C.; Medina-Sánchez, M.; Rivas, L.; Ozkan, S. A.; Merkoçi, A. *Biosensors and Bioelectronics*.

(21) Francino, O.; Altet, L.; Sánchez-Robert, E.; Rodriguez, A.; Solano-Gallego, L.; Alberola, J.; Ferrer, L.; Sánchez, A.; Roura, X. *Veterinary Parasitology* **2006**, *137*, 214-221.

(22) Boo, H.; Jeong, R.-A.; Park, S.; Kim, K. S.; An, K. H.; Lee, Y. H.; Han, J. H.; Kim, H. C.; Chung, T. D. *Analytical Chemistry* **2006**, *78*, 617-620.

(23) Mirbagheri, N.; Chevallier, J.; Kibsgaard, J.; Besenbacher, F.; Ferapontova, E. E. *ChemPhysChem* **2014**, *15*, 2844-2850.

(24) Zhao, Y.; Hernandez-Pagan, E. A.; Vargas-Barbosa, N. M.; Dysart, J. L.; Mallouk, T. E. *The Journal of Physical Chemistry Letters* **2011**, *2*, 402-406.

(25) Chen, R.-S.; Huang, Y.-S.; Liang, Y.-M.; Tsai, D.-S.; Chi, Y.; Kai, J.-J. *Journal of Materials Chemistry* **2003**, *13*, 2525-2529.

Chapter 5

General conclusions and future perspectives

5.1 Conclusions

Novel and improved biosensing systems taking advantage of gold nanoparticles (AuNPs) and Iridium oxide Nanoparticles (IrOx NPs) have been developed. These biosensing approaches have been adapted for the detection of both protein and DNA short sequences.

Considering the detailed objectives described in chapter 2 and the obtained results in chapter 3 and 4 the conclusions are detailed as follows:

Electrochemical Impedance Spectroscopy (EIS) combined with hydrogen evolution reaction (HER). HER induced by AuNPs read by EIS has been demonstrated to constitute a high reproducible and efficient method for the detection of different amounts of AuNPs in acidic medium. This EIS-HER method combines the advantages of EIS with HER induced by AuNPs. The proposed method displays a satisfactory analytical performance in terms of a linear range of response and sensitivity for the detection of a model protein (human IgG) in a magnetoimmunoassay, and in the gold nanoparticle size characterization. In addition, it is also important to emphasize that with this new strategy for the magneto immunosandwich a reduction of one order of magnitude in the LOD is obtained, compared with chroamperometric technique normally used for this detection reported before. We envisage the use of such sensing technology to be with interest for various sensing and biosensing applications where nanoparticles or other nanomaterials may be involved.

Iridium oxide nanoparticle and Polythionine thin film based platform for sensitive Leishmania DNA detection: A simple and sensitive platform for the impedimetric label free genosensor taking advantage of conventional screen printed carbon electrode (SPCE) modified by polythionine and IrO2 nanoparticles is developed. The combined modification of polythionine layers and IrO2 NPs show suitable properties for good impedimetric measurements and the modification with DNA oligonucleotides. Moreover, in order to improve selectivity, reproducibility and sensitivity the blocking procedure and hybridization steps have been optimized. This new genosensor is able to detect a target sequence in up to 1000 times diluted samples of PCR amplified DNA.

A Lateral Flow Immunoassay (LFIA) for the detection of PTHLH has been designed and tested (annex A). As far as we know this is the first time that LFIA has been applied for the detection of PTHLH taking advantage of the properties that paper based nanobiosensors offer (easy to use, quick tests, good sensitivity) being capable to perform the detection of such factor at ng mL^{-1} levels in real samples obtained from HaCaT, LA-N-1 and SK-N-AS cell cultures (cell lysates and cell media). This pioneer study offers a novel alternative for the quick and robust detection of PTHLH avoiding the need of complex or expensive requirements. The developed method offers a new tool for the study

of fundamental aspects related to the mechanisms and the factors associated to PTHLH secretion, which can be of great importance for therapeutic applications. Furthermore the low matrix effects found when analysing a human serum sample, demonstrate the ability of the developed system to perform analysis in scenarios of interest for future diagnostic applications.

Electrochemical DNA and aptamer biosensors (E-DNA and E-AB respectively) have been successfully prepared. Gold disk electrodes following the standard procedure haven been used to fabricate sensors for the detection of linear DNA, cocaine and Thrombin. The feasibility of the technique on screen printed electrodes was tested using gold screen printed electrodes (GSPE) and latter extended to carbon screen printed electrodes (SPCE). Although electrochemical signals of MB could be read using SPCE, SAM formation of mecaptohexanol on the sensor surface , introduced an increase in the irreproducibility of sensor fabrication depleting the MB peak. The obtained results show firstly the possibility to use MB labelled DNA probes with the home made SPCE and obtain a readable signal and secondly, the problems related to the performed immobilization, based in the thiol gold interaction: impossibility to successfully fabricate a E-AB sensor have been related to this last issue.

In situ detection of protein secreted by cells cultured on a nanochannel based sensing platform has been tested (Annex C). The work presented has been done as a continuation of previous studies within the group; it has been possible to go one step beyond applying the previous work in the development of a biosensing system based on the use of nanochannels for the in situ detection of biomarkers secreted by cell cultures. Therefore an in situ cell culture/electrochemical detection set-up system has been built and tested to be capable of detecting secreted PTHLH with cells being incubated up to 20h. The performed detection is label-free and take advantage of using PBNPs as indicator.

5.2 Future perspectives

Thanks to the unique properties which nanomaterials exhibit, nanotechnology has expanded the scope for the development of new sensing strategies and improvements in biosensors. Owing to the large number of possibilities introduced by new nanomaterials, characterization, study of their properties and their applications in biosensing are still being explored. New modifications and combinations with already existing techniques seem to be a promising field for the improvement of already stablished approaches fulfilling demands for specific properties from other fields of science.

The application of new sensing techniques for AuNPs detection based in catalysis of HER, achieving a more sensitive approach, open the possibility to develop new devices based in impedance measurement. Furthermore, the more sensitive detection of HER allow at the same time to perform a better sensing of the presence of protons in the sample. This issue can be exploited in the development of pH sensing strategies using small carbon electrodes modified with AuNPs, as an alternative to the traditional benchtop pHmeters.

Integration of polythionine films and IrOxNPs on a carbon screen printed electrode developing a label free sensor for detection of specific DNA sequences, represent an interesting platform which can further be adapted to the detection of different DNA sequences by changing the capturing DNA oligonucleotide.

LFIA (work presented in Annex A) are applied in the detection of PTHLH fulfilling the requirements for POC testing. The developed assay represents a potentially interesting method for researchers working in the study of PTHLH expression and roles in cell cycle. However, due to the versatility of LFIA, components of the assay can be easily modified with the aim of adapting the assay to a different detection context or even improve sensitivity. In case that further works make possible to enhance the LOD down to levels of PTHLH found in human blood (pg mL^{-1}), this cheap, fast and non-hazardous alternative would make feasible studies of PTHLH levels in patients, allowing researchers to achieve a better understanding in the complex role that PTHLH plays in physiological conditions, as well as exploit the chance to explore the potential use of PTHLH as molecular biomarker. Besides, LFIA represents a versatile and easy adaptable technique. This kind of paper-based diagnostics are suitable for largescale production, making them a very cheap and efficient technology.

In order to overcome the limitations of the compatibility of the E-DNA and A-AB technology with SPCE (Annex B) and move forward in the integration of both technologies we believe that two main alternatives could be followed: on the one hand, change the immobilization procedure of

thiolated probes on the AuNPs; carry out AuNPs modification in solution and then deposit the constructs on the SPCE instead. The other alternative could be by changing the immobilization principle, instead of using the thiol gold interaction, directly attach covalently the labelled DNA probes on the electrodes, avoiding the use of AuNPs as connecting platform. Overcoming these limitations would allow to integrate the E-DNA and E-AB technology on SPCE, combining advantages of both, resulting a robust and cost effective sensing platform a close to real world application product.

The development of a sensing platform for in situ detection of protein secreted by cells cultured onto nanochannel platform (annex C), represents a highly interesting tool with potential future applications in the study of protein secretion of a cell line in a single device. Both the cell culture and the detection are performed in situ being this technology easy to be used and adapted into a high throughput system, paving the way to fast and simple approaches for the study of expression pattern of proteins or any related phenomena.

Annex A

Annex A 1.

Detection of Parathyroid Hormone-like Hormone in Cancer Cell Cultures by Gold Nanoparticle-based Lateral Flow Immunoassays

Related publication

Submitted, in revision.

Detection of Parathyroid Hormone-like Hormone in Cancer Cell Cultures by Gold Nanoparticle-based Lateral Flow Immunoassays

Chamorro-Garcia Alejandro [a,b], de la Escosura-Muñiz Alfredo [a], Espinosa-Castañeda Marisol [a], Rodriguez-Hernandez Carlos J. [b], de Torres Carmen [b], Merkoçi Arben [a,c].

[a] ICN2 – Nanobioelectronics& Biosensors Group, Institut Catala de Nanociencia i Nanotecnologia, Campus UAB, 08193 Bellaterra, Barcelona, Spain

[b]Hospital Sant Joan de Déu andFundació Sant Joan de Déu, Passeig Sant Joan de Déu 2, 08950 Esplugues de Llobregat, Barcelona, Spain.

[c] ICREA - Institucio Catalana de Recerca i Estudis Avançats, 08010 Barcelona, Spain.

Summary

Parathyroid Hormone-like Hormone (PTHLH) exerts relevant roles in the progression and dissemination of several tumours. However, factors influencing its production and secretion have not been fully characterized. The main limitation is the lack of specific, sensitive and widely available techniques to detect and quantify PTHLH. We have developed a Lateral Flow Immunoassay using gold nanoparticles label for the fast and easy detection of PTHLH in lysates and culture media of three human cell lines (HaCaT, LA-N-1, SK-N-AS). Levels in culture media and lysates ranged from 11 to 20 ng/mL and 0.66 to 0.87 µg/mL respectively. Results for HaCaT are in agreement to the previously reported, whereas LA-N-1 and SK-N-AS have been evaluated for the first time. The system also exhibits good performance in human serum samples. This methodology represents a helpful tool for future in-vitro and in-vivo studies of mechanisms involved in PTHLH production as well as for diagnostics.

Index

A1.1 Introduction

Parathyroid Hormone-like Hormone (PTHLH) is a secreted factor that is present in virtually all organs and tissues of the body. It was initially identified in cancer patients with hypercalcemia. The syndrome was named humoral hypercalcemia of malignancy (HHM) and was apparently caused by a factor released by the tumour (1). Parathyroid hormone (PTH) was first proposed as the factor responsible of these effects, but it was never demonstrated that increased levels of PTH could cause HHM. The sequencing and cloning of the PTHLH gene in 1987 showed the high homology of the N-terminal region between PTH and PTHLH. This homology allows PTHLH to signal through the PTH receptor (2). Once isolated and characterized as the factor responsible for HHM (3), PTHLH was reported to exert other functions in cancer as well as in normal tissues (2-7). In cancer, it has been reported to be involved in the initiation, survival and progression of primary tumors (8, 9), as well as in the generation and development of metastases (10-12). Moreover, novel functions of this cytokine are still being described in recent papers (13). Nevertheless, the mechanisms that control its production and secretion are only partially understood.

One of the limitations to characterize the multiple mechanisms that control its production and secretion is the lack of specific, sensitive and easy techniques to detect and quantify this molecule in in vitro models. After the description and characterization of PTHLH, few methodologies were adapted to detect circulating PTHLH (14), mostly radioimmunoassays (RIAs) and immunoradiometric assays (IRMAs) which have been successfully applied in cancer patients (15,16). Advantages of the radioactive assays rely in the ease of isotope conjugation, signal detection with little optimization and low limit of detection, around 0.7 pmol/L. Nevertheless, these assays have serious drawbacks mostly related to the half-life of the isotope, the potential hazard of radioactivity and, consequently the strict requirements needed to implement these procedures. For this reason, in most cell biology and molecular research laboratories PTHLH is analyzed at the mRNA level by quantitative reverse transcriptase polymerase chain reaction (qRT-PCR) and the protein is evaluated by immunocyto/histochemistry (17), Western blot (18) and ELISA (12,19). However, these methods are expensive, time-consuming and require trained personnel, thus making alternative approaches of potential interest in a number of settings.

In this context, biosensors based on nanomaterials, or nanobiosensors, constitute an outstanding alternative for a low-cost, fast, efficient, large scaling and user-friendly analysis (20,21). For example, an electrochemical immunoassay based on nanoparticles and nanochannels for the detection of standard PTHLH solutions (spiked in cell culture media) has been very recently reported

by our group (22). However, the developed immunosensing system requires the assembling of nanoporous membranes on the electrode surface together with different incubation/washing steps before the electrochemical reading, being a non-integrated and relatively time-consuming system.

Lateral-flow immunoassays (LFIAs), very well-known for the popular pregnancy test (23), are highly integrated systems that appear as ideal candidates for rapid PTHLH analysis, thanks to their characteristics of simple use, rapid result, low cost, good specificity and long shelf life (24). In these systems, all the reagents are preloaded in paper strips, the samples are casted on a pad of the strip and flow by capillarity through all the components, mixing with the reagents and reaching the detection zones. As a result, the assay is done by just adding the sample on the corresponding pad, and adding washing solution afterwards. Finally qualitative results can be read by naked eye and, in case that quantification is required, only a simple colorimetric reader is needed. In addition to the pregnancy test, LFIAs have been extensively applied for the detection of different analytes such as cancer biomarkers (25), DNA (26), toxins (27) and metals (28).

The inherent limitations of LFIA technology in terms of sensitivity and reproducibility have been overcome in the last years thanks to the tools offered by the nanotechnology, mostly taking advantage of the plasmonic properties and large surface area of gold nanoparticle (AuNPs) tags (29-32).

In the aforementioned context of increasing relevance of PTHLH in cancer the objective of this work is to develop and optimize a rapid, sensitive, cheap, easy-to-use and non-hazardous technique to detect and quantify PTHLH secreted in cell cultures, with the aim of offering a new tool for the study of fundamental aspects related to the mechanisms and the factors associated to PTHLH secretion, which can be of great importance for therapeutic applications. We here present a novel LFIA approach based on AuNPs for the rapid and simple determination of this protein production and secretion in three human cell lines: two neuroblastoma cell lines (SK-N-AS and LA-N-1), a tumor where high PTHLH expression has been associated with benign subgroups (33) and immortalized keratinocytes (HaCaT) as a control of high PTHLH production.

The proposed LFIA method allows for the quantification of PTHLH in cell lysates as well as in cell culture media. This is relevant because PTHLH exerts different functions inside the cell (as an intracrine, autocrine factor) and as a secreted protein that mediates a cross-talk with neighbour cells (paracrine functions) (2,7). A schematic view of the process is displayed in Figure A1. Finally, the suitability of the system to perform detection in a complex matrix (human serum) spiked with commercial PTHLH has been proved.

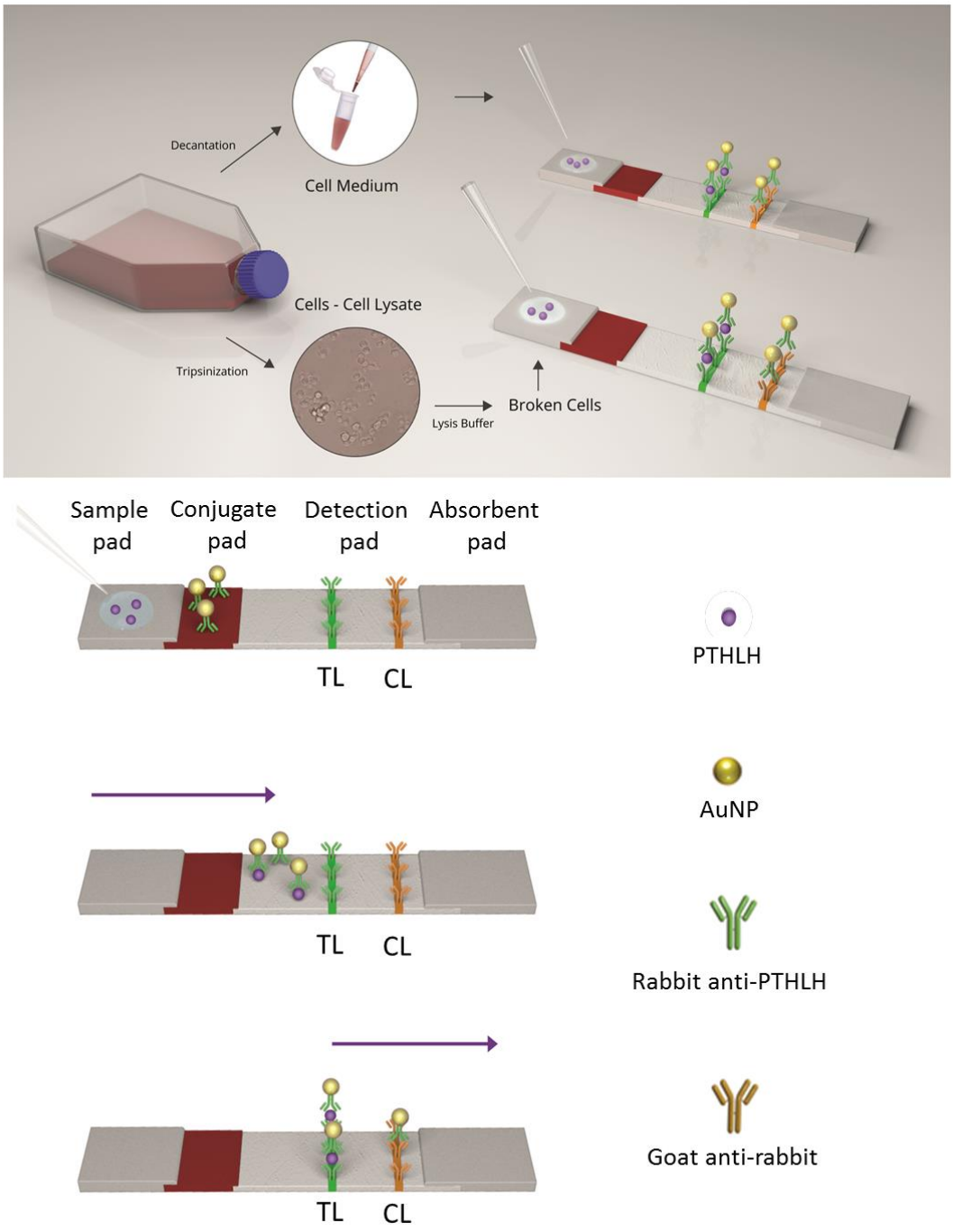

Figure A1: (Top) Schematic view of the experimental procedure for PTHLH quantitation in cell culture media and cell lysates using a gold nanoparticle (AuNP)-based lateral flow immunoassay (LFIA).(Bottom) Depiction of sequential steps involved, and materials and reagents used in the designed LFIA. TL and CL stand for test line and control line, respectively.

A1.2 Experimental section

A1.2.1 Reagents and apparatus

Gold(III) chloride trihydrate ($HAuCl_4 \cdot 3H_2O$), trisodium citrate, sodium chloride, boric acid (powder, for electrophoresis), sodium phosphate dibasic, sodium dihydrogen phosphate, sucrose, Tween 20, 10mM pH 7.4 phosphate buffered saline in tablets (referred in the main text as PBS), HEPES buffer solution, NaCl, $MgCl_2$, NaF, Triton x100, EDTA, PMSF, DTT, trypan blue, Bradford reagent and Bovine serum albumin (BSA) were purchased to Sigma Aldrich (Spain). was purchased to Millipore (USA). An IsoFlow reagent dispensing system (Imagene Technology, USA) was used to dispense the detection and control lines. A commercially available strip reader, model ESE Quant Lateral Flow reader (Qiagen Inc., Germany) was used for quantitative measurements.

PTHLH recombinant was purchased to Sigma Aldrich (Spain). Polyclonal rabbit antibody (38-208) against PTHLH was purchased to Pro-Sci (USA). Polyclonal goat antibody (Ab6702) against rabbit IgG was purchased to Abcam (UK). SK-N-AS cells were purchased from the European Collection of Cell Cultures. LA-N-1 cells were kindly provided by Dr.Nai-Kong Cheung (Memorial-Sloan Kettering Cancer Center, New York, USA) and HaCaT cells by Dr. Joan Guinovart (Institut de Recerca Biomèdica, Barcelona, Spain).

RPMI media, L-Glutamine, Penicillin streptomycin solution, trypsin 0.25% EDTA, and Fetal Bovine Serum (FBS) EU approved were purchased to Fisher scientific (Spain). Nitrocellulose filters were purchased to Bio-Rad. Anti-Rabbit IgG (W4011) Horseradish Peroxidase (HRP) conjugate was purchased to Promega (Spain). Immobilon Western Chemiluminescent HRP Substrate was purchased to Merck Millipore (Spain). Enhanced chemiluminiscence reagents for immunoblotting were purchased to Amersham Pharmacia (Piscataway, USA). Glass fibre conjugate pad (GFCP00080000), cellulose fibre sample and absorbent pad (CFSP001700), nitrocellulose pad HFB180 (SHF1800425) and backing card (HF000MC100) were purchased to Millipore (USA). Solutions were prepared in purified (<18.2 MΩ cm^{-1}; mQ) water, produced using the Milli-Q system (Millipore, Sweden). A guillotine (Dahle 533, Germany) was used to cut the strips. The stirrer used was a TS-100 Thermo-Shaker (Biosan, Latvia). TEM images were obtained with a FEI Tecnai™ G2F20 field emission gun transmission electron microscope (FEI, USA). UV-Abs spectra were performed using a SpectraMax $M2^e$ spectrophotometer (Molecular Devices, USA). The pictures of the Lateral Flow strips were taken with a S6D Leica optical microscope (Leica, Germany).

Serum samples for the spiking and recovery experiments were obtained from blood samples (1-3 mL) from healthy donors collected at the time of a minor surgery. Residual volumes were

processed and stored for research purposes after all necessary diagnostic procedures were performed. Written informed consent was obtained to store these samples in the Tumor Bank and to use them as anonymized controls. Serum was obtained from blood as per Standard Operating Protocols at Developmental Tumor Biology laboratory, Hospital Sant Joan de Déu, Barcelona.

A1.2.2 Methods and procedures

A1.2.2.1 Synthesis of gold nanoparticles (AuNP) and preparation of AuNP/antibody conjugates

AuNP of 15 nm in diameter were prepared by reduction of HAuCl4·3H2O following the procedure described by Turkevich et al (34): all glassware was cleaned with aqua regia (HCl and HNO3 at 3:1 parts in volume) and thoroughly rinsed with milliQ water. Aqueous solution of HAuCl4·3H2O 0.25mM in milliQ water was heated to boiling point under strong stirring. Then 1.25 mL of 34mM trisodium citrate solution was added, the heating and stirring was held constant for 10 minutes, at this point the colourless solution becomes violet and later red. The AuNP solution was cooled down and stored at 4°C protected from light. The resulting nanoparticles were characterized by ultraviolet/visible spectroscopy (UV-Vis) and Transmission Electron Microscopy (TEM).

Modification of AuNPs with specific antibodies against PTHLH (Pro-Sci 38-208) antibodies were done accordingly to the experimental procedure already reported by the group (35). Optimal conditions for proper conjugation were obtained by performing a Gold Aggregation Test (GAT), so as to estimate the minimum amount of antibodies required for fully covering the surface of all the AuNPs and the minimum bovine serum albumin (BSA) for covering the AuNPs in order to prevent perform the nonspecific site blocking. Briefly, the GAT was carried out as follows: 150 µL of 3nM AuNP suspension were added in each well of a multi-well plate. pH was adjusted using 30 µL of borate buffer at different pHs: 6.5, 8, 9 and 10.5. Then 10 µL of the anti-PTHLH polyclonal antibody solution at different concentrations (0, 10, 50, 100, 200 µg/mL) were added to each well. The plates were incubated on a shaker for 20 min at 600 rpm. Then 20 µL of 10% NaCl solution were added to each well and incubated on the shaker for 10 min at 600 rpm. (note: NaCl causes the aggregation of AuNPs and shifts the maximum absorbance peak from 520 nm to 580 nm).

AuNPs were modified with the anti-PTHLH polyclonal antibody and BSA for nonspecific binding sites blocking by adding the minimum concentration of antibody previously calculated by the GAT. Briefly, the pH of 1.5 mL of 3nM AuNP suspension was adjusted to 9 by adding 300 µL of 0.1M pH 9.2

borate buffer. Next 100 µL of the antibody at the previously optimized concentration (100 µg/mL) in aqueous solution was added, the resulting mixture was incubated in a shaker for 30 min at 650 rpm and room temperature. Then a blocking step was performed by adding 100 µL of BSA aqueous solution at the optimized concentration (1 mg/mL) and incubating in a shaker for 30 min at 650 rpm and at room temperature. Finally the AuNP/antibody conjugates were purified from the excess of reagents by centrifugation at 18000 g and 4ºC for 30 minutes and the pellet of conjugates was solubilized in 500µL of 10% sucrose (w/v).

A1.2.2.2 Preparation of the conjugate, sample and detection pads

In order to prepare the conjugate pads, the fibre glass strips were soaked by drop casting with the solution of AuNP/antibody conjugates (prepared as described in section A1.2.2.1). The resulting conjugate containing fibre glass was dried in a vacuum chamber for 1.5 hours. The sample pad was prepared by dipping the cellulose fibre strips in a 0.5% (w/v) BSA, 0.05% (v/v) Tween 20, 10mM pH7.4 PBS solution, and dried in the oven at 70ºC for 30 minutes. Capturing antibodies for both the test and control line were deposited on the nitrocellulose pad using the isoflow dispenser. The polyclonal antibody anti-PTHLH at 100 µg/mL in 1 mg/mL BSA 10mM pH 7.4 Phosphate buffer (PB) was deposited in the test line, while a polyclonal antibody against rabbit IgG at 1mg/mL in 10mM pH 7.4 PB was deposited in the control line. The substrates were dried in an oven at 37ºC for 1.5 hours. Last step was the assembly of the 4 the components of the LFIA on the backing card: detection pad, conjugate pad, sample pad and absorbent pad were placed by this order. Pads were placed so one pad overlaps the next one where they meet in order to assure the flow of the liquid from one pad to the other. The resulting assemblies are cut in 7 mm wide strips and stored in a sealed flask with desiccating pearls in the fridge until the moment of use.

A1.2.2.3 Cell lines culture, lysates preparation and human serum samples

Cells were grown in Roswell Park Memorial Institute (RPMI)-1640, 10% fetal bovine serum (Invitrogen, Carlsbad, CA), 2 mM L-glutamine, penicillin (100 U/mL) and streptomycin (100 µg/mL), at 37ºC and 5% CO_2. Mycoplasma polymerase chain reaction (PCR) tests were routinely performed. Cells were seeded in T-75 flasks, and after reaching 80% confluence, supernatants (also referred to as cell culture media) were collected by decantation. Cells were trypsinized and counted (see Figure A2 and Table A1). To obtain cell lysates, cell suspensions were centrifuged for 5 min at 250 x*g*.

Pellets were re-suspended in 1 mL of PBS, centrifuged 5 min at 91 *g* and then re-suspended in 100 µL of extraction buffer (25mM HEPES, 300mM NaCl, 0.1mM Orthovanadate, 10mM sodium fluoride, 1.5mM magnesium chloride, 0.1% Triton X100, 0.2mM EDTA, 0.5mM phenylmethylsulfonyl fluoride, 0.5mM dithiothreitol in milliQ water). Following incubation on ice for 10 min, mixtures were centrifuged 15 min at 13000 *g* and lysates were then stored at -80ºC. A pool of serum samples was obtained by mixing 500µL of serum from 6 different patients. The resulting mixture was used as serum matrix to perform the spiking of commercial PTHLH in order to carry out the signal recovery study.

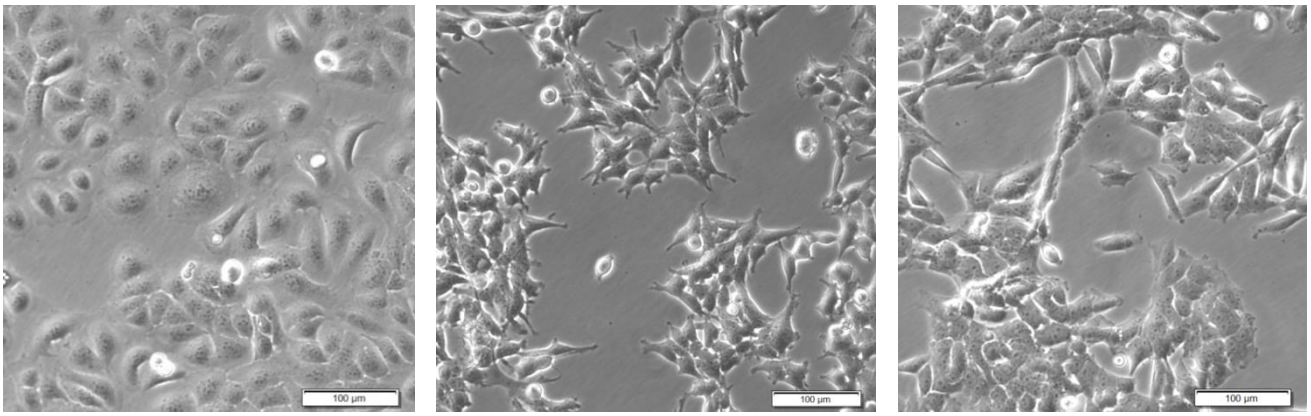

Figure A2: Cell cultures before trypsinization and lysis process. Cell lines from left to right: HaCaT, LA-N-1, SK-N-AS. Scale bar: 100µm.

Cell line	Amount of cells after tripsinization
HaCaT	$1.00 \cdot 10^6$ cells/mL
SK-N-AS	$1.24 \cdot 10^6$ cells/mL
LA-N-1	$0.64 \cdot 10^6$ cells/mL

Table A1: Calculated amount of cells after trypsinization for each cell line.

A1.2.2.4 Immunoblotting

Total protein amount was quantified according to the Bradford method (36). Indicated quantities of proteins were electrophoresed in 15% SDS-PAGE gels and transferred onto nitrocellulose membranes. Incubation with primary polyclonal antibody anti-PTHLH was followed by

HRP-conjugated secondary antibodies. Immunoreactive bands were detected with enhanced chemiluminiscence reagents.

Standards of BSA at known concentration, diluted in milli-Q water, were used to calculate the ampount of total protein present in the lysate samples. Mixtures of 2 µL of sample and 200 µL of Bradford reagent were prepared (Figure A1).

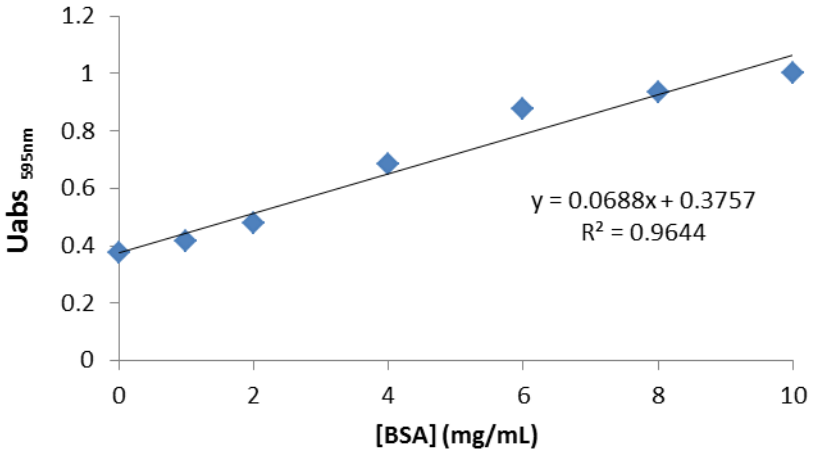

Figure A3: Calibration curve of BSA standards, carried out to estimate the total protein in the samples of lysate.

A1.2.2.5 Analysis of the samples by Lateral Flow Immunoassay (LFIA)

Samples were analysed following a LFIA, in which 150µL of the sample were added on the sample pad. After 4 minutes, 50µL of Tween 20 at 0.05% in PBS (washing solution) were added on the conjugate pad. This process was repeated 3 times in order to wash the excess of conjugates and the non-specific adsorbed conjugates onto the nitrocellulose and printed lines. The total time required for the tests was between 15 and 20 minutes. The strips were let dry at room conditions for 20 minutes and afterwards read using a colorimetric reader for lateral flow strips. For all the measurements the background signal of PBS was subtracted. All the measurements were repeated 3 times, and the corresponding error bar calculated.

First a calibration curve using standard solutions of PTHLH in PBS was performed. Due to the high concentration of proteins in the cell lysate samples, the LFIA showed some limitations, mostly related with the difficulties of migration of the conjugates through the detection pad, and the lack of formation of both lines: test and control. In order to overcome this limitation the samples were

diluted in PBS until the dilution in which the LFIA worked properly, which happened to be 1:250 (see dilution optimization in Figure A4). The cell lysate was diluted to 1:250 in PBS and measured by LFIA, being the content of PTHLH extrapolated from the calibration curve.

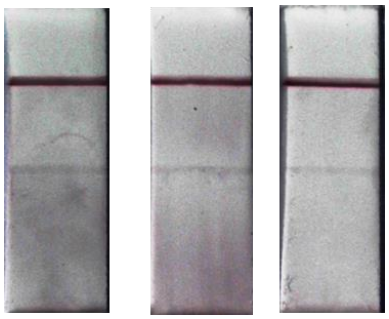

Figure A4: Lateral Flow strips obtained after analysis of HaCaT cell lysates. From left to right: lysate 1:20, lysate 1:50, lysate 1:250.

For the determination of PTHLH in cell culture media, the method of the standard additions was applied for samples without any previous dilution. Additions of 0, 10 and 50 ng/mL of the standard PTHLH solution were evaluated.

The regular experimental procedure of lateral flow analysis was applied for the commercial PTHLH spiked (to reach final concentrations of 0, 5 and 100 ng/mL) in both PBS and human serum samples. With the only exception that the background signal was not subtracted from the measurement in order to calculate the recoveries.

A1.3 Results and discussion

A1.3.1 Assay principle

A LFIA based on AuNPs is designed (see details at Figure A1 in A1.1.Introduction section) and applied for the quantification of PTHLH in HaCaT, LA-N-1 and SK-N-AS cell culture media and cell extracts. Samples are casted onto the pre-treated cellulose fibre (sample pad) and flows by capillarity towards the other end (adsorption pad) of the strip. In this pathway, sample meets the conjugate pad, where conjugates of 15nm AuNPs modified with polyclonal anti-PTHLH antibodies have been pre-stored. The PTHLH is recognized by the conjugates thereby forming an AuNP/Antibody/PTHLH conjugate. These conjugates keep flowing through the nitrocellulose. Immobilized antibodies anti-PTHLH bind the PTHLH forming an immunosandwich with the AuNP/Antibody/PTHLH, holding the conjugates in the detection line and making a red band (detection line) due to the accumulation of AuNPs. Excess of AuNP/Antibody conjugates migrate

further, and are captured on the control line, where antibodies against the anti-PTHLH are previously immobilized. The appearing of the control line is necessary to confirm the good performance of the assay and the migration of the reagents along the strip. The colour density or optical density (OD) of the detection line is proportional to the analyte concentration. A schematic view of both the LFIA working principle and the experiments procedure can be observed in Figure A1. Three different cell lines were evaluated and two types of samples from each one were analysed: cell culture media and cell lysates. A calibration curve using standard solutions of the protein was made so as to quantify PTHLH in cell lysates. As the low levels of PTHLH in cell media did not allow the sample dilution before analysis, standard additions technique was applied so as to avoid matrix effects. Cell lysates were also analyzed by means of Western Blot as reference method. It is important to note that the polyclonal antibody used in this work recognizes the central region of the PTHLH (amino acids 37-122).

A1.3.2 Characterization of AuNPs and AuNP/antibody conjugates

Homemade AuNP were characterized by UV-Vis spectroscopy showing the typical absorption band at 520 nm which evidences the formation of a well-dispersed colloidal suspension. TEM analysis confirms a narrow size distribution of spherical AuNPs of 15 ± 2 nm and (Figure A5 A and Figure A5 B). Antibodies are conjugated onto the AuNP surface through a simple adsorption, with a random orientation, as extensively previously reported (24-25, 27-32, 35, 37). The well-known affinity of the thiol groups contained in the cysteine (present in the constant region of the antibodies) to gold substrates also contributes to this binding. Gold Aggregation Test (GAT) is preliminarily performed to determine the minimum antibody concentration to use for conjugation, discussed in section A1.2.2.1: “Synthesis of gold nanoparticles (AuNP) and preparation of AuNP/antibody conjugates” in material and methods). NaCl dislocates surface charges on AuNPs causing their aggregation while antibody-coated AuNPs do not aggregate since NaCl is not able to break the Au–S bond (35). The minimum antibody concentration for avoiding AuNP aggregation was determined by measuring the difference between the absorbance at 520 nm (dispersed AuNPs) and at 580 nm (aggregated AuNPs) for different antibody concentrations. Different pHs were also evaluated. Based on the results shown in Figure A5 C and Figure A5 D, the optimum conditions were an anti-PTHLH concentration of 100 µg/mL and incubation at pH 9 (see BSA concentration optimization Figure A6).

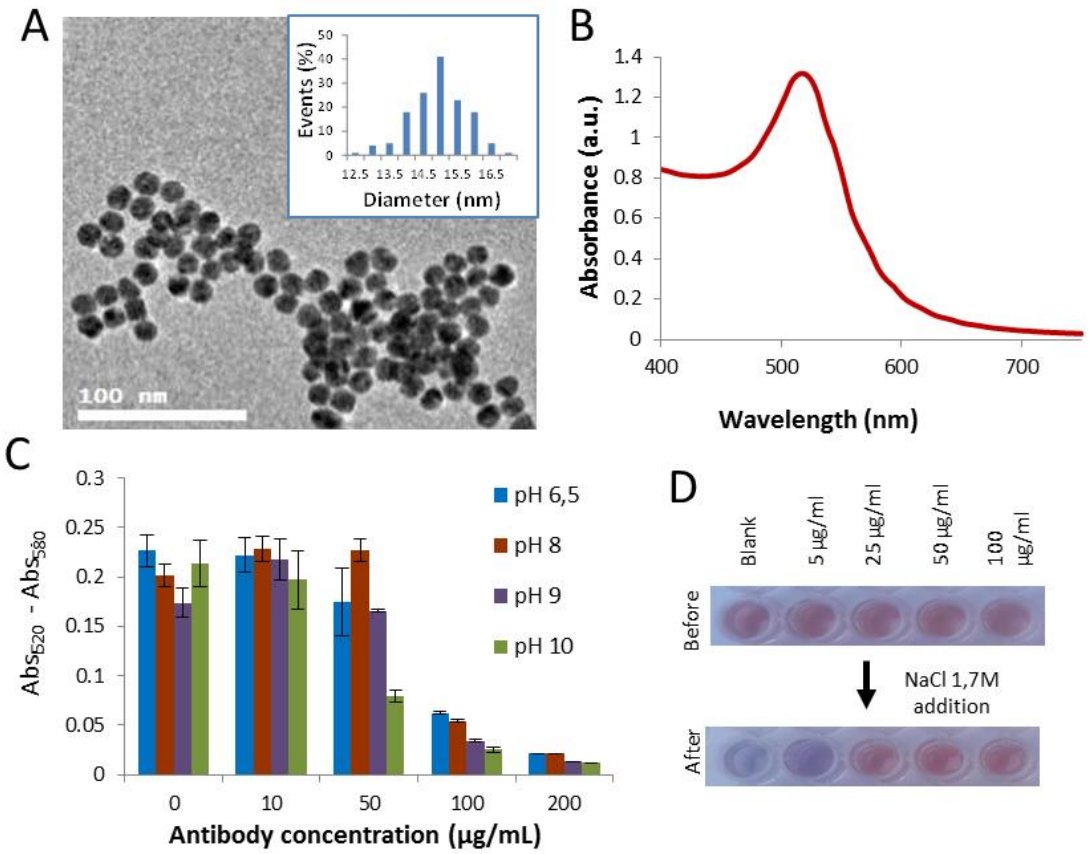

Figure A5: Characterization of gold nanoparticles (AuNPs) and AuNP/anti-PTHLH conjugates. (A) TEM image (inset graph corresponds to size distribution diagram) and (B) UV-Vis spectrum of the AuNPs suspension. (C) Difference in absorbance (Abs 520-Abs 580) plotted against anti-PTHLH concentration in the gold aggregation test (GAT) for different pH values. (D) Pictures of the corresponding solutions (incubation at pH 9).

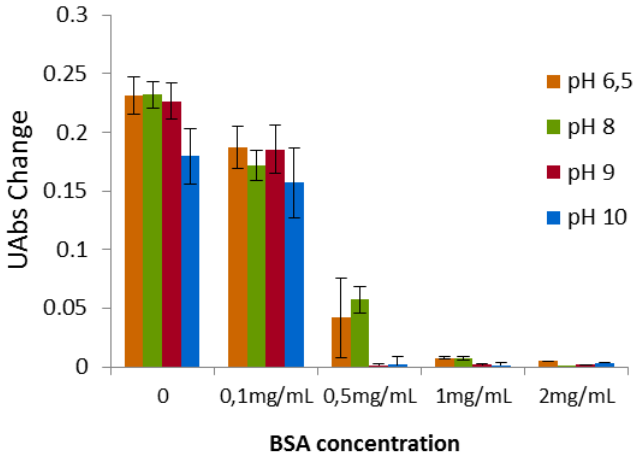

Figure A6: Gold aggregation tests performed to find the optimal concentration of BSA for the proper gold nanoparticle conjugation blocking. Results of the tests for incubations using different concentrations of proteins and at different pH.

A1.3.3 PTHLH detection in cell lysates

The proposed LFIA was used to calculate the amount of PTHLH present in cell lysates from three different cell lines: HaCaT, LA-N-1, SK-N-AS. As far as we know, PTHLH levels in neuroblastoma (LA-N-1 and SK-N-AS cell lines) have not been evaluated yet, while the levels in HaCaT lysates are expected to be at ng/mL order (12,38). Real-time quantitative PCR performed in these three cell lines showed a wide range of PTHLH expression varying from low (LA-N-1), medium (SK-N-AS) to high (HaCaT) (data not shown).

Standard solutions of PTHLH in PBS buffer were initially used to evaluate the effect of the PTHLH concentration on the analytical signal (Optical density). As shown in Figure A7 A (left), a gradual increase in the colour intensity of the test line was observed for increasing concentrations of PTHLH**,** being possible to detect up to 5 ng/mL even with the naked eye. As shown in Figure A7 B**,** a logarithmic relationship between the value of the Optical density (measured with a strip reader) and the protein concentration was found in the range from 5 ng/mL to 100 ng/mL (correlation coefficient: 0.995), as adjusted to the following equation:

$$\text{Optical density (AU)} = 48.201 \cdot \text{Ln}[\text{PTHLH}]\ (\text{ng/mL}) - 29.935 \quad (n=3) \quad (\text{Eq 1}).$$

where *n* corresponds to the number of individual assays.

The limit of detection (LOD), calculated by extrapolating from the calibration plot the concentration of analyte required to give a signal equal to the blank plus three times its standard deviation was 1.42 ng/mL (41), while the limit of quantification (LOQ) calculated as the smallest amount of detectable analyte with a CV<20% was 2 ng/mL(42). The reproducibility of responses of 5 ng/mL (n=10) gave a relative standard deviation (RSD) of 4%.

Since high concentrations of PTHLH are expected to be found in cell lysates (in the order of μg/mL) 1:250 dilutions of lysates were prepared with PBS buffer (1:250 before LFIA analysis to obtain analytical signals within the calibration curve range. This approach produced significant signals for the three cell lines (HaCaT, SK-N-AS and LA-N-1), as shown in Figure A7 A (right). The corresponding values of optical density are shown in the graph of Figure A7 B as discrete dots. As matrix effects are not relevant in these highly diluted samples, the concentration of PTHLH in each lysate was directly extrapolated from the calibration curve made with standard solutions. In this way, PTHLH concentrations between 0.66 and 0.87 μg/mL were estimated in cell lysates for the three lines evaluated, as summarized in Table A2**.**

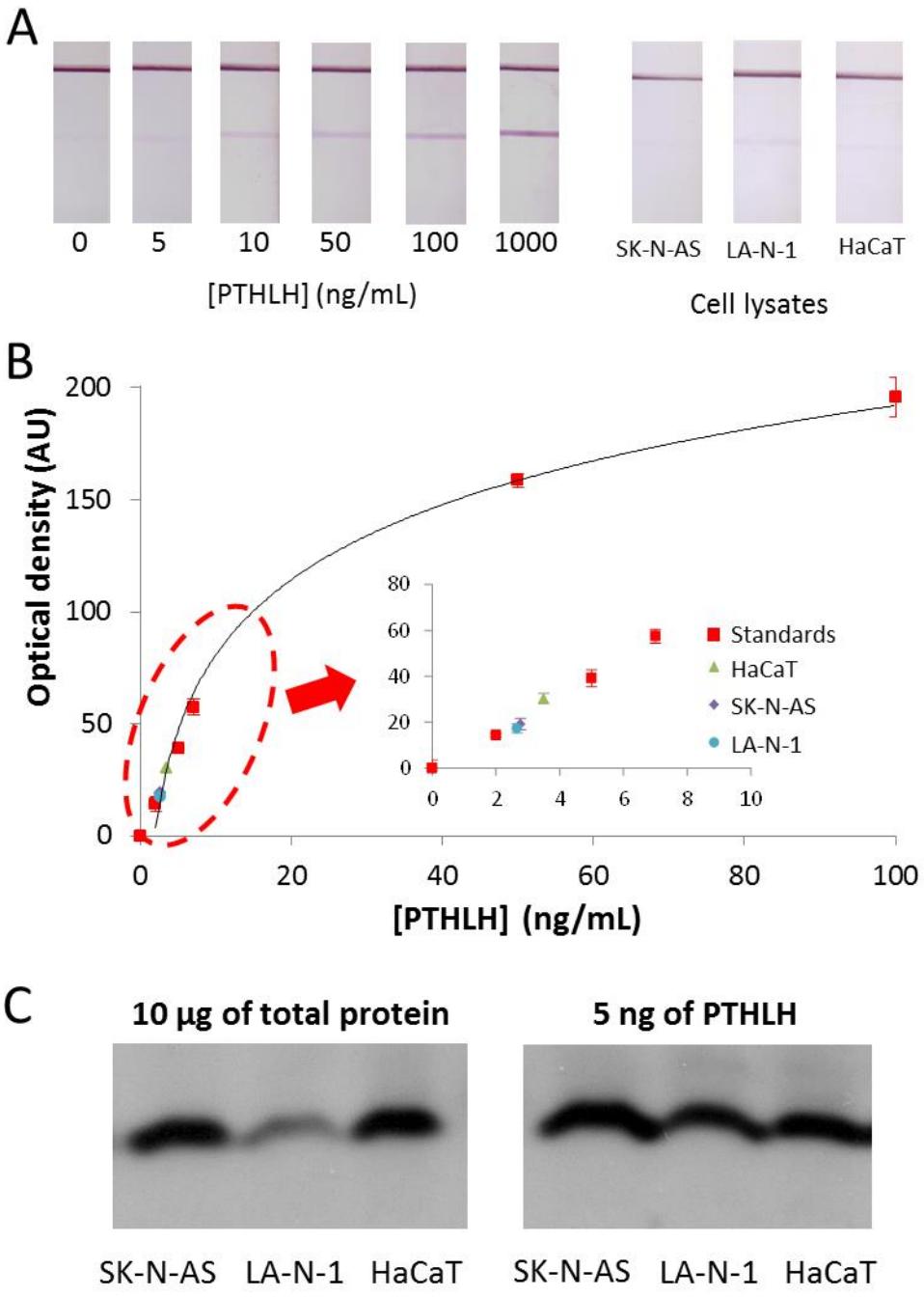

Figure A7: PTHLH evaluation in cell lysates. (A) Pictures of the LF strips after assays run with different standard solutions of PTHLH and with lysates(diluted at 1:250). (B)Effect of PTHLH concentration (standard solutions) on the optical density. The signals obtained for the three cell lines, diluted at 1:250 are inserted. (C) Western blot experiments for cell lysates.

Total protein content in each sample was calculated by Bradford method (see section A1.2.2.4 in materials and methods). The ratio PTHLH (measured by LFIA)/total protein (Bradford) amount was also calculated (Table A2).

For an independent detection of PTHLH we performed immunoblot (or Western Blots) to detect the protein. As Figure A7 C) (left panel) shows, when the gels are loaded with the same concentration of total protein, different signals are observed being the weakest signal corresponding to the LA-N-1 sample. But the relative differences did not precisely match those observed with LFIA. As a semi-quantitative technique, Western Blot provides only relative information about differences in PTHLH content between different samples. Its accuracy relies on several factors as protein quantity, primary and secondary antibodies concentration or even the housekeeping protein selected (38). So a proper quantification by this technique would require many different tests for each sample. If the quantification performed with the easier, quicker method of LFIA is trustworthy, we could correct the loading of gels to an equal PTHLH amount that we could observe in a Western Blot. Figure A7 C) (right panel) shows that, when we load equal PTHLH quantity, calculated with data in we obtain bands with similar intensity, despite the preliminary and apparent disagreement of the numbers. These results validate the LFIA quantification as a reliable method for PTHLH quantification in a complex mixture of proteins as a cell lysate sample.

Cell line	[PTHLH] in cell lysate (μg/mL)	[Total protein] in cell lysate (mg/mL)	[PTHLH]/[Total protein] %
HaCaT	0.87 ± 0.01	5.05 ±0.16	0.017%
SK-N-AS	0.69 ± 0.01	4.22 ±0.13	0.016%
LA-N-1	0.66 ± 0.01	4.86 ± 0.10	0.013%

Table A2: PTHLH quantification in cell lysates by LFIA (second column), total protein content in cell lysates according to the Bradford method (third column), and percentage of PTHLH in each samples (fourth column)

This assay to detect PTHLH production in cell lysates could also be applied for the detection of PTHLH in tissue samples, including tumours. Thus, it might be a useful tool, together with mRNA expression analysis, to analyse PTHLH regulation *in vitro* and also in *in vivo* models.

A1.3.4 PTHLH detection in cell culture media

Presence of secreted PTHLH in HaCaT, LA-N-1 and SK-N-AS cell culture media was calculated by LFIA. Cells morphology before collecting cell media can be observed in images shown in Figure A8.

Cell culture media represents a very complex matrix composed by the supplemented media (proteins mainly coming from Fetal Bovine Serum) and also proteins secreted by the cells. Since the expected amount of secreted PTHLH found in the cell culture media is at ng/mL levels (39), which is close to the LOD of the developed LFIA, the sample itself cannot be diluted before analysis. As matrix effects are expected to play a significant role in these non-diluted samples, PTHLH standard solution was added several times to a sample aliquot to estimate the PTHLH levels in cell culture media (40).

PTHLH standards (0, 10 and 50 ng/mL) were added to samples as detailed in the Materials and Methods section. As shown in Figure A8, the gradual increase in the obtained analytical signal is proportional to the added concentration of PTHLH according to the linear relationships shown in the inset.

Extrapolating from such equations the point on the *x*-axis at which OD = 0, the negative intercept on the *x*-axis corresponds to the amount of the PTHLH (ng/mL) in the sample. In this way, the amounts of secreted PTHLH present in cell media were 20.16 ng/mL, 14.19 ng/mL and 11.73 ng/mL respectively. As in the case of cell lysates, the highest levels of PTHLH were found in HaCaT cells media, while the other cell lines showed similar amounts of secreted PTHLH. Hence, secreted PTHLH seems to be in correlation with the PTHLH present inside the cell in these particular cell contexts.

The advantages of our methodology mainly rely in the fact of having all the reagents preloaded in the tests, making it possible to perform a quick detection (less than 20 minutes) even with the naked eye, without incubations and washing steps, in which only the samples have to be drop casted onto the sample pad of the already made LFIA strips. Other reported techniques require long incubations (hours or even overnight), washing steps, and usually reaction kinetics are involved in the final reading step. Furthermore no hazardous reagents are necessary, specialized facilities (RIA and IRMA) are not required and simple and cheap equipment is used.

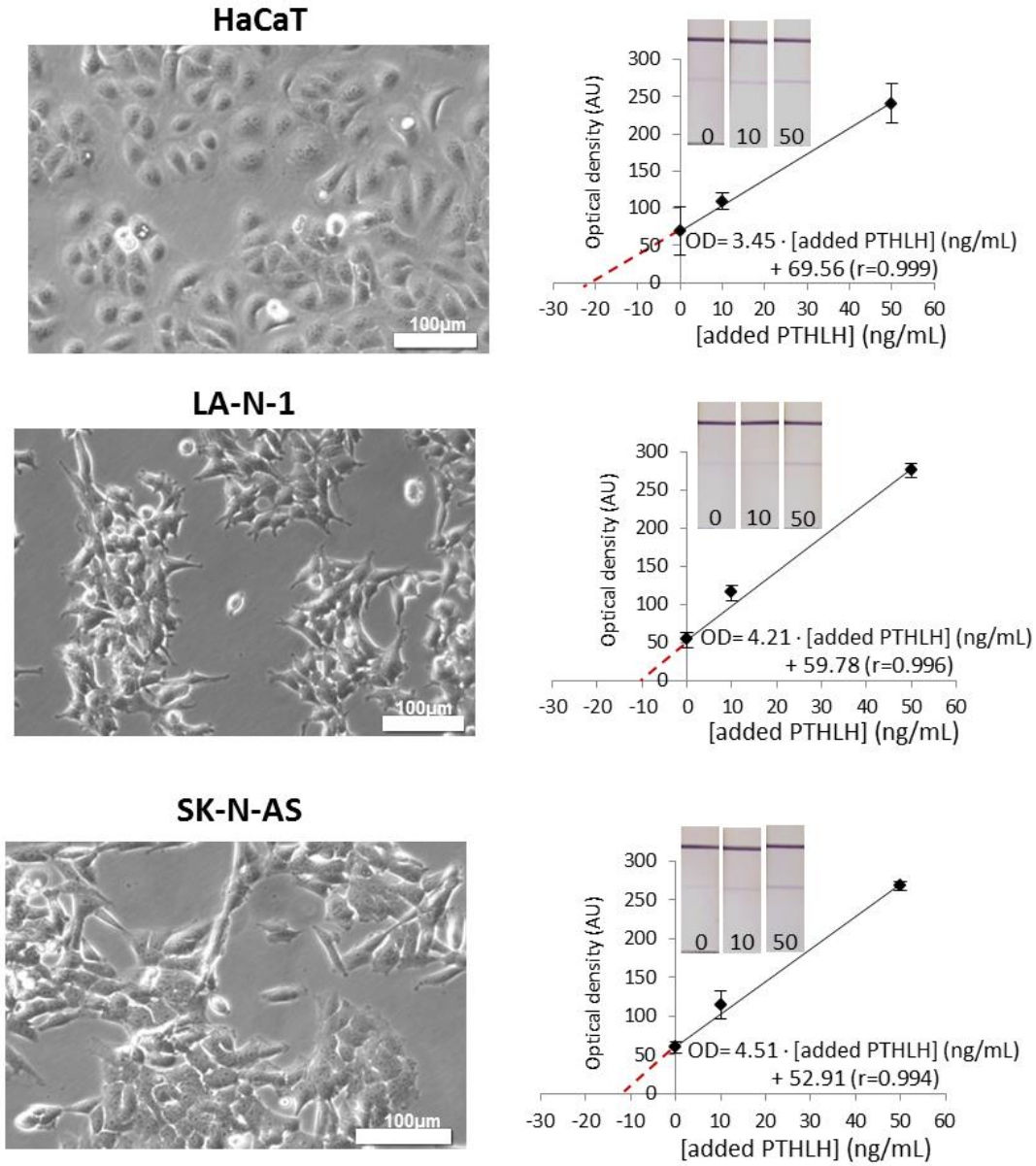

Figure A8: PTHLH quantitation in HaCaT, LA-N-1 and SK-N-AS cells culture media.(Left)Optical microscope images of cell cultures before the assay.(Right)Standard additions of PTHLH in cell culture media of the three cell lines. Insets in graphics show the strips after each addition (in ng/mL).

A1.3.5 Performance in real samples: spike and recovery

Although the main goal of this work is the quick and easy detection of PTHLH in cell cultures, with the aim to give researchers a new resource to help the studies of the expression levels and secretion of this PTHLH in cell cultures, the performance of the LFIA assay in human serum was also evaluated so as to demonstrate the potential of our system for diagnostics. Since the levels of PTHLH in human serum of healthy donors (few pg/mL) (15,16) are below the LOD of the our system, the native amount of PTHLH present in the serum will be neglected and considered only the spiked PTHLH. A pool of human serum from 6 different donors was used to spike 0, 5 and 100 ng/mL. The obtained analytical signals and their comparison to those obtained in PBS buffer are shown in Table A3.

Recoveries around 90% for all the concentrations assayed were achieved. These results suggest that the developed LFIA has acceptable recovery rates for human serum samples making it a promising candidate to perform detection of PTHLH in a scenario of great interest for future diagnostic applications.

Spiked PTHLH (ng/mL)	Optical density in PBS (U.A.)	Optical density in Serum (U.A.)	Recovery (%)
0	70.86±2.22	62.73±7.93	88.6
5	111.26±25.27	100.67±10.90	90.5
100	354.06±39.75	309.495±7.13	87.4

Table A3: Spike and recovery assay data. The study was done by spiking 0, 5 and 100ng/mL of PTHLH in human serum. (n=3 for each sample). Percentage of recovery was obtained as comparing with PBS buffer

A1.4 Conclusions

In summary, a LFIA for the detection of PTHLH has been designed and tested, being capable to perform the detection of such factor at ng/mL levels in real samples obtained from HaCaT, LA-N-1 and SK-N-AS cell cultures (cell lysates and cell media). Secreted PTHLH in cell lysates and cell culture media has been evaluated. These results are in agreement with the obtained by Western Blot analysis, used as a semi-quantitative reference method.

Our approach represents a fast and easy methodology to detect PTHLH in cell lysates and cell culture media, As far as we know this is the first time that LFIA has been applied for the detection of PTHLH taking advantage of the properties that paper based nanobiosensors offer (easy to use, quick tests, good sensitivity). We would like to remark the advantage that means the possibility of taking a sample from cell culture media and quantify PTHLH in less than one hour. This pioneer study offers a novel alternative for the quick and robust detection of PTHLH avoiding the need of complex or expensive requirements. Besides, LFIA represents a versatile and easy adaptable technique. Components of the assay can be easily modified with the aim of adapting the assay to a different detection context. This kind of paper-based diagnostics are suitable for largescale production, making them a very cheap and efficient technology.

The developed method offers a new tool for the study of fundamental aspects related to the mechanisms and the factors associated to PTHLH secretion, which can be of great importance for therapeutic applications. Furthermore the low matrix effects found when analysing a human serum sample, demonstrate the ability of the developed system to perform analysis in scenarios of interest for future diagnostic applications. The present study opens the way to future applications of LFIA for the rapid determination of a relevant protein in the biology and treatment of several malignancies.

A1.5 References

(1) Moseley JM, Kubota M, Diefenbachjagger H, Wettenhall REH, Kemp BE, Suva LJ, et al. *Proc Natl Acad Sci USA* **1987**; 84:5048-52.

(2) Moseley JM, Gillespie MT. *Crit Rev Clin Lab Sci* **1995**; 32:299-343.

(3) Suva LJ, Winslow GA, Wettenhall RE, Hammonds RG, Moseley JM, Diefenbach-Jagger H, Rodda CP, Kemp BE, Rodriguez H, Chen EY, et al. *Science*. **1987**; 237(4817):893-896.

(4) McCauley LK, Martin TJ. *J Bone Miner Res* **2012**; 27:1231-9.

(5) Wysolmerski JJ, Stewart AF. *Annu Rev Physiol* **1998**; 60:431-60.

(6) Soki FN, Park SI, McCauley LK. *Future Oncology* **2012**; 8:803-17.

(7) Liao J, McCauley LK. *Cancer and Metastasis Reviews* **2006**; 25:559-71.

(8) Park SI, Lee C, Sadler WD, Koh AJ, Jones J, Seo JW, et al. *Cancer Res* **2013**; 73:6574-83.

(9) Li J, Karaplis AC, Huang DC, Siegel PM, Camirand A, Yang XF, et al. *J Clin Invest* **2011**; 121:4655-69.

(10) Iguchi H, Tanaka S, Ozawa Y, Kashiwakuma T, Kimura T, Hiraga T, et al. *Cancer Res* **1996**; 56:4040-3.

(11) Wang Y, Lei R, Zhuang X, Zhang N, Pan H, Li G, et al. *J Clin Invest* **2014**; 124:1646-59.

(12) Urosevic J, Garcia-Albéniz X, Planet E, Real S, Céspedes MV, Guiu M, et al. *Nat Cell Biol* **2014**; 16:685-94.

(13) Urosevic J, Garcia-Albéniz X, Planet E, Real S, Céspedes MV, Guiu M, Fernandez E, Bellmunt A, Gawrzak S, Pavlovic M, Mangues R, Dolado I, Barriga FM, Nadal C, Kemeny N, Batlle E, Nebreda AR, Gomis RR. *Nat Cell Biol*. **2014**; 16(7):685-94.

(14) Bilezikian JP. *Clin Chem* **1992**; 38:179-81.

(15) Fraser WD, Robinson J, Lawton R, Durham B, Gallacher SJ, Boyle IT, et al. *Clin Chem* **1993**; 39:414-9.

(16) Pandian MR, Morgan CH, Carlton E, Segre GV. *Clin Chem* **1992**; 38:282-288.

(17) Raison D, Coquard C, Hochane M, Steger J, Massfelder T, Moulin B, et al. *American Journal of Physiology-Renal Physiology* **2013**; 305:F333-F42.

(18) Cafforio P, Savonarola A, Stucci S, De Matteo M, Tucci M, Brunetti AE, et al. *J Bone Miner Res* **2014**; 29:55-66.

(19) Kir S, White JP, Kleiner S, Kazak L, Cohen P, Baracos VE, Spiegelman BM. *Nature* **2014**; 513:100-4.

(20) De la Escosura-Muñiz A, Merkoçi A. *Expert Opinion on Medical Diagnostics* **2010**; 4(1): 21-37.

(21) De la Escosura-Muñiz A, Parolo A, Merkoçi A. *Materials Today* **2010**; 13(7-8):24-34.

(22) Espinoza-Castañeda M, de la Escosura-Muñiz A, Chamorro A, de Torres C, Merkoçi A. *Biosens Bioelectron*. **2015**; 15(67):107-114.

(23) Osikowicz G, Beggs M, Brookhart P, Caplan D, Ching SF, Eck P, et al. *Clin. Chem.* **1990**; 36:1586-.

(24) Parolo C, Merkoci A. Paper-based nanobiosensors for diagnostics. *Chem. Soc. Rev*. **2013**; 42:450-457.

(25) Fernández-Sánchez C, McNeil CJ, Rawson K, Nilsson O, Leung HY, Gnanapragasam, V. *J. Immunol. Methods* **2005**; 307:1-12.

(26) Lie P, Liu J, Fang Z, Dun B, Zeng L. *Chem. Commun*. **2012**; 48;236-238.

(27) Anfossi L, Baggiani C, Giovannoli C, D'Arco G, Giraudi G. *Anal. Bioanal. Chem.* **2013**; 405:467-480.

(28) López Marzo AM, Pons J, Blake DA, Merkoçi A. *Anal. Chem*. **2013**;85:3532-3538.

(29) Parolo C, de la Escosura-Muñiz A, Merkoçi A. *Biosens. Bioelectron*. **2013**; 40:412-416.

(30) Parolo C, Medina-Sánchez M, de la Escosura-Muñiz A, Merkoçi A. *Lab Chip* **2013**; 13:386-390.

(31) Rivas L, Medina-Sánchez M, de la Escosura-Muñiz A, Merkoçi A. *ab Chip* **2014**;14:4406-4414.

(32) (a)Nunes-Pauli GE, de la Escosura-Muñiz A, Parolo C, Helmuth-Bechtold I, Merkoçi, A. *Lab Chip*, **2015**; 15:399-405. (b) A. de la Escosura-Muñiz, C. Parolo, F. Maran, A. Merkoçi. *Nanoscale* **2011**,3(8); 3350-3356.

(33) de Torres C, Beleta H, Diaz R, Toran N, Rodriguez E, Lavarino C, Garcia I, Acosta S, Sunol M, Mora J. *Cancer.* **2009;** 115 (12); 2792-2803.

(34) Turkevich J, Stevenson PC, Hillier J. *Discussions of the Faraday Society* **1951**; 11:55-75.

(35) Ambrosi A, Castañeda MT, Killard AJ, Smyth MR, Alegret S, Merkoçi A. *Anal Chem* **2007**; 79:5232-40.

(36) Bradford, MM. *Anal. Biochem*. **1976**; 72: 248–254.

(37) (a) Parolo C, de la Escosura-Muñiz A, Polo E, Grazú V, de la Fuente JM, Merkoçi A. *ACS Appl Mater Interfaces* **2013**; 5:10753-9. (b) Kim E. Sapsford, W. Russ Algar, Lorenzo Berti, Kelly Boeneman Gemmill, Brendan J. Casey, Eunkeu Oh, Michael H. Stewart, and Igor L. Medintz. *Chemical Reviews* **2013** 113 (3), 1904-2074.

(38) Ferguson RE, Carroll HP, Harris A, Maher ER, Selb, PJ, Banks RE. *Proteomics* **2005**; 5(2): 566-571.

(39) Heath JK, Southby J, Fukumoto S, Okeeffe LM, Martin TJ, Gillespie MT. *Biochem J* **1995**; 307:159-167.

(40) Ellison SLR, Thompson M. Standard additions: Myth and reality. *Analyst* **2008**; 133:992-7.

(41) Daniel MacDougall, Warren B. Crummett, et al. *Analytical Chemistry* **1980** 52 (14), 2242-2249

(42) Armbruster DA, Pry T. *The Clinical Biochemist Reviews*. **2008**; 29 (Suppl 1):S49-S52.

Annex B

Annex B 1.

Electrochemical DNA biosensors (E-DNA sensors) technology based on carbon screen printed electrodes and gold nanoparticles

Research Stay Report

Work carried out in a research stay at the University of California Santa Barbara (UCSB) in USA between 20 January 2015 and 10 May 2015, at Prof. Kevin W. Plaxco Group in the Department of Chemistry and Biochemistry.

This research was done in the framework of the project IRSES "PEPTIDE NANOSENSORS". Funded by European Commission, Marie Curie Actions, Programme "PEOPLE" (Call identifier: FP7-PEOPLE-2011-IRSES Proposal No 294901).

Summary

Electrochemical DNA sensors (E-DNA) and Electrochemical Aptamer based sensors (E-AB) present remarkable properties that make them good candidates to be used in the field of biosensing. To date, all reported E-DNA and E-AB sensors have been fabricated on gold electrodes, or electrodes modified with electroplated gold. As an appealing alternative, screen printed carbon electrodes (SPCE) represent an inexpensive type of electrodes, suitable thanks to the broad potential window, the high overpotential needed for the oxygen or hydrogen reaction catalysis, and their mass production possibility. A feasible possibility non explored to date, as far as we know, is the combination of gold nanoparticles with thiol and methylene blue (MtB) modified aptamers or DNA sequences onto SPCE. E-DNA and E-AB sensors using conventional gold sensors were fabricated and applied for three different analytes: Linear DNA-40 base pairs (pb), Cocaine and Thrombin. Thrombin was chosen to be used as detection system to be adapted to the proposed biosensor. The system feasibility on planar printed electrodes was tested on gold screen printed electrodes and later applied to carbon electrodes to develop the proposed SPCE E-AB sensor using AuNPs.

Index

B.1.1 Introduction

Electrochemical DNA sensors (E-DNA) and Electrochemical Aptamer based sensors (E-AB) present remarkable properties that make them good candidates to be used in the field of biosensing[4,5]. In the particular case of methylene blue labeled DNA oligos and aptamers, the most significant properties, as already reported by Plaxco and coworkers are three[1,4-10]: a) reagent less sensor, no need to perform incubations, washings or blocking steps once the sample has been casted in the detection system; b) one recognition element, no need of secondary labeled probes, just one binding event necessary, therefore one binding area in the analyte is required; c) good performance when challenged in complex matrices such as blood or plasma.

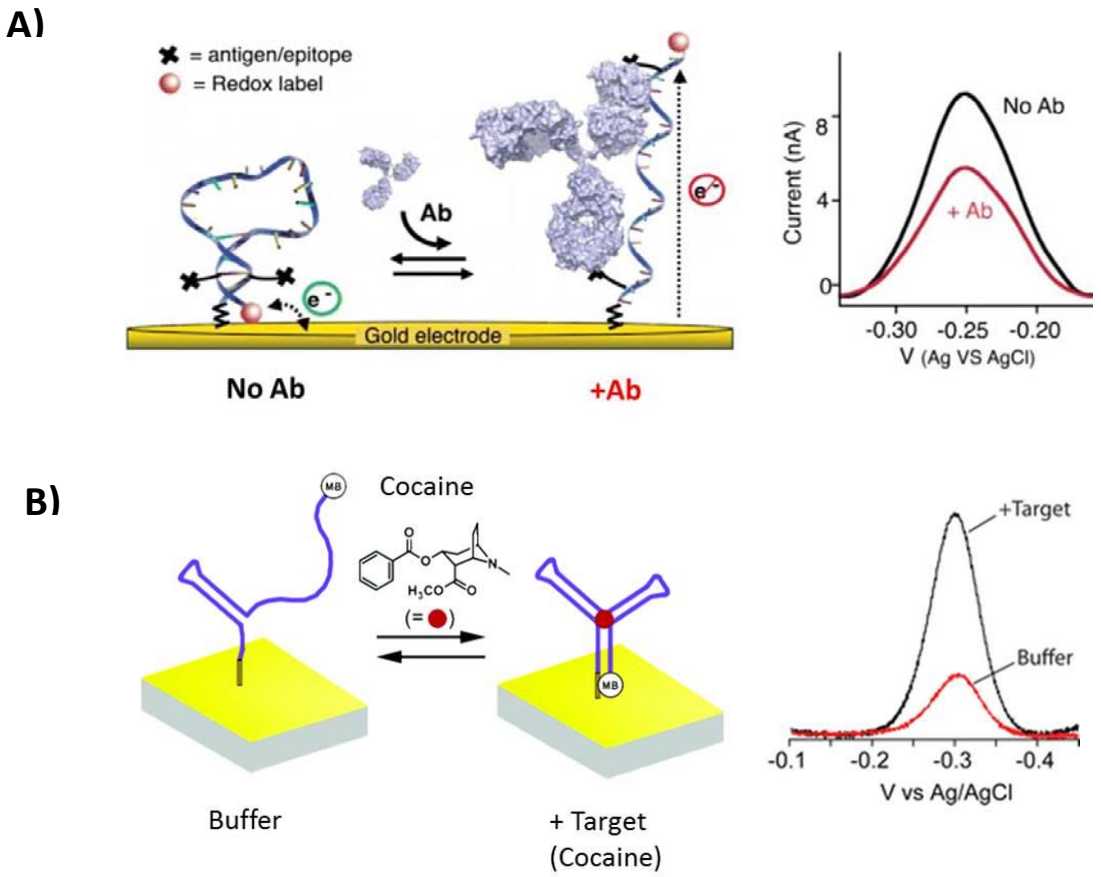

Figure B1 : Example of E-DNA and E-AB sensors using methylene blue (MtB) labelled DNA probes. A) Scheme of working principle of a E-DNA for the detection of antibodies in undiluted serum. Signal off detection: The more analyte (antibodies) the more DNA probes are opened and the MtB pulled away from the surface reducing the electrochemical signal in the SWV. Image adapted from reference [1]. B) Example of signal on E-AB sensor for cocaine detection through methylene blue labelled cocaine aptamer. Image adapted from references [2,3].

To date, all reported E-DNA and E-AB sensors have been fabricated on gold electrodes, or electrodes modified with electroplated gold[11]. Although the good properties presented by gold electrodes such as, high conductivity, flat surface, chemical inertness, they are limited by the high reactivity in certain electrochemical conditions, mainly due to the oxidation at positive potentials, the strong binding of undesired biological components containing mercapto groups and on top of all: the cost. As an appealing alternative, screen printed carbon electrodes (SPCE) represent an inexpensive type of electrodes, suitable thanks to the broad potential window, the high overpotential needed for the oxygen or hydrogen reaction catalysis, and the possibility to mass produce them.

There is significant amount literature related DNA and aptamers immobilized on gold nanoparticles. Most of the described approaches are based in the use of gold as optical label: taking advantage of the plasmon resonance and use them in aggregation assays [12-14]. In lesser extent electrochemical approaches for the detection of AuNP conjugated with aptamers have been also described. In this case the AuNP are used for different purposes: as direct labels detected taking advantage of the electrochemical properties of the AUNP, or as carriers to conjugate both the aptamer specific for detection and an electrochemical label (e.g HRP) that generates the electrochemical signal [15-17]. A shared fact among many of the described works is the use of aptamers as mere substitutes of antibodies, performing the same constructs as in regular immunosandwiches. The main interest lays on the advantages of using aptamers compared to antibodies. In some cases aptamers have been used for label free detection, using a redox indicator. The interaction with the analyte modifies the disposition of the aptamer and alters the surface available for the redox indicator.

Xingwang Yang and coworkers reported the use of nanoparticles as platforms linked to aptamers in order to perform detection of Ocratoxin (OTA). However the problem is tackled by performing an indirect assay using complex constructs of DNA – AuNP – DNA – Apatamer – Electrode, in which the OTA interferes with the interaction DNA-Aptamer, and releases the DNA-AuNP-DNA assembly. The electrochemical signal is obtained by measuring the amount of MtB in the solution which is accumulated in the G of DNA chains, giving a signal associated to the amount of DNA.

A feasible possibility non-explored to date, as far as we know, is the combination of gold nanoparticles with thiol and methylene blue (MtB) modified aptamers or DNA sequences onto SPCE. The principle of detection is the conformation change of the aptamer/DNA sequence when bounds to the analyte. This change will bring the MtB label closer, more accessible or away or isolated from the surface and hence increase or decrease the electrode signal. The aptamers were immobilized on

gold nanoparticles. Measurements were performed with carbon SPCE. The main advantage of the proposed system is the use of gold nanoparticles as carriers, to easily modify the carbon electrodes exploiting also their advantageous properties. The use of MtB- modified aptamer gives the possibility to make detection with just one recognition element avoiding the need of performing and immunosandwich. The system developed would represent a useful platform for quick modification of the SPCE surfaces with the AuNP-Aptamer assemblies, and perform the quantification of the analyte.

In order to reach the objective first steps were focused in E-DNA and E-AB sensors fabrication and use. The conventional gold sensors (using gold disk electrodes, 2mm diameter) were done for three different analytes: Linear DNA-40 base pairs (pb), Cocaine and Thrombin. For both the linear DNA and Thrombin the detection system is a signal off (see Figure B1 A), therefore when anlyte binds there is a loss in the electrochemical signal. Cocaine is a signal on system (see Figure B1 B), when cocaine is captured by the aptamer the charge transfer to the electrode is enhanced, hence the signal is increased. Capturing agents were DNA sequences modified with Methylene Blue in the 3' end. In the case of the linear DNA, capturing agent consisted in just a linear labelled DNA complementary to the 40pb DNA used as analyte. However, for the detection of Cocaine and Thrombin, specific sequences of aptamers were used. The labelled DNA sequences were anchored on the gold surfaces thanks to a thiol group conjugated to the sequence through a 6 carbon alkane spacer on the 5'end, following the host lab procedures as previously reported. Next, thrombin was chosen to be used as detection system to be adapted to the proposed biosensor: SPCE E-AB sensor through AuNPs. Previous to directly work with AuNPs and SPCE, the feasibility of the E-AB on planar printed sensors was proved using gold screen printed electrodes (GSPE).

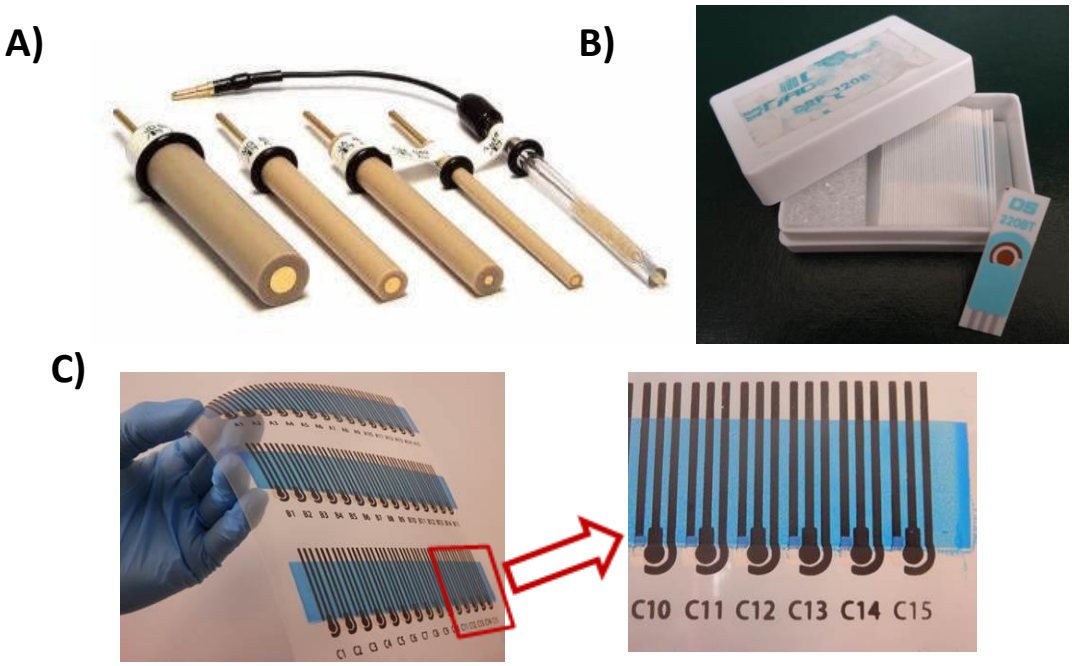

Figure B2: Examples of electrodes used to fabricate sensors.A) gold disk electrodes of different diameters. B) Gold screen printed electrode (GSPE) from Dropsens, showing the working, counter and reference electrode. C) Sheet of screen printed carbon electrodes (SPCE) on polyester substrate. Inset displays magnification of the image of the SPCE individually, reference, working and counter electrode can be better appreciated.

B.1.2 Experimental section

B.1.2.1 Reagents and apparatus

PDMS membranes of 0.008 inches thick (200µm) were obtained from Speciality Silicon Products, Inc (Ballton Spa, NY, US). Gold(III) chloride trihydrate ($HAuCl_4 \cdot 3H_2O$), Mercapto hexanol, TCEP (tris(2-carboxyethyl)phosphine hydrochloride) , cocaine were purchased to sigma Aldrich. Sodium hydroxide, sodium chloride, magnesium chloride, trisodium citrate, phosphoric acid and alumina powder for electrode polishing were purchased from Fisher scientific. All buffers were filtered before use. Human alpha Thrombin (referred as Thrombin in the chapter) was purchased to Haematologic Technologies Inc.

Thrombin aptamer sequence was 5'd Thiol C6 SS-TAAGTTCATCTCCCCGGTTGGTGTGGTTGGT-Methylene Blue 3', Cocaine aptamer sequence was 5'd Thiol C6 SS-GACAAGGAAAATCCTTCAATGAAGTGGGTC Methylene Blue 3', Linear DNA sequence used was 5'd Thiol C6 SS-CGCGATAGAAGAACTGGCGCTCCGTGTGATCGCGCGCGATA Methylene Blue 3' and the

corresponding target 5'-TATCGCGCGCGATCACACGGAGCGCCAGTTCTTTATCGCG-3 . The 4 DNA sequences were purchased to Biosearch technologies (Petaluma, CA, USA).

Gold disk electrodes 1mm of diameter were purchased to CH Instruments, Austin, Tx, US). Gold screen printed electrodes, printed on ceramic substrate, were purchased to Drop Sens (Oviedo, Spain). SPCEs on polyester were home-made using a semiautomatic machine DEK248. Polyester substrates were purchased from MacDermid Autotype (Manchester, UK). All the inks, Carbon ink, Ag/AgCl ink and the insulating ink were purchased from Gwent electronics (Pontypool, UK).

Electrochemical measurements were performed with a CH potentiostat (CH Instruments Inc., Austin Tx, US). Z potential and DLS measurements were performed with a Z sizer instrument, Malvern insturments (Malvern, UK).

B.1.2.2 Methods and Procedures

B.1.2.2.1 Carbon screen printed fabrication

SPCEs consist of counter electrode, reference electrode of Ag/AgCl and working Electrode. They are fabricated on sheets of polyester substrate by the sequential deposition of different ink layers. First the graphite ink layer on the polyester substrate for working and counter electrodes, next the Ag/AgCl ink for the reference electrode and finally the isolating ink. Each layer is printed using a screen printing machine with a stencil specific for each layer, which contains the patterns of the electrodes. After its deposition each layer was cured by keeping the printed sheet at 120 ºC for 30 minutes.

B.1.2.2.2 Gold nanoparticle synthesis

AuNP of 15 nm in diameter were prepared by reduction of $HAuCl_4 \cdot 3H_2O$ following the procedure described by Turkevich et al [18] : all glassware was cleaned with aqua regia (HCl and HNO3 at 3:1 parts in volume) and thoroughly rinsed with milliQ water. Aqueous solution of HAuCl4·3H2O 0.25mM in milliQ water was heated to boiling point under strong stirring. Then 1.25 mL of 34mM trisodium citrate solution was added, the heating and stirring was held constant for 10 minutes, at this point the colourless solution becomes violet and later red. The AuNP solution was cooled down and stored at 4°C protected from light. The resulting nanoparticles were characterized by Z potential and Dynamic Light Scattering (DLS).

B.1.2.2.3 Gold electrodes and gold screen printed electrodes activation and modification

Gold electrodes and GSPE E-DNA and E-AB sensors were prepared using the well-established previously described procedure [4,19]. In brief, prior to sensor fabrication, gold disk electrodes were cleaned both mechanically (polished using alumina powder of 1µm diameter size) and electrochemically (applying cycles of in NaOH and H_2SO_4)[4]. GSPE were just electrochemically cleaned by applying immersing the electrodes in a 0.05M H_2SO_4 solution and applying 20 cycles from -0.2V to +1.4V.

Right before electrode modification, DNA probes were incubated 1h in TCEP 10mM, in order to reduce the thiol bond of the C6 alkane protecting group attached by S-S bond to the C6 spacer on the 5' end. Gold electrodes and GSPE were modified by immersion in a PBS solution containing the DNA to be anchored.

Gold electrodes for the specific case of DNA linear probe, were immersed in a PBS solution containing 50nM of methylene blue labelled DNA solution. For the thrombin aptamer they were immersed in 500nM of methylene blue labelled thrombin aptamer solution of PBS. For the cocaine aptamer gold electrodes were immersed in 500nM of methylene blue labelled cocaine aptamer solution of PBS. All gold electrodes were immersed in 100µl.

GSPE were modified with thrombin aptamer by covering the working electrode with 50µl of 1µM of methylene blue labelled thrombin aptamer solution in PBS. Electrodes were incubated for 2 hours in a humid chamber in order to prevent evaporation of the drop. Next, the electrodes were washed by immersion in fresh PBS, the procedure was repeated 3 times per electrode. Then, the electrodes were immersed in 20mM mercapto hexanol in PBS for 3 hours, in order to form a self-assembled monolayer (SAM) on the gold surfaces; which acts as blocking agent and helps the packaging of the C6 spacers of the DNA sequences on the electrodes. Washing steps after blocking consisted in immersing the electrodes in PBS three times, each time using fresh buffer.

Incubation of the electrodes with the analytes were performed by immersion of the sensors, gold electrodes and GSPE, in 5ml and 2.5ml samples respectively. Measurements were performed after 1h incubation of the sensor with the sample (as optimized in previous reports of the group [20]).

B.1.2.2.4 SPCE electrodes modification with Gold Nanoparticles and DNA probes

SPCE were first modified with AuNPs by dropcasting them on the WE. A PDMS frame with a circular window exposing just the WE and protecting the CE and RE was used to drop cast 30µl of AuNPs and modify selectively just the WE. The dropcasted electrodes were dryed in an oven at 60ºC for 1 hour. After the modification the PDMS was removed and the modified SPCE rinsed with distillate water. Measurement of presence of AuNPs on the SPCE was done thanks to the gold signal in presence of H_2SO_4, cyclic voltammetry between -0.5 and +1.5V in 0,05M showed the reduction peak related to the gold presence.

SPCE were modified with thrombin aptamer by covering the working electrode with 50µl of 1µM of methylene blue labelled thrombin aptamer solution in PBS. Electrodes were incubated for 2 hours in a humid chamber with the Methylene Blue labelled DNA solutions. Then, the electrodes were immersed in 20mM mercapto hexanol in PBS for 3 hours, in order to form a self-assembled monolayer (SAM) on the gold surfaces. Washing steps after blocking consisted in immersing the electrodes in PBS three times, each time using fresh buffer. Incubation of the electrodes with the analytes were performed by immersion of the sensors, in tubes containing 500µl of sample. Measurements were performed after 1h incubation of the sensor with the sample (as optimized in previous reports of the group).

B.1.2.2.5 Electrochemical measurements

Square Wave voltammetry (SWV) was performed to interrogate the sensors. The presence of methylene blue under the potential scan from 0V until -0.5V gives a peak signal at -0.3V corresponding to the reduction of methylene blue. The peak intensity is extracted from the measurements, using the CH instrument software, and used as analytical signal.

Gold sensors were measured in electrochemical cell with 5ml of sample volume, and external RE and CE are added. Screen printed electrodes, both Carbon and Gold, are measured in drop, using a 60µl of sample drop covering all three components: WE, CE and RE.

B.1.3 Results and discussion

B.1.3.1 Gold nanoparticles (z potential and DLS)

One synthetized, the resulting AuNPs were characterized using a Zeta sizer equipment. The results obtained are displayed in Figure B3. The average value of particle diameter is 21.43 nm, which is close to the expected 20nm. Furthemore, the -32.4mM of Z potential granted good stability of the AuNPs colloidal solution.

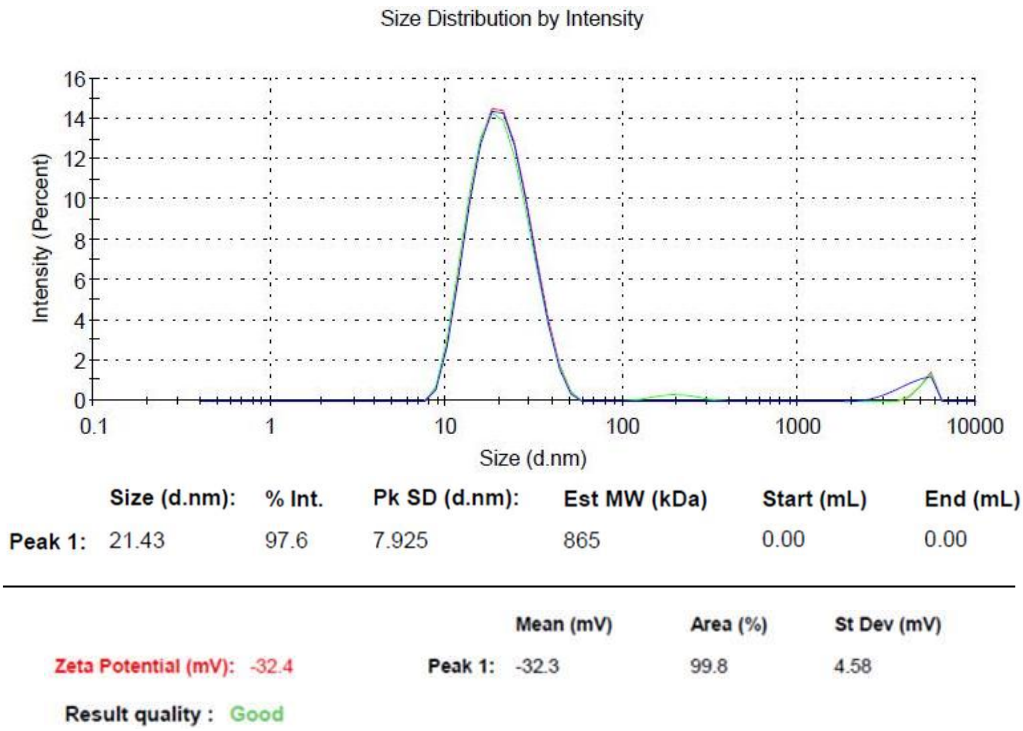

Figure B3: Dynamic light scattering (DLS) and Z potential measurements obtained for the synthetized gold nanoparticles (AuNPs). Top: output graphic of DLS showing the peak of average diameter at 21.43 nm (as shown in the table right under the graphic). Bottom: Z potential results, mean value -32mV, probing the stability of the AuNPs.

B.1.3.2 Gold disk electrodes calibrations titration curves

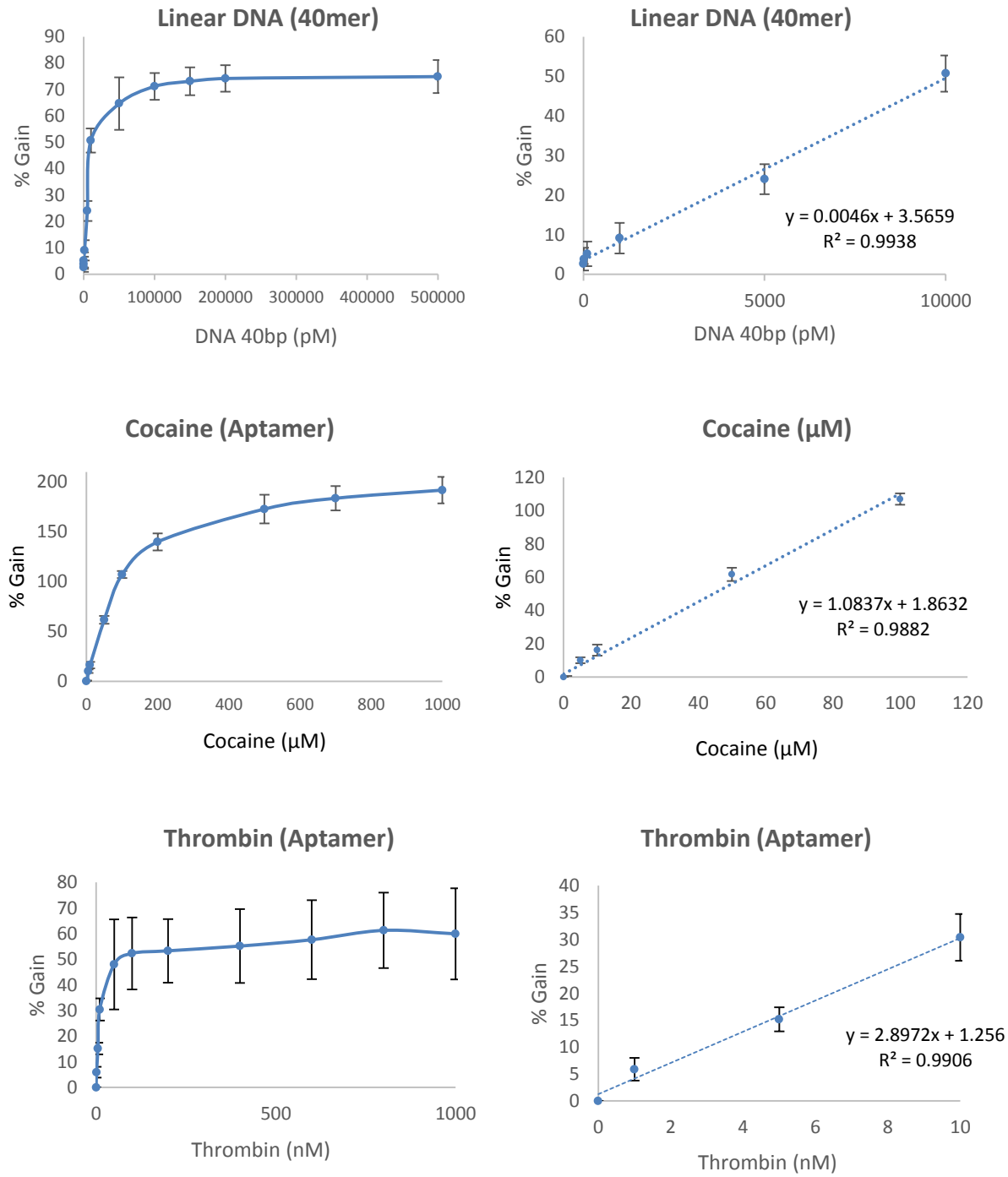

Figure B4: Titration curves obtained for three different analytes using gold disk electrodes. **Left:** % of Gain over the analyte concentration is displayer. **Right:** Titration curb of the linear region for each analyte and the corresponding linear adjustment.

Results of the measurements performed with sensors fabricated with gold disk electrodes are shown in Figure B4. Standard solution of known concentration was done in buffer. Analytical values in the measurement were the reduction peak of methylene blue in the SWV measurement. Left of the image the percentage of Gain is plotted. Gain is signal of the samples in reference to the signal of the blank. Measurements of each point were performed at different frequencies of the SWV. The results presented correspond to the frequency to which maximum signal was achieved; for linear DNA 100Hz was used, for cocaine aptamer 100Hz, for and Thrombin aptamer 240Hz. On the right of Figure B4 the corresponding linear behaviour region is presented with its respective line adjustment. Since the corresponding capturing agent is used for each analyte, the particular affinity they presents for their analytes results different for the increasing amounts of analyte. This is why the linear region for each situation is different. The fact that the signal change is mediated by the interaction of the analyte with the capturing DNA, detection systems for each analyte will present different final percentage of Gain. For instance, the interaction of the cocaine aptamer with cocaine results in such a conformation that the electron transfer to the gold surface is greatly increased achieving gains over 100%, while the two other systems, thrombin and linear DNA, present gains of 60% and 70% respectively.

The fabrication of E-DNA and A-AB sensors have been successfully carried out and checked with samples in buffer. Proving the reproducibility and robustness of the systems developed and reported by the host institution.

After the good performance of all the tried analytes, thrombin, due to the interest of working on protein detection, was chosen as model analyte for later works adapting the proved electrochemical detection system to the screen printed electrodes.

B.1.3.3 Gold Screen printed electrodes

Although the E-DNA and E-AB technology represent well established and reliable technology, as confirmed in the previous section, it still became of interest to prove its performance using screen printed electrodes. As intermediate, before moving to the use of AuNPs modified SPCE, and in order to check the feasibility of the system on printed electrodes GSPE were used to fabricate A-AB sensors using thrombin aptamer, and tested for the detection of thrombin in buffer.

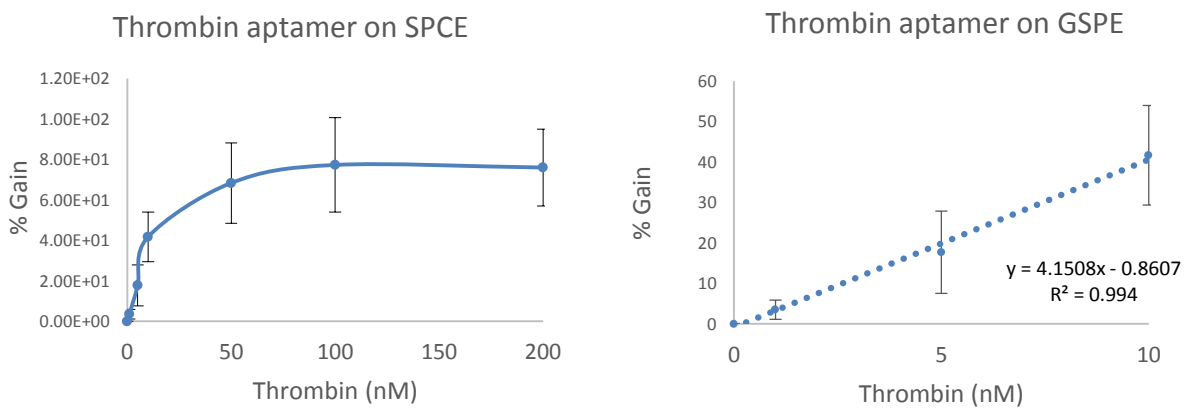

Figure B5: Detection of thrombin using Gold Screen Printed Electrodes (GSPCE) modified with thrombin aptamer. Left: representation of the % signal Gain. Right: magnification of the linear behaving region, adjusted to a line.

Interrogating the electrodes after incubation with the analyte through SWV, a titration curve was built (see Figure B5). For these sensors maximum current signal was achieved at 80Hz. From measurements using this frequency the % of gain was calculated for the different samples. Although significant bigger error bars were obtained for the GSPE, compared to the Gold disk electrodes, the slope in the linear adjustment is higher for the GSPE, meaning that better discrimination of different amounts of analyte can be achieved.

Two main issues were under study: first, in the case gold disk electrodes just the working electrode was modified, since the counter and reference are externally incorporated in the electrochemical cell in order to perform the measurement. On the contrary, GSPE constitute one entity, therefore all three electrodes, WE, CE and RE have to be subjected to the modification procedure. Second, for gold disk electrodes all incubations, modifications and measurements were performed by immersing the electrode in the modifying solution, while in the case of screen printed electrodes, some steps such as modifications and measurements are performed in drop instead of immersing the electrode in the solution. As conclusion of this experiment, the main objective was proved: screen printed electrodes are compatible with E-AB technology.

B.1.3.4 SPCE modification with gold nanoparticles

Modification of SPCE with gold nanoparticles was studied. It was necessary to find the proper deposition procedure, and stable modification of the WE. Due to its easiness and simplicity drop casting was chosen as modification procedure. In order to avoid dealing with AuNPs aggregation in solution and coverage, it was decided to perform all the immobilization procedure on surface by different steps, trying to act as closer as possible as the developed E-DNA A-AB reported technology with gold electrodes. First the gold nanoparticles were attached on the electrodes surface, then the MtB labelled DNA and finally the SAM.

Drop casting was performed as described in section B.1.2.2.4). Stability of modification was checked by observing the signal change of gold reduction peak after rinsing thoroughly the electrodes with buffer.

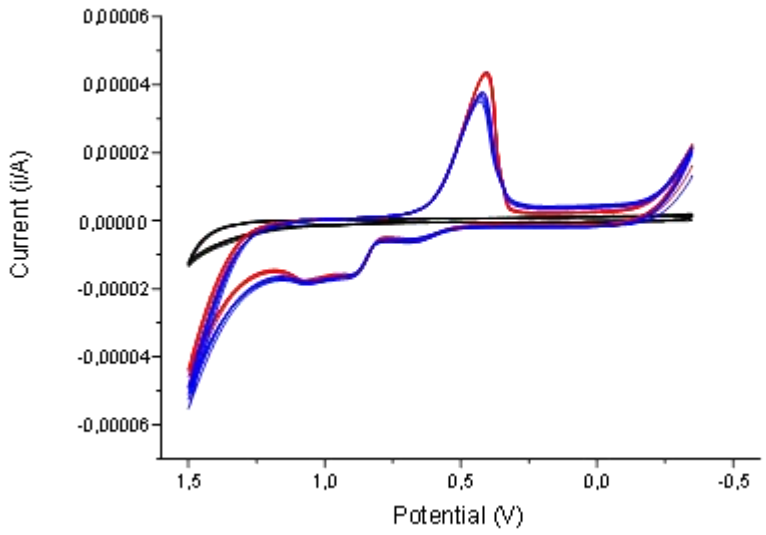

Figure B6: Example of cyclic voltammetry (cv) of Gold nanoparticle (AuNPs) modified screen printed carbon electrodes (SPCE). The cycles were performed in 0,05M of H_2SO_4. Black: signal obtained for bare SPCE, without any modification. Red: the signal achieved for a SPCE modified with AuNPs and rinsed just once. Blue: SPCE modified with AuNPs, rinsed, measured by CV, rinsed again and measured for a second time.

Although the small signal change, the gold peaks of AuNPs were stable after washings. Black line corresponding to a bare SPCE proves that the peak obtained belongs to the deposited AuNPs. The small changes in peak currents can be explained by the modifications created by the harsh conditions applied to the system at the highest and lowest potentials in the CV cycles. When measuring, high positive and negative potentials are applied, henceAuNPs can be altered. As

conclusion, drop casting gold nanoparticles on the WE of the SPCE and drying in the oven represents an easy procedure for the stable modification of the electrodes.

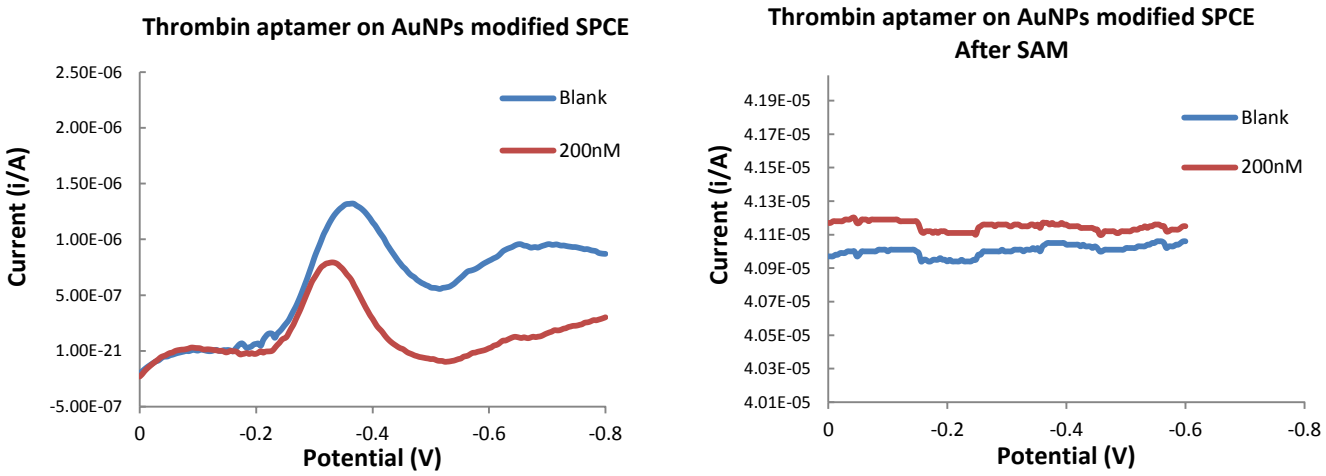

Figure B7: Example of results obtained for different Screen printed Carbon electrodes (SPCE) modified with thrombin aptamer labelled with Methylene blue (MtB). **Left:** SPCE modified with labelled aptamer.Measurements performed for blank, and 200nM of Thrombin. **Right:** aptamer modified SPCE after incubation in mercaptohexanol (MHX) for Self-assembled monolayer (SAM) formation. Square wave voltammetry performed at 20Hz .

In Figure B7 examples of results obtained for modified SPCE are displayed. When SPCE are just modified with the MtB labelled aptamer, through the interaction between the thiol group on the aptamer and the gold on the AuNPs, a current peak corresponding to the MtB reduction signal can be seen. When the same sensor is incubated in 200nM of Thrombin a reduction in the signal is achieved. The peaks obtained for the blank and the samples at 200nM were $1.32 \cdot 10^{-6}$A and $8.64 \cdot 10^{-7}$A respectively. In order to carry out the whole sensor fabrication procedure, a SAM has to be performed, to help the well package and stabilize the DNA chains immobilized through thiol gold chemistry. Examples of results of these sensors are displayed in Figure B7 right. No signal peak is achieved after incubation with MHX. These results together with the lack of reproducibility of the modification (data not shown), suggest that the peaks obtained before performing the SAM on the sensors, were achieved thanks to the MtB modified aptamers that have been non-specifically attached to the surface of the AuNPs modified SPCE.

B.1.4 Conclusions

E-DNA and E-AB sensors have been fabricated following previously reported procedures. The devices have been used for the detection of linear DNA, cocaine and Thrombin by making a titration curve for each of the analytes. In order to proof the feasibility of the E-DNA and E-AB technology on printed electrodes, a sensor for Thrombin detection has been successfully fabricated on GSPE. When the technology has been applied on SPCE, signals of MtB could be read if no SAM of mercaptohexanol was performed on the electrodes. After the SAM formation step, an increase in the irreproducibility of sensor fabrication was found, and the MtB peak disappeared. As conclusion, two phenomena have been proved, first the possibility to use MtB labelled DNA probes with the home made SPCE and obtain a readable signal, second, the problems related to the immobilization preformed, based in the thiol gold interaction; impossibility to successfully fabricate an E-AB sensor have been related to this last issue. In order to overcome this point and move forward in the topic we believe that two main alternatives could be followed: on the one hand optimize the modification of gold nanoparticles in solution and then deposit the constructs on the SPCE to later perform the measurement. On the other hand, changing the immobilization principle, instead of using the thiol gold interaction, attach covalently the labelled DNA probes on the electrodes, avoiding the use of AuNPs as connecting platform.

B.1.5 Bibliography

(1) Vallee-Belisle, A.; Ricci, F.; Uzawa, T.; Xia, F.; Plaxco, K. W. *Journal of the American Chemical Society* **2012**, *134*, 15197-15200.

(2) Baker, B. R.; Lai, R. Y.; Wood, M. S.; Doctor, E. H.; Heeger, A. J.; Plaxco, K. W. *Journal of the American Chemical Society* **2006**, *128*, 3138-3139.

(3) Idili, A.; Amodio, A.; Vidonis, M.; Feinberg-Somerson, J.; Castronovo, M.; Ricci, F. *Analytical Chemistry* **2014**, *86*, 9013-9019.

(4) Xiao, Y.; Lai, R. Y.; Plaxco, K. W. *Nat. Protocols* **2007**, *2*, 2875-2880.

(5) Rowe, A. A.; White, R. J.; Bonham, A. J.; Plaxco, K. W. *Journal of visualized experiments : JoVE* **2011**.

(6) Bonham, A. J.; Hsieh, K.; Ferguson, B. S.; Vallee-Belisle, A.; Ricci, F.; Soh, H. T.; Plaxco, K. W. *Journal of the American Chemical Society* **2012**, *134*, 3346-3348.

(7) Bonham, A. J.; Paden, N. G.; Ricci, F.; Plaxco, K. W. *Analyst* **2013**, *138*, 5580-5583.

(8) Fan, C.; Plaxco, K. W.; Heeger, A. J. *Proceedings of the National Academy of Sciences* **2003**, *100*, 9134-9137.

(9) White, R. J.; Kallewaard, H. M.; Hsieh, W.; Patterson, A. S.; Kasehagen, J. B.; Cash, K. J.; Uzawa, T.; Soh, H. T.; Plaxco, K. W. *Analytical Chemistry* **2012**, *84*, 1098-1103.

(10) Xiao, Y.; Dane, K. Y.; Uzawa, T.; Csordas, A.; Qian, J.; Soh, H. T.; Daugherty, P. S.; Lagally, E. T.; Heeger, A. J.; Plaxco, K. W. *Journal of the American Chemical Society* **2010**, *132*, 15299-15307.

(11) Yang, W.; Gerasimov, J. Y.; Lai, R. Y. *Chemical Communications* **2009**, 2902-2904.

(12) Liu, J.; Lu, Y. *Journal of the American Chemical Society* **2003**, *125*, 6642-6643.

(13) Cheng, F.; He, Y.; Xing, X.-J.; Tan, D.-D.; Lin, Y.; Pang, D.-W.; Tang, H.-W. *Analyst* **2015**, *140*, 1572-1577.

(14) He, P. L.; Shen, L.; Cao, Y. H.; Lia, D. F. *Analytical Chemistry* **2007**, *79*, 8024-8029.

(15) Yeh, F.-Y.; Liu, T.-Y.; Tseng, I. H.; Yang, C.-W.; Lu, L.-C.; Lin, C.-S. *Biosensors and Bioelectronics* **2014**, *61*, 336-343.

(16) Ma, X.; Jiang, Y.; Jia, F.; Yu, Y.; Chen, J.; Wang, Z. *Journal of Microbiological Methods* **2014**, *98*, 94-98.

(17) Zhao, J.; Lin, F.; Yi, Y.; Huang, Y.; Li, H.; Zhang, Y.; Yao, S. *Analyst* **2012**, *137*, 3488-3495.

(18) Turkevich, J.; Stevenson, P. C.; Hillier, J. *Discussions of the Faraday Society* **1951**, *11*, 55-75.

(19) Rowe, A. A.; White, R. J.; Bonham, A. J.; Plaxco, K. W. *Journal of Visualized Experiments : JoVE* **2011**, 2922.

(20) Xiao, Y.; Lubin, A. A.; Heeger, A. J.; Plaxco, K. W. *Angewandte Chemie International Edition* **2005**, *44*, 5456-5459.

Annex C

Annex C 1.

In situ detection of PTHLH secreted by cells cultured on a nanochannel-based sensing platform.

Summary

A nanochannel array device that operates through Prussian blue nanoparticles (PBNPs) as red-ox indicator for sensitive label-free immunodetection of a protein secreted by a cell line directly cultured in the device is presented. The detection principle is based on the nanochannel (20 nm pore sized) blockage due to the immunocomplex formation. This novel application of the system previously developed in the group has proved its capability for detecting Parathyroid like hormone (PTHLH) secreted by cells directly grown on the sensing platform. In this specific case two cell lines were chosen, HaCat and SK-N-AS, and PTHLH measured after different incubation times, being able to observe differences in expression between both cell lines.

Index

C1.1. Introduction

In this annex, preliminary results for the application of nanochannels in the detection of PTHLH secreted by cells directly cultured on a nanochannel membrane are presented. In section 1.3.2 in the introduction of the thesis biosensing based in the use of nanochannels is discussed.

Immunodetection using nanochannels can be accomplished by the blockage effect of the immunocomplex formed by the capturing antibody immobilized on the nanochannel membrane and the analyte, when formed it prevents the redox indicator from reaching the electrode surface through the nanochannels, and hence, there's a loss of electrochemical signal. As stated previously in the thesis intro, this principle has been successfully applied in biosensing, not only for the detection of proteins, but DNA as well[1-3].

Previously in our group, nanochannel based detection of proteins has been successfully performed and reported for the detection of Parathyroid Like Hormone (PTHLH) present in cell culture medium[4]. Levels of detection achieved (50 ng/mL) are still far from those found in human bloodstream, however PTHLH produced by certain cell lines are within the LOD of the developed system. Therefore, study of PTHLH expression of cells in culture can be performed using the proposed technique. PTHLH is secreted by tumour cells and circulates in the bloodstream until the target cells. Its activity has been described mainly for the specific case of hypercalcemia [5,6]. Moreover, other roles and actions have been reported for PTHLH in different contexts [7-9], demanding more studies to achieve better and more complete understanding of the protein. As consequence the possibility to perform PTHLH detection in cell culture models still represents an interesting research and application area. Hence, integration of sensing device for expressed PTHLH and growing the cells in the same platform becomes of special interest for expression studies of PTHLH under different conditions.

Preliminary work has been performed within the group setting the conditions and preparing the set up for growing cells on a nanochannel based sensing device [10]. These optimizations include: checking the compatibility of cells being seed on anodized aluminium oxide (AAO) nanochannel membranes, compatibility of cells with plastic materials used in the set up and proper sealing of the set up to prevent leaks of cell medium. As a continuation of this work what this annex presents now is the integration of both: on one side the sensing of PTHLH through nanochannels, and on the other the cell growing on nanochannel membranes, for the detection of the PTHLH expressed by the cells grown directly onto the device.

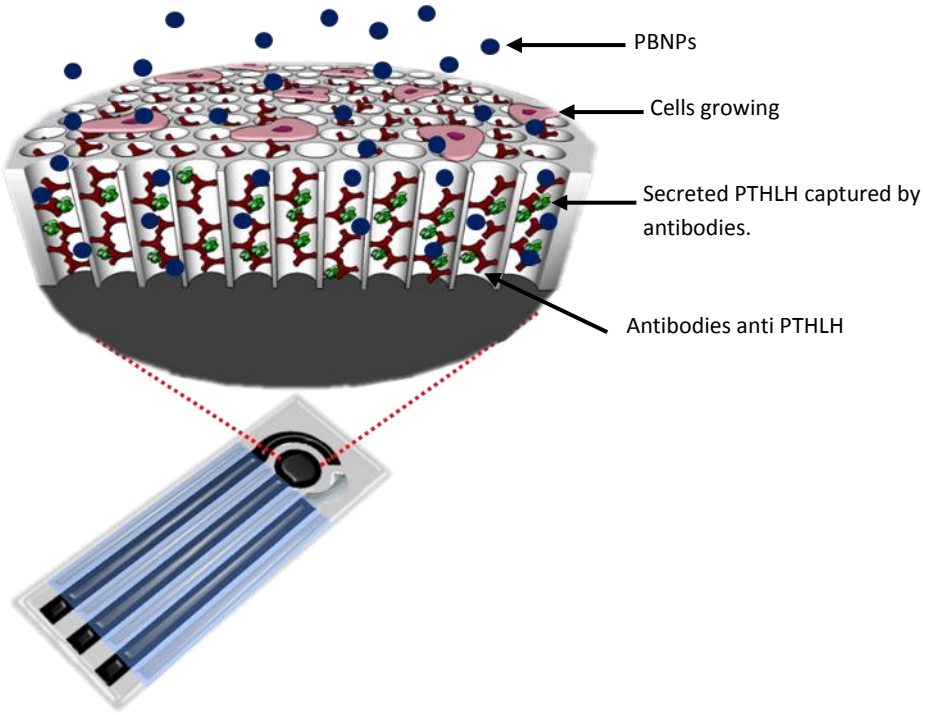

Figure C1: Schematic view of the nanochannel based detection of parathyroid like hormone (PTHLH) secreted by cells grown on the nanochannel device. Red-ox indicator: Prussian Blue nanoparticles (PBNPs). Figure adapted from reference [10].

C1.2. Experimental section

C1.2.1. Reagents and equipment

Thermostatic bath ISOTEMP was purchase from Fisher Scientific. Incubator NU-5100E/GCO$_2$ was purchase from Nuaire (USA). A BIOII A/Pbiosecurity cabinet (from Telstar, Spain) was used. TC Flask 75 cm², Multiple Well Cluster Plate, TC-Treated, Sterile individual pipettes of 25, 10, 5, 2 mL were purchased from Cultek (Spain). Screen-printed carbon electrodes (SPCEs) used as transducers were fabricated following the experimental procedure detailed in Chapter 3. SPCEs consisted of three electrodes: working electrode, reference electrode and counter electrode in a single strip fabricated with a semi-automatic screen-printing machine DEK248 (DEK International, Switzerland). Plastic used as substrate was Autostat HT5 polyester sheet purchased to McDermid Autotype (Manchester, UK), pastes or inks used to print the electrodes were C2030519P4 carbon/graphite paste, C2130809D5 silver/silver chloride paste and D2070423P5 dielectric paste purchased to Gwent

electronic materials Ltd. (Pontypool, Wales, UK). Anodized alumina oxide filter membranes (Whatman anodisc AAO filters, 13 mm diameter; 60 µm thickness; containing 20 nm diameter pores) were purchased from Scharlab (Spain). A homemade methacrylate electrochemical cell set-up with capacity for six and three samples was developed (see Figure C2) and used for electrochemical measurements that were performed with an Autolab 20 (Eco-chemie, The Netherlands) connected to a PC. All the measurements were carried out at room temperature with a working volume of 200 µL, which was enough to fill the well conformed by the home-made pieces with the nanochannels membranes and where cells are grown, besides is the volume that covers the three electrodes contained in the SPCEs connected to the potentiostat by a homemade edge connector module. Olympus IX71 (Spain) inverse microscope and Scanning Electrochemical Microscopy FEI Quanta 650 FEG ESEM (The Netherlands) were used for the optical characterizations.

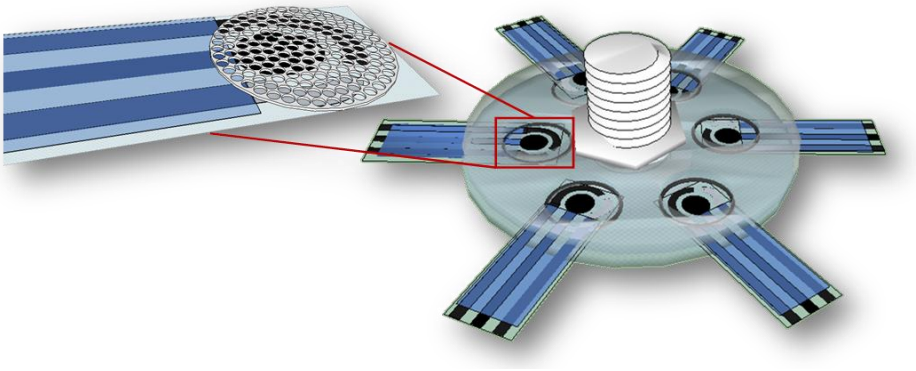

Figure C2: Scheme of home-made methacrylate set-up for processing 6 samples at the same time. The lower piece holds the electrodes in position, while the upper piece fixes the membrane on the electrodes. The upper methacrylate piece is in contact with the alumina membrane through a rubber ring to prevent the membrane from breaking. Figure adapted from [10].

The HaCaT and SK-N-AS cell lines were provided from Hospital Sant Joan de Deú, (Barcelona, Spain). Anti-PTHLH (PC09) polyclonal antibody developed in rabbit was purchased from Calbiochem (Spain). Aliquots of this antibody were prepared in 0.01 M PBS buffer pH 7.4, containing 5 mM EDC/sulfo-NHS. Bottle of CO_2 was purchased from Carburos Metálicos (Spain). PTHLH (SRP4651; human recombinant, expressed in E.coli) was purchased from Sigma-Aldrich (Spain). $FeCl_2 \cdot 4H_2O$ and $K_3[Fe(CN)]_6$) were purchased from Panreac Química SA (Spain). fPolyvinylpyrrolidone (PVP) (average MW 40 KDa), 3-aminopropyltrimethoxysilane (APS), [N -(3-dimethylamino) propyl)]-N-ethylcarbodimide (EDC), sulfo N-hydroxysuccinimide (sulfo-NHS), phosphate buffer solutions tablets (PBS) were purchased from Sigma-Aldrich (Spain). RPMI-1640 w/o l-glutamine (CE), Fetal Bovine Serum EU approved (southamerica), L-glutamine 200MM (100X), penicillin streptomycin sol, trypsin

0.25% and EDTA were purchase from Fisher Scientific (Spain). All chemicals were of analytical grade and used as received. All aqueous solutions were prepared in Milli-Q water.

C1.2.2. Protocols and procedures

Prussian blue nanoparticles (PBNPs) were synthetized following the experimental procedure[11] described as follows: 8 mL of an aqueous solution of PVP/FeCl2·4H_2O (concentration ratio 20:1) containing 10 mM FeCl2·4H2O was first prepared. After that, 2 mL of a 10 mM $K_3[Fe(CN)]_6$ aqueous solution was added at 500 µL/min using a syringe pump and left reacting for 2h at room temperature with vigorous stirring. 2.5 mL of acetone for each mL of the reaction mixture were added. This procedure was repeated several times and the obtained PBNPs were dried at room temperature giving a blue powder that was dissolved by using a 1 M HCl solution. A 10 µg/mL of PBNPs solution was used for the electrochemical measurements.

Cell cultures of HaCat and SK-N_AS were done in Gibco® RPMI medium supplemented with glutamine 2 mM, 10% of fetal bovine serum and penicillin streptomycin. All the cell manipulations were carried out in a biosafety cabinet with laminar flow, using sterile materials and specific waste containers. The cells were incubated in TC Flask at 37 °C in humidified atmosphere of 95% air and 5% CO2. The medium was renovated every 3 days, and the cells were sub cultured every week. All the mediums were pre-warmed at 37 °C (in a thermostatic bath) before using. Cells were trypsinized adding 3 mL of 0.25% tripsin and EDTA and incubate at 37º C for 15 min. Later supplemented medium in a ratio of 3 mL to 1 mL of tripsin is added to inactivate trypsin, then cells were counted using a Neubauer Chamber and adjusted to the desired concentration before use.

Protocol followed for the alumina membranes modification with anti PTHLH antibodies was based in the covalent immobilization of the antibodies through their amine group in the lysines with the carboxylic groups introduced on the alumina membranes through a silanization process (see Figure 1.20 in the introduction of the thesis, section 1.3.2.1). Briefly, the anodized alumina oxide membranes (AAO) were boiled in Milli-Q water for 1 h. After drying in argon, they were immersed into a 5% acetone solution of APS for 1 h. Then they were washed in acetone several times and dried again at 120 ºC for 30 min. Once dried a 30 µL drop of a 1 mg/mL solution of anti-human IgG in PBS buffer (control membranes), containing 5 mM EDC/sulfo-NHS, were placed on the membrane filtering side and left there overnight at 4 ºC. The same procedure was followed for the immobilization of the anti-PTHLH antibodies PC09, using in this case an antibody concentration of 20 µg/mL. Finally membranes were thoroughly washing with PBS buffer. AAO membranes were fixed on

the SPCE by physical attachment inside a methacrylate cell (as displayed in Figure C2), then the sample was added in the well conformed by the membrane and the upper methacrylate piece.

For the standard curb of PTHLH, the membranes were incubated with 30 µL of the commercial PTHLH solution on membrane's filtering side during 1 hour. Finally the membranes were thoroughly washed and stored in Milli-Q water before electrochemical measurements (explained later).

For the cells growing on the membrane, 200 µL of supplemented medium with the corresponding cell concentration was added in each well with the alumina membrane and the SPCE underneath. Two sets of samples were prepared, seeding two different amounts cells: 4,800 cells/mL (low) and 24,000 cells/mL (high). Cells were incubated on the membranes 3, 10 and 20 hours, in the cell incubator until the electrochemical measurement was performed.

Electrochemical measurements of each electrode after the incubation was performed as follows: electrochemical cells wells were emptied, and washed with PBS twice, next the electrochemical cell was filled with 100 µL of a 10 µg/mL PBNPs suspension. A pre-treatment at -550 mV was applied for 30s and immediately after a differential pulse voltammetry (DPV) scan from -550 mV to +700 mV (step potential 10 mV, modulation amplitude 50 mV) was applied resulting in an analytical signal due to the oxidation of Prussian Blue (PB) at approximately +500 mV. The measurement was carried out at room temperature under no stirring conditions. Each measurement was performed with a new membrane.

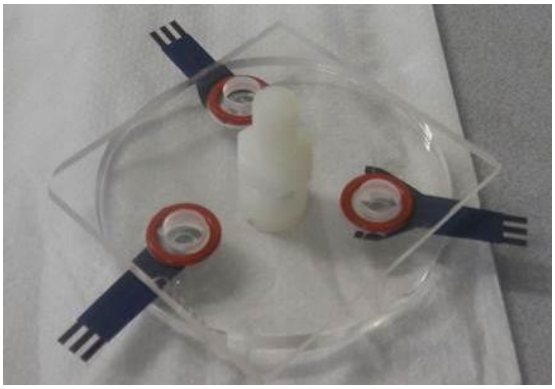

Figure C3: Picture of an example of electrochemical cell with three electrodes right after being assembled, before casting the 200 µL of cell suspension in the well. In red, the rubber rings used to press the anodized aluminum oxide membrane (AAO) on the screen printed electrode (SPCE) can be seen through the transparent methacrylate pieces of the set up.

C1.3. Results and discussion

The aim of the study is to carry out a proof of concept of the possibility to grow cell on a sensing platform and perform detection of a protein (PTHLH) secreted by the cell itself. As first step in the study a titration curb for the detection of PTHLH spiked in cell culture medium like previously reported [4] was made. Obtaining a LOD of 55 ng/mL similar to the previously reported within the group by Espinosa-Castañeda et al.[4].

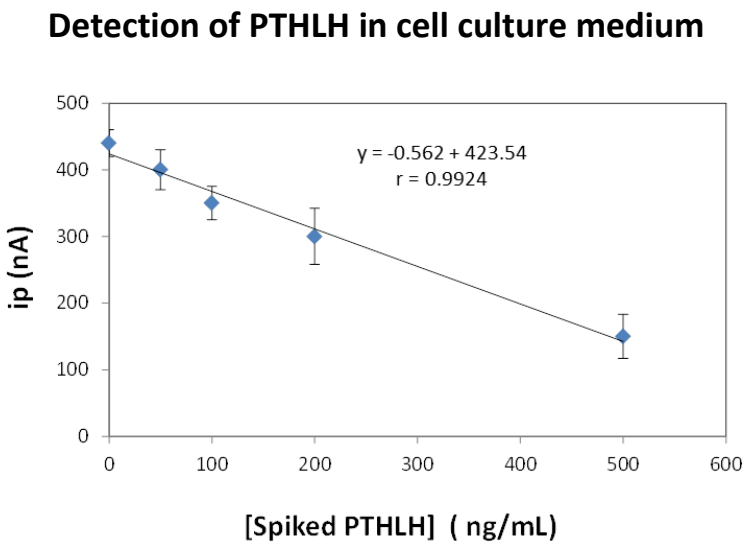

Figure C4: Standard curb of Parathyroid Like hormone (PTHLH) spiked in cell culture medium, by nanochannel detection using Prussian Blue Nanoparticles (PBNPs) as indicators. LOD calculated 55 ng/mL.

Once checked that the detection approach was successfully reproduced, detection of secreted PTHLH by cells directly cultured on the nanochannel membranes was carried out. Intensity signal obtained in each situation of cell culture was extrapolated in the titration curb (Figure C4) to estimate the amount of PTHLH in ng/mL. Data obtained is presented in a table with the values of PTHLH in ng/mL for the different situations. Graphic representation of the current signals obtained in each situation is also displayed. Working principle of the proposed technique (discussed previously in the thesis, section 1.2.2.2 and figure 1.21 in the introduction of the thesis) lays on the signal change caused by the blockage of the channel towards the indicator (PBNPs) diffusion to the working electrode. Therefore, the more analyte, the better blocking and hence the less signal/intensity will be obtained.

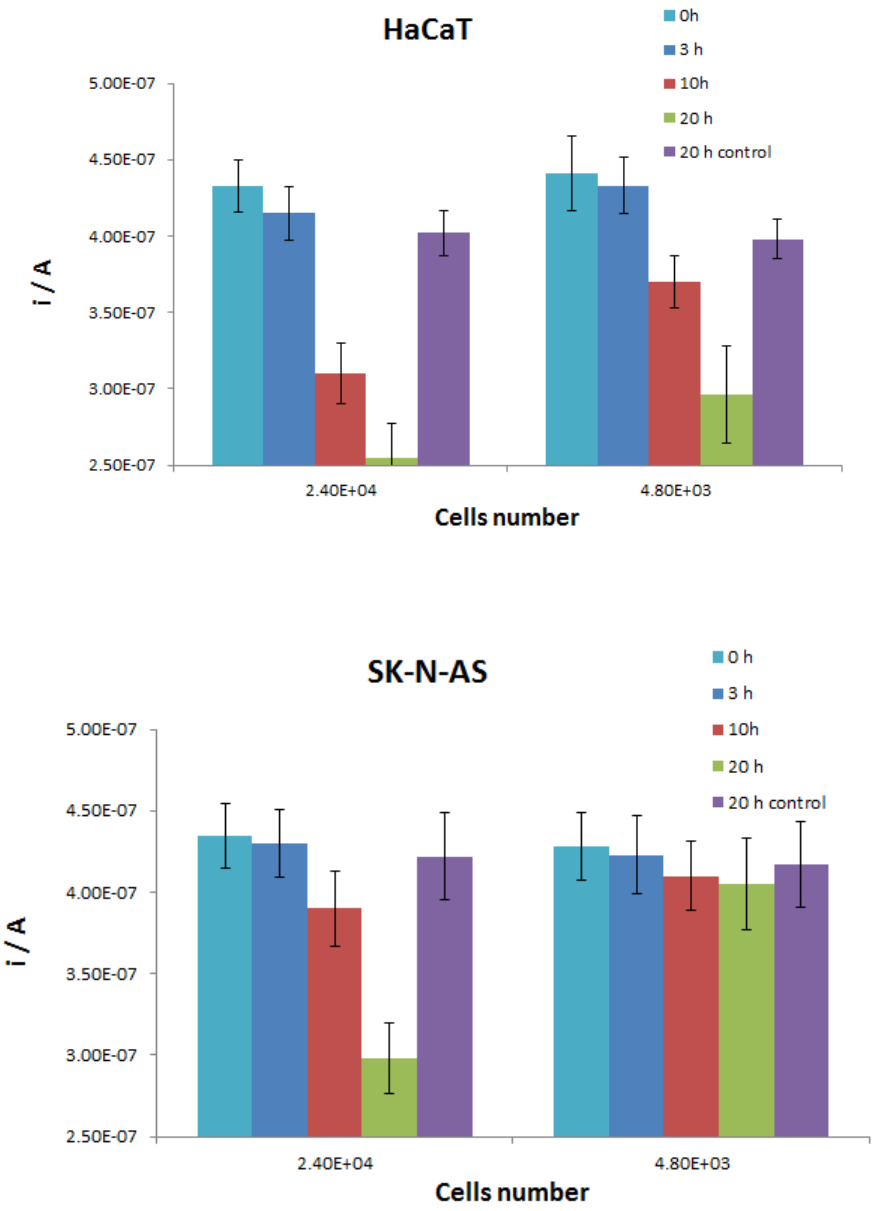

Figure C5: Results obtained for the cell culturing on anodized alumina membranes (AAO). Each graphic show the results obtained for each cell line cultured HaCat (human keratinocyte) and SK-N-AS (human neuroblastoma cell). Set of columns on the left correspond to the high concentration of cells seed ($2.4 \cdot 10^4$ cells/mL) while set of columns on the right correspond to the low concentration of cells seed ($4.8 \cdot 10^3$ cells/mL). The different colour columns correspond to the times of incubation, from 0h to 20h. Control column correspond to membranes modified with a non-specific antibody for PTHLH , a anti-human IgG antibody.

Cell	Cell number	Incubation time (h)	[PTHLH] (ng/mL)
HaCaT	24000	3	< 50
		10	202±35
		20	299±38
	4800	3	< 50
		10	95±30
		20	227±56
SK-N-AS	24000	3	< 50
		10	59±33
		20	223±41
	4800	3	< 50
		10	< 50
		20	< 50

Table C1: Table with the values obtained for the cell culturing on anodized aluminium oxide (AAO) membranes. Values in red are signals too similar to the blank signal, hence a concentration below 50 ng/mL that cannot be discriminated.

Data shown in Figure C5 and Table C1 proof the feasibility of PTHLH detection secreted by cells cultured on the same nanochannel sensing platform.

In the described experiment the signal decrease along different times of incubation evidences the accumulation of protein and hence the more blocking effect in the channels. This blocking effect can be attributed to the PTHLH thanks to the signal achieved in the control samples , in which the nanochannel membrane is modified with antibodies not specific for PTHLH, anti-human IgG was used instead. The value of the control sample after 20h of incubation similar to the blank signal at the beginning of the not only proofs that the signal comes from the blocking performed by PTHLH but also the low contribution of nanochannel blocking by the cell growing on the channels.

Another issue related to the results is the different final values achieved by the two different cell concentration cultured, resulting in a bigger decrease of signal those samples with more initial cells in the experiment. Meaning that $4.8 \cdot 10^3$ cells/mL need more time to produce the sufficient PTHLH to generate the same signal as in the case of $2.4 \cdot 10^4$ cells/mL. Furthermore, HaCat cells are

known to be stronger producers of PTHLH than SK-N-AS cells, discussed previously in Annex A section A1.3.3, which is corroborated by the higher intensities achieved by the SK-N-AS, which means that lower amounts of PTHLH were produced.

C1.4. Conclusions and future perspectives

On basis of previous preliminary studies within the group, in which the ability of cell lines to adhere and grow on AAO membranes was proved, it has been possible to go one step beyond applying the cited optimizations in the development of a biosensing system based on the use of nanochannels for the in situ detection of biomarkers secreted by cell cultures. Therefore a in situ cell culture/electrochemical detection set-up system has been built and tested to be capable of detecting secreted PTHLH with cells being incubated up to 20h in the set up. Finally, it is worth to mention that the detection performed is a label-free detection using PBNPs as indicator.

The developed sensing platform represents a highly interesting tool with potential future applications in basic research laboratories. The study of protein secretion of a cell line in a single device, where both the cell culture and the detection are performed in situ, by principle is an easy approach to be adapted into a high throughput system, paving the way to fast and simple approach for the study of an expression pattern of a protein, or factor implied in it.

C1.5. References

(1) Li, S.-J.; Li, J.; Wang, K.; Wang, C.; Xu, J.-J.; Chen, H.-Y.; Xia, X.-H.; Huo, Q. *ACS Nano* **2010**, *4*, 6417-6424.

(2) de la Escosura-Muñiz, A.; Merkoçi, A. *Small* **2011**, *7*, 675-682.

(3) de la Escosura-Muñiz, A.; Merkoçi, A. *ACS Nano* **2012**, *6*, 7556-7583.

(4) Espinoza-Castañeda, M.; Escosura-Muñiz, A. d. l.; Chamorro, A.; Torres, C. d.; Merkoçi, A. *Biosensors and Bioelectronics* **2015**, *67*, 107-114.

(5) Burtis, W. J.; Brady, T. G.; Orloff, J. J.; Ersbak, J. B.; Warrell, R. P.; Olson, B. R.; Wu, T. L.; Mitnick, M. E.; Broadus, A. E.; Stewart, A. F. *New England Journal of Medicine* **1990**, *322*, 1106-1112.

(6) Mundy, G. R.; Edwards, J. R. *Journal of the American Society of Nephrology* **2008**, *19*, 672-675.

(7) Mak, I. W. Y.; Turcotte, R. E.; Ghert, M. *Bone* **2013**, *55*, 198-207.

(8) McCauley, L. K.; Martin, T. J. *J. Bone Miner. Res.* **2012**, *27*, 1231-1239.

(9) Soki, F. N.; Park, S. I.; McCauley, L. K. *Future Oncol.* **2012**, *8*, 803-817.

(10) Espinoza Castañeda , M.; Thesis: *Study and development of new biosensors based on nanoparticles and nanochannels.* Link: http://www.tdx.cat/handle/10803/284878?show=full, Autonomous University of Barcelona, 2014.

(11) Uemura, T.; Kitagawa, S. *Journal of the American Chemical Society* **2003**, *125*, 7814-7815.

Annex D

Accepted publications

Biosensors and Bioelectronics 67 (2015) 53–58

Contents lists available at ScienceDirect

Biosensors and Bioelectronics

journal homepage: www.elsevier.com/locate/bios

Electrochemical Impedance Spectroscopy (bio)sensing through hydrogen evolution reaction induced by gold nanoparticles

Carmen C. Mayorga-Martinez [a,1], Alejandro Chamorro-Garcia [a,b,1], Arben Merkoçi [a,c,*]

[a] Nanobioelectronics & Biosensors Group, Institut Catala de Nanociencia i Nanotecnologia (ICN2), Edifici ICN2, Campus UAB, Bellaterra (Barcelona) 08193, Spain
[b] Autonomous University of Barcelona, UAB Campus, 08193 Bellaterra, Spain
[c] Institució Catalana de Recerca i Estudis Avançats (ICREA), Passeig Lluís Companys 23, 08010 Barcelona, Spain

ARTICLE INFO

Available online 10 June 2014

Keywords:
Gold nanoparticles
Electrochemical Impedance Spectroscopy
Hydrogen evolution reaction
Magneto-immunoassay

ABSTRACT

A new gold nanoparticle (AuNP) based detection strategy using Electrochemical Impedance Spectroscopy (EIS) through hydrogen evolution reaction (HER) is proposed. This EIS–HER method is used as an alternative to the conventional EIS based on $[Fe(CN)_6]^{3-/4-}$ or $[Ru(NH_3)_6]^{3+/2+}$ indicators. The proposed method is based on the HER induced by AuNPs. EIS measurements for different amounts of AuNP are registered and the charge transfer resistance (R_{ct}) was found to correlate and be useful for their quantification. Moreover the effect of AuNP size on electrical properties of AuNPs for HER using this sensitive technique has been investigated. Different EIS–HER signals generated in the presence of AuNPs of different sizes (2, 5, 10, 15, 20, and 50 nm) are observed, being the corresponding phenomena extendible to other nanoparticles and related catalytic reactions. This EIS–HER sensing technology is applied to a magneto-immunosandwich assay for the detection of a model protein (IgG) achieving improvements of the analytical performance in terms of a wide linear range (2–500 ng mL^{-1}) with a good limit of detection (LOD) of 0.31 ng mL^{-1} and high sensitivity. Moreover, with this methodology a reduction of one order of magnitude in the LOD for IgG detection, compared with a chroamperometric technique normally used was achieved.

1. Introduction

Gold nanoparticles (AuNPs) possess unique electrochemical and optical properties including high surface-to-volume ratio and excellent biocompatibility making these interesting materials in developing a variety of biosensors (Bonanni et al., 2008).

Hydrogen evolution reaction (HER) induced by AuNPs have been used in a variety of analytical applications for novel and improved sensing and biosensing devices with high specificity and high sensibility (de la Escosura-Muñiz et al., 2010; de la Escosura-Muniz et al., 2011; Espinoza-Castañeda et al., 2013; Maltez-da Costa et al., 2010, 2012a, b; Saha et al., 2012).

In addition AuNPs are also used in Electrochemical Impedance Spectroscopy (EIS) to either enhance the impedimetric signal or modify electrodes in order to increase the amount of analites adsorbed onto their surface, or to exploit a dendritic signal amplification in various applications (Bonanni et al., 2008; Derkus et al., 2013; Gao et al., 2013; Ren et al., 2013; Shen et al., 2013).

EIS is a powerful, non-destructive and highly informative technique, which is usually used for interface characterization and kinetic parameter determination for different reactions carried out on interfaces (Bonanni et al., 2011; Katz and Willner 2003; Park and Yoo 2003; Xianzong et al., 2013; Xie et al., 2012). EIS besides other techniques is used to study HER at different pure metals (Pd, Pt, Ni, Re, Au, and Ir) and alloys (Pt–Rh, Ni – rare earth) establishing a qualitative relation between metal loading and potential variation (Castro and Milocco, 2005; Chen et al., 2012; Khanova and Krishtalik, 2011; Ortega-Chavez et al., 2008).

In the current study a new and efficient AuNPs-based detection strategy using EIS and HER in acid solution monitored through carbon screen printed electrodes (SPCE) is described. Chronoamperometry and differential pulse voltammetry (DPV) are commonly used techniques to detect AuNPs (de la Escosura-Muñiz et al., 2010; de la Escosura-Muniz et al., 2011; Espinoza-Castañeda et al., 2013; Maltez-da Costa et al., 2010, 2012a, b). This EIS–HER method is used as an alternative to the conventional EIS based on the $[Fe(CN)_6]^{3-/4-}$ or $[Ru(NH_3)_6]^{3+/2+}$ indicators (Chang and Park, 2010; Rodriguez et al., 2005; Wei et al., 2011). This new detection

* Corresponding author at: Nanobioelectronics & Biosensors Group, Institut Catala de Nanociencia i Nanotecnologia (ICN2), Edifici ICN2, Campus UAB, Bellaterra (Barcelona) 08193, Spain. Tel.: +34 937374604.
E-mail address: arben.merkoci@icn.cat (A. Merkoçi).
[1] These authors contributed equally.

http://dx.doi.org/10.1016/j.bios.2014.05.066
0956-5663/

approach is successfully applied in a magneto-immunosandwich assay for HIgG detection achieving a low limit of detection (0.31 ng mL^{-1}). Furthermore, the effect of size on the EIS signals of AuNPs has been investigated demonstrating the applicability of this techniques to evaluate the particles size. This EIS–HER method is very sensitive toward AuNPs quantification and consequently may be offered for several biosensing applications.

2. Materials and Methods

2.1. Chemicals

Magnetic beads (Dynabeads M-280 Tosylactivated) were purchased to Invitrogen™ (Paisley, UK). Gold colloid, gold nanoparticles of different diameters were obtained from British Biocell (BBi, Cardiff, UK). Tetrachloroauric acid, sodium citrate, boric acid, PBS 10 mM pH 7.4, Albumin from Bovine Serum (BSA) in powder, HCl 37% (v/v) , human IgG from serum and antihuman IgG produced in goat were purchased from Sigma Aldrich (SA, St Quentin Fallavier, France). The anti-human IgG produced in rabbit was purchased from Sigma Aldrich (Schnelldorf, Germany). Polyester substrates were purchased from MacDermid Autotype. All the inks, Carbon ink, Ag/AgCl ink and the insulating ink were purchased from Acheson™, Henkel group.

2.2. Apparatus

For electrochemical measurement Autolab302 potentiostat/galvanostat/frequency-response analyzer PGST30, controlled by GPES/FRA Version 4.9, was used. Transmission electron microscope (TEM) images were taken with a JEM-2011 (Jeol, Ltd., Japan).

2.3. Gold nanoparticles synthesis

Gold nanoparticles were made following the procedure reported before (Turkevich et al., 1951). A solution of 0.01% (w/v) of tetrachloroauric acid is brought to boiling point under vigorous stirring, then 1.25 mL of sodium citrate at 1% (w/v) is added quickly maintaining the same conditions of stirring and the temperature for 15 more minutes until the color of the solution turned to deep red. It was left to cool down keeping the stirring. The concentration of gold nanoparticles in the resulting product is 3 nM. For the study, different concentrations of gold nanoparticles were used: 3 nM, 300 pM, 30 pM, 3 pM and 0 pM. For the characterization of gold nanoparticles at different sizes, the commercial gold nanoparticles of different diameters (2, 5, 10, 15, 20, and 50 nm) were used at a concentration of 3 nM. The initial concentration of the gold nanoparticles in the commercial samples were given by the supplier.

2.4. Screen printed electrodes fabrication

Screen printed electrodes (SPCE) consists of counter-electrode, reference electrode of Ag/AgCl and working electrode. They are fabricated on sheets of polyester substrate by the sequential deposition of different ink layers, first the graphite ink layer on the polyester substrate for working electrode and counter-electrode, next the Ag/AgCl ink for the reference electrode and finally the isolating ink. Each layer is printed using a screen printing machine with a stencil specific for each layer, which contains the patterns of the electrodes. After its deposition each layer was cured by keeping the printed sheet at 120 °C for 30 min.

2.5. Magneto-immunosandwich formation

The magneto-immunosandwich was prepared according to previously reported procedures (Ambrosi et al., 2007; de la Escosura-Muñiz et al., 2010; Maltez-da Costa et al., 2010). To prepare the immunosandwich assembly magnetic beads (Dynabeads M-280) were used as support (3 mg/ml per sample). The magnetic beads are washed in borate buffer pH 9.2, and incubated overnight (37 °C and agitation of 400 rpm) with anti-human IgG, at a final concentration of 40 μg/ml in the mixture. After the incubation the samples were washed with PBS tween 20 at 0.5% (v/v). In order to perform a blocking step, the conjugated magnetic beads were resuspended in a solution of PBS and 5% (w/v) BSA for 1 h. After the blocking step the samples were washed with PBS. Then the blocked conjugate is incubated with the antigen (in this specific case human IgG) for 1 h at 25 °C and 400 rpm.

For the gold nanoparticle conjugation to the anti-human IgG, first the pH of the gold nanoparticle is adjusted to 9.2 using borate buffer. Then the gold nanoparticles are incubated with the antibody at a final concentration of 5 μg/ml for 1 h at 25 °C and 400 rpm. After the incubation a solution of BSA in milliQ water was added to reach a final concentration of 0.15 mg/ml and incubated for 1 h at 650 rpm and 25 °C. Next, the sample was centrifuged at 14000 rpm for 20 min at 4 °C. The pellet was reconstituted to the initial volume in PBS.

The last incubation consisted in mixing the magnetic bead assembly with the conjugated gold nanoparticles at a ratio of 1:1 (v/v). The incubation was done for 30 min long under 600 rpm agitation and 25 °C. After the incubation different washing steps with PBS tween 20 at 0.5% (v/v), PBS and milliQ water were carried out. The assembly was finally resuspended in milliQ water.

2.6. Electrochemical measurements

In the EIS–HER measurements a first oxidation step for 60 s at +1.35 V was applied followed by a signal composed of DC of −1 V plus AC of 0.05 V_{RMS}. The range of frequencies went from 0.1 to 10 kHz. The resulting data was fitted in a regular Randless circuit to extract the value of charge transfer resistance (R_{ct}).

The magneto-immunosandwich assay for HIgG detection using EIS–HER was done. A small magnet is placed under the working electrode of the SPCE to direct the magnetic beads towards it. A mixture of 25 μl of the magnetoimmunosandwich and 25 μl of a 2 M HCl solution is placed onto the surface of the electrode.

3. Results and discussion

AuNPs, prepared by the Turkevich method (Turkevich et al., 1951), were characterized by Transmission Electron Microscopy (TEM). Fig. 1 (inset) shows a typical TEM image of AuNPs. Highly regular and uniform nanoparticles in the size range of 21 ± 3 nm can be observed. In order to explore the HER of AuNPs by EIS reading, a fixed concentration of AuNPs solution (1500 pM) was measured by holding the working electrodes (where AuNPs were deposited) at a constant potential of +1.35 V for 1 min (electro-oxidizing Au° to Au^{+3}) followed by applying a composed signal of high negative DC potential (polarization potential) plus 0.05 V of AC potential in a range frequency from 0.1 Hz to 10 kHz. Different DC potentials were evaluated; Fig. 2 shows the Nyquist representation.

For interface modelling, equivalent circuit (corresponds to Randles model) which includes the solution resistance (R_s), double layer capacitance (C_{dl}) and the charge transfer resistance (R_{ct}) is used (see scheme in Fig. 1). The performed fitting using the Randles model is fairly good and the calculated parameters

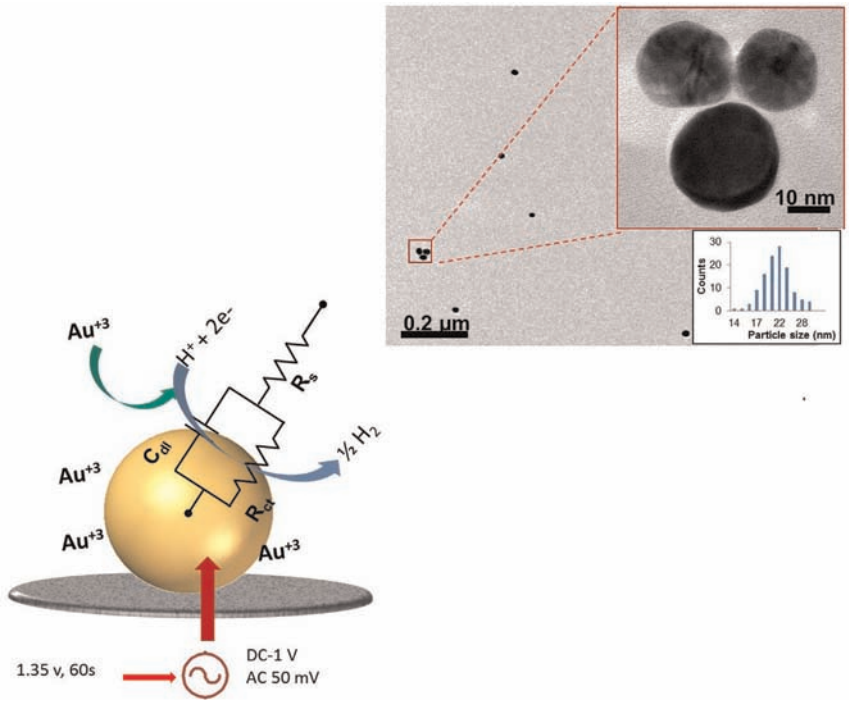

Fig. 1. Schematic of EIS sensing principle through hydrogen evolution reaction induced by gold nanoparticles. Inset: Transmission Electron Microscopy (TEM) images of AuNPs including a magnified image.

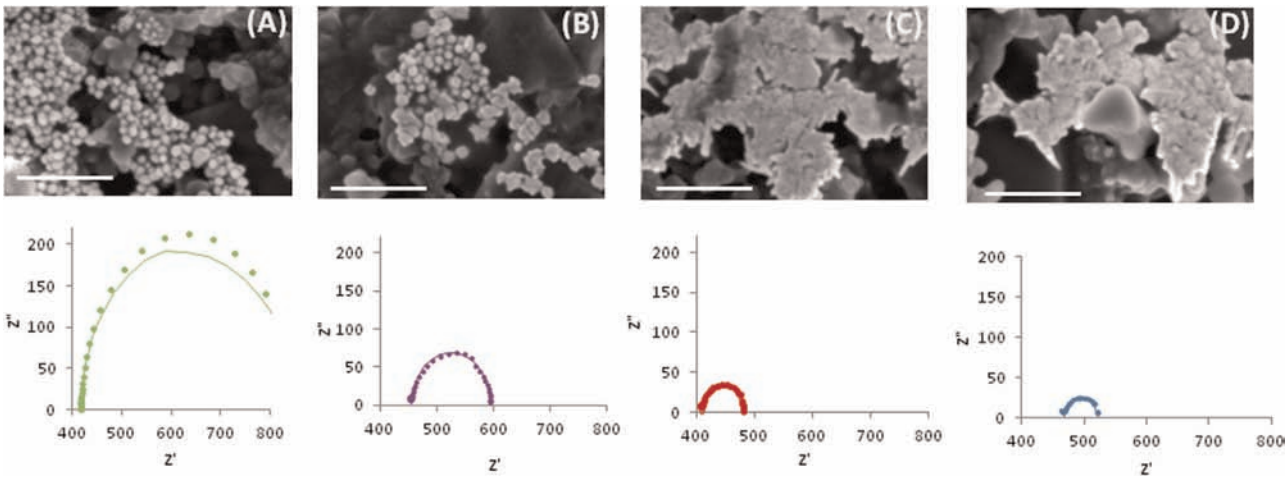

Fig. 2. Scanning electron micrograph (SEM) and Nyquist plot for AuNPs after potentiostatic cathodic polarization: (A) −0.6 V, (B) −0.8 V, (C) −1 V and (D) −1.2 V. The scale bar of all the SEM images is 250 nm and continuous line corresponds to fit data.

obtained at different potentials (Table S1 in Supporting information) show that the R_{ct} values decrease when the polarization potential increases. These measurements show the impedance response dependency from the applied DC potential.

This fact is due to a large dependence of the HER kinetics on AuNPs' surfaces in HCl solution and at negative over potentials. The total two-electron process of hydrogen evolution proceeds at least in two steps: first, the proton donors discharge with formation of adsorbed H atoms, and, second, the desorption of these atoms. In this case the hydrogen adsorption by the AuNPs is not observed, for these reason the experimental data was fitted in a common Randless circuit and used to evaluate HER. This phenomenon has been reported for metal electrodes such as gold that poorly adsorbs hydrogen (Khanova and Krishtalik 2011).

From the SEM images shown in Fig. 2 it is possible to notice the physical deformation of the circular shape of the AuNPs, which after hydrogen evolution becomes irregular; furthermore the level of irregularities in the shape increases with the increase of the negative potential applied on the AuNPs (Fig. 2B–D). This indicates that high negative potential applied changes the nanostructure of AuNPs. For later measurements −1 V was fixed as a polarization potential due to the stable impedance response and less observed deformation of the circular shape of the AuNPs compared to the case where higher potentials are used.

Different AC potentials (10, 20, 50 and 100 mV) also were tested. Fig. S1 in supporting information shows the obtained Nyquist plot without a significant difference in terms of R_{ct}. Nevertheless, at low potentials (10, 20 mV) the impedance response is not stable at low frequency. On the other hand being the 100 mV AC a relatively large potential an AC of 50 mV was used.

Finally, the +1.35 V was applied to release Au^{+3} ions from the surface of the gold nanoparticles into the measuring solution. This pretreatment condition enhances the catalytic effect on the HER

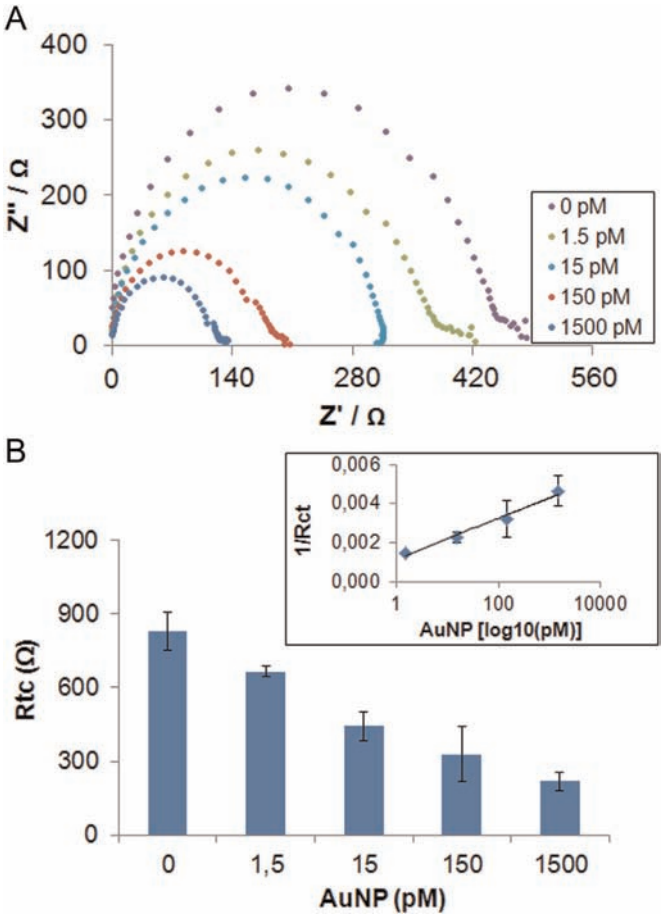

Fig. 3. (A) Argand diagram recorded for increasing concentrations of AuNPs in 1 M HCl ranging from 1.5 to 1500 pM (top to bottom). (B) Histogram representing R_{ct} as a function of different AuNPs concentrations. Inset: calibration curve obtained by plotting the R_{ct} inverse value with logarithm of AuNPs concentration.

and was previously optimized (Ambrosi et al., 2007; de la Escosura-Muñiz et al., 2010; Maltez-da Costa et al., 2010).

After optimizing the experimental procedure, a series of EIS measurements for different amounts of AuNP are registered under the optimal conditions. Fig. 3A shows the impedance measurements in a Nyquist plot. The smallest semicircle corresponds to the 1500 pM AuNPs, while the biggest semicircle corresponds to the blank (HCl without AuNP). The resulting charge transfer resistances are directly represented in a histogram (Fig. 3B) and the inverse of these resistances is plotted vs. the logarithm of the concentration to adjust the calibration curve (inset Fig. 3B). The LOD of 0.67 pM is calculated by the value obtained by interpolation of the blank plus three times its standard deviation. The method shows high reproducibility being its RSD of around 13%, obtained for 3 repetitive assays.

Once the impedimetric detection of AuNP catalysis was performed and its effectiveness as a transduction method demonstrated, it is afterwards applied in a standard immunoassay for protein detection. In Fig. 4A a schematic of the performed magneto-immunosandwich for human IgG (HIgG) detection is displayed. The capturing antibody, immobilized onto the magnetic bead, is an antihuman IgG, polyclonal, developed in goat. The detection antibody, conjugated with gold nanoparticles, is another antihuman IgG developed in rabbit. Fig. 4B shows the obtained R_{ct} values with the corresponding error bars achieved using different amounts of HIgG. The signal of AuNP is directly related to the amount of the formed immunoconjugates. A linear biosensing response within the range from 2 to 500 ng mL^{-1} IgG with 0.31 ng mL^{-1} as limit of detection (LOD) was obtained from the inverse of the obtained R_{ct}.

Fig. 5 shows TEM image of magnetic beads with (Fig. 5A) and without (Fig. 5B) gold nanoparticles anchored through the immunosandwich (magnetic bead-anti-human IgG/human IgG/anti-human IgG-AuNPs). The small black points corresponding to AuNPs covering the surface of the MBs (big spheres) can be observed in Fig. 5A demonstrating the magneto-immunosandwich formation.

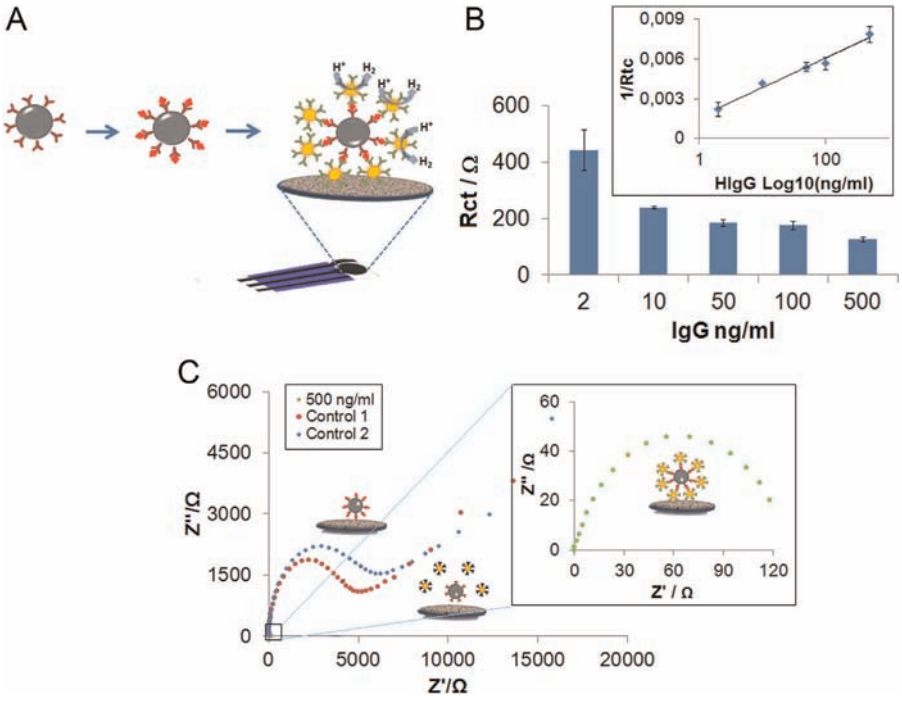

Fig. 4. (A) Schematic of the magneto-sandwich immunoassay for HIgG detection using AuNPs as label. (B) R_{ct} values vs. different concentrations of HIgG. Inset: calibration curve obtained by plotting $1/R_{ct}$ vs. the logarithm of different concentrations of HIgG. (C) Selectivity of the immunosandwich assay: Nyquist plots obtained for the control 1 (BSA), no antibody as a control two and 500 ng mL^{-1} as a positive.

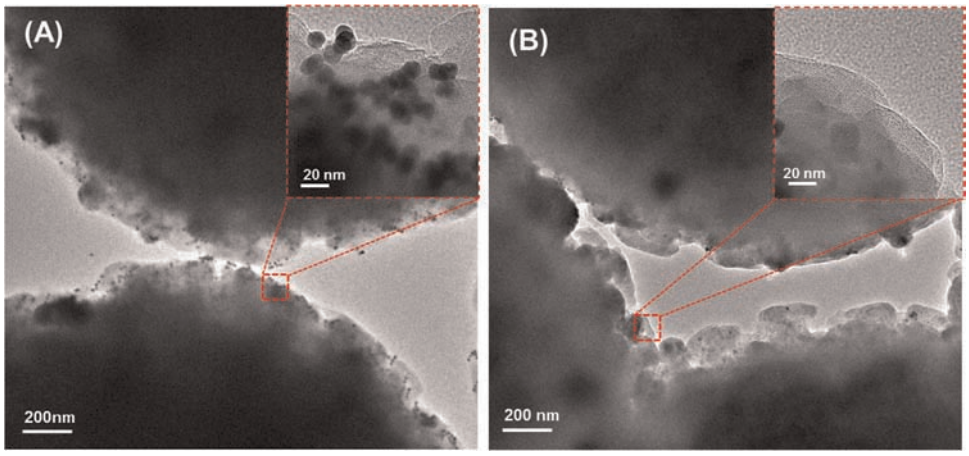

Fig. 5. TEM images of magnetic beads modified with (A) and without (B) AuNP anchored through the immunosandwich (magnetic bead-anti-human IgG/humanIgG/anti-human IgG-AuNPs).

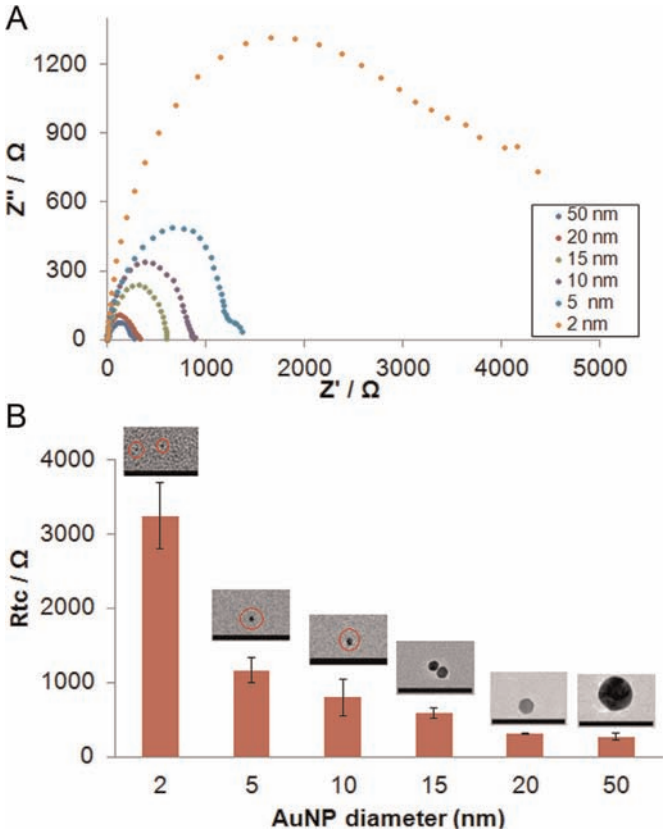

Fig. 6. Impedimetric measurement of AuNPs of various diameters and in the same concentration. Nyquist plot (A) and histograms of R_{ct} value vs. AuNPs diameter (B). The scale bar of all the TEM images is 100 nm.

LOD was calculated by the interpolation of the blank plus three times the standard deviation of the blank. With this new AuNP based strategy using EIS the LOD is improved in comparison to the previously one obtained when the chronoamperometry was used for AuNPs detection (Maltez-da Costa et al., 2010). Moreover, high reproducibility with an RSD of around 13% was observed for HIgG detection. The selectivity of the assay is demonstrated performing two control assays using a non-specific protein (BSA instead of HIgG) as 'control 1' and another one without AuNPs as 'control 2' (see Fig. 4C).

On the other hand, the Au NP size effect in the electrochemical signal amplification was evaluated before (Bonanni et al., 2011). For this reason, this new method represents a quite fast and cost efficient method to determine the size of AuNPs. Fig. 6 shows the results of EIS–HER characterization of AuNPs (from BritishBiocell) of different sizes (2, 5, 10, 15, 20, and 50 nm). In Fig. 6A the EIS–HER data is presented in a Nyquist plot, showing the semicircles resulting from the measurement of the nanoparticles of different diameters. The biggest semicircles correspond to the smallest gold nanoparticles (2 nm diameter) with a clear tendency of EIS decrease when AuNPs size is increased. Although EIS is applied before for AuNP size evaluation (Bonanni et al., 2011) this EIS–HER method clearly shows an improvement of the sensitivity and a better discrimination of AuNPs in the size range of 2–50 nm. The histograms for different AuNPs sizes as a function of R_{ct} were presented in Fig. 6B and the corresponding TEM images as insets are also shown. High reproducibility of the EIS–HER measurements with an RSD of 12% is observed.

4. Conclusion

In summary we have demonstrated that the Electrochemical Impedance Spectroscopy (EIS) combined with hydrogen evolution reaction (HER) constitutes a high reproducible and efficient method for the detection of different amounts of AuNPs in an acidic medium. This EIS–HER method combines the advantages of EIS with HER induced by AuNPs. Furthermore, the proposed method displays dramatic improvements of the analytical performance in terms of a wide linear range (2–500 ng mL^{-1}) of response along with a good LOD (0.31 ng mL^{-1}) and sensitivity for a model protein (Human IgG) detection in a magnetoimmunoassay and the gold nanoparticle size characterization. In addition, it is also important to emphasize that with this new strategy for the magneto-immunosandwich a reduction of one order of magnitude in the LOD is obtained, compared with the chroamperometric technique normally used for this detection reported before. On the other hand, the use of this EIS–HER as a sensitive technique capable of differentiating the signal generated by the presence of AuNPs of different sizes can be extended to other nanoparticles and related catalytic reactions. We envisage the use of such sensing technology to be with interest for various sensing and biosensing applications where nanoparticles or other nanomaterials may be involved.

Acknowledgments

MINECO (Spain) for Project MAT2011-25870 is acknowledged.

Appendix A. Supplementary information

Supplementary data associated with this article can be found in the online version at 10.1016/j.bios.2014.05.066.

References

Ambrosi, A., Castañeda, M.T., Killard, A.J., Smyth, M.R., Alegret, S., Merkoçi, A., 2007. Anal. Chem. 79 (14), 5232–5240.
Bonanni, A., Esplandiu, M.J., del Valle, M., 2008. Electrochim. Acta 53 (11), 4022–4029.
Bonanni, A., Pumera, M., Miyahara, Y., 2011. Phys. Chem. Chem. Phys. 13 (11), 4980–4986.
Castro, B.E., Milocco, R.H., 2005. J. Electroanal. Chem. 579 (1), 113–123.
Chang, B.Y., Park, S.M., 2010. Electrochemical impedance spectroscopy. In: Yeung, E.S., Zare, R.N. (Eds.), Annual Review of Analytical Chemistry, Vol. 3. Annual Reviews, Palo Alto, pp. 207–229.
Chen, F.Y., Liu, J.G., Chen, H., Yan, C.W., 2012. Int. J. Electrochem. Sci. 7 (4), 3750–3764.
de la Escosura-Muñiz, A., Maltez-da Costa, M., Sánchez-Espinel, C., Díaz-Freitas, B., Fernández-Suarez, J., González-Fernández, Á., Merkoçi, A., 2010. Biosens. Bioelectron. 26 (4), 1710–1714.
de la Escosura-Muniz, A., Parolo, C., Maran, F., Merkoci, A., 2011. Nanoscale 3 (8), 3350–3356.
Derkus, B., Emregul, E., Yucesan, C., Cebesoy Emregul, K., 2013. Biosens. Bioelectron. 46 (0), 53–60.
Espinoza-Castañeda, M., de la Escosura-Muñiz, A., González-Ortiz, G., Martín-Orúe, S.M., Pérez, J.F., Merkoçi, A., 2013. Biosens. Bioelectron. 40 (1), 271–276.
Gao, Z., Deng, H., Shen, W., Ren, Y., 2013. Anal. Chem. 85 (3), 1624–1630.
Katz, E., Willner, I., 2003. Electroanalysis 15 (11), 913–947.
Khanova, L.A., Krishtalik, L.I., 2011. J. Electroanal. Chem. 660 (2), 224–229.
Maltez-da Costa, M., de la Escosura-Muniz, A., Merkoci, A., 2010. Electrochem. Commun. 12 (11), 1501–1504.
Maltez-da Costa, M., de la Escosura-Muniz, A., Nogues, C., Barrios, L., Ibanez, E., Merkoci, A., 2012a. Small 8 (23), 3605–3612.
Maltez-da Costa, M., de la Escosura-Muniz, A., Nogues, C., Barrios, L., Ibanez, E., Merkoci, A., 2012b. Nano Lett. 12 (8), 4164–4171.
Ortega-Chavez, L., Herrera-Peraza, E., Verde, Y., 2008. J. New Mater. Electrochem. Syst. 11 (2), 125–130.
Park, S.M., Yoo, J.S., 2003. Anal. Chem. 75 (21), 455A–461A.
Ren, Y., Deng, H., Shen, W., Gao, Z., 2013. Anal. Chem. 85 (9), 4784–4789.
Rodriguez, M.C., Kawde, A.N., Wang, J., 2005. Chem. Commun. 34, 4267–4269.
Saha, K., Agasti, S.S., Kim, C., Li, X.N., Rotello, V.M., 2012. Chem. Rev. 112 (5), 2739–2779.
Shen, W., Deng, H., Ren, Y., Gao, Z., 2013. Biosens. Bioelectron. 44 (0), 171–176.
Turkevich, J., Stevenson, P.C., Hillier, J., 1951. Discuss. Faraday Soc. 11, 55–75.
Wei, Y., Kong, L.T., Yang, R., Wang, L., Liu, J.H., Huang, X.J., 2011. Chem. Commun. 47 (18), 5340–5342.
Xianzong, X., Rieth, L., Caldwell, R., Diwekar, M., Tathireddy, P., Sharma, R., Solzbacher, F., 2013. IEEE Trans. Biomed. Eng. 60 (10), 2943–2951.
Xie, X., Rieth, L., Merugu, S., Tathireddy, P., Solzbacher, F., 2012. Appl. Phys. Lett. 101 (9), 093702.

Journal of Materials Chemistry B

COMMUNICATION

View Article Online
View Journal | View Issue

Cite this: J. Mater. Chem. B, 2015, 3, 5166

Received 25th March 2015,
Accepted 5th June 2015

DOI: 10.1039/c5tb00545k

www.rsc.org/MaterialsB

An iridium oxide nanoparticle and polythionine thin film based platform for sensitive *Leishmania* DNA detection†

Carmen C. Mayorga-Martinez,‡[a] Alejandro Chamorro-García,‡[ab] Lorena Serrano,[c] Lourdes Rivas,[ab] Daniel Quesada-Gonzalez,[ab] Laura Altet,[c] Olga Francino,[bc] Armand Sánchez[ce] and Arben Merkoçi*[ad]

An impedimetric label-free genosensor for high sensitive DNA detection is developed. This system is based on a screen-printed carbon electrode modified with the thionine layer and iridium oxide nanoparticles (IrO_2 NP). An aminated oligonucleotide probe is immobilized on the IrO_2 NP/polythionine modified electrode and ethanolamine was used as a blocking agent. Different diluted PCR amplified DNA samples have been detected. The selectivity and reproducibility of this system are studied and the system was highly reproducible with RSD ≈ 15% and sensitive enough while using 2% of ethanolamine during the blocking step employed for genosensor preparation.

Introduction

In the field of biosensors electrochemical impedance spectroscopy (EIS) has become especially well-suited for the detection of binding events which take place on the electrode's surface.[1–3] This capability to discriminate small changes on surfaces makes EIS capable of detecting interactions of biomolecules close to the surface of the electrodes, and hence enabling a label free detection of biomolecules thanks just to the changes caused by them due to the biological recognition event.[3] Especially, impedimetric label free DNA genosensors based on nucleic acid hybridization have received considerable attention due to the screening of samples in search of specific DNA sequences related to a specific disease, or state of risk and represent a powerful tool in the field of diagnosis.[4–6] They offer great advantages due to simplicity, speed, miniaturization, sensitivity, selectivity and low cost for detection of desired DNA sequences or mutant genes.[5,7]

The EIS response depends on the modifications of the electrode surface and the interaction of the analyte with the specific recognition elements. Such alterations affect the capability of the redox indicator to reach the electrode surface and consequently its redox conversion. In this way the charge transfer may either increase or decrease. In this type of measurement the nature of the electrode surface is of special importance, which determines to a great extent the electron transfer between the electrode and the redox indicator. It is common to find the bibliography examples of electrode surface modifications by electropolymerized layers or self-assembled monolayers, in order to enhance the electron transfer between the electrode surface and a redox indicator.[8] With this aim, polythinoine layers have been reported to be used for proper modifications of sensors.[9,10]

The immobilization of the single stranded DNA (ss-DNA; to be used as receptor) has been studied over a variety of substrates/electrodes using various methods such as adsorption, covalent coupling and entrapment.[11–14] However, various issues like poor compatibility of immobilizing materials on the transducer, poor binding of DNA, creation of inactive or poor conducting layers and less surface area including poor stability were raised.[15,16] Nanomaterials including metal nanoparticles, nanowires, nanorods, carbon nanotubes, and graphene have been successfully used in impedimetric biosensors to amplify the detection signal and achieve a lower detection limit due to their high surface area, favorable electronic properties and electrocatalytic activity as well as good biocompatibility induced by the nanometer size and specific physicochemical characteristics.[17] Nanoparticles, due to their small size, display interesting properties at the nanoscale level. First, due to their shape and size they can increase the surface area. Second, thanks to the electrostatic interactions they can be adsorbed or attached onto different surfaces. Third, thanks to the functional groups on their surface, they can be used as anchor points for other molecules.[18]

[a] Nanobioelectronics & Biosensors Group, Institut Catala de Nanociencia i Nanotecnologia (ICN2), Edifici ICN2, Campus UAB, Bellaterra (Barcelona) 08193, Spain. E-mail: arben.merkoci@icn.cat; Tel: +34 937374604
[b] Autonomous University of Barcelona, UAB Campus, 08193 Bellaterra, Spain
[c] Vetgenomics, Edifici Eureka, Parc de Recerca UAB, 08193 Bellaterra (Barcelona), Spain
[d] Institució Catalana de Recerca i Estudis Avançats (ICREA), Passeig Lluís Companys 23, 08010 Barcelona, Spain
[e] Centre for Research in Agricultural Genomics-CSIC-IRTA-UAB-UB, Campus UAB, 08193 Cerdanyola del Valles, Catalonia, Spain

† Electronic supplementary information (ESI) available. See DOI: 10.1039/c5tb00545k

‡ These authors contributed equally to this work.

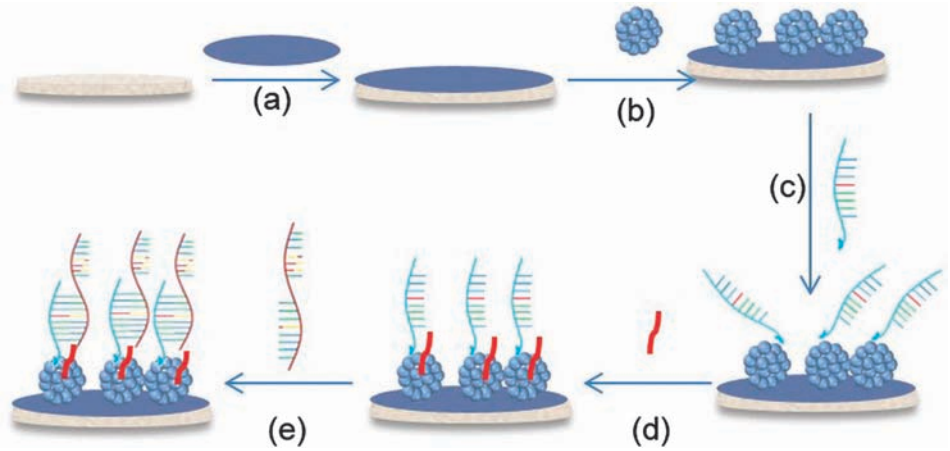

Scheme 1 Schematic representation of the procedure for the impedimetric label-free genosenor fabrication. Thionine electropolymerization (a), deposition of IrO_2 NPs (b), immobilization of ss-DNA (c), blocking step with etanolamine (d) and hybridization with a complementary target (e).

Here we exploit the iridium oxide nanoparticles (IrO_2 NPs) deposited over a polythionine layer which has been electro polymerized onto the carbon transducer with the aim to enhance the properties of the sensor for the detection of amplified DNA (see Scheme 1). IrO_2 NPs has proved to be good candidates for being applied in biosensing platforms, especially thanks to the citrate groups they present on their surface. The citrate groups allow tailoring of different biomolecules thanks to the non-covalent bond formation between with amino groups on the biomolecule.[19,20] The platform developed shows good performance for electrochemical sensing of PCR amplified DNA of dog affected by *Leishmania*, this target is used as a proof a concept. Different dilutions of PCR amplified DNA samples are detected showing high sensitivity while detecting up to 1000 times diluted samples. The system offers the possibility to be applied for diagnostics based on DNA detection, as the pathogen detection (or infectious disease) both in veterinary and human file.

Experimental

Apparatus

Electrochemical experiments were performed using an electrochemical analyzer Autolab 20 (Eco-Chemie, The Netherlands) which was connected to a personal computer using a software package GPS 4.9 (General Purpose Electrochemical System). Impedance measurements were performed by using an Autolab302 potentiostat/galvanostat/frequency-response analyzer PGST30, controlled by GPES/FRA Version 4.9. A semi-automatic screen-printing machine DEK248 (DEK International, Switzerland) was used for the fabrication of the screen-printed carbon electrodes (SPCEs).

Reagents and solutions

The reagents used for SPCEs fabrication were: Autostat HT5 polyester sheet (McDermid Autotype, UK), Electrodag 423SS carbon ink, Electrodag 6037SS silver/silver chloride ink, and Minico 7000 Blue insulating ink (Acheson Industries, The Netherlands). Trizma hydrochloride, sodium chloride, sodium citrate, ethylenediaminetetraacetic acid disodium salt dihydrate (EDTA), ethanolamine, potassium hexachloroiridate(IV), sodium hydrogencitrate and thionine acetate were purchased from Sigma-Aldrich (St. Louis, MO). Potassium hexacyanoferrate(II) three hydrate, potassium hexacyanoferrate(II) and sulphuric acid were purchased from Panreac Quimica S.A. (Barcelona, Spain). Milli-Q water was obtained from purification system and all solutions were prepared with ultra-pure water from a Millipore-MilliQ system. Washing solutions in the label-free assay consisted of TE (0.01 M tris and 0.001 M EDTA) buffer, pH 8, 2 × SSC (300 mM Sodium Chloride and 30 mM sodium citrate) buffer, buffer pH 7.2, containing 1% ethanolamine and Tris (0.1 M).

Synthesis of iridium oxide nanoparticles

Potassium hexachloroiridate(IV) 2.6×10^{-5} M solution was mixed with sodium hydrogencitrate 1.6×10^{-2} M solution. The pH of the red brown solution was adjusted to 7.5 with a 0.25 M NaOH solution and then refluxed in an oil bath with constant stirring for 30 min. As the mixture cooled to room temperature, the pH was again adjusted to 7.5 with a reflux for 30 min. This procedure was repeated until pH reached a constant value of 7.5. Finally the solution was refluxed 2 h more with oxygen bubbling. At the end of this step, a deep blue solution of IrO_2 nanoparticles was obtained. The solution was stocked in a glass-stoppered flask and at 4 °C when not in use.

PCR amplified products

The samples used in the study are PCR amplified products of extracted DNA as described in Francino *et al.* 2006.[21] Briefly, for the DNA extraction, peripheral whole blood was washed in TE buffer pH 8.0 to disrupt the erythrocyte membranes until the leukocyte pellet was white. Leukocytes were then lysed by incubation of the pellet in 0.1 ml of PK buffer (50 mM KCl, 10 mM Tris pH 8.0, 0.5% Tween-20 and 23 μg of proteinase K) at 56 °C for 5 h. Before running the PCR the proteinase K was inactivated by incubation of the samples at 90 °C for 10 min. DNA was then diluted 1/5 in water.

The PCR amplification *Leishmania*, target is used as a proof of concept for the developed system. TaqMan-MGB probe (FAM-

50-AAAAATGGGTGCAGAAAT-30-non-fluorescent quencher-MGB) and PCR primers (Forward:AACTTTTCTGGTCCTCCGGGTAG and Reverse:ACCCCCAGTTTCCCGCC) were used to target conserved DNA regions of the kinetoplast minicircle DNA from *L. infantum*. *Leishmania* primers and probe were added at 900 and 200 nM, respectively. PCR was carried out in 25 ml final volume reaction mixture containing TaqMan Universal PCR Master Mix with UNG Amperase (Life technologies). The thermal cycling profile was 50 °C for 2 min, 95 °C for 10 min, 40 cycles at 95 °C for 15 s and 60 °C for 1 min. Each amplification run contained positive and negative controls.

Genosensor preparation

Screen printing electrodes were fabricated by sequential deposition of a graphite ink, Ag/AgCl ink and insulating ink on a polyester substrate. The polyester substrate was dried at 120 °C for 45 min (graphite) and 30 min (Ag/AgCl and insulating) after the deposition of each layer.

Before modification with thionine layer and IrO_2 NPs, SPCEs were activated by applying a 3 μA current during 120 s in 0.1 M H_2SO_4 and then the electrodes were washed with Milli-Q water. 100 μL of thionine solution 0.5 mM was dropped onto the working surface of SPCE, and 20 CVs scans from 0.1 to −0.55 V at 50 mV s^{-1} were applied. The electrodes were washed with TE buffer. Afterwards 8 μL solution of IrO_2 NPs suspension were dropped onto the working surface of SPCE and dried at room temperature (1 hour), and the electrodes were washed with TE buffer.

After modification of SPCE with thionine and IrO_2 NPs, adsorption of a 0.5 ng μL^{-1} of 3′-aminated oligonucleotide probe (5′-NH_2-TEG-atatatatatatataTTTTCTGGTCCTCCGGGTAGGGGCG-TTCTG-3′) onto the electrode modified surface was performed, leaving an aliquot of 10 μL overnight at 4 °C. Then the electrode was washed with TE buffer pH, to remove the excess of oligonucheotide. Free surface sites were blocked placing a drop of 40 μL of ethanolamine solution contained desired concentration for 90 min, followed by a washing step with SSC, pH 7.2, buffer containing 1% ethanolamine.

Hybridization step was performed using synthetic oligonucleotide (for system optimization) and PCR amplified product. The hybridization with synthetic oligonucleotide target was performed at room temperature by placing 30 μL of synthetic complementary target solutions (5′-TTTCTGCACCCATTTTTCC-ATTTTCGCAGAACGCCCCTACCCGGAGGACCAGAAAA-3′) in 2 × SSC buffer, pH 7.2, containing 1% ethanolamine, onto the surface of the genosensor for 45 min and then rinsing with Tris buffer pH 7.2 containing 1% ethanolamine.

The PCR amplified DNA of dog with *Leishmania* (140 bp) was used to perform the hybridization instead of commercial oligonucleotide target using the same experimental condition as those used for commercial oligonucleotide. Before the hybridization, the PCR amplified DNA was denatured by heating at 95 °C for 5 min followed by immersing in ice until the use. The experimental control was performed using PCR amplified DNA of dog without *Leishmania* (blank).

Electrochemical measurements

The electrochemical measurement was performed by electrochemical impedance spectroscopy (EIS) in 1 mM $[Fe(CN)_6]^{3-/4-}$ with 0.1 M KCl as a redox probe. A sinusoidal potential modulation of ±10 mV amplitude in the 0.1 Hz to 100 kHz frequency range, with logarithmic scale of 10 points per decade, was superimposed onto the formal potential of the redox couple, $[Fe(CN)_6]^{3-/4-}$ (0.24 V *vs.* Ag/AgCl). Nyquist diagrams were also recorded. Electrochemical experiments were carried out at room temperature.

Results and discussion

Electrochemical impedance spectroscopy (Fig. 1) and cyclic voltammetry (Fig. S1, ESI†) were used for the characterization of each fabrication step of the genosensor (Scheme 1). Impedance data is usually studied using an equivalent circuit which helps understanding the behavior of the electrode–electrolyte interface onto the biosensor surface.[2]

The observed high electron transfer rate (Fig. 1A and Fig. S1A, ESI†) indicates that the redox mediator doesn't face any obstacle while reaching the surface of the bare electrode. Nevertheless, when the electrode is modified by electrodeposited polythionine layer, the R_{ct} value decreases and a capacitive behavior is observed (Fig. 1B and Fig. S1B, ESI†). This demonstrates that the polythionine layer is well deposited and it enhances the electron transfer. However, once IrO_2 NPs are adsorbed onto the modified electrode, a well-defined semicircle (Fig. 1C) and a decreasing of the ΔE of around 20 mV (Fig. S1C, ESI†) were observed. The improvement of the change transfer was probably due to an electrode effective area increases (see SEM images of Fig. 2) and the redox activity of the IrO_2 NPS.[19,22–24] After the oligonucleotide capture probe was attached to the IrO_2 NPs a charge transfer increase is observed (Fig. 1D and Fig. S1D, ESI†). The negative charges surrounding the IrO_2 NPs allow the attachment of the positively charged amino groups through non-covalent bonding. The charge transfer increase is due to negative charge from oligonucleotide capture probe that acts as an electrostatic barrier between SPCE/PTH and the redox indicator. The blocking effect of ethanolamine was evidenced by a decrease of charge transfer (Fig. 1E and Fig. S1E, ESI†). The hybridization of DNA target with the capture probe represents a greater obstacle to the redox mediator due to the negative charge of phosphate backbone of DNA (Fig. 1F and Fig. S1F, ESI†).

The R_{ct} values obtained from Nyquist plots after each surface modification step of the proposed system are shown in Fig. S2 of ESI.† On the basis of the charge transfer kinetics of the $[Fe(CN)_6]^{3/4}$ (redox probe), the faradaic impedance spectra were modelled using the equivalent circuit approach of Randles model modified with Warburg impedance (Fig. S2, inset, ESI†).

The morphological characterization of IrO_2 NPs was studied. Fig. 2A displays a transmission electron microscopy (TEM) micrograph, where a clusters morphology of around 20 nm composed by smaller IrO_2 NPs was observed.

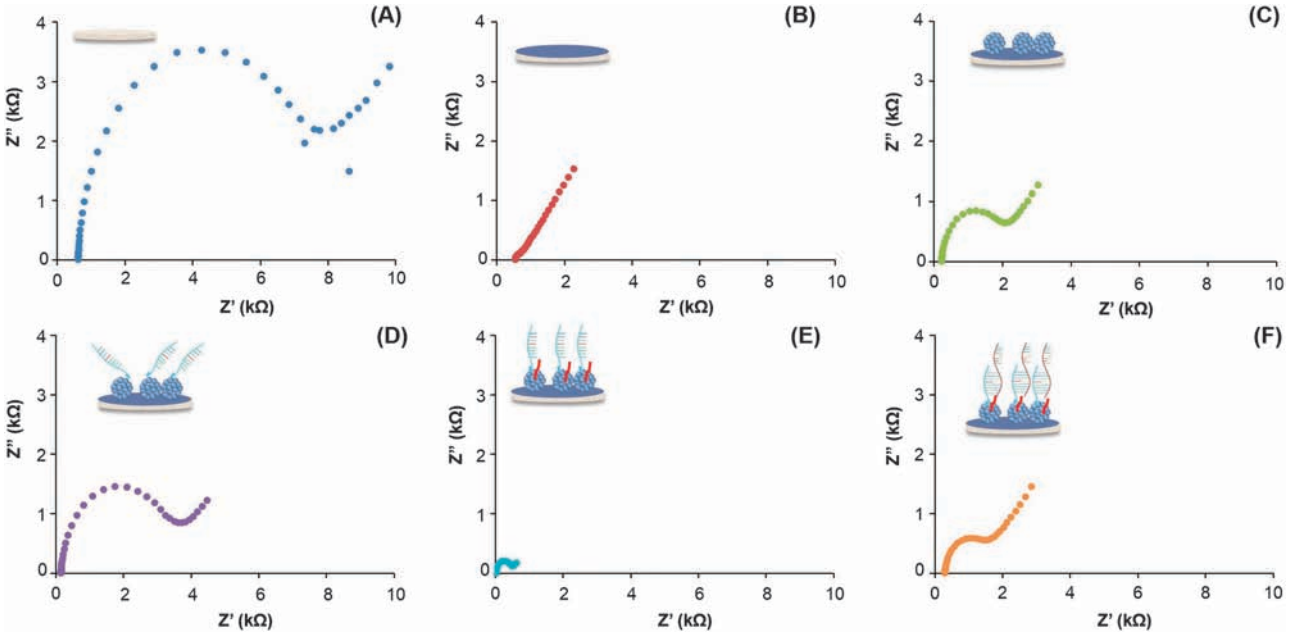

Fig. 1 EIS characterization of the bare electrode (A) and after the electrodeposition of polythionine (B), IrO_2 NP adsorption (C), oligonucleotide probe immobilization (D), blocking step with ethanolamine (E) and hybridization with a complementary target (F).

X-ray photoelectron spectroscopy and UV-visible spectrophotometry studies also were performed (see Fig. S3 and S4, ESI†). Fig. S3 (ESI†) shows the survey XPS analysis (Fig. S3A, ESI†) and high-resolution XPS spectra of the Ir 4f and O 1s regions (Fig. S3B, ESI†). The XPS spectra of the Ir 4f region revealed two main features with signals at 62.5 and 65.3 eV, which correspond to Ir 4f 7/2 and Ir 4f 5/2 orbitals, respectively. Furthermore, the O 1s region shows two features. The position of the main feature is around 532.5 eV that is similar of O 1s observed in standard IrO_2 single crystal,[25] the additional feature present the binding energy of 530.2 eV. The UV-Vis spectra reveals a characteristic peak of Ir(IV) oxides with a maximum around 580 nm (Fig. S4, ESI†). These results are in good agreement with high oxidation state 4^+ of iridium reported before.[19,24,25]

The morphological modification of SPE were also studied using scanning electron microscopy (SEM). Fig. 2B shows a SPE after activation step using H_2SO_4, while Fig. 2C displays the polythionine layer as a thin film smoothing the SPE surface. Finally in Fig. 2D, the distribution of the IrO_2 NPs (brighter dots) onto the SPE/polythionine were observed. Backscatter electrons mode was used for the enhancement of the contrast between IrO_2 NPs and SPE/polythionine surface.

Different dilutions of PCR amplified DNA (1 : 10, 1 : 100 and 1 : 1000) were detected using the system described above. The R_{ct} values were recorded as a function of PCR amplified DNA (see Fig. S5A, ESI†) showing lower impedance values for more diluted samples. These results demonstrate that the system is suitable to detect DNA but with a relatively poor reproducibility (RSD of 26%).

Selectivity is a very important parameter to be considered for DNA genosensors. To evaluate the selectivity of this system,

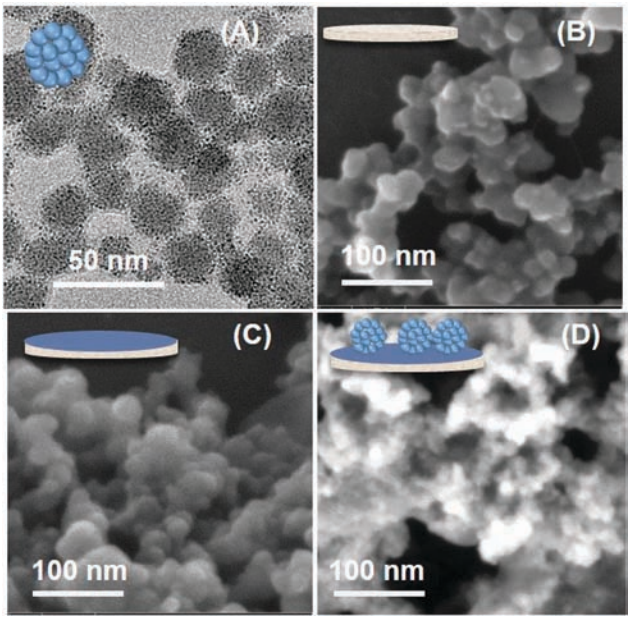

Fig. 2 Electrode surface characterization. (A) TEM images of IrO_2 NPs. SEM images of SPCE (B), SPCE with polythionine electrodeposited onto the working electrode surface (C) and SPCE/polythionine with IrO_2 NPs adsorbed onto its surface (D). SEM images were taken using backscattered electrons mode.

PCR product of dog with (positive) and without (blank) *Leishmania* were compared. Blank diluted 1 : 10 had a signal comparable to the positive sample diluted 1 : 100 (see Fig. S5B in the ESI†). To improve the selectivity and the reproducibility of this system, the blocking step during genosensor fabrication was modified using 2% of ethanolamine instead of 0.1%. The resulting data

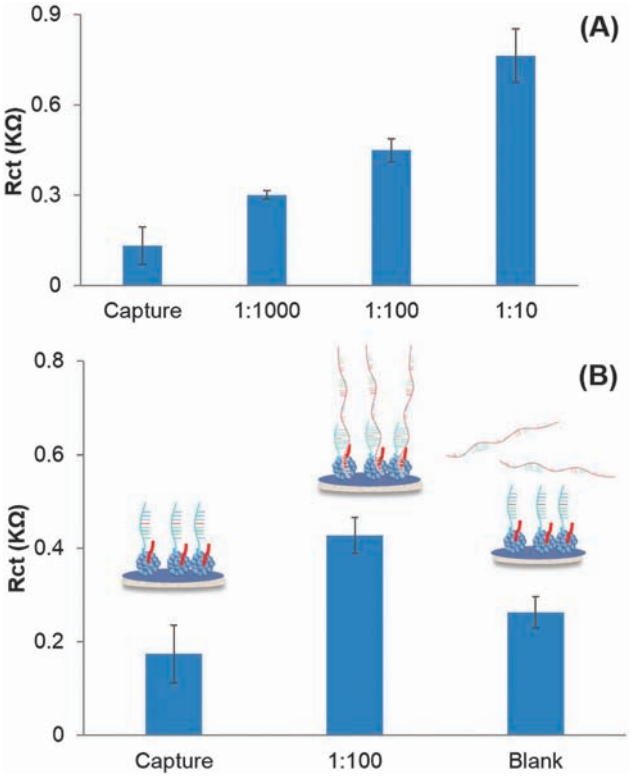

Fig. 3 (A) R_{ct} as a function of different dilutions of PCR amplified DNA samples. (B) Comparison of R_{ct} values of the genosensor modified with the capture probe and hybridized with PCR amplified DNA samples of dog affected (positive) or not (blank) with *Leishmania*. Dilution of 1 : 10 and 1 : 100 for the blank and positive samples, respectively, and 2% ethanolamine during the blocking step was used.

are shown in Fig. 3A. The R_{ct} values are quite different for the different dilutions of the PCR product (RSD of 15%) therefore we could say that this system is more sensitive. A good selectivity of the genosensor toward DNA detection was also evidenced by the neglected responses toward blank (see Fig. 3B) while the difference between the capture probe and blank was of 0.09 kΩ.

Conclusions

A simple and sensitive platform for the impedimetric label free genosensor taking advantage of a conventional screen printed carbon electrode (SPCE) modified by polythionine and IrO_2 nanoparticles is developed. Although the SPCE electrodes have several advantages such as low cost, miniaturization, mass production, *etc.* they are not directly suitable as such for impedimetric label free detection, mainly because they present a high resistivity and rough surface. In order to overcome these limitations a polythionine layer was electrodeposited on the surface of the working electrode. This modification at the same time decreases the roughness and increases the conductivity of the working electrode. Furthermore, the IrO_2 NPs show suitable redox properties in addition to the capability to attach the bioreceptor thanks to the surrounding citrate groups used as capping agents. Moreover, regarding the adsorption of capture DNA probe, the blocking procedure and hybridization steps have been optimized. To improve selectivity, reproducibility and sensitivity the concentration of ethanolamine used as a blocking agent was optimized and found to be 2% (v/v), which is the optimal concentration level. This new genosensor is able to detect up to 1000 times diluted samples of PCR amplified DNA.

Acknowledgements

We acknowledge the E.U.'s support under FP7-SME-2012-1 contract number 315653 "POC4PETS". ICN2 also acknowledges support of the Spanish MINECO under Project MAT2011-25870 and through the Severo Ochoa Centers of Excellence Program under Grant SEV-2013-0295.

References

1 A. Bonanni and M. del Valle, *Anal. Chim. Acta*, 2010, **678**, 7–17.
2 B.-Y. Chang and S.-M. Park, *Annu. Rev. Anal. Chem.*, 2010, **3**, 207–229.
3 F. Lisdat and D. Schaefer, *Anal. Bioanal. Chem.*, 2008, **391**, 1555–1567.
4 Q. Xu and J. J. Davis, *Electroanalysis*, 2014, **26**, 1249–1258.
5 E. Spain, R. Kojima, R. B. Kaner, G. G. Wallace, J. O'Grady, K. Lacey, T. Barry, T. E. Keyes and R. J. Forster, *Biosens. Bioelectron.*, 2011, **26**, 2613–2618.
6 J. P. Tosar, G. Brañas and J. Laíz, *Biosens. Bioelectron.*, 2010, **26**, 1205–1217.
7 T. Ito, K. Hosokawa and M. Maeda, *Biosens. Bioelectron.*, 2007, **22**, 1816–1819.
8 S. A. Emr and A. M. Yacynych, *Electroanalysis*, 1995, **7**, 913–923.
9 Q. Gao, X. Q. Cui, F. Yang, Y. Ma and X. R. Yang, *Biosens. Bioelectron.*, 2003, **19**, 277–282.
10 R. Yang, C. M. Ruan, W. L. Dai, J. Q. Deng and J. L. Kong, *Electrochim. Acta*, 1999, **44**, 1585–1596.
11 H. Peng, C. Soeller, N. Vigar, P. A. Kilmartin, M. B. Cannell, G. A. Bowmaker, R. P. Cooney and J. Travas-Sejdic, *Biosens. Bioelectron.*, 2005, **20**, 1821–1828.
12 S. Liu, J. Liu, L. Wang and F. Zhao, *Bioelectrochemistry*, 2010, **79**, 37–42.
13 A. Bonanni, M. J. Esplandiu and M. del Valle, *Biosens. Bioelectron.*, 2009, **24**, 2885–2891.
14 A. C. Honorato Castro, E. G. França, L. F. De Paula, M. M. C. N. Soares, L. R. Goulart, J. M. Madurro and A. G. Brito-Madurro, *Appl. Surf. Sci.*, 2014, **314**, 273–279.
15 M. Gebala and W. Schuhmann, *Phys. Chem. Chem. Phys.*, 2012, **14**, 14933–14942.
16 T. Doneux, A. De Rache, E. Triffaux, A. Meunier, M. Steichen and C. Buess-Herman, *ChemElectroChem*, 2014, **1**, 147–157.
17 Y. Wang, Z. Ye and Y. Ying, *Sensors*, 2012, **12**, 3449–3471.
18 R. W. Murray, *Chem. Rev.*, 2008, **108**, 2688–2720.

19 L. Rivas, A. de la Escosura-Muñiz, J. Pons and A. Merkoçi, *Electroanalysis*, 2014, **26**, 1287–1294.
20 S. Kurbanoglu, C. C. Mayorga-Martinez, M. Medina-Sánchez, L. Rivas, S. A. Ozkan and A. Merkoçi, *Biosens. Bioelectron.*, 2015, **67**, 670–676.
21 O. Francino, L. Altet, E. Sánchez-Robert, A. Rodriguez, L. Solano-Gallego, J. Alberola, L. Ferrer, A. Sánchez and X. Roura, *Vet. Parasitol.*, 2006, **137**, 214–221.
22 H. Boo, R.-A. Jeong, S. Park, K. S. Kim, K. H. An, Y. H. Lee, J. H. Han, H. C. Kim and T. D. Chung, *Anal. Chem.*, 2006, **78**, 617–620.
23 N. Mirbagheri, J. Chevallier, J. Kibsgaard, F. Besenbacher and E. E. Ferapontova, *ChemPhysChem*, 2014, **15**, 2844–2850.
24 Y. Zhao, E. A. Hernandez-Pagan, N. M. Vargas-Barbosa, J. L. Dysart and T. E. Mallouk, *J. Phys. Chem. Lett.*, 2011, **2**, 402–406.
25 R.-S. Chen, Y.-S. Huang, Y.-M. Liang, D.-S. Tsai, Y. Chi and J.-J. Kai, *J. Mater. Chem.*, 2003, **13**, 2525–2529.